Synthese von funktionalisierten Diazocinen für die Photopharmakologie, Molekularbiologie und für responsive Materialien

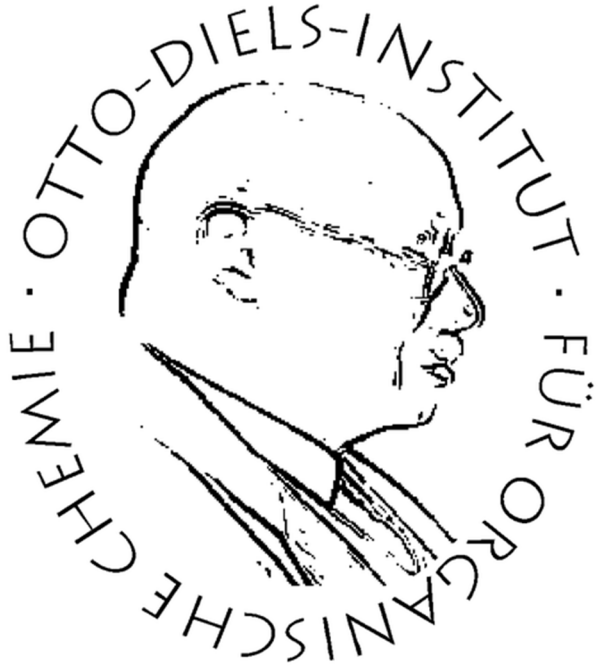

Dissertation

Zur Erlangung des Doktorgrades

der Mathematischen-Naturwissenschaftlichen-Fakultät

der Christian-Albrecht-Universität

zu Kiel

vorgelegt von

Widukind Moormann

Otto-Diels-Institut für Organische Chemie

Kiel 2020

Erster Gutachter: Prof. Dr. R. Herges

Zweiter Gutachter: Prof. Dr. F. D. Sönnichsen

Tag der mündlichen Prüfung: 17.4.2020

Zum Druck genehmigt: 21.4.2020

Ort, Datum

Widukind Moormann

Die vorliegende Arbeit wurde unter Anleitung von

Prof. Dr. Rainer Herges

am Otto-Diels-Institut für Organische Chemie

der Christian-Albrechts-Universität

und im Rahmen des SFB 677

im Zeitraum von Dezember 2015 bis Februar 2020 angefertigt.

Eidesstattliche Erklärung

Hiermit erkläre ich, Widukind Moormann, an Eides statt, dass ich die vorliegende Doktorarbeit selbstständig und nur mit den angegebenen Quellen und Hilfsmitteln angefertigt habe. Die Arbeit ist nach Inhalt und Form, abgesehen von der Beratung durch meinen Betreuer Prof. Rainer Herges, von mir eigenständig erarbeitet und erstellt worden. Diese Arbeit ist unter Einhaltung der Regeln guter wissenschaftlicher Praxis der Deutschen Forschungsgemeinschaft entstanden. Die Arbeit hat an keiner anderen Stelle im Rahmen eines Prüfungsverfahren vorgelegen und mir wurde kein akademischer Grad entzogen.

_____ _____

Ort, Datum Widukind Moormann

Danksagung

An dieser Stelle möchte ich mich bei allen bedanken, die mich während meiner Dissertation unterstützt haben. An erster Stelle möchte ich bei Prof. Herges für die Möglichkeit bedanken, an diesem interessanten und herausfordernden Thema arbeiten zu können. Er hat mich stets, auch zur später Stunde, mit interessanten Gesprächen unterstützt und mir dadurch geholfen, den richtigen Zugang zu Problemen zu finden. Außerdem möchte ich mich dafür bedanken, dass ich während meiner Promotion ein Biochemiestudium durchführen konnte. Dies hat mich zeitweise stark gefordert, aber auch zu sehr interessanten Kooperationen motiviert. Unter anderem konnte unsere Expertise in der Diazocinsynthese dazu genutzt werden, um in Kooperation mit Gisela Cabré von der Unversität aus Barcelona synthetische Neurotransmitter zu entwickeln. Gleichermaßen erfolgreich und interessant war die Zusammenarbeit mit dem Arbeitskreis Sönnichsen aus dem Otto-Diels-Institut, dem Arbeitskreis Faupel von der Technischen Fakultät in Kiel und Prof. Sijbesma von der Technischen Universität in Eindhoven. Weiterhin möchte ich mich auch bei Prof. Gescheidt und Eduard Stadler von der TU in Graz für die Messungen zahlreicher Quantenausbeuten bedanken. Meine Arbeit wäre ohne die Unterstützung der analytischen Abteilung der gesamten Fakultät nicht möglich gewesen. An selber Stelle möchte ich mich auch dafür bedanken, dass ich in der Biochemie der CAU wochenlang das CD-Spektrometer von Prof. Grötzinger nutzen konnte. In den zehn Jahren an der Universität habe ich mit vielen Menschen zusammen für Tests und Klausuren gelernt, Protokolle und später Paper geschrieben. Bei allen möchte ich mich für die spannende Zeit bedanken. Besonders möchte ich Nils Preußke danken, der mich von PC-1 bis zu meinem zweiten Bachelor stets begleitet hat und mir durch seine konstruktive Kritik immer wieder geholfen hat. Genauso danke ich Miri, die nicht weniger kritisch war, aber dadurch vier Jahre mit mir in einem Labor ausgehalten hat. Außerdem möchte ich Nils, Prof. Sönnichsen und Prof. Herges dafür danken, dass sie mir es ermöglichten, weiter an meinen Zielen zu arbeiten, als ich nicht mehr laufen konnte. Vielen Dank auch an alle, die meine Arbeit korrekturgelesen haben (Torsten, Miri, Nils, Pascal). Meiner Familie danke ich dafür, dass sie es mir ermöglichte, stets meinem Hobby, dem Mounted Games Sport, nachgehen zu können, auch wenn ich viel Zeit an der Uni verbracht habe. Zudem boten sie mir immer einen Ort, an dem ich den Kopf frei bekommen konnte. Zuletzt danke ich meiner Frau Svea, die während der gesamten Zeit an der Universität an meiner Seite stand und es auch hoffentlich in unserem neuen Lebensabschnitt weiter mit mir aushält.

Abstract

The development of artificial photoswitches, which can change their configuration upon activation with light, has paved the way to numerous applications. These applications include drugs that can be activated in the affected tissue and no longer cause side effects elsewhere in the body, peptide cross-linkers, allowing the investigation of complex interactions in biological systems with high spatiotemporal resolution and stress sensing polymers. So far, many of the available artificial photoswitches were suffering from imperfect photophysical properties limiting their use in practical applications. To achieve this objective, improved systems are required, which overcome the systematic limitations of their predecessors. With high quantum yields and superior switching efficiency, diazocines have the potential to meet these requirements. One major advantage is the fact that already the parent system switches upon irradiation with visible light. The diazocine, often referred to as bridged azobenzene, in contrast to azobenzene is thermally stable in its *cis* configuration and should thus be suitable for photopharmacology and as a mechanophore in mechanoresponsive materials. Furthermore, it should be advantageous as a cross-linker for macromolecules, since its structure reduces hydrophobic interactions. To demonstrate the applicability of diazocines in a broad range of fields, it was essential to develop a synthesis strategy, allowing specific functionalization. The synthesis started from commercially or synthetically available 2-nitrotoluene derivatives. These were dimerized in an oxidative C-C coupling and subsequently converted either in reductive or oxidative azo cyclization reactions. In combination with a suitable protecting group strategy, several functional diazocines were synthesized and tested regarding their applicability in photopharmacology, molecular biology and materials science. In collaboration, diazocine-based synthetic neurotransmitters were synthesized and used to successfully activate and deactivate neuronal signaling and thereby prove the concept of diazocines in photopharmacology. Furthermore, it was shown that diazocines are suitable cross-linkers in both artificial and bio macromolecules.

Kurzdarstellung

Die Entwicklung künstlicher Fotoschalter, die bei Aktivierung mit Licht ihre Konfiguration ändern können, hat zu zahlreichen Anwendungen geführt. Diese reichen von Wirkstoffen, welche nur im betroffenen Gewebe aktiviert werden können und im übrigen Körper keine Nebenwirkungen mehr verursachen, über Peptid Cross-Linker, mit denen sich komplexe Wechselwirkungen in biologischen Systemen mit hoher räumlich-zeitlicher Auflösung untersuchen lassen bis hin zu stressempfindlichen Polymeren. Bisher verwendete Fotoschalter schränken die Möglichkeit einer kommerziellen Verwendung auf Grund ihrer nicht hinreichenden fotochemischen Eigenschaften oft ein. Um den erklärten Zielen näher zu kommen, bedarf es verbesserten Systemen, welche die systematischen Probleme ihrer Vorgänger umgehen. Mit hohen Quantenausbeuten und überlegener Schalteffizienz könnte das Diazocin ein geeignetes System darstellen, das ohne weitere Funktionalisierung bereits mit sichtbarem Licht schaltet. Das Diazocin, oft als verbrücktes Azobenzol bezeichnet, ist im Gegensatz zu diesem in der *cis*-Konfiguration thermisch stabil und sollte daher für die Photopharmakologie und als Mechanophor in mechano-sensitiven Materialien geeignet sein. Weiterhin sollte es als Cross-Linker für Makromoleküle vorteilhaft sein, da seine Struktur hydrophobe Wechselwirkungen nicht begünstigt. Um die Anwendbarkeit von Diazocinen zu demonstrieren, musste eine Synthesestrategie entwickelt werden, die die erforderliche Funktionalisierung ermöglicht. Es erschien sinnvoll, die Synthese von handelsüblichen oder synthetisch erhältlichen 2-Nitrotoluolderivaten aus zu beginnen. Diese wurden in einer oxidativen C-C-Kupplung dimerisiert und anschließend entweder in einer reduktiven oder oxidativen Azozyklisierung umgesetzt. In Kombination mit einer geeigneten Schutzgruppenstrategie wurden auf diese Weise eine Vielzahl funktionalisierter Diazocine synthetisiert und auf ihre Anwendbarkeit in der Photopharmakologie, Molekularbiologie und in responsiven Materialien getestet. In Zusammenarbeit wurden auf Diazocinen basierende synthetische Neurotransmitter genutzt, um die neuronale Reizleitung reversibel zu kontrollieren und auf diese Weise die Anwendbarkeit von Diazocinen in der Photopharmakologie zu erweisen. Weiterhin konnte gezeigt werden, dass Diazocine sowohl in künstlichen als auch in biologischen Makromolekülen als Cross-Linker geeignet sind.

Contents

1 Introduction

All functions of the macroscopic world are accomplished on a molecular level. Each function is generally triggered by an external stimulus and causes a response that ultimately results in an effect. In nature, processes such as vision, ion and proton transport are just a few examples that are accomplished through a light-driven switching function. The group of retinal-carrying proteins (rhodopsin, halorhodopsin, bacteriorhodopsin) performs a number of biological functions through the photon-absorbing co-factor retinal.[1] Upon absorption of light the retinal residue undergoes a very fast and high-yielding *cis* → *trans* isomerization.[2] In the visual pigment rhodopsin, the formation of the photoproduct, photorhodopsin is accomplished within 200 fs and results in the activation of the visual phototransduction through the coupled G-protein transducin (**Figure 1.1**).[3]

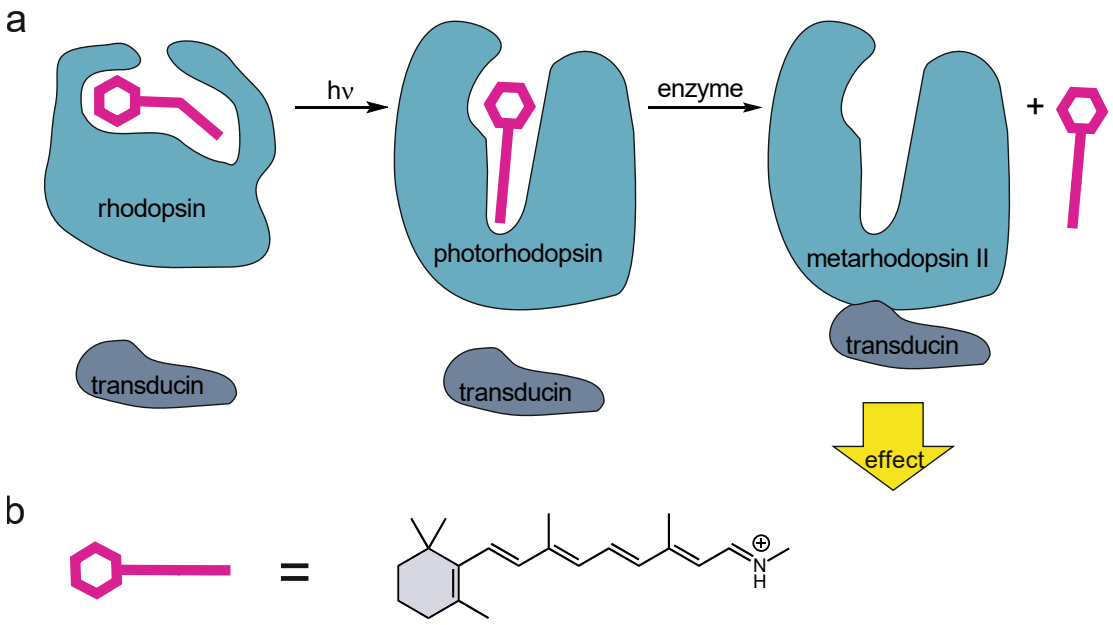

Figure 1.1: a) The first step in the visualization process is triggered through light-activated isomerization of 11-*cis* retinal. After isomerization, rhodopsin undergoes conformational changes and all-*trans* retinal is cleaved. Thereupon the binding site for transducin becomes available and activates the transduction cascade.[4] b) Structure of all-*trans* retinal.

The understanding of photo-induced control of biological function has inspired investigations on a number of artificial, biotic and abiotic functions using molecules that change their structure and properties upon the absorption of light similar to retinal. Research is focused on

the development of novel functional materials, miniaturization of technical processes, understanding of biological interactions and treating diseases more selectively.[5–10] The most frequently used artificial photoswitch is azobenzene.[11] It is thermodynamically stable in the planar and slender *trans* configuration. Upon excitation with light of 365 nm, *trans* → *cis* isomerization is induced, resulting in the formation of a metastable *cis* isomer, which isomerizes back to the *trans* isomer thermally or upon irradiation using 440 nm (**Figure 1.2**).[12] The utilization of azobenzene in biological systems and materials is dependent on the isomerization wavelength. UV light has a low tissue penetration depth and above all damages tissue.[13] The influence of substitution on the isomerization wavelength of azobenzene has been elucidated and particular, derivatives allow to some extend the isomerization of azobenzene with visible light.[14–16]

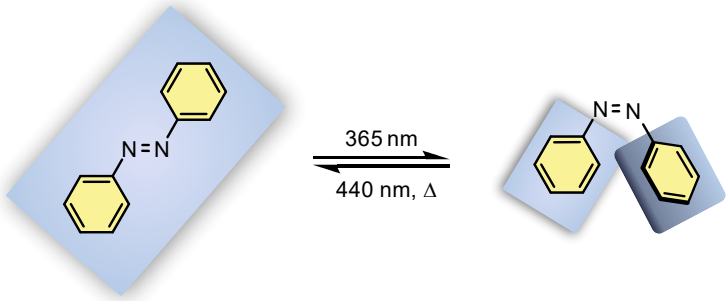

Figure 1.2: Azobenzene is thermodynamically stable in its planar *trans* configuration. Upon irradiation with UV light (365 nm), it is isomerized into the metastable *cis* configuration. The back-isomerization can be accomplished by irradiation with light of 440 nm or thermally.[11]

The stimulation of molecular photoswitches like azobenzene with light holds a number of advantages, especially when applied to biological systems. Due to spatiotemporal resolution and selection of different wavelengths, light is a highly selective trigger, which allows fast and reversible control. The stimulation with visible light is neither invasive nor toxic and orthogonal to most biological processes.[17] Biological functions are controlled through a complex network of biochemical interactions, the relationships of which have not yet been fully determined.[18] To get a better understanding of the interaction pathways, mechanism and kinetics within a biological system, it would be ideal to switch the activity of the relevant component on and off with high spatiotemporal control. Introduction of photoswitchable molecules into bioactive compounds similar to retinal in rhodopsin has been a successful strategy towards this end.[7–10, 18] A photoswitchable molecule can be introduced into a

biologically active compound as part of an organic small molecule or as a macromolecule conjugate.[7, 10] Peptides and proteins have diverse functions inside biological systems and are involved in the largest part of interactions. Thus, they are ideal targets for the functionalization with photoswitchable molecules.

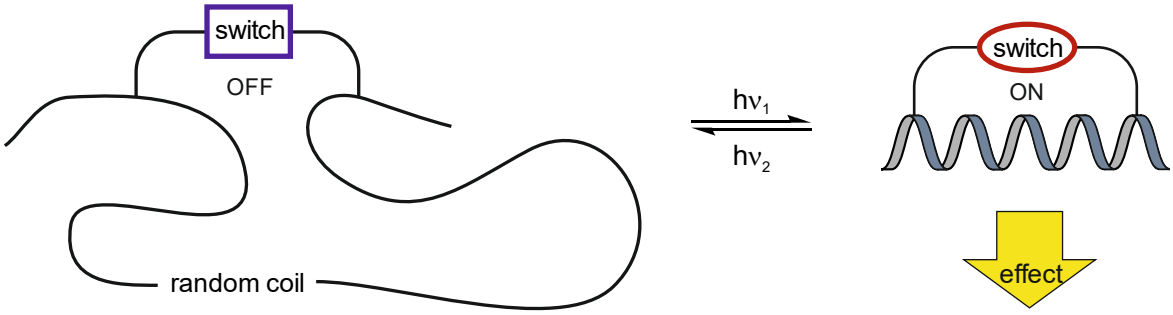

Figure 1.3: One way to control the biological activity of peptides and proteins with high spatiotemporal resolution is by cross-linking it with a photoswitchable compound. Upon irradiation, a change in the properties of the photoswitch influences the fold and thereby the activity of peptides and proteins.

The biological activity of peptides and proteins largely depends on their secondary and tertiary structure. Controlling the fold is therefore desired.[7, 9, 18] To achieve this, photoswitchable molecules can be introduced in the side-chain, in the backbone or as a cross-linker between attachment sides.[9] The functionalization of α-helices with a photoswitchable cross-linker has proven to be a successful concept (**Figure 1.3**). Starting with the model peptide FK-11, Woolley *et al.* have introduced a number of azobenzene derivatives into α-helical proteins and peptides, thereby successfully controlling the fold of the α-helix and the activity in a reversible manner. Thereupon, but not limited to, DNA binding, transcription factor controlled gene expression, apoptosis and cell adhesion, have been investigated.[18] The use of photoswitchable molecules in biological systems, however, is not limited to an analytical tool but it has also been directly employed in the field of photopharmacology. The combination of photochemistry and pharmacology is defined as photopharmacology.[10] Photopharmacology aims to control the selectivity of active pharmaceutical ingredients (API) with high spatiotemporal resolution through the introduction of a photoswitchable moiety (**Figure 1.4 a**). Conventional drugs can cause side effects in the body before they reach the target and afterwards when entering the environment. The environmental contamination of APIs has been of particular interest in ongoing investigations concerning bacterial drug

resistance and the consequences. However, the environmental toxicity caused through APIs is not limited to antibiotics, but also hormones and anti-inflammatory products have contributed significantly.[19–22]

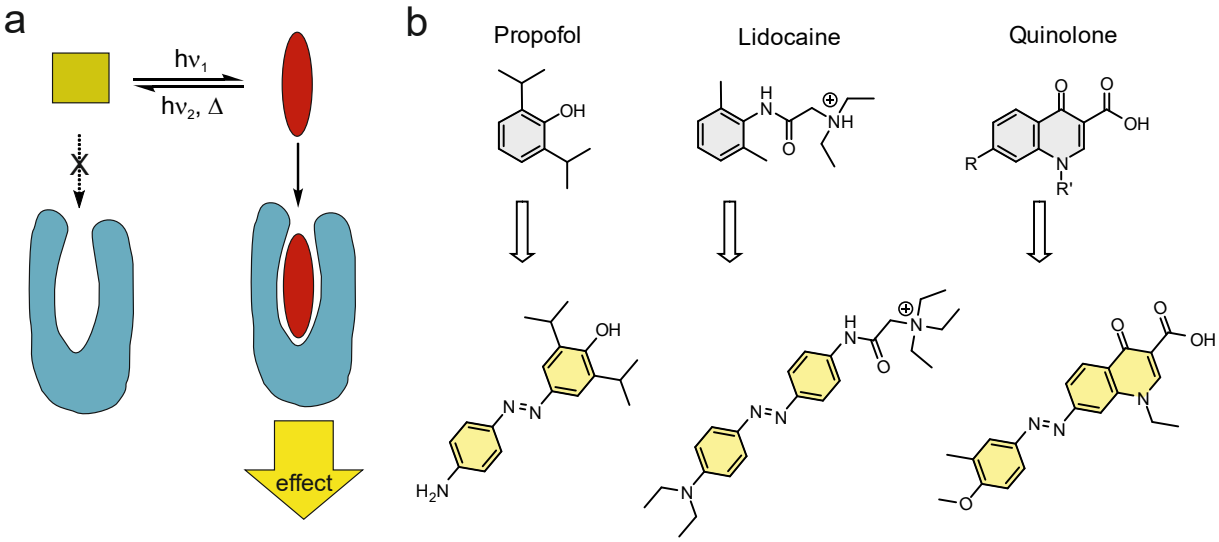

Figure 1.4: a) Photopharmacology ideally aims to decrease side effects by only activating the drug at a desired location and time. To achieve this, the compound must undergo conformational changes upon irradiation, resulting in one conformation, which has a high affinity to the target, whereas the original configuration does not interact with the target. b) Through the introduction of azobenzene into existing drugs, a number of compounds were successfully tested. However, with the exception of quinolone-derived photopharmacophores, most compounds have been active in their dark-adapted state and only allow deactivation upon irradiation with light.

Azobenzene has been implemented into the structures of numerous pharmaceutically active small molecules. A common target are gated ion channels, as the pharmacology of ion channels has been extensively investigated and matches the fast kinetics of photoswitches.[23] The early design of these photopharmacophores appeared to be rather simple. One of the first successfully tested components was an azobenzene-propofol analogue (**Figure 1.4 b**).[24] Propofol acts as an allosteric modulator at $GABA_A$ gated ion channels and is used as an anesthetic. This photopharmacophore simply consisted of an azobenzene with the substitution pattern of propofol. In a similar fashion, azobenzene was functionalized with the binding motif of lidocaine, which targets sodium channels to achieve local anesthesia (**Figure 1.4 b**).[25] In most reports, the planar *trans* configuration has an increased affinity to the binding pocket, in comparison to the sterically demanding and bent

cis configuration. The azobenzene-based quinolone derivative reported by Feringa, however, is an exception and has increased activity in the bulkier *cis* configuration (**Figure 1.4 b**).[26]

Due to their key role in excitatory synaptic transmission in the nervous system, glutamate ion channels have been among the first targets of photopharmacology. The ionotropic glutamate receptors (iGluRs) are divided into groups depending on their genomic sequence and interaction with the agonists; AMPA (α-amino-3-hydroxyl-5-methyl-4-isoxazolepropionic acid), Kainate (kainic acid), NMDA (N-methyl-D-aspartate). They are activated upon presynaptic binding of glutamate, which ultimately results in postsynaptic neuronal firing. The action potential of neurons can easily be detected in patch-clamp and multielectrode arrays (MEA), which enable standardized *in vitro* and *in vivo* testing.

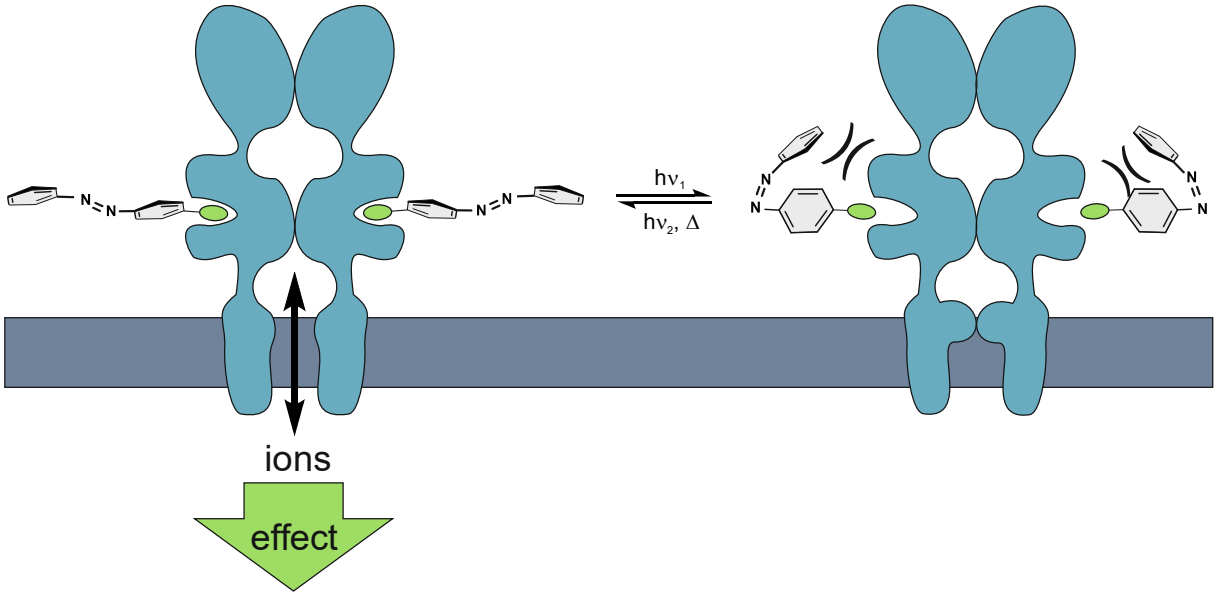

Figure 1.5: Kainate receptors belong to the group of ionotropic glutamate receptors. These tetrameric cation channels open upon binding of presynaptically released glutamate. Photocontrol of postsynaptic action potentials have been achieved with azobenzene derivatives equipped with a glutamate moiety. In the slender *trans* configuration, these compounds show activity. After isomerization of azobenzene, binding is sterically prohibited and no action potential can be measured.

A number of photoswitchable glutamate neurotransmitters have been synthesized and used to investigate the deactivation and activation of neuronal firing (**Figure 1.5**). Controlling the activity of single neurons has helped to understand the connectivity of the nervous system in more detail.[23]

1.1 Smart Materials

Besides photopharmacology, additional strategies have been developed to decrease side effects of drugs.[17, 27–29] A prominent example is the spatiotemporally controlled release of drugs by smart materials.[30–32] Smart materials, also called intelligent or responsive materials, are defined by the ability to react to an external stimulus with a controlled change of material properties. A large number of materials have been engineered either by changing their sensitivity to the external stimuli, their polymer properties or the specific response of the material.[33] In order to stimulate the material, a responsive group needs to be incorporated into the material. Stimulation has been achieved mechanically, optically, thermally, electrically and chemically.[33, 34] The incorporation of novel mechano- and/or photoresponsive elements has increased the functionality of polymers and thereby enabled a great variety of applications ranging from rewritable optical storage, artificial muscles and catalysis.[34–36] In particular, stress indicating, drug and fragrance releasing and self-healing materials have recently been brought to attention.[34, 37, 38] Stress indication can be achieved by incorporation of mechanochromic groups into materials. These mechanophores change their color upon the application of force.[37] Ideally, this could prevent accidents caused by material exhaustion, simply by a change of color, visible to the eye.

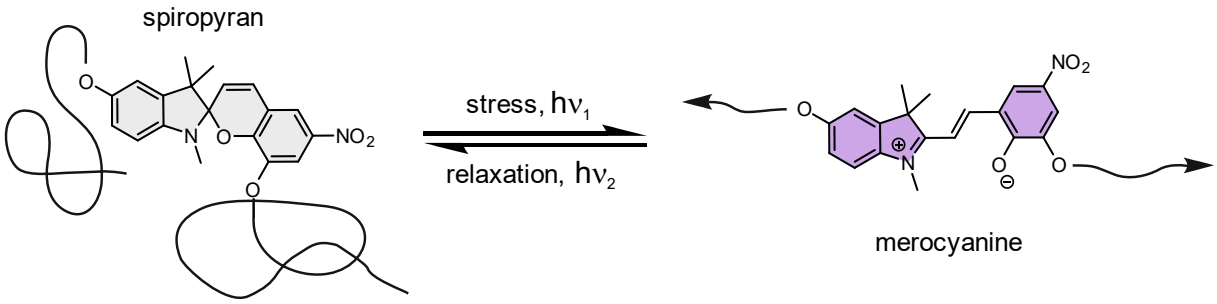

Figure 1.6: Spiropyran can act as a mechanosensitive unit when embedded into a polymer. When tensile force is applied, the shorter and colorless spiropyran is stretched into the elongated and colored merocyanine. The merocyanine can thermodynamically relax back to the spiropyran. Additionally, spiropyran-containing polymers can also change their properties through light-triggered isomerization of the spiropyran, thereby acting as mechano and photosensitive materials.

Spiropyran was used as a mechano and photoresponsive unit in the pioneering work of Sottos, Moore and White.[37–39] Spiropyran is thermodynamically stable in its colorless closed form, yet upon irradiation with UV light (photosensitive) or mechanical force (mechanosensitive) it undergoes ring opening and the colored merocyanine is formed (**Figure 1.6**). The merocyanine can be converted back to the spiropyran upon irradiation or by thermal relaxation.[40] Although the Spiropyran has served as an ideal model system for stress sensing, actuators and shape-recovery polymers, its applicability is limited. Irradiation with UV light causes material damage and the open merocyanine is unstable towards oxygen.[40] In contrast, azobenzene derivatives have proven to be stable under oxygen, and irradiation of tetra *ortho* substituted derivatives with visible light is possible.[12, 14, 16] However, azobenzenes are not suitable as mechanophores, as the thermodynamically stable but elongated *trans* configuration cannot be isomerized upon the application of force.[41]

1.2 Requirements for Photoswitches

Photoswitch-based investigations have opened up a number of very promising applications, but the photochemical properties of the implemented photoswitches must be further optimized prior to commercialization.

To implement photopharmacology as a relevant alternative to conventional API treatment, the integrated photoswitch must be non-toxic and metabolically stable in aqueous solution, under physiological pH, high ionic strength and upon irradiation.[17] Additionally, high absorbance, quantum yields and conversion rates are ideal to generate high concentrations of the active pharmaceutical ingredient upon irradiation. When considering the advantages of photopharmacophores over conventional drugs, the ideal strategy is to administer the API in its dark adapted inactive state and to activate it upon irradiation at the site of interest. Although exceptions are reported, azobenzene derivatives are commonly isomerized upon irradiation with UV light. UV light is toxic and causes tissue damage.[13] Tetra *ortho* substituted derivatives are an exception, but might not be synthetically accessible in every required substitution pattern. Furthermore, affinity to the binding site can be disturbed by the steric hindrance and the change in dipole moment.[42] Additional attention must be paid to the substitution pattern in regard to the stability of azobenzene derivatives in the cellular environment.[43, 44] Especially the functionalization with electron-withdrawing or amino groups has increased the likelihood of glutathione-caused reduction. The reduction of azobenzenes to their corresponding anilines has been extensively investigated and correlations to a carcinogenic effect have been identified.[45, 46]

1.3 Diazocines

Although already synthesized in 1910 by Duval, it was not until 2009 that bridged azobenzenes, also called diazocines, were investigated for the first time with regard to their photochemical properties by Herges and Temps.[47–50] Through addition of an *ortho* ethylene bridge, the diazocine forms an 8-membered ring with the diazene embedded. In contrast to azobenzene, diazocines are thermodynamically stable in their bent *cis* configuration (**Figure 1.7 a**). The twist and chair configurations are much more strained than the boat, which forces the azo group into the *cis* configuration. Upon irradiation with visible light, the diazocine can undergo a very fast and reversible isomerization to the twisted *trans* configuration.

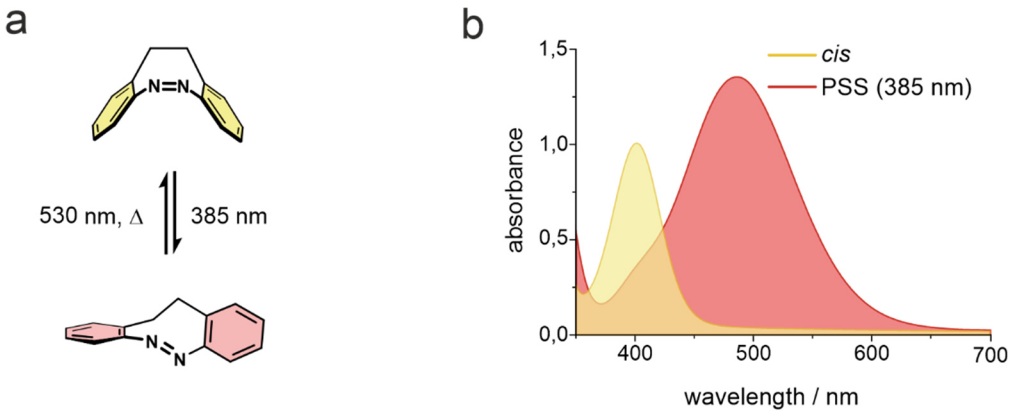

Figure 1.7: Diazocines have an inverse thermal stability in comparison to azobenzenes. The sterically demanding and bent *cis* isomer is thermodynamically stable and isomerizes upon irradiation with visible light. The isomerization is accompanied by a color change from yellow (*cis*) to red (*trans*). The back-isomerization of the twisted *trans* isomer can be accomplished with green light or by thermal relaxation.

It is worth noting that the n-π* transition of the *trans* diazocine is shifted bathochromically enabling the isomerization with visible light. This is an advantage as compared to *trans* azobenzene, which isomerized upon excitation of the π-π* transition. The n-π* transition of the *cis* and *trans* isomer are clearly separated by about 100 nm resulting in exceptionally high photostationary states (PSS) *cis* → *trans* (87%) and *trans* → *cis* isomerization (>99%) (**Figure 1.7 b**). Diazocines are stable under atmospheric conditions and no fatigue or photo degradation is observed after hundreds of switching cycles. The ethylene bridge suppresses the conformational freedom in diazocines; therefore it is more likely that

an excited state will follow the isomerization reaction path, resulting in exceptionally high quantum yields (parent diazocine $\Phi_{E\rightarrow Z}$ = 0.9, $\Phi_{Z\rightarrow E}$ = 0.72).[47, 51] The unique photochemical properties of diazocines render them as ideal photoswitches in biological systems and for photopharmacology. Due to the inverse stability, diazocines are an ideal replacement for a number of azobenzene-based photopharmacophores. Azobenzene derivatives are generally active in their dark-adapted state and can only be deactivated (**Figure 1.8**). To decrease side effects, the drug would have to be irradiated constantly, except in the affected tissue. Resulting from the investigations on azobenzene-derived photopharmacophores, diazocine-based pharmacophores should be inactive in their dark-adapted *cis* configuration and activated upon irradiation with visible light. Additionally, diazocines are less prone to hydrophobic interactions in the sterically demanding *cis* configuration and in the twisted *trans* configuration, which has caused problems when switching azobenzene derivatives in biological systems and materials.[35]

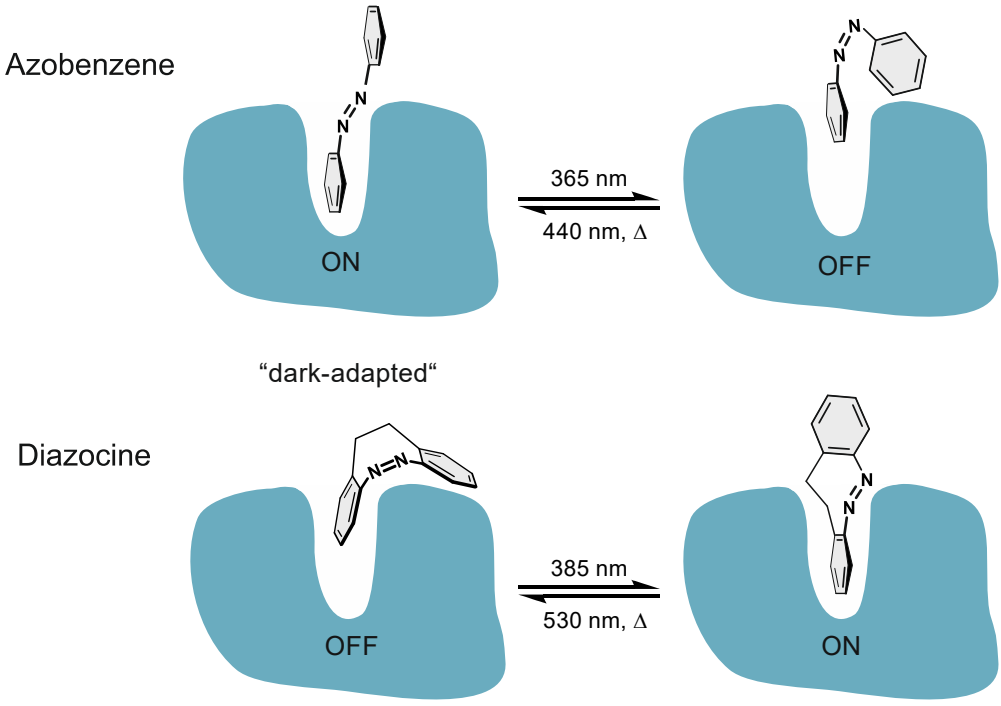

Figure 1.8: Most azobenzene-derived drugs are active in their dark-adapted state and deactivated upon irradiation with UV or visible light. The inverse stability of diazocines render them as an ideal system to avoid constant irradiation. Only when activated upon irradiation the drug would be active and could relax back to the inactive isomer or isomerize with light of a different wavelength.

Due to the reverse stability, diazocines are suitable as a mechanosensitive units in mechanoresponsive materials.[35] When incorporated into a suitable polymer, the short, yellow *cis* diazocine isomerizes into the stretched, red *trans* isomer upon the application of tensile force. In consequence, this system is a valid alternative to the currently investigated spiropyrans in stress-sensing and shape recovery polymers. (**Figure 1.9**).

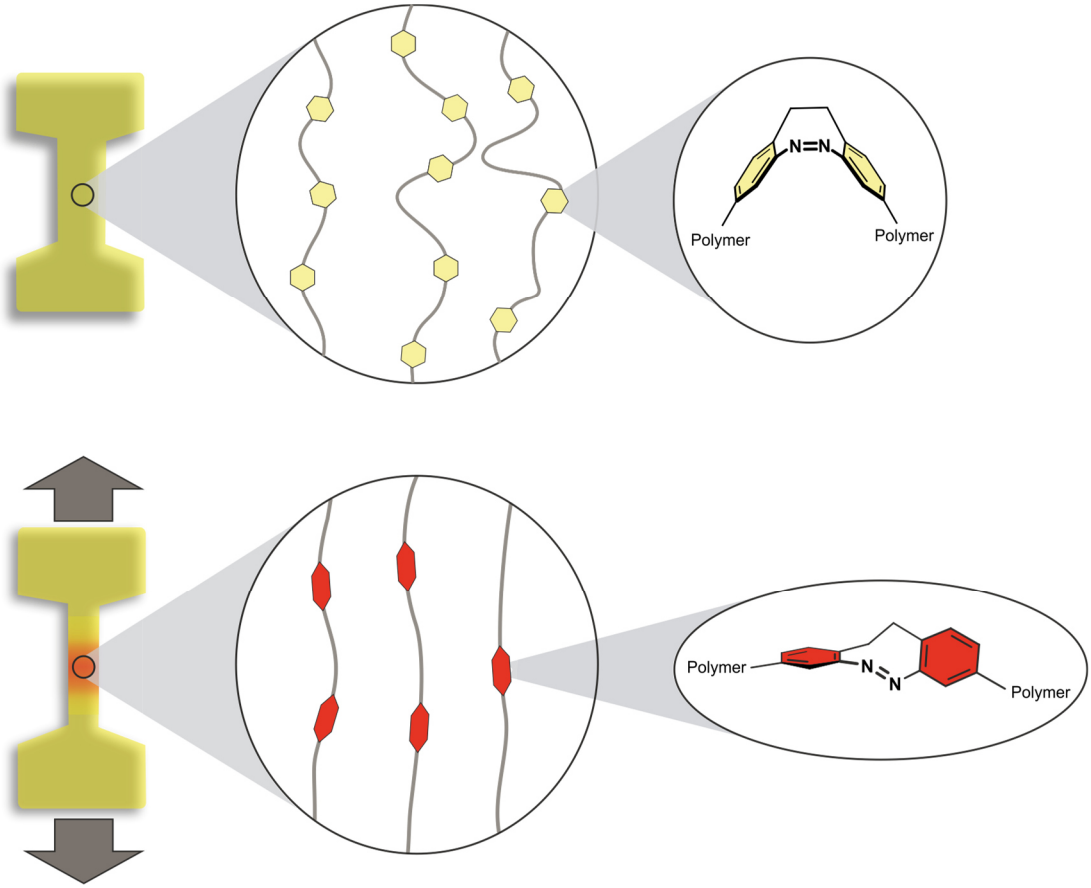

Figure 1.9: When a force is applied on the shorter and bent *cis* isomer, embedded into a polymer, it can be stretched into the longer and twisted *trans* isomer, thereupon changing the color from yellow to red and functioning as a stress sensing tool.

Since the parent diazocine has very promising photochemical properties, it is interesting to see whether the properties can be further optimized. Because of the difficult synthesis in comparison to azobenzene, only little is known on the effect of derivatization of diazocine. So far modified diazocines were investigated by the introduction of a heteroatom in the -C-C- ethylene bridge. It is known that *ortho* substitution in azobenzene has shifted the n-π^* transition of the *trans isomer* bathochromically and thus improved the separation of

absorption bands. By substitution of a methylene group of the bridge with a heteroatom (NR, O, S) the absorption of the diazocine has also shifted bathochromically and allowed isomerization with near infrared light.[51, 52] Through the introduction of an additional 5-membred bridge, chiral diazocines have been developed. They are particularly interesting for the chiral induction of liquid crystal phasing with circular polarized light and directional motion on surfaces.[53]

2 Scope

Due to their unique properties, diazocines are suitable for various applications.[35, 53–58] Because of their inverse stability, they are of specific interest in photopharmacology and for the development of mechano- and photoresponsive materials.[35, 51, 59] Preliminary work has focused on investigating and improving the photochemical properties of the diazocine parent system for example by substitution of a bridge methylene group with a heteroatom.[51, 52] In order to design drugs using diazocines as cross-linkers in peptide and protein chemistry or in mechanosensitive materials, it was necessary to develop a synthetic strategy, which allows a desired functionalization of diazocines. In contrast to azobenzene very little was known about the synthesis of substituted diazocines.[49, 53, 56–58] A small number of functionalized diazocines have been published previously; the synthesis, however, appeared to be limited to few functional groups and the yields were low and unreliable. In addition to the difficult synthesis, in some cases, the chosen substitution pattern resulted in the loss of the excellent photochemical properties.[54, 56–58] Thus, strategies were sought to achieve functionalization that would allow the implementation into macromolecules, but also retain the photochemical properties. After the development of a suitable synthesis strategy, selected compounds for photopharmacology and cross-linkage of macromolecules were synthesized and characterized with regard to their photochemical properties. In order to validate the concepts, these compounds were tested in collaborations concerning their behavior after implementation in biological systems and materials.

3 Publications

3.1 Diazocine Synthesis

Despite the promising features of diazocines in photopharmacology, materials science and supramolecular chemistry, after the discovery of their photochemical properties by Herges and Temps, diazocines were mainly used as a reference substance to azobenzene-based photoswitches.[47, 60–62] Only a limited number of new diazocines and applications were published.[43, 55–57] The synthetic procedures in each of the published works varied and was never mechanistically elusive. It appeared that the original synthesis of Duval and later Paudler had good yields but still was not considered ideal. Alternative syntheses failed to be reproducible, high yielding, reliable, versatile for derivatization or up-scalable.[47, 55–57, 63] In comparison to the azobenzene synthesis, diazocine synthesis generally includes one additional C-C coupling step. In principle, the C-C coupling can be accomplished before or after the azo cyclization step (**Figure 3.1.1**). However, there was no reported synthesis of diazocines in which the azo cyclization was followed by the C-C coupling (**Figure 3.1.1 b**).

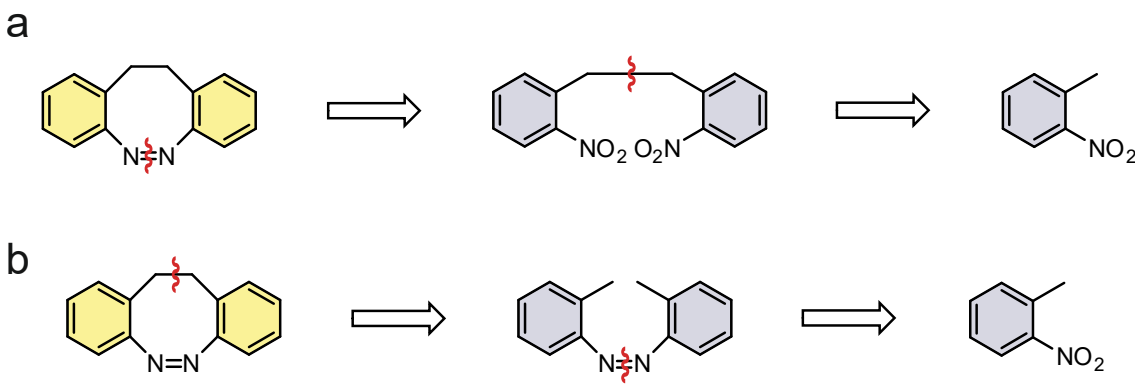

Figure 3.1.1: There are generally two conceivable routes for the synthesis of diazocine, a) and b). a) A two-step diazocine synthesis starting from 2-nitrotoluene has, however, only been accomplished through C-C coupling in the first step followed by azo cyclization. b) So far, it has not been possible to form the ethylene bridge following the azo cyclization.

Using a reductive azo cyclization starting from a dinitro precursor would allow a desired two-step diazocine synthesis (**Figure 3.1.1 a**). The dinitro precursor can be synthesized in an oxidative C-C coupling starting from 2-nitrotoluene.[64] These derivatives are commercially available and easy to synthesize. Thus, they would be ideal starting compounds for the derivatization of diazocines if the two consecutive steps were reliable and high yielding.

3.1.1 Summary of Solvent-Free Synthesis of Diazocine

In this work we developed a convenient two-step diazocine synthesis starting from the commercially available 2-nitrotoluene. At first, we investigated the oxidative C-C coupling of 2-nitrotoluene. Addition of potassium butoxide leads to deprotonation of the α-proton to form an anion, which is stabilized by the nitro group in *ortho* position. As a result of delocalization, the anion can no longer act as a nucleophile in substitution reactions. Upon addition of an oxidant, the anions are oxidized to form radicals, which dimerize subsequently.[64] The original reaction by Chaudhuri and Ball was carried out with air as oxidant.[64] However, it was difficult to reproduce the reaction conditions including parameters such as temperature, stirring speed and water content of the air. The use of bromine as an oxidant allowed to establish a reliable reaction. Further optimization of reaction conditions resulted in a reliable, fast and high yielding C-C coupling of 2-nitrotoluene (**Figure 3.1.2**).

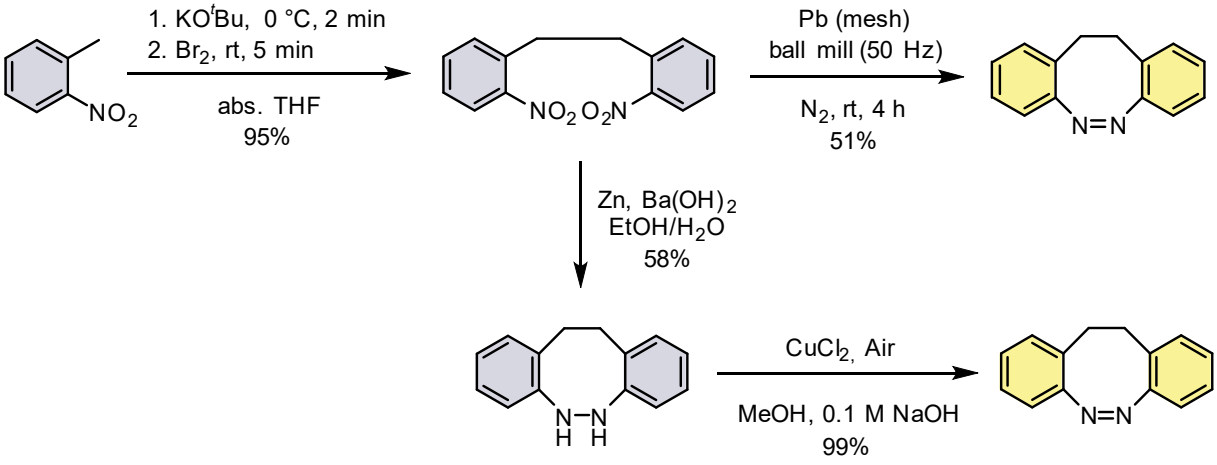

Figure 3.1.2: The developed synthesis of the diazocine starts from commercially available 2-nitrotoluene, which is deprotonated and oxidized to form radicals, that dimerize. The dinitro dimer was converted in a two-step azo cyclization using Zn, $Ba(OH)_2$ to form the hydrazine, which was subsequently oxidized with $CuCl_2$ and air. To avoid a two-step synthesis we investigated the reduction of the dinitro dimer in a ball mill with lead under nitrogen atmosphere.

As the reductive azo cyclization is the second step in this diazocine synthesis strategy, we investigated the procedure by Duval and Paudler with regard to the formation of intermediates during the reaction.[49, 65] This reaction allows reduction of the dinitro precursor

to the hydrazine using Zn, $Ba(OH)_2$ under conditions, which prevent the formation of diamines. In a second step, the hydrazine is oxidized quantitatively to the diazocine with highly toxic mercury oxide. In previous experiments, the outcome of the reaction very much varied in dependence of the zinc quality. Based on the monitoring of the reaction conditions a method was developed that allows to perform the reaction, independent of the zinc reactivity. Additionally the use of mercury oxide was avoided by implementing $CuCl_2$ and air as an alternative. (**Figure 3.1.2**).

To avoid the second oxidation step we investigated a one-step solvent-free azo cyclization, using lead powder in a ball mill under nitrogen atmosphere, which yielded 51% (**Figure 3.1.2**).[66] In view of possible applications in pharmacology, the stability of diazocine towards glutathione was tested. It appeared that the parent diazocine is stable when isomerized under the presence of glutathione. Thus, it can be expected to be intracellularly stable and not carcinogenic.[45, 46]

3.1.2 Solvent-Free Synthesis of Diazocine

Widukind Moormann, Daniel Langbehn and Rainer Herges

Synthesis **2017**, *49 (15)*, 3471-3475

DOI: 10.1055/s-0036-1590685

Scientific contribution to this paper

I developed the synthetic route. I carried out all the syntheses and investigations, with the help of Daniel Langbehn as in his role as a research associate. Prof. Dr. R. Herges and I wrote the manuscript.

3471

Synthesis W. Moormann et al. Paper

Solvent-Free Synthesis of Diazocine

Widukind Moormann
Daniel Langbehn
Rainer Herges*

Otto Diels Institute for Organic Chemistry, University of Kiel, Otto-Hahn-Platz 4, 24118 Kiel, Germany
rherges@oc.uni-kiel.de

Dedicated to Professor Herbert Mayr on the occasion of his 70th birthday

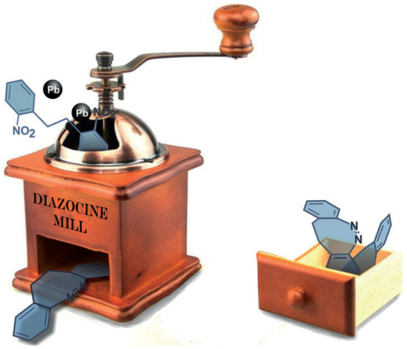

Received: 17.05.2017
Accepted after revision: 29.06.2017
Published online: 11.07.2017
DOI: 10.1055/s-0036-1590685; Art ID: ss-2017-z0341-op

Abstract A convenient two-step synthesis of diazocine starting from 2-nitrotoluene is described. The first step, the oxidative dimerization of 2-nitrotoluene, is improved to 95% yield. The second step, the reductive azo cyclization, is performed as a solvent-free reaction with lead powder in a ball mill (51% yield). As a reference, the previously described azo cyclization with $Zn/Ba(OH)_2$ is investigated in detail. The results explain why in previous experiments the yields are low and extremely dependent on the reaction conditions. In view of potential applications in photopharmacology, we checked the stability under reducing conditions. Diazocine does not react with glutathione, indicating intracellular stability.

Key words bridged azobenzene, diazocine, reductive azo-cyclization, solvent-free synthesis, oxidative C–C coupling, lead, azoxy, hydrazine, glutathione

Diazocines have been known for more than 100 years, however, it was only recently discovered that they exhibit extraordinary photophysical and photochemical properties.[1,2] As compared to the most frequently used photoswitch, azobenzene, the parent diazocine has higher switching efficiencies (100% *E*→*Z*, 96% *Z*→*E*), and higher quantum yields (50% *E*→*Z*, 72% *Z*→*E*). Moreover, diazocines can be isomerized with visible light (400 nm *E*→*Z*, 500 nm *Z*→*E*), and the photodynamics are ultrafast.[3] Most importantly, in contrast to azobenzene, diazocine is more stable in its sterically demanding *Z* form than in the slender *E* configuration. Hence, diazocines are ideal switches in photopharmacology.[4,5] Most drugs equipped with an azobenzene unit are active in their more stable and less hindered *E* configuration. Biological activity is switched off upon isomerization with UV light because the bent *Z* isomer no longer fits into the binding site of the receptor. Diazocines, however, are more stable in their *Z* state, and could be administered in their inactive form. At the site of illness, the drug would be switched on with light with high spatiotemporal control. Several examples prove the practicability of diazocines in biochemical applications. Peptides and DNA strands with switchable conformations have been prepared by incorporation of diazocines, and spatiotemporal regulation of DNA functions has been suggested.[6,7] However, the synthesis of diazocines proceeds with notoriously poor yields and low reproducibility. We therefore optimized and investigated in detail the most frequently used preparation method, i.e., the oxidative coupling of 2-nitrotoluene and the reduction of 2,2′-dinitrodibenzyl with Zn powder and $Ba(OH)_2$. Based on the mechanistic information, we have developed a convenient, reliable, and solvent-free synthesis of diazocine.

The synthesis of diazocine started with dimerization of 2-nitrotoluene using *t*-BuOK as a base, and air as the oxidizing agent. According to our observations, 2,2′-dinitrodibenzyl is formed in low yields, even in the absence of additional oxidizing agents, because part of the nitro compound is sacrificed in the oxidation step (and reduced). We therefore screened the effect of external oxidizing agents on the reaction time, temperature and yields. The yield reported by Chaudhuri and Ball[8] (65%) was increased to 95% by addition of bromine as the oxidizing agent (Scheme 1). Thereby, the reaction time was reduced from several hours to 7 minutes.

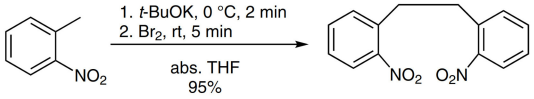

Scheme 1 Improved method for the oxidative coupling of 2-nitrotoluene to 2,2′-dinitrodibenzyl

The majority of procedures describing the synthesis of diazocines are based on the reduction of 2,2′-dinitrodibenzyl with Zn and $Ba(OH)_2$, as published by Duval (Scheme 2).[1,2,6,9–12] The reported yields vary substantially.

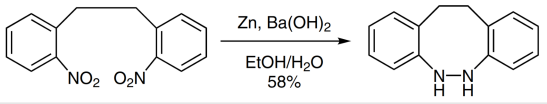

Scheme 2 Reduction of 2,2′-dinitrodibenzyl with Zn and $Ba(OH)_2$ as reported by Duval et al.

According to our observations the process is strongly dependent on the reaction conditions. We therefore investigated the mechanism in detail by monitoring the intermediates and their concentrations during the reduction (Figure 1).

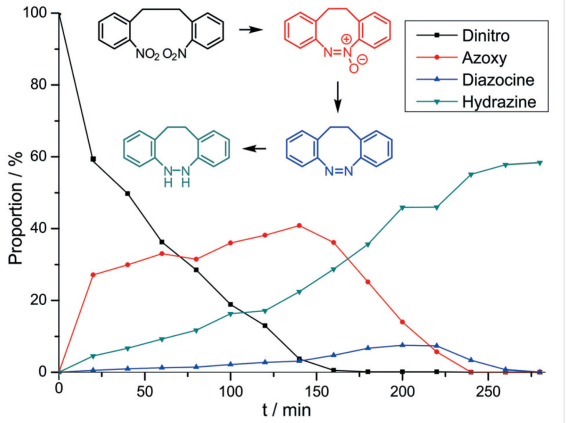

Figure 1 Fractions of products and intermediates during reduction of 2,2′-dinitrodibenzyl with $Zn/Ba(OH)_2$ as a function of time

Several facts are worth noting. The azoxy compound is the first isolable reduction product, and it is obviously an intermediate with a peak concentration of 41% after about 2 hours (16 equiv of Zn powder, 3 equiv $Ba(OH)_2$, ethanol, reflux). The azoxy compound is further reduced to the diazocine (peak concentration ~8% after ~3 h) which again is reduced to the hydrazine (~58%). Further reduction to the diamine is slow (if no further Zn is added). We checked this mechanistic hypothesis by resubmitting the intermediate azoxy compound to the same reduction conditions, and observed an analogous concentration dependence of diazocine and hydrazine as shown in Figure 1. The sum of azoxy compound, diazocine, and hydrazine remains constant during reduction. There is no loss of material after formation of the azoxy compound. By-products, such as the dimer and higher oligomers, are formed in the first reductive ring-closure step of the dinitrodibenzyl. We conclude that reduction to the hydrazine and reoxidation is the most convenient method to prepare the diazocine giving the highest yields. The reaction can be easily monitored by TLC. Diazocine gives rise to a yellow spot which can be switched to a red color upon irradiation with UV light (and back to yellow with green light). The colorless hydrazine spot is converted into the yellow diazocine upon very short exposure to fuming nitric acid vapor, and thus easily identified by subsequent switching with UV light. Oxidation of the hydrazine to diazocine with air and $CuCl_2$ is an almost quantitative reaction (Scheme 3).

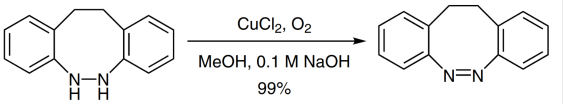

Scheme 3 Formation of diazocine by oxidation of the corresponding hydrazine

A reason for the varying yields in previous syntheses might be the fact that upon standing in air the hydrazine autoxidizes to the diazocine. By-products during reduction are the cyclic dimer (16-membered ring) and oligomers.[13]

Ring-closure reactions are favored over oligomerization under high dilution conditions, or if performed as heterogeneous reactions keeping the local concentration of the reactant low.[14,15] Besides reduction with $Zn/Ba(OH)_2$, reactions with lead under basic conditions (pH 9.5) in methanol and formic acid as a proton source have been successfully performed.[7,10] Under these reaction conditions the cyclic azoxy compound is formed, which subsequently is reduced with PCl_3 or $Ph_3P/MoCl_2O_2(dmf)_2$. Hence, both procedures reported in the literature are two-step reactions. To avoid over-reduction to the hydrazine [$Zn/Ba(OH)_2$], or incomplete reduction to the azoxy compound ($Pb/Et_3N/HCOOH$), we investigated the one-step, solvent-free reduction with lead powder in a ball mill (Scheme 4).[16] Avoiding moisture (dry nitrogen atmosphere), or other additional proton sources should prevent formation of the hydrazine or diamine. Various substituted azobenzenes have been prepared on small scale by Suzuki et al. using this method.[17]

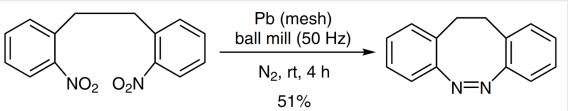

Scheme 4 Solvent-free reduction of 2,2′-dinitrodibenzyl with lead powder in a ball mill

We mixed 2,2′-dinitrodibenzyl with a 10-fold molar excess of lead powder, and agitated the mixture in a ball mill under a nitrogen atmosphere. At regular intervals, probes were taken and analyzed. As in the case of $Zn/Ba(OH)_2$ reduction, the cyclic azoxy compound is the first isolable compound with a peak concentration of 45% after about 2 hours (vibrational frequency 50 Hz). Upon further milling,

the diazocine is formed at the expense of the azoxy compound concentration (Figure 2). The isolated yield of diazocine after 3.5 hours is 51%. No further reduction takes place after extended periods of milling. The reaction time depends on the scale of the reaction and the milling frequency.

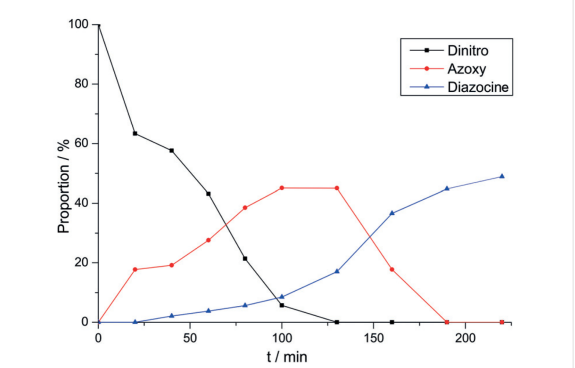

Figure 2 Fractions of products and intermediates during reduction of 2,2′-dinitrodibenzyl with lead powder in a ball mill as a function of time

The product is separated from the lead powder by extraction with acetone and filtration. Lead should be removed quickly, or protic solvents or moisture should be carefully avoided. Upon standing of the suspension with lead under air, further reduction to the hydrazine was observed. Small amounts (~6%) of the dimer (16-membered ring with both azo groups in *E* configuration) and higher cyclic oligomers are formed as well.[13]

Under physiological conditions, a number of azobenzenes (particularly amino-substituted azobenzenes) are reduced *in vivo* to the corresponding anilines, some of which are carcinogenic.[18] Good correlations have been observed between the glutathione-inducing effect of azo dyes in the liver and their carcinogenic activities.[19] For applications in photopharmacology, the stability of the switchable drugs toward reduction by glutathione inside cells is essential.

We therefore subjected diazocine to reduction by glutathione. For solubility reasons, the experiments were performed in a 1:1 acetonitrile/PBS buffer. After incubation of diazocine for 24 hours, no change in UV–vis absorption was detected. Furthermore, the diazocine was switched 22 times between the *Z* and the *E* configuration with light of 385 and 530 nm in the presence of glutathione. No fatigue, or side products were detected (Figure 3). Our experiments indicate that diazocine is stable toward reduction by glutathione. Besides photopharmacology, diazocines have been proposed as substitutes for azobenzenes in demonstration experiments, because they can be switched with visible light and they exhibit a distinct color change.[20] The negative glutathione test gives a first indication that diazocine is physiologically benign.

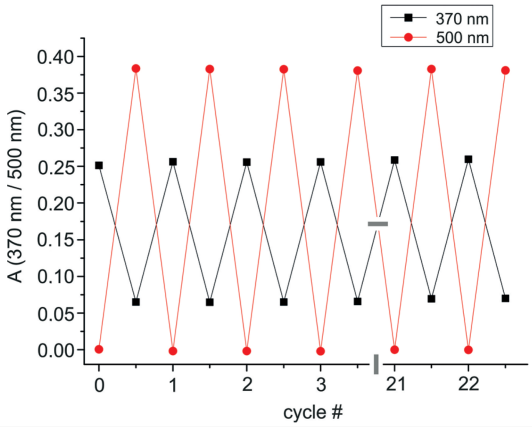

Figure 3 Switching of diazocine with light of 385 and 530 nm in an alternating sequence in the presence of glutathione in acetonitrile/water (1:1) after incubation for 24 h. Absorption at 370 and 500 nm was recorded after each switching cycle. No fatigue was observed.

In conclusion, we optimized the synthesis of parent diazocine. The yield of the first step (oxidative dimerization of 2-nitrotoluene) was improved to 95% by using bromine as the oxidizing agent (instead of air). The eight-membered ring in diazocines is rather strained (ring strain ~16 kcal mol^{-1}). Reductive azo-cyclization of the dinitro precursor, therefore, competes with cyclic oligomer and polymer formation. Further problems on the reaction pathway to diazocine arise from incomplete reduction (azoxy compound), or over-reduction (hydrazine), or further reductive ring cleavage (diamino compound). We minimized oligomer formation, and avoided over-reduction by performing the reduction of the dinitro compound under dry and solvent-free conditions with metallic lead in a ball mill. In contrast to a number of azobenzenes, diazocine is stable towards reduction by glutathione which is an important prerequisite for applications in photopharmacology.

Milling reactions were carried out in a 15 mL stainless steel grinding cup using stainless steel balls of 10 mm diameter in a laboratory ball milling apparatus (Pulverisette 23, Fritsch GmbH, Idar-Oberstein, Germany). Test for stability to glutathione reduction: Diazocine was incubated (24 h, 27 °C) in 1:1 acetonitrile/PBS (1X phosphate-buffered saline:137 mM NaCl, 2 mM KCl, 8 2 mM Na_2PHO_4, 2 mM KH_2PO_4, pH = 7.4) in a 10 mM solution of glutathione. A reaction control was performed with the use of an Agilent Technologies 1100 Series HPLC and Agilent Zorbax 5 µm Eclipse XDB-C8, 4.6 × 150 mm column. TLC plates (Polygram Sil G/UV254 Macherey–Nagel) were used for reaction control. Flash column chromatography was carried out with a Biotage® Isolera system using Biotage® SNAP ULTRA (HP-Sphere™ 25 µm) columns. Melting points were obtained using a Büchi, Melting Point M-560 apparatus. IR spectra were recorded with a Perkin–Elmer 1600 series FT-IR spectrophotometer, using a Golden Gate Diamond ATR unit, A531-G. NMR spectra were recorded using a Bruker DRX 500 spectrometer [^{1}H NMR (500.1 MHz), ^{13}C NMR (125.8 MHz)]

without an internal standard. Mass spectra were recorded on a Finnigan MAT 8230 (EI, 70 eV) spectrometer. UV–Vis spectra were recorded with a Lambda 14 UV/Vis spectrometer, Perkin–Elmer. Irradiation was performed with LED light sources [385 nm: 12 × Nichia NC-SU034A, FWHM = 9 nm, P(opt) = 12 × 340 mW, 530 nm: 16 × Luxeon LXML-PM01-0080, FWHM = 33 nm, P(opt) = 16 × 200 mW], Sahlmann Photochemical Solutions.

2,2′-Dinitrodibenzyl

[CAS Reg. No. 16968-19-7]

Under a nitrogen atmosphere, 2-nitrotoluene (2.00 g, 15.0 mmol) was dissolved in dry THF (90 mL), cooled to 0 °C, followed by addition of potassium butoxide. The reaction was stirred for 2 min before addition of bromine (3.12 g, 19.5 mmol). After further stirring for 5 min, the reaction was added to 500 mL of ice/water. The precipitate was filtered and the filtrate extracted with CH_2Cl_2 (3 × 100 mL). The combined organic layers were washed with saturated sodium thiosulfate solution and saturated sodium chloride solution, then dried over $MgSO_4$ and concentrated under reduced pressure. The crude product was purified by crystallization (H_2O/EtOH, 1:2) to give 2,2′-dinitrodibenzyl as a white solid (1.94 g, 7.13 mmol, 95%); mp 121 °C; R_f = 0.33 (*n*-pentane/CH_2Cl_2, 1:1).

IR (ATR): 2962, 2854, 2343, 1608, 1576, 1509, 1443, 1344, 1310, 1262, 1201, 1164, 1126, 1073, 1041, 959, 859, 787, 749, 704, 666, 567, 531, 421 cm^{-1}.

^1H NMR (500.1 MHz, $CDCl_3$, 300 K): δ = 7.96 (dd, *J* = 8.2 Hz, *J* = 1.2 Hz, 2 H, *H*-3), 7.54 (pseudo t, 2 H, *H*-5), 7.42 (dd, *J* = 7.7 Hz, *J* = 1.3 Hz, 2 H, *H*-6), 7.38 (pseudo t, 2 H, *H*-4), 3.25 (s, 4 H, CH_2).

^{13}C NMR (125.8 MHz, $CDCl_3$, 300 K): δ = 149.37, 136.01, 133.30, 132.49, 127.56, 124.84, 34.44.

MS (EI, 70 eV): *m*/*z* (%) = 273 (1) $[M + H]^+$, 255 (8), 237 (9), 178 (21), 136 (100), 120 (70), 92 (85).

5,6,11,12-Tetrahydrodibenzo[*c*,*g*][1,2]diazocine (Hydrazine)

[CAS Reg. No. 2225-55-0]

To a solution of 2,2′-dinitrodibenzyl (201 mg, 738 µmol) in EtOH (40 mL) were added an aqueous solution of barium hydroxide [$Ba(OH)_2{\cdot}8H_2O$] (695 mg, 2.20 mmol) in H_2O (20 mL) and zinc powder (778 mg, 11.9 mmol), and the mixture was stirred for 5 h under reflux. The reaction mixture was filtered through Celite and the solvent was removed under reduced pressure. The crude product was dissolved in CH_2Cl_2, filtered through Celite, and the solvent evaporated. The residue was purified by flash column chromatography (cyclohexane/EtOAc, 3:1, R_f = 0.72) to afford the product as a colorless solid (90.0 mg, 429 µmol, 58%); mp 151 °C.

IR (ATR): 3337, 3327, 3049, 2939, 2902, 1606, 1580, 1495, 1454, 1441, 1406, 1234, 1101, 935, 864, 746, 717, 542, 484, 441, 405 cm^{-1}.

^1H NMR (500 MHz, acetone-d_6, 300 K): δ = 7.03 (d, *J* = 7.3 Hz, 2 H, *H*-6), 6.99 (dt, *J* = 7.6 Hz, *J* = 1.5 Hz, 2 H, *H*-2), 6.83–6.76 (m, 4 H, *H*-3, *H*-5), 6.55 (s, 2 H, N-*H*), 3.18 (s, 4 H, CH_2).

^{13}C NMR (125 MHz, acetone-d_6, 300 K): δ = 148.9, 133.8, 131.3, 127.0, 122.0, 117.8, 32.0.

MS (EI, 70 eV): *m*/*z* (%) = 210 (100) $[M]^+$.

HRMS (EI, 70 eV): *m*/*z* $[M]^+$ calcd for $C_{14}H_{14}N_2$: 210.1157; found: 210.1154.

(*Z*)-11,12-Dihydrodibenzo[*c*,*g*][1,2]diazocine

[CAS Reg. No. 1194317-15-1]

By Reduction/Reoxidation of 2,2′-Dinitrodibenzyl: To a solution of 2,2′-dinitrodibenzyl (201 mg, 738 µmol) in EtOH (40 mL) were added an aqueous solution of barium hydroxide [$Ba(OH)_2{\cdot}8H_2O$] (695 mg, 2.20 mmol) in H_2O (20 mL) and zinc powder (778 mg, 11.9 mmol), and the mixture was stirred for 5 h under reflux. The reaction mixture was filtered through Celite, and the solvent was removed under reduced pressure. The crude product was dissolved in CH_2Cl_2 and filtered through Celite, and the solvent was removed under reduced pressure. The crude product was dissolved in 0.1 M methanolic NaOH solution (50 mL), $CuCl_2$ (4 mg, 29.8 µmol) was added, and air was bubbled through the solution until completion of the reaction. The reaction was neutralized with 1 M HCl solution. After addition of saturated sodium bicarbonate solution, the aqueous layer was extracted with CH_2Cl_2. The combined organic layers were dried over $MgSO_4$ and the solvent was removed under reduced pressure. The crude product was purified by flash column chromatography (cyclohexane/EtOAc, 3:1, R_f = 0.51) to afford the product as a yellow solid (89.1 mg, 428 µmol, 58%); mp 103–105 °C.

IR (ATR): 3058, 2898, 1813, 1568, 1522, 1480, 1438, 1153, 1083, 1037, 949, 924, 864, 805, 763, 747, 682, 631, 596, 566, 535, 481, 459, 422, 405 cm^{-1}.

^1H NMR (500.1 MHz, $CDCl_3$, 300 K): δ = 7.13 (pseudo t, 2 H, H-4), 7.02 (pseudo t, 2 H, H-5), 6.98 (d, *J* = 7.7 Hz, 2 H, H-6), 6.83 (d, *J* = 7.8 Hz, 2 H, H-3), 2.87 (m_c, 4 H, CH_2).

^{13}C NMR (125.8 MHz, $CDCl_3$, 300 K): δ = 155.49, 129.60, 128.08, 127.01, 126.66, 118.70, 31.65.

MS (EI, 70 eV): *m*/*z* (%) = 208 (19) $[M]^+$, 179 (100), 165 (61).

HRMS (EI, 70 eV): *m*/*z* $[M]^+$ calcd for $C_{14}H_{12}N_2$: 208.1001; found: 208.1004.

UV–Vis (MeCN): λ_{max} (log ε) = 401 (2.99), 281 (3.48), 245 (3.96) nm.

By One-Step Reduction of 2,2′-Dinitrodibenzyl with Pb in a Ball Mill: Under a nitrogen atmosphere, 2,2′-dinitrodibenzyl (320 mg, 1.18 mmol), lead mesh (2.44 g, 11.8 mmol; Alfa Aesar lead powder, 200 mesh, 99.9%), and two stainless steel balls (10 mm diameter) were added to a stainless steel grinding cup (15 mL). The reaction vessel was shaken at a rate of 50 Hz for 4 h. The black pasty product was extracted twice with acetone (200 mL). The extracts were filtered over Celite and the solvent was evaporated. The crude residue was purified by flash column chromatography (cyclohexane/EtOAc, 3:1, R_f = 0.51) to afford the product as a yellow solid (125 mg, 602 µmol, 51%).

Funding Information

The authors gratefully acknowledge financial support by the Deutsche Forschungsgemeinschaft (DFG) within the Sonderforschungsbereich SFB677, ‘Function by Switching’.

References

(1) Duval, H. *Bull. Soc. Chim. Fr.* **1910**, *7*, 727.
(2) Siewertsen, R.; Neumann, H.; Buchheim-Stehn, B.; Herges, R.; Näther, C.; Renth, F.; Temps, F. *J. Am. Chem. Soc.* **2009**, *131*, 15594.
(3) Siewertsen, R.; Schönborn, J. B.; Hartke, B.; Renth, F.; Temps, F. *Phys. Chem. Chem. Phys.* **2011**, *13*, 1054.

(4) Lerch, M. M.; Hansen, M. J.; van Dam, G. M.; Szymanski, W.; Feringa, B. L. *Angew. Chem. Int. Ed.* **2016**, *55*, 10978.
(5) Broichhagen, J.; Frank, J. A.; Trauner, D. *Acc. Chem. Res.* **2015**, *48*, 1947.
(6) Samanta, S.; Qin, C.; Lough, A. J.; Woolley, G. A. *Angew. Chem. Int. Ed.* **2012**, *51*, 6452.
(7) Eljabu, F.; Dhruval, J.; Yan, H. *Bioorg. Med. Chem. Lett.* **2015**, *25*, 5594.
(8) Chauduri, N. K.; Ball, T. J. *J. Labelled Compd. Radiopharm.* **1980**, *18*, 1189.
(9) Paudler, W. W.; Zeiler, A. G. *J. Org. Chem.* **1969**, *43*, 3237.
(10) Joshi, D. K.; Mitchell, M. J.; Bruce, D.; Lough, A. J.; Yan, H. *Tetrahedron* **2012**, *68*, 8760.
(11) Tellkamp, T.; Shen, J.; Okamoto, Y.; Herges, R. *Eur. J. Org. Chem.* **2014**, *25*, 5456.
(12) Deo, C.; Bogliotti, N.; Métivier, R.; Retailleau, P.; Xie, J. *Chem. Eur. J.* **2016**, *22*, 9092.
(13) Tauer, E.; Machinek, R. *Liebigs Ann. Chem.* **1996**, 1213.
(14) Fan, Q.; Wang, T.; Dai, J.; Kuttner, J.; Hilt, G.; Gottfried, J. M.; Zhu, J. *ACS Nano* **2017**, *11*, 5070.
(15) Bielawski, C. W.; Benitez, D.; Grubbs, R. H. *Science* **2002**, *297*, 2041.
(16) Tanaka, K.; Toda, F. *Chem. Rev.* **2000**, *100*, 1025.
(17) Wada, S.; Urano, M.; Suzuki, H. *J. Org. Chem.* **2002**, *67*, 8254.
(18) Mori, H.; Mori, Y.; Sugie, S.; Yoshimi, N.; Takahashi, M.; Hiroaki, N.-i.; Yamazaki, H.; Toyoshi, K.; Williams, G. M. *Cancer Res.* **1986**, *46*, 1654.
(19) Neish, W. J. P.; Davies, H. M.; Reeve, P. M. *Biochem. Pharm.* **1964**, *13*, 1291.
(20) Krämer, R. *Dissertation*; Bergische Universität Wuppertal: Germany, **2016**.

3.2 Synthesis of Functionalized Diazocines

Due to their inverse stability in comparison to azobenzenes, diazocines are suitable as mechanochromic mechanophores. The bent and yellow *cis*-configuration should be stretched into the longer and red *trans*-configuration with the application of force. The isomerization of Spiropyran has been used to establish stress-indicating materials and shape recovery polymers in a similar manner.[37–39] However, this mechanophore is partially oxidized in the open merocyanine form, wherby restricting its use.[40] Not only is the diazocine more stable, it also has improved photochemical properties which makes them suitable for photoresponsive materials.[47, 48]

To achieve this, functionalized diazocines need to be synthetically accessible, the functionalization needs to enable cross-linkage and implementation must retain the excellent photochemical properties. Hitherto only a few diazocines have been implemented into macromolecules.[35, 54] In those, the chosen substitution pattern resulted in poor *cis* → *trans* isomerization rates and thus did not implement the improved photochemical properties of the diazocine parent system (**Figure 3.2.1**).[43, 56]

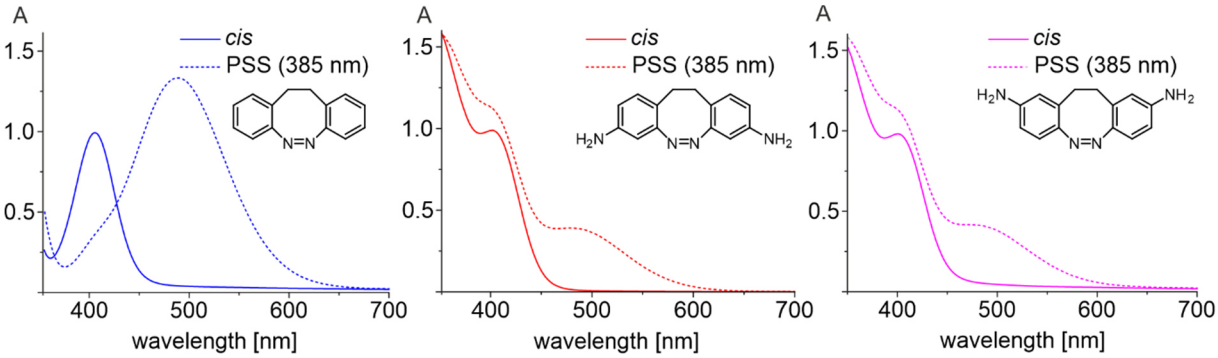

Figure 3.2.1: UV-spectra of the parent diazocine (left), 3,3'-diaminodiazocine (middle) and 4,4'-diaminodiazocine (right) in acetonitrile. The 3,3'-diaminodiazocine (middle) and 4,4' diaminodiazocine (right) have both been implemented in macromolecules but show uncharacteristic photochemical properties in comparison to the parent system (left). It appears that the π–π* transition of the *trans*-isomer is bathochromically shifted and thus interfering with the n-π* transition of the *cis*-isomer, resulting in poor photostationary states.

3.2.1 Summary of Synthesis of Functionalized Diazocines for Application as Building Blocks in Photo- and Mechanoresponsive Materials

In this work, the photochemical properties of previously published diazocines used as photoswitches in macromolecules were compared with several new functionalized diazocines in solution.[54, 56] To enable a comparison of photochemical properties of different compounds, these needed to be tested under the same conditions. Thereupon we synthesized and investigated the previously published 3,3'-diaminodiazocine, 4,4'-diaminodiazocine and parent diazocine. The $PSS_{385\ nm}$ of both amino substituted diazocines were evidently poor. We attributed this to the electronic interactions between the substituents and azobenzene and concluded that electronic decoupling of the azobenzene unit and its substituents by insertion of one or two CH_2 groups would improve the PSS at 385 nm. Consequently, a synthesis route for seven symmetrically functionalized diazocines bearing the functional groups amine, alcohol, azide and vinyl, was developed. The synthesis route was based on the previously published oxidative C-C coupling and reductive azo cyclization, which have shown to be suitable for derivatization of diazocines (**Figure 3.2.2 a**).[67]

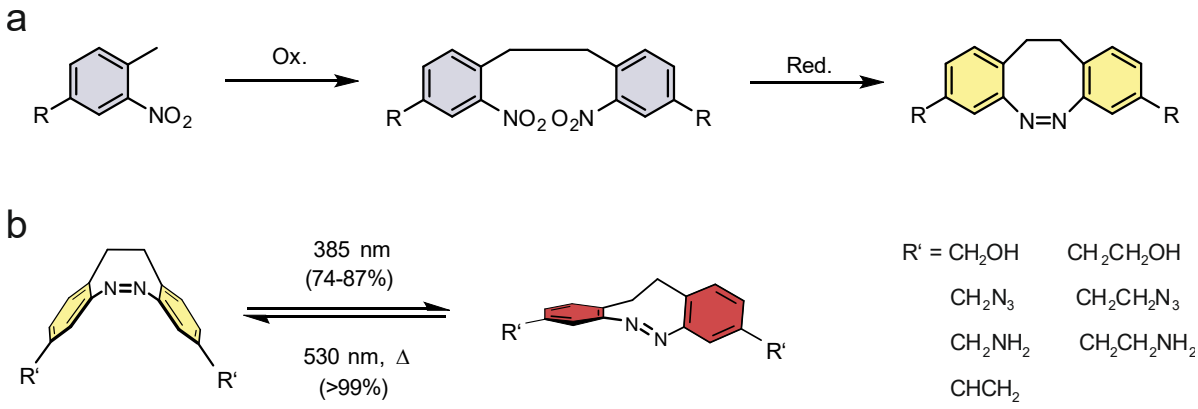

Figure 3.2.2: a) The previously published procedure starting from 2-nitrotoluene derivatives was applied to synthesize seven symmetrically substituted diazocines. b) The introduction of a methylene group between the aromatic ring and the functional group improved the photostationary states at 385 nm.

The photochemical properties of the diazocines were investigated in UV-vis and NMR experiments. The switching efficiency was significantly improved ($PSS_{385\ nm}$: 74-85%) in comparison to the diaminodiazocines ($PSS_{385\ nm}$: 25-30%) (**Figure 3.2.2 b**) and thus enable the use of diazocines with improved photochemical properties in a variety of polymers such as polyurethanes, polyesters, polyamides, polyureas and polyolefines.

3.2.2 Synthesis of Functionalized Diazocines for Application as Building Blocks in Photo- and Mechanoresponsive Materials

Widukind Moormann, Daniel Langbehn and Rainer Herges

*Beilstein J. Org. Chem.***2019**, *15*, 727–732.
doi:10.3762/bjoc.15.68

Scientific contribution to this paper

I developed the synthetic route. I carried out the syntheses and investigations together with Daniel Langbehn. Prof. Dr. Herges and I wrote the manuscript.

BEILSTEIN JOURNAL OF ORGANIC CHEMISTRY

Synthesis of functionalized diazocines for application as building blocks in photo- and mechanoresponsive materials

Widukind Moormann, Daniel Langbehn and Rainer Herges*

Full Research Paper

Open Access

Address:
Otto Diels Institute for Organic Chemistry, Christian-Albrechts-University, Otto-Hahn-Platz 4, 24118 Kiel, Germany

Email:
Rainer Herges* - rherges@oc.uni-kiel.de

* Corresponding author

Keywords:
bridged azobenzene; diazocine; mechanophor; oxidative C–C coupling; photochrome; reductive azo cyclization

Beilstein J. Org. Chem. **2019,** *15,* 727–732.
doi:10.3762/bjoc.15.68

Received: 12 December 2018
Accepted: 09 March 2019
Published: 20 March 2019

Associate Editor: J. A. Murphy

Abstract

Seven symmetrically 3,3'-substituted diazocines were synthesized. Functional groups include alcohol, azide, amine and vinyl groups, which are suitable for polymer synthesis. Upon irradiation at 385 and 530 nm the diazocines perform a reversible, pincer-type movement switching the 3,3'-distance between 6.1 Å (*cis*, stable isomer) and 8.2 Å (*trans*, metastable isomer). Key reactions in the synthesis are an oxidative C–C coupling of 2-nitrotoluenes (75–82% yield) and a reductive ring closure to form the diazocines (56–60% yield). The cyclization of the dinitro compound to the azo compound was improved in yield and reproducibility, by over-reduction to the hydrazine and reoxidation to the azo unit. In contrast to 3,3'- and 4,4'-diaminodiazocine, which have been implemented in macromolecules for conformation switching, our compounds exhibit improved photophysical properties (photostationary states, separation of absorption bands in the *cis* and *trans* configuration). Hence they are promising candidates as molecular switches in photo and mechanoresponsive macromolecules and other smart materials.

Introduction

The field of photoresponsive materials is of growing interest [1-3]. Several mechanophores such as azobenzene [4-8], diarylethene [9-13] and spiropyrans [14-18] have been investigated as photoswitchable building blocks. Bridged azobenzenes also known as diazocines exhibit excellent photochemical properties but applications are limited and suitably functionalized compounds are rare [19-23]. In contrary to azobenzenes, diazocines **1** are stable in their *cis* configuration. The bent *cis* isomer is less prone to π–π stacking which is known to reduce the switching efficiency (Figure 1a) [19,24]. The reverse stability of the *cis* and *trans* isomers in azobenzenes and diazocines should allow reciprocal applications in mechanoresponsive materials and in photopharmacology [25]. Another advantage of diazocines over azobenzenes is their switchability in the visible range (400 nm *cis* → *trans*, 530 nm *trans* → *cis*) preventing deterioration of the material or tissue damage by UV light [19]. Well separated absorption bands, high switching efficiency and high quantum yields are further advantages

Beilstein J. Org. Chem. 2019, 15, 727–732.

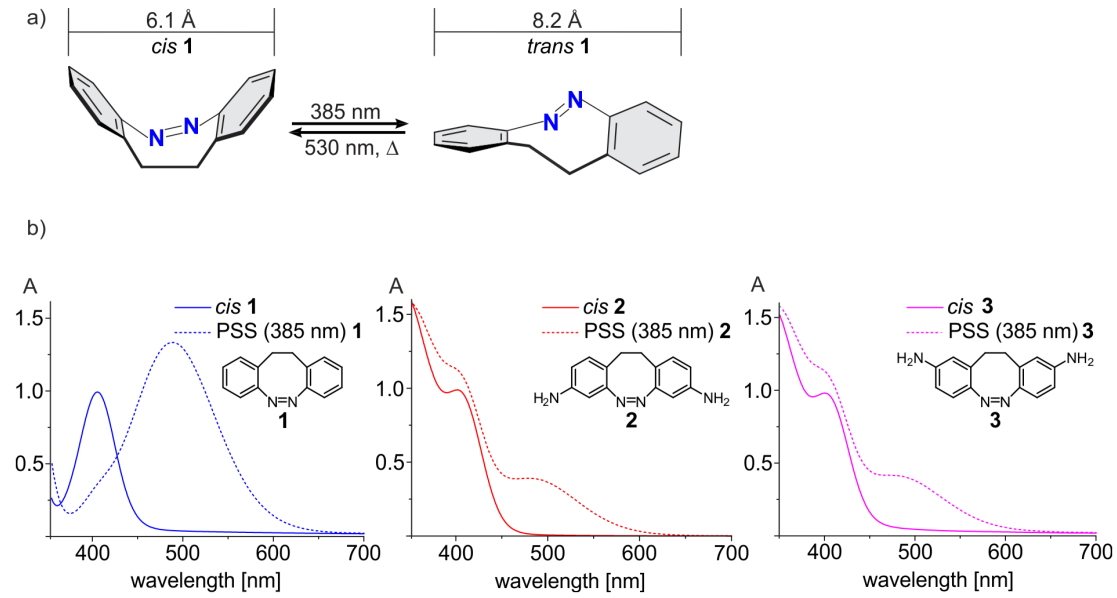

Figure 1: (a) Isomerization of parent diazocine **1**. Distances of carbon atoms *para* to the ethylene bridge were determined at the B3LYP/6-31g* level of DFT [23]. (b) UV–vis spectra of parent diazocine **1** (left), 3,3'-diaminodiazocine **2** (center) and 4,4'-diaminodiazocine **3** (right). Continuous lines: 100% *cis* and dashed lines: PSS (385 nm) at 298.15 K in acetonitrile.

regarding their application as switches in photoresponsive materials [19,24,26]. In contrast to spiropyrans which have been frequently used as photoswitches in materials, diazocines are stable over several thousand switching cycles under air [19,24,26,27]. Notwithstanding their excellent properties, to date only 3,3'- and 4,4'- functionalized diazocine **2** and **3** have been implemented in polymers [19] and proteins [28]. Unfortunately, similar to azobenzenes, aminosubstitution at the phenyl rings reduces switching efficiency [29]. In contrast to the parent system, separation of absorption bands of the *cis* and *trans* isomer in **2** and **3** is poor. Upon irradiation of the corresponding *cis*-configured compounds at 385 nm only 30% of the *trans* isomer of 3,3'-diazocine **2** and 25% of the 4,4'-diazocine **3** are formed (Figure 1b). Applications of diazocines **2** and **3** are further hampered by the low yields of their synthesis [19,20].

To decouple the electronic influence of the functional groups from the azo switching process and to improve yields of the azo cyclization step, we separated the functional groups from the aromatic system by one or two methylene groups and restricted substitution to the position *meta* with respect to the azo group (Figure 2) [19,20].

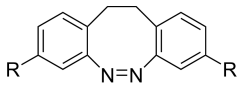

R = CH_2OH	**4a**	CH_2CH_2OH	**4b**
CH_2N_3	**5a**	$CH_2CH_2N_3$	**5b**
CH_2NH_2	**6a**	$CH_2CH_2NH_2$	**6b**
$CHCH_2$	**7**		

Figure 2: Synthesized target diazocines **4–7** for applications in responsive materials.

Results and Discussion

The synthesis of the targeted diazocines **4–7** is based on two key reactions, an oxidative C–C coupling of nitrotoluenes and the reductive ring closure of the dinitro compounds (Scheme 1). We recently improved the yield of the C–C coupling through

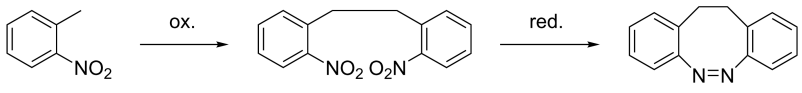

Scheme 1: Key reactions in diazocine synthesis.

Beilstein J. Org. Chem. **2019,** *15,* 727–732.

addition of bromine as an oxidizing agent [27]. The reaction times thus are reduced to several minutes as compared to several hours in previous procedures using oxygen and the yields are increased from 65% to 95% in the parent system [30].

In a recent work we observed that the reduction of 2,2′-dinitrodibenzyl is difficult to stop at the azo stage because further reduction to the hydrazine is faster than the preceding cyclization reaction [27]. The hydrazine is quite stable towards reduction to the diamine, and can easily be reoxidized to the azo compound using $CuCl_2/O_2$. The yields are higher and more reproducible using the above reduction/reoxidation scheme. Previously applied reducing agents include $Ba(OH)_2/Zn$ [27], glucose/NaOH [20], $Pb/NEt_3/HCOOH$ [22,23], or the Baeyer–Mills reaction via Zn/NH_4Cl [25]. We chose the $Ba(OH)_2/Zn$ method because it provided superior yields even at larger scales. The syntheses of the functionalized diazocines **4–7** started with (4-methyl-3-nitrophenyl)methanol (**8a**) and (4-methyl-3-nitrophenyl)ethanol (**8b**). In a first step the hydroxy groups in **8a** and **8b** were protected as *tert*-butyl ethers (Scheme 2) to prevent oxidation in the following oxidative C–C coupling [31]. The *tert*-butyl ether was chosen as the protecting group because it is stable towards the oxidizing conditions of the C–C coupling reactions and the reducing conditions of the azo cyclization. Moreover, the *tert*-butyl group can be conveniently removed under acidic conditions. As described in [27] potassium butoxide is used as a non-nucleophilic base to remove the α-toluene protons of **9a** and **9b**. By addition of bromine as an oxidizing agent dimers **10a** and **10b** are formed, most probably through radical intermediates. Then the dinitro compounds **10a** and **10b** were reduced with $Ba(OH)_2/Zn$ to the hydrazine intermediates and subsequently oxidized with $CuCl_2$ and air in a two-step reductive azo cyclization in a similar manner as described in [27]. After deprotection with $TiCl_4$ the hydroxy-functionalized diazocines **4a** and **4b** were obtained [32]. The hydroxy groups in **4a** and **4b** were successfully converted into azides using 2-azido-1,3-dimethylimidazolinium hexafluorophosphate (ADMP) and DBU [33]. The synthesis was completed with a Staudinger reaction to obtain the amino-functionalized diazocines **6a** and **6b** [34]. Additionally, the diazocine **4b** was converted into the divinyldiazocine **7**. Towards this end, the hydroxy groups were tosylated, followed by elimination with potassium butoxide [35,36].

The photochemical and photophysical properties of compounds **4–7** were investigated by NMR and UV–vis spectroscopy and the results are listed in Table 1. Photostationary states (PSS) as well as half-lives ($t_{1/2}$) were determined in acetonitrile at 300 K and 298.15 K, respectively. The (*cis* → *trans*) and (*trans* → *cis)* isomerization were achieved by irradiation into the appropriate

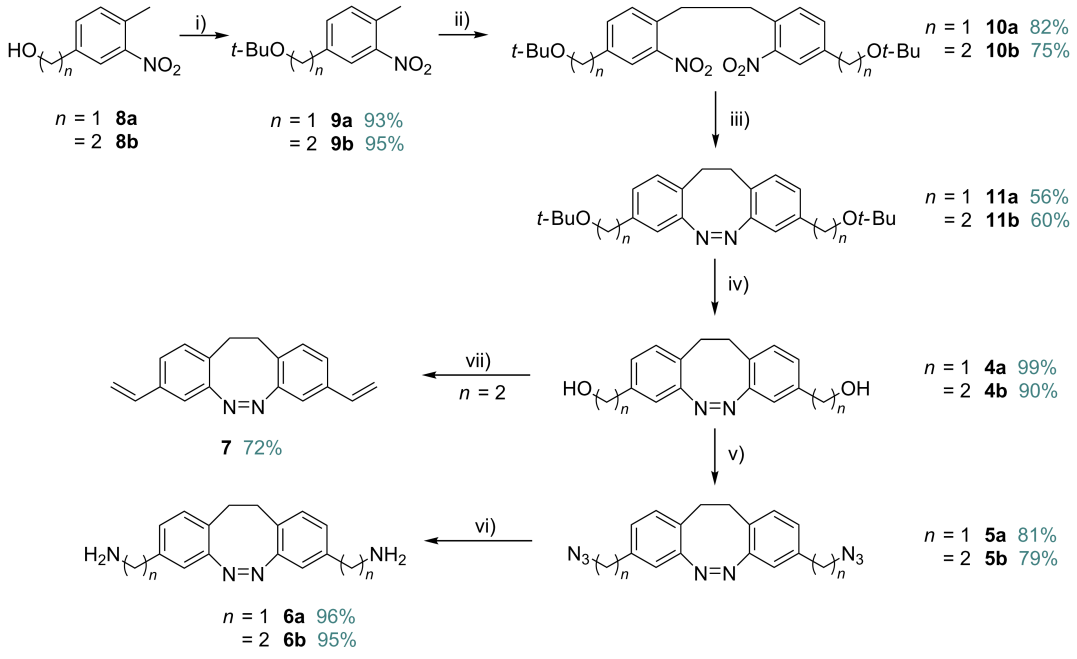

Scheme 2: Syntheses of the functionalized diazocines **4–7**. Reaction conditions: i) Isobutylene, sulfuric acid, DCM; ii) *t*-BuOK, Br_2, THF; iii) Zn, $Ba(OH)_2$ H_2O/EtOH, and $CuCl_2/O_2$, NaOH/MeOH; iv) $Ti(Cl)_4$, DCM; v) ADMP, DBU, THF; vi) PPh_3, H_2O, THF; viii) TsCl, DMAP, TEA, DCM, and *t*-BuOK, THF.

Beilstein J. Org. Chem. **2019,** *15,* 727–732.

Table 1: Photostationary states (300 K), absorption maxima and half-lives (298.15 K), determined by ^{1}H NMR and UV–vis spectroscopy in acetonitrile.

molecule	PSS (385 nm) [%] *trans*	PSS (530 nm) [%] *cis*	λ_{max} (*cis*) [nm]	λ_{max} (*trans*) [nm]	$t_{1/2}$ (UV) [h] at 298.15 K
1	87	>99	402	486	15.3
2	30	>99	401	487	24.8
3	25	>99	400	475	20
4a	83	>99	404	485	11.4
4b	81	>99	405	487	16.7
5a	85	>99	402	484	11.2
5b	82	>99	405	489	14.0
6a	81	>99	405	488	14.7
6b	78	>99	400	485	10.1
7	74	>99	403	484	13.1
11a	82	>99	403	487	10.2
11b	81	>99	405	488	15.9

n–π* bands at 385 and 530 nm. As a result of electronic decoupling the absorption bands are well separated and the photostationary states of diazocines **4**–**7** are considerably improved compared to 3,3'- (**2**) and 4,4'-diaminodiazocine **3** (Figure 3). The (*cis* → *trans*) isomerization of diazocines **4**–**7** was achieved after 2 min of irradiation at 385 nm in yields of 74–85%. All *trans*-diazocines were converted quantitatively to the *cis*-configuration either by thermal relaxation or by irradiation at 530 nm. In general, the (*trans* → *cis)* isomerization can be accomplished with wavelengths between 520 and 620 nm. The half-lives ($t_{1/2}$) for the thermal relaxation (*trans* → *cis*) at 298.15 K of diazocines **4**–**7** in acetonitrile are between 10.2–16.7 h and thus are in the same order of magnitude as the parent system **1** (15.3 h). In comparison, the 3,3'-diaminodiazocine **2** has a much longer half-life ($t_{1/2}$) of 24.5 h. The electronic decoupling of substituents in diazocines **4**–**7** has proven to retain the excellent photochemical properties in regard to PSS and half-life ($t_{1/2}$) of the parent system **1**.

Conclusion

Seven symmetrically substituted diazocines **4**–**7** were synthesized and characterized. Oxidative C–C coupling and reductive azo condensation proved to be reliable key steps in the synthesis of these substituted diazocines. The photophysical properties of compounds **4**–**7** were investigated by NMR and UV–vis experiments. The previously investigated 3,3'-diaminodiazocine **2** and 4,4'-diaminodiazocine **3** exhibited poor photostationary states (PSS (385 nm): 25–30% *trans*). The electronic decoupling of the azobenzene unit and the oxygen and nitrogen containing functional groups (OH, OR, N_3, NH_2) was achieved by insertion of one or two CH_2 groups. Thereby, the switching efficiencies were increased by about a factor of two (PSS

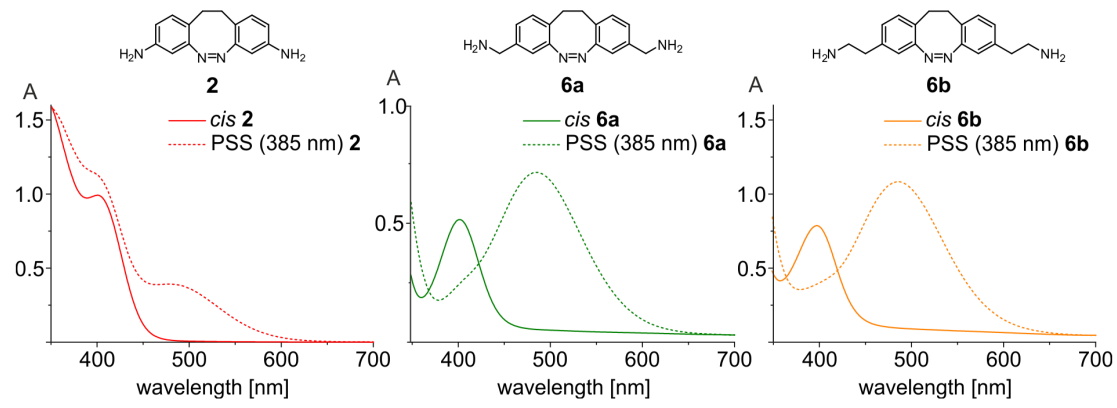

Figure 3: UV–vis spectra of 3,3'-diaminodiazocine **2** (left), 3,3'-di(aminomethyl)diazocine **6a** (center), and 3,3'-di(aminoethyl)diazocine **6b** (right). Continuous lines: 100% *cis* and dashed lines: PSS (385 nm) at 298.15 K in acetonitrile.

Beilstein J. Org. Chem. **2019,** *15,* 727–732.

(385 nm): 74–85% *trans*), and thus are close to the parent system **1** (87%). Moreover, the yields of the two synthetic key steps, the oxidative C–C coupling and the azo cyclization have been improved. Diazocines **4**–**7** are easily accessible and valuable building blocks for the synthesis of photo- and mechanoresponsive polymers such as polyurethanes, polyesters, polyamides, polyureas and polyolefines.

Supporting Information

Supporting Information File 1

Analytical equipment, experimental procedures, NMR and UV–vis spectra.
[https://www.beilstein-journals.org/bjoc/content/supplementary/1860-5397-15-68-S1.pdf]

Acknowledgements

The authors gratefully acknowledge financial support by the Deutsche Forschungsgesellschaft (DFG) within the Sonderforschungsbereich 677, “Function by Switching”.

ORCID® iDs

Rainer Herges - https://orcid.org/0000-0002-6396-6991

References

1. Ikeda, T.; Mamiya, J.-i.; Yu, Y. *Angew. Chem., Int. Ed.* **2007,** *46,* 506–528. doi:10.1002/anie.200602372
2. Davis, D. A.; Hamilton, A.; Yang, J.; Cremar, L. D.; Van Gough, D.; Potisek, S. L.; Ong, M. T.; Braun, P. V.; Martínez, T. J.; White, S. R.; Moore, J. S.; Sottos, N. R. *Nature* **2009,** *459,* 68–72. doi:10.1038/nature07970
3. Potisek, S. L.; Davis, D. A.; Sottos, N. R.; White, S. R.; Moore, J. S. *J. Am. Chem. Soc.* **2007,** *129,* 13808–13809. doi:10.1021/ja076189x
4. Kim, S.-J.; Reneker, D. H. *Polym. Bull.* **1993,** *31,* 367–374. doi:10.1007/bf00692965
5. Hosono, N.; Kajitani, T.; Fukushima, T.; Ito, K.; Sasaki, S.; Takata, M.; Aida, T. *Science* **2010,** *330,* 808–811. doi:10.1126/science.1195302
6. Kim, C. B.; Wistrom, J. C.; Ha, H.; Zhou, S. X.; Katsumata, R.; Jones, A. R.; Janes, D. W.; Miller, K. M.; Ellison, C. J. *Macromolecules* **2016,** *49,* 7069–7076. doi:10.1021/acs.macromol.6b01848
7. Yu, Y.; Nakano, M.; Ikeda, T. *Nature* **2003,** *425,* 145. doi:10.1038/425145a
8. Bandara, H. M. D.; Burdette, S. C. *Chem. Soc. Rev.* **2012,** *41,* 1809–1825. doi:10.1039/c1cs15179g
9. Luo, Q.; Cheng, H.; Tian, H. *Polym. Chem.* **2011,** *2,* 2435–2443. doi:10.1039/c1py00167a
10. Ryo, S.; Ishibashi, Y.; Murakami, M.; Miyasaka, H.; Kobatake, S.; Irie, M. *J. Phys. Org. Chem.* **2007,** *20,* 953–959. doi:10.1002/poc.1190
11. Corredor, C. C.; Huang, Z.-L.; Belfield, K. D.; Morales, A. R.; Bondar, M. V. *Chem. Mater.* **2007,** *19,* 5165–5173. doi:10.1021/cm071336b
12. Stellacci, F.; Bertarelli, C.; Toscano, F.; Gallazzi, M. C.; Zotti, G.; Zerbi, G. *Adv. Mater. (Weinheim, Ger.)* **1999,** *11,* 292–295. doi:10.1002/(sici)1521-4095(199903)11:4<292::aid-adma292>3.0.co;2-v
13. Pu, S.-Z.; Sun, Q.; Fan, C.-B.; Wang, R.-J.; Liu, G. *J. Mater. Chem. C* **2016,** *4,* 3075–3093. doi:10.1039/c6tc00110f
14. Gossweiler, G. R.; Hewage, G. B.; Soriano, G.; Wang, Q.; Welshofer, G. W.; Zhao, X.; Craig, S. L. *ACS Macro Lett.* **2014,** *3,* 216–219. doi:10.1021/mz500031q
15. Celestine, A.-D. N.; Beiermann, B. A.; May, P. A.; Moore, J. S.; Sottos, N. R.; White, S. R. *Polymer* **2014,** *55,* 4164–4171. doi:10.1016/j.polymer.2014.06.019
16. Lee, C. K.; Beiermann, B. A.; Silberstein, M. N.; Wang, J.; Moore, J. S.; Sottos, N. R.; Braun, P. V. *Macromolecules* **2013,** *46,* 3746–3752. doi:10.1021/ma4005428
17. Beiermann, B. A.; Davis, D. A.; Kramer, S. L. B.; Moore, J. S.; Sottos, N. R.; White, S. R. *J. Mater. Chem.* **2011,** *21,* 8443. doi:10.1039/c0jm03967e
18. Klajn, R. *Chem. Soc. Rev.* **2014,** *43,* 148–184. doi:10.1039/c3cs60181a
19. Li, S.; Han, G.; Zhang, W. *Macromolecules* **2018,** *51,* 4290–4297. doi:10.1021/acs.macromol.8b00687
20. Sell, H.; Näther, C.; Herges, R. *Beilstein J. Org. Chem.* **2013,** *9,* 1–7. doi:10.3762/bjoc.9.1
21. Tellkamp, T.; Shen, J.; Okamoto, Y.; Herges, R. *Eur. J. Org. Chem.* **2014,** 5456–5461. doi:10.1002/ejoc.201402541
22. Joshi, D. K.; Mitchell, M. J.; Bruce, D.; Lough, A. J.; Yan, H. *Tetrahedron* **2012,** *68,* 8670–8676. doi:10.1016/j.tet.2012.06.007
23. Hammerich, M.; Schütt, C.; Stähler, C.; Lentes, P.; Röhricht, F.; Höppner, R.; Herges, R. *J. Am. Chem. Soc.* **2016,** *138,* 13111–13114. doi:10.1021/jacs.6b05846
24. Siewertsen, R.; Neumann, H.; Buchheim-Stehn, B.; Herges, R.; Näther, C.; Renth, F.; Temps, F. *J. Am. Chem. Soc.* **2009,** *131,* 15594–15595. doi:10.1021/ja906547d
25. Schehr, M.; Hugenbusch, D.; Moje, T.; Näther, C.; Herges, R. *Beilstein J. Org. Chem.* **2018,** *14,* 2799–2804. doi:10.3762/bjoc.14.257
26. Siewertsen, R.; Schönborn, J. B.; Hartke, B.; Renth, F.; Temps, F. *Phys. Chem. Chem. Phys.* **2011,** *13,* 1054–1063. doi:10.1039/c0cp01148g
27. Moormann, W.; Langbehn, D.; Herges, R. *Synthesis* **2017,** *49,* 3471–3475. doi:10.1055/s-0036-1590685
28. Samanta, S.; Qin, C.; Lough, A. J.; Woolley, G. A. *Angew. Chem.* **2012,** *124,* 6558–6561. doi:10.1002/ange.201202383
29. Rau, H. Azo Compounds. *Photochromism: Molecules and Systems,* 1st ed.; Elsevier: Amsterdam, The Netherlands, 2003; pp 165–192. doi:10.1016/b978-044451322-9/50008-7
30. Chaudhuri, N. K.; Ball, T. J. *J. Labelled Compd. Radiopharm.* **1981,** *18,* 1189–1196. doi:10.1002/jlcr.2580180814
31. Beyerman, H. C.; Bontekoe, J. S. *Proc. Chem. Soc., London* **1961,** 249.
32. Schlessinger, R. H.; Nugent, R. A. *J. Am. Chem. Soc.* **1982,** *104,* 1116–1118. doi:10.1021/ja00368a044
33. Kitamura, M.; Koga, T.; Yano, M.; Okauchi, T. *Synlett* **2012,** *23,* 1335–1338. doi:10.1055/s-0031-1290958
34. Meguro, T.; Yoshida, S.; Hosoya, T. *Chem. Lett.* **2017,** *46,* 473–476. doi:10.1246/cl.161159
35. Stokes, B. J.; Opra, S. M.; Sigman, M. S. *J. Am. Chem. Soc.* **2012,** *134,* 11408–11411. doi:10.1021/ja305403s

Beilstein J. Org. Chem. **2019,** *15,* 727–732.

36. Thiraporn, A.; Rukachaisirikul, V.; Iawsipo, P.; Somwang, T.; Tadpetch, K. *Eur. J. Org. Chem.* **2017,** 7133–7147. doi:10.1002/ejoc.201701272

3.3 Diazocine-based Photocontrol of the Trp-cage Fold

It is required to understand and unravel the complex network of interactions in biological systems in order to find new targets and treatments of complex diseases. Photocontrol of the biological activity of peptides and proteins is a novel approach to accomplish this.[7, 9, 18] In numerous studies, the control of peptide and protein activity has been achieved through the isomerization of a conjugated azobenzene.[18] However, when hydrophobic interactions are the driving force for the formation of tertiary structures, the hydrophobic character of the planar *trans*-azobenzene can be disruptive. The tendency to form aggregates through π-π interactions with aromatic amino acids could be reduced through the utilization of diazocine cross-linkers. Diazocines are stable in the bent and sterically demanding *cis*-configuration and can be isomerized to the twisted *trans*-configuration. Both isomers are less prone towards aggregation and thus an alternative to azobenzene-based cross-linkers.

In a previous study, Woolley and co-workers were able to incorporate a diazocine cross-linker between two side-chains of an α-helix. Upon irradiation with visible light, the originally unfolded FK-11 model peptide formed the characteristic α-helix in a reversible manner.[54] This observation is raising the question, if this approach can be extended to reversible fold and unfold the tertiary structure through a single, solvent-exposed α-helix of particular importance to the fold of a small, but stable protein. Although Woolley's concept proved the applicability of diazocines as cross-linkers in peptide and protein chemistry, the photochemical properties of the chosen 4,4'-diaminodiazocine were not beneficial. To comprise the excellent photochemical properties of diazocines a new diazocine cross-linking strategy was necessary. As reported in earlier studies the implementation of a methylene or ethylene group between the aromatic rings of the diazocine and the functional group has improved the photostationary states significantly in organic solvents.

3.3.1 Summary of Visible-Light-Driven Photocontrol of the Trp-cage Protein Fold by a Diazocine Cross-Linker

In this work a functionalized diazocine cross-linker was used to reversibly fold and unfold the tertiary structure of the globularly folded Trp-cage, the smallest protein with a fold and thus an ideal system for the elucidation of protein folding (**Figure 3.3.1 a**). Under assistance of computational calculations, an appropriate conjugation strategy was established, utilizing a novel dicarboxylic diazocine linker. This linker, functionalized as NHS active ester, enabled the incorporation through amino group-bearing residues (**Figure 3.3.1 b**). The design aimed to attach the diazocine cross-linker at the side-chains of the α-helix, one of the secondary structures of the Trp-cage, and thereby stabilizing the tertiary structure. Upon irradiation with visible light, the bent, shorter *cis*-diazocine should be isomerized to the longer *trans*-diazocine, leading to a destabilization of the α-helix (**Figure 3.3.1 a**). Assuming that the α-helix serves as a folding nucleus, not only the α-helix is unfolded but the complete tertiary structure of the Trp-cage.

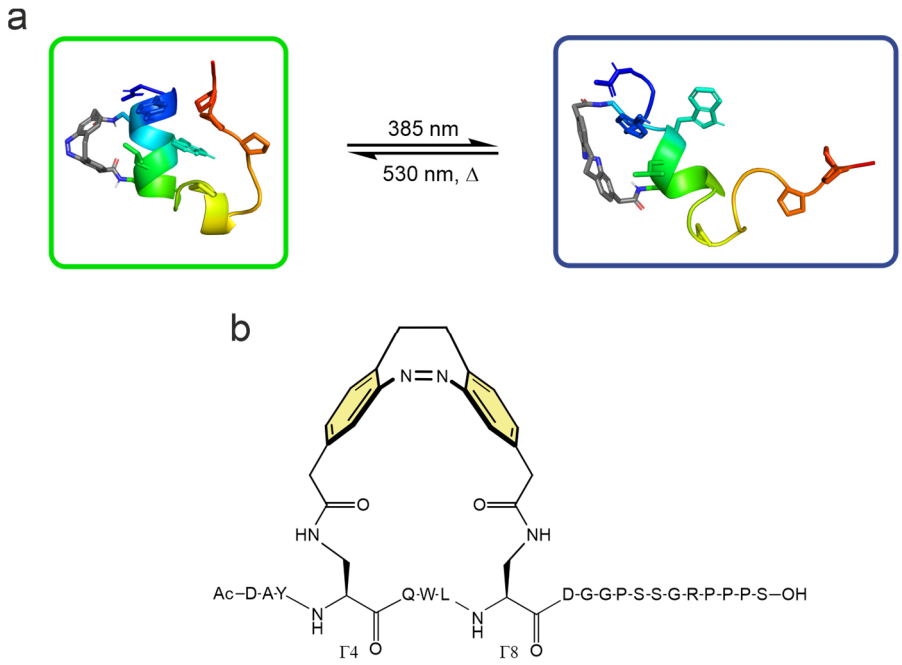

Figure 3.3.1: a) The switchable Trp-cage called switch cage (SC) is stable in the dark-adapted *cis*-state of the diazocine or upon irradiation with light of 530 nm. Irradiation with light of 385 nm leads to *cis* → *trans* isomerization and thus prevents the formation of the helix and the associated tertiary structure. b) The diazocine cross-linker was attached at side-chain 4 and 8 of the Trp-cage.

The chosen peptide sequence (Ac-DAYΓQWLΓDGGPSSGRPPPS) was synthesized using Fmoc-based solid phase peptide synthesis. L-2,3-diaminopropionic acid (Γ) was used as a lysine homologue with decreased side-chain length thereby limiting flexibility upon conjugation in 4 and 8 position. The synthesis of the diazocine cross-linker was based on the previously reported oxidative C-C coupling and reductive azo cyclization.[67] Following conjugation, the switch cage (SC) was investigated in NMR and CD measurements to confirm the concept (**Figure 3.3.2 a**). The peptide was significantly stabilized upon cross-linking. Irradiation with visible light of 385 nm achieved a PSS of around 46% *trans*-SC and complete unfolding of the tertiary structure in the *trans*-SC. Irradiation with 530 nm and thermal relaxation completely recovered the original Trp-cage fold confirming the reversibility of this process.

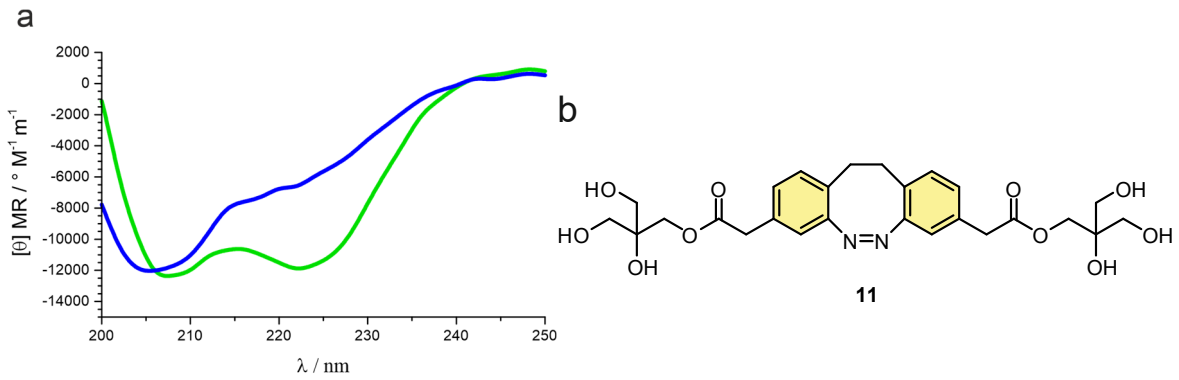

Figure 3.3.2: a) The CD spectrum of *cis*-SC (green) shows two minima at 206 nm and 222 nm indicating an α-helix. The minimum at 222 nm is significantly reduced after irradiation with 385 nm (blue) confirming the destabilization of the α-helix. b) The PSS of diazocine ester **11** was compared with the SC. in organic solvents.

In the context of the folded protein in aqueous solution, the PSS at 385 nm (46 % *trans*-isomer) of the chosen diazocine cross-linker (**Figure 3.3.1 b**) is hampered in comparison with the ester **11** in organic solvents (MeOH: 78% *trans*-isomer, MeCN: 82% *trans*-isomer) (**Figure 3.3.2 b**). Most recent research suggests that this effect is more heavily influenced by the highly polar solvent (water) than by the folded protein environment.[23, 59, 68] Nevertheless, this concept has proven that it is possible to reversibly fold and unfold the tertiary structure through a single, solvent-exposed α-helix of particular importance to the tertiary structure, of a globularly folded protein using diazocines as photoswitchable cross-linkers. Accordingly, it should be possible to apply this concept to larger proteins with biological activity.

3.3.2 Visible-Light-Driven Photocontrol of the Trp-cage Protein Fold by a Diazocine Cross-Linker

Nils Preußke, Widukind Moormann, Katrin Bamberg, Matthias Lipfert, Rainer Herges and Frank D. Sönnichsen

Accepted at Org. Biomol. Chem.

Scientific contribution to this paper

Nils Preußke, Matthias Lipfert and I developed the concept. Nils Preußke planned and performed the MD simulations, the synthesis and characterization of the Trp-cage and switch-cage. I planned and performed the synthesis and characterization of the cross-linker. Nils Preußke and I prepared the original draft. Prof. Dr. F. D. Sönnichsen and Prof. Dr. R. Herges revised the manuscript.

Organic & Biomolecular Chemistry

ROYAL SOCIETY OF CHEMISTRY

PAPER

Visible-light-driven photocontrol of the Trp-cage protein fold by a diazocine cross-linker†

Cite this: DOI: 10.1039/c9ob02442e

Nils Preußke, Widukind Moormann, Katrin Bamberg, Matthias Lipfert, Rainer Herges* and Frank D. Sönnichsen *

Received 12th November 2019,
Accepted 19th December 2019
DOI: 10.1039/c9ob02442e
rsc.li/obc

Diazocines are characterized by extraordinary photochemical properties rendering them of particular interest for switching the conformation of biomolecules with visible light. Current developments afford synthetic access to unprecedented diazocine derivatives promising particular opportunities in photocontrol of proteins and biological systems. In this work, the well-established approach of photocontrolling the secondary structure of α-helices was exploited using a diazocine to reversibly fold and unfold the tertiary structure of a small protein. The protein of choice was the globulary folded Trp-cage, a widely used model system for the elucidation of protein folding pathways. A specifically designed, short and rigid dicarboxy-functionalized diazocine-based crosslinker was attached to two solvent-exposed side chains at the α-helix of the miniprotein through the use of a primary amine-selective active ester. This cross-linking strategy is orthogonal to the common cysteine-based chemistry. The cross-linked Trp-cage was successfully photoisomerized and exhibited a strong correlation between protein fold and diazocine isomeric state. As determined by NMR-spectroscopy, the *cis*-isomer stabilized the fold, while the *trans*-isomer led to complete protein unfolding. The successful switching of the protein fold in principle demonstrates the ability to control protein function, as the activity depends of their structural integrity.

Introduction

Biological systems comprise a complex network of biochemical interactions, *e.g.* signal transduction cascades, of very diverse compounds including small molecules (second messengers, metabolites), peptides (hormones), and proteins (enzymes, receptors). The ability to control the biological activities of peptides or proteins with high spatio-temporal resolution is a powerful tool to elucidate the mechanisms, kinetics and sequence of these biochemical pathways.[1–4] Visible light is a perfect trigger as it transfers a desired amount of energy with the required spatial and temporal resolution, does not contaminate the sample, is non-toxic and has a high penetration depth (except through blood-supported tissue). Consequently, irradiation-induced configurational changes of incorporated light-sensitive chromophores have been used to control the three-dimensional structure of peptides and proteins.[1–4]

By far the most frequently used photoswitches are azobenzenes.[1–4] Upon irradiation, they undergo reversible isomerization between two states of significantly different geometries (Fig. 1, top). The thermodynamically stable extended *trans*-configuration can be converted to the shorter, bent *cis*-isomer with high yields upon irradiation with ultraviolet (UV) light. Due to its planarity, *trans*-azobenzene exhibits a tendency to aggregate when incorporated into peptides.[5,6] Additionally, it may influence condensation and melting of DNA when equipped with positive charges.[7–9] Therefore, most peptide or protein switching applications[10–19] make use of a water soluble sulfonic acid-substituted azobenzene.[20] However, even this cross-linker may lead to aggregation when

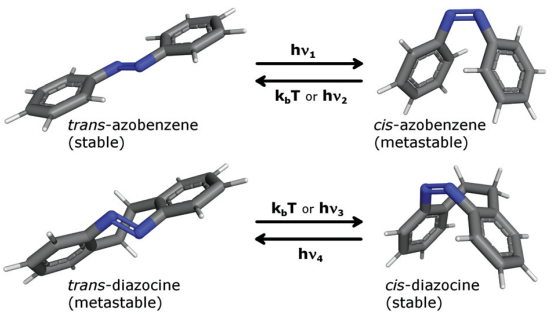

Fig. 1 *cis*–*trans*-Isomerization of azobenzene (top) and diazocine (bottom).

Otto-Diels-Institute for Organic Chemistry, Christian-Albrechts-University of Kiel, Otto-Hahn-Platz 4, 24118 Kiel, Germany. E-mail: rherges@oc.uni-kiel.de, fsoennichsen@oc.uni-kiel.de

†Electronic supplementary information (ESI) available: Additional experimental procedures and spectroscopic data. See DOI: 10.1039/c9ob02442e

incorporated into a peptide[10] or can unintendedly interfere with the protein fold due to interactions of the sulfonic acid moieties with guanidinium groups of arginine.[15]

Compared to azobenzenes, diazocines show a reversed switchability (Fig. 1, bottom): the ethylene bridge stabilizes the bent and bulky *cis*-configuration rendering it the thermodynamically stable isomer.[21–24] *trans*-Diazocine is not planar, but adopts a twist or chair conformation. It is therefore not prone to π–π-stacking. Diazocines also display improved photochemical properties in organic solvents when compared to azobenzenes.[21,22] These include a better separation of absorption bands and exceptionally high quantum yields resulting in higher switching efficiencies, *i.e.* better isomer ratios in the photostationary states (PSS).[21,22,24] Importantly, switching in both directions can be achieved with visible light, which is essential for applications in biological systems. Recent developments in the synthesis of diazocines now render them almost as easily accessible as azobenzenes.[25–27]

If carefully designed and attached to a protein, the relatively subtle structural change of the molecular switch affects the fold of the much larger biomacromolecule. Photocontrolling the biological function of α-helical peptides by reversibly allowing or preventing formation of their secondary structure is already well-established and has been applied to DNA recognition,[10–12,14] protein–protein interactions[5,6,12–14,16–19] or RNA binding.[15] These examples make use of cross-linking the respective peptide using an azobenzene moiety with both attachment points at the same side of the α-helix. In contrast to azobenzene, a diazocine was applied only once to achieve photocontrol over a simple α-helical peptide in a study by Woolley *et al.*[28]

The *cis*-configuration of an azobenzene or diazocine stabilizes the helical backbone conformation when the cross-linker is connected to residues *i*, *i* + 4[13,19] or *i*, *i* + 7[5,6,10,12–19] while switching to its *trans*-isomer prevents formation of the secondary structure. In contrast, connected to residues *i*, *i* + 11 the *trans*-cross-linker would stabilize the α-helical fold, which in turn adapts a disordered state upon isomerization to the contracted *cis*-state of the cross-linker.[11,13,28]

Either of these approaches is useful to switch single, bioactive helices. A question of greater interest is whether they could be used to control the tertiary structure and thus function of cooperatively folded proteins. α-Helices are central and essential elements of the fold, particularly in small globular proteins or domains. Examples are the apoptosis-regulating Bcl-family of proteins,[29,30] the engrailed homeodomain transcription factor,[31,32] the KIX domain of CBP,[33] the ribonuclease T_1,[34] the villin headpiece subdomain[35] or the Trp-cage.[36,37] In these, a solvent-exposed α-helix is of particular importance for establishing a network of tertiary contacts. Reversibly preventing the formation of secondary structure in these domains would be expected to result in their unfolding. This will perturb the integrity of the entire protein or protein complex which can be used as a tool to control their function.

The Trp-cage miniprotein[36,37] displays typical protein properties[38] despite its length of only 20 residues. It comprises three elements of secondary structure, *i.e.* an N-terminal α-helix, a short 3_{10}-helix and a polyproline II (PPII) helix. The eponymous encapsulation of a central tryptophan residue is driven by hydrophobic interactions and additionally stabilized by hydrogen bonds and a salt bridge. The highly stable and well characterized mutant 'TC10b' exhibits characteristics of folding cooperativity including reversible, sigmoidal thermal unfolding curves with a T_m above 55 °C.[37] Because of its protein-typical features yet small size the Trp-cage is a well-established model system for the experimental[36,37,39–44] and theoretical[37,40,45–48] elucidation of protein folding pathways with the aim to deduce general mechanisms applicable to larger proteins.

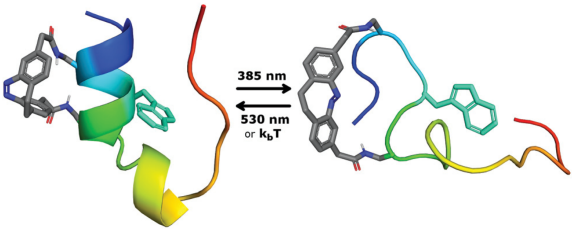

Fig. 2 The switchable Trp-cage (switch cage) was designed to exhibit a stable fold in the dark or under irradiation with green light (530 nm) when the diazocine cross-linker is present in its *cis*-configuration. Upon irradiation with violet light (385 nm) the diazocine is converted to the *trans*-isomer which prevents formation of the helix and in turn disrupts the tertiary structure.

In this work, the Trp-cage was chosen to evaluate the hypothesis that folding of a surface-exposed α-helix reversibly influences the complete tertiary structure of a protein. Here, we describe the design, synthesis and characterization of a Trp-cage miniprotein conjugated with a diazocine-based cross-linker (Fig. 2). The cross-linker was conjugated with the protein through the use of an active ester which constitutes an adequate alternative to the common cysteine-based chemistry. We set out to reversibly fold and unfold the Trp-cage through visible-light-driven photocontrol of its α-helix. This approach explores the application of diazocines in aqueous environments and their use in achieving photocontrol of proteins.

Results and discussion

The Trp-cage

Due to its small size, most residues in the Trp-cage significantly contribute to the fold stability which limits the options for attaching the cross-linker. Moreover, the short α-helix of the Trp-cage only allows cross-linking to residues *i*, *i* + 4 or *i*, *i* + 7. Residues 4 and 8 (*i*, *i* + 4) of TC10b seemed most suitable for conjugation because they are solvent exposed and contribute relatively little to the fold stability.[37] Incidentally, Markiewicz and co-workers came to the same conclusion when investigating the folding dynamics of the Trp-cage using a rigid, non-switchable cross-linker.[40]

In our hands,[49] the use of primary-amine-selective active esters in peptide conjugation reactions has proven superior to

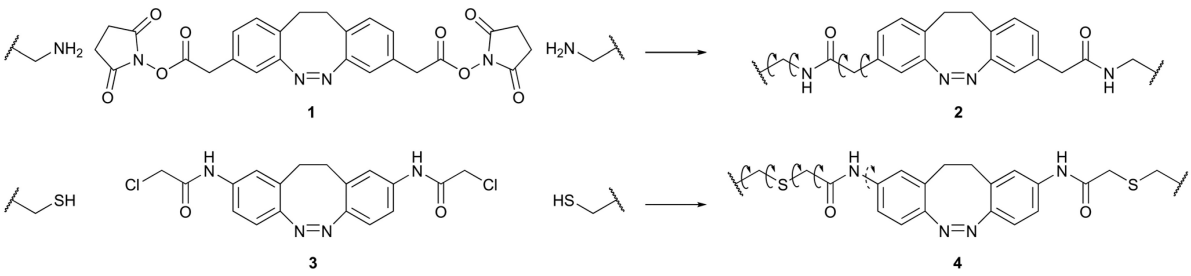

Scheme 1 Comparison of the primary amine-reactive cross-linker (**1**) presented in this work with the thiol-reactive cross-linker (**3**) by Woolley *et al.* Curved arrows indicate rotational degrees of freedom of single bonds of the cross-linker incorporated into a peptide or protein (**2** and **4**). The dashed arrow indicates reduced rotational freedom due to partial double bond character.

the usually employed cysteine-based cross-linking chemistry.[1,3,28,40] In order to enable selective cross-linking, residues Ala4 and Lys8 of TC10b were mutated to L-2,3-diaminopropionic acid (Dpr, Γ)‡ and the N-terminus was acetylated resulting in a Trp-cage named TC(4,8). Dpr was chosen over lysine because it has a drastically reduced side chain length and flexibility, which is necessary to efficiently couple the geometric properties of the diazocine with the fold state of the Trp-cage.

TC(4,8) was synthesized *via* Fmoc-based solid phase peptide synthesis. It was confirmed to exhibit the Trp-cage fold as evidenced by CD and two-dimensional (2D) ^{1}H-NMR spectroscopy. However, with a T_m of (31.6 ± 2.7) °C the fold stability of TC(4,8) was reduced compared to TC10b (~55 °C). This destabilization can be ascribed to the repulsion between the positively charged amines of Dpr4 and Dpr8. It leads to the presence of unfolded by-forms of the Trp-cage (Fig. S5†).

The cross-linking strategy

The diazocine-based cross-linker **1** (Scheme 1) was designed to match the distance between the amino side chains of Dpr4 and Dpr8 (*i*, *i* + 4) of the folded Trp-cage. The chosen design is based on an "unfolding-upon-extension/folding-upon-contraction" switching mechanism where the short, contracted *cis*-diazocine supports the stable fold of the protein. Upon switching to the extended *trans*-state of cross-linker formation of the Trp-cage fold is prevented (Fig. 2). This concept is in contrast to the diazocine-based photoswitchable α-helix by Woolley and co-workers, which relies on an *i*, *i* + 11 approach (folding-upon-extension/unfolding-upon-contraction).[28]

When incorporated into the protein, advantages of cross-linkage **2** over the cysteine-dependent diazocine cross-linkage **4** by Woolley and co-workers[28] include reduced length and flexibility (decreased number of rotable bonds) in the *cis*- as well as in the *trans*-configuration (Scheme 1). Furthermore, methylene groups in **2** serve as spacers between the diazocine moiety and the amide groups. This should preserve the excellent photochemical properties of the parent diazocine.[25]

‡IUPAC did not define any one-letter code for the artificial amino acid L-2,3-diaminopropionic acid. Therefore, in this work we assigned it the greek letter Γ.

In order to validate the proposed cross-linking strategy, molecular dynamics (MD) simulations of the uncross-linked TC(4,8) and of the hypothetical amidated diazocine **5** (*cis*-**5** and *trans*-**5**) were performed (Fig. 3). The distance between the cross-linker attachment points at TC(4,8), *i.e.* γN of Dpr4 and γN of Dpr8 was measured during the simulation. Similarly, the *cis*- and *trans*-isomer of the amidated diazocine **5** were constructed *in silico* to assess the accessible N–N′-distance of the cross-linker during the simulations.

The side chain amines (N^γ) of TC(4,8) are always less than 9.8 Å apart. With an accessible distance range of 9.8 Å to 15.2 Å *trans*-**5** does not match this distance. On the other hand, *cis*-**5** displays a large variance in its N–N′-distance covering a range between 3.3 Å and 13.1 Å that largely overlaps with the attachment point distances in TC(4,8). Finally, a model of the peptide-cross-linker-conjugate (*cis*-SC_a, Fig. 3) was constructed and its MD simulation resulted in a narrow distribution of N^γ_{Dpr4}–N^γ_{Dpr8}-distances between 5.6 Å and 7.0 Å.

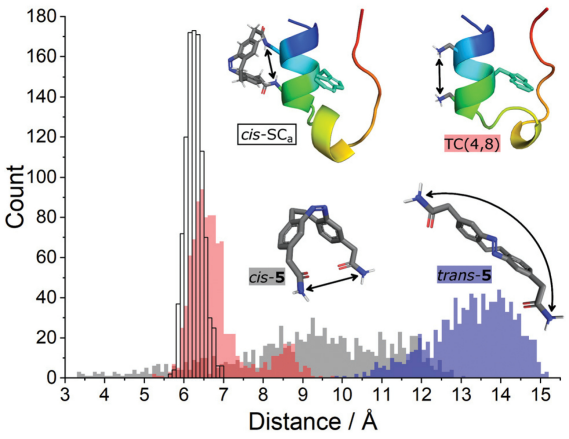

Fig. 3 The histograms of the switchable Trp-cage '*cis*-SC_a' (open), the uncross-linked Trp-cage 'TC(4,8)' (red), as well as the diazocines *cis*-**5** (gray) and *trans*-**5** (blue) result from an MD simulation over a period of 100 ns for each displayed molecule. Each simulation resulted in 1000 structures from which the indicated N–N′-distances were measured and plotted with a bin-size of 0.1 Å.

Thus, MD simulations indicated that the *trans*-cross-linker would prevent a stable fold when conjugated with the Trp-cage while the *cis*-diazocine supports a stable fold. Importantly, both observations confirm the concept.

The linear five step synthesis of the cross-linker **1** (Scheme 2) was based on a previously published oxidative C–C coupling and reductive azo cyclization.[25,26] Initially, the carboxylic acid functional group of 3-nitro-4-methyl-phenylacetic acid (**6**) was protected with an 4-methyl-2,6,7-trioxa-bicyclo [2.2.2]octane-1-yl (OBO) protecting group. This protection according to Corey and Raju[50] starts with an esterification with 3-methyl-3-oxetanemethanole (**7**) followed by a $BF_3{\cdot}Et_2O$-catalysed rearrangement that yields the desired orthoester **9**. Potassium butoxide is used as a non-nucleophilic base to selectively deprotonate the toluene α protons of **9**. By addition of bromine as an oxidizing agent, the anions are converted into radicals and C–C-bond formation leads to the desired dinitro dimer **10**. In the ensuing reductive azo cyclization, **10** is reduced with $Ba(OH)_2$/Zn to a hydrazine intermediate and subsequently oxidized with $CuCl_2$ and air. During work-up, the orthoester is hydrolysed to the open ester **11**, which was cleaved with Cs_2CO_3. Without purification, the resulting free carboxylic acid was converted with 1-ethyl-3-(3-dimethylaminopropyl)carbodiimide (EDC) and *N*-hydroxysuccinimide (NHS) into the active ester **1**.

The PSS of diazocine **11** was determined at 385 nm in MeOH or MeCN at 298 K (Fig. S23†). With 78% and 82% *trans*-isomer, respectively, **11** largely retains the outstanding properties of the parent diazocine (87% *trans*-isomer[25] at 385 nm in MeCN). In addition to its use in bio- and organic chemistry the dicarboxy-diazocine can therefore be applied as a monomer of polyamides or polyesters in photo- and mechanoresponsive materials.

The folded *cis*-switch cage

Conjugation of TC(4,8) with cross-linker **1** was carried out in high dilution in dimethylsulfoxide (DMSO) by means of a double syringe pump and resulted in the photo-switchable Trp-cage that we designate 'switch cage' (SC; Fig. 2).

Dark-adapted *cis*-SC shows all characteristics of a stable Trp-cage fold as evidenced by NMR chemical shift deviations (CSDs; Table S4†), number and intensity of nuclear Overhauser enhancement (NOE) cross-peaks and CD spectroscopy (Fig. 4). As expected, conjugation with the *cis*-diazocine markedly increases the stability of the fold reaching a T_m of (48.5 ± 1.4) °C compared to TC(4,8) ((31.6 ± 2.7) °C; Fig. 4a).

The Trp6 indole NH proton ($H^{\varepsilon 1}$) is a particularly valuable indicator for the existence of the hydrophobic cluster, as its resonance frequency is not overlapping with other signals. Most importantly, it lies in the centre of the fold and its chemical shift deviation from the random coil chemical shift (~10.2 ppm (ref. 51 and 52)) correlates with the stability of the Trp-cage. Interestingly, the indole region of the ^{1}H-NMR spectrum indicates two folded species of *cis*-SC (*cis*-SC_a: 9.728 ppm,

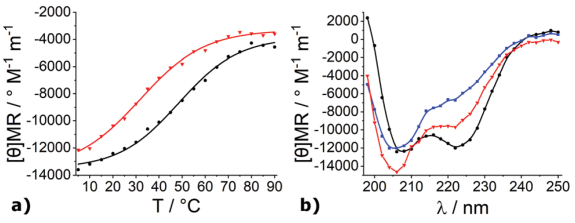

Fig. 4 (a) The mean residue molar ellipticity [θ]MR at 222 nm of TC(4,8) (red triangles) and *cis*-SC (black circles) is plotted over the temperature. A sigmoidal Boltzman function was fitted to each plot to obtain the midpoint of thermal unfolding (melting temperature, T_m). Details regarding the fitted function can be obtained from the ESI.† (b) The CD spectrum of *cis*-SC (black circles) displays two minima at 206 nm and 222 nm indicative of an α-helix. TC(4,8) (red triangles) appears to have a lower helical propensity as the minimum at 222 nm is less pronounced. Compared to the spectrum of *cis*-SC, the spectrum of the switch cage after having reached the PSS at 385 nm (blue squares) indicates significantly reduced helical propensity.

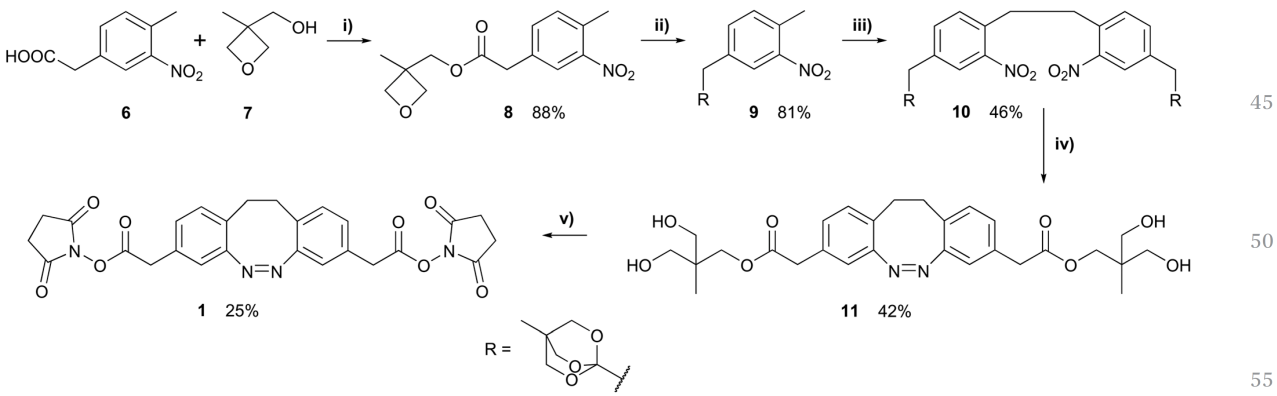

Scheme 2 Reaction conditions: (i) *N*,*N*′-Dicyclohexylcarbodiimide (DCC), 4-dimethylaminopyridine (DMAP), dichloromethane (DCM); (ii) $BF_3{\cdot}Et_2O$, triethylamine (TEA), DCM; (iii) *t*BuOK, Br_2, tetrahydrofuran (THF); (iv) 1. Zn, $Ba(OH)_2$ H_2O/EtOH; 2. $CuCl_2/O_2$, NaOH/MeOH; (v) 1. Cs_2CO_3, MeOH, H_2O; 2. 1-ethyl-3-(3-dimethylaminopropyl)carbodiimide (EDC), *N*-hydroxysuccinimide (NHS), *N*,*N*′-dimethylformamide (DMF).

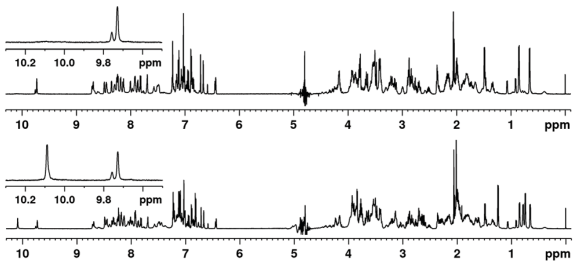

Fig. 5 The 1D ^{1}H-NMR spectra of *cis*-SC in its dark adapted state (top) and after having reached the PSS at 385 nm (bottom) are shown. In the expansion of the spectrum at the top the two folded species *cis*-SC_a and *cis*-SC_b are indicated by the two singlets of the Trp6 $H^{\varepsilon 1}$ at 9.728 ppm and 9.757 ppm. The expansion of the important indole region between 10.3 pmm and 9.5 ppm clearly shows the rise of an unfolded species indicated by the intense singlet at 10.089 nm (bottom).

cis-SC_b: 9.757 ppm; Fig. 5, top). In fact, there is a second set of resonances for the spin systems of many, but not all residues and the diazocine moiety. NMR chemical shifts and NOE cross-peaks confirm that the major (*cis*-SC_a) and the minor (*cis*-SC_b) form both comprise the correctly folded protein and differ only in the orientation of the cross-linker (Fig. 6). The two diastereomers are the result of conjugating the prochiral diazocine moiety with the chiral protein. The *cis*-cross-linker is incorporated so that either its ethylene bridge (*cis*-SC_a, Fig. 6, left) or its azo-group (*cis*-SC_b, Fig. 6, right) is oriented towards residue Leu7. NOE spectroscopy (NOESY) indicates that the ethylene bridge side of the diazocine is in close vicinity to $H^{\beta 2/\beta 3}$ and $H^{\delta 1/\delta 2}$ of Leu7 in *cis*-SC_a. Similarly, the orientation of the cross-linker in *cis*-SC_b was also derived from the NOESY data. Notably, *cis*-SC_a is the main form with an approximately 3-fold higher population than its diastereomer *cis*-SC_b.

Switching from *cis*-SC to *trans*-SC

Irradiation with light at the wavelength of 385 nm produces a photo stationary state (PSS) with approximately 46% *trans*-SC and 54% *cis*-SC (Table S6†). At first glance, this ratio appears to be low for a diazocine, but few conversion ratios of diazocines in water have been published. For instance, Woolley and colleagues[28] provided information on the PSS of their diazocine only in DMSO. In fact, the PSS of the switch cage compares well with the few published PSSs of diazocine derivatives in aqueous solution that range between 16% and 60% of *trans*-isomer.[53–56] Although the conditions differ in pH, buffer and DMSO content, it appears that the PSSs of ethylene bridged diazocines§ in aqueous environment are generally lower than the PSS of the parent diazocine[21,22] in organic solvents (>90% *trans*-species in *n*-hexane). In addition to the solvent effect, in *cis*-SC the folding free energy of the Trp-cage has to be overcome in order to unfold the miniprotein upon *cis* → *trans*-isomerization which also may lower the PSS.

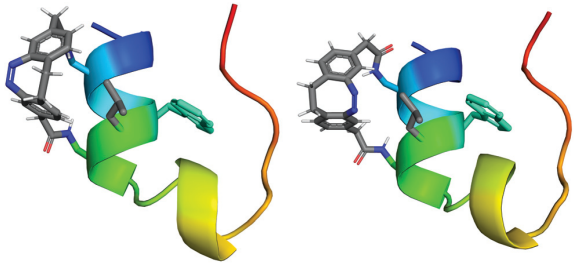

Fig. 6 The two different possible orientations of the cross-linker produce the two diasteromers *cis*-SC_a (left) and *cis*-SC_b (right). Structural models of the Trp-cage are shown in cartoon mode with the Trp6 side chain in the center of the molecule. The side chain of Leu7 is shown in grey in stick representation omitting hydrogens for clarity.

After irradiation with light at 385 nm, new resonances are observed in the NMR spectra (Fig. 5) belonging to the *trans*-species of the switch cage (*trans*-SC). It was not possible to assign many atoms of *trans*-SC, as their resonances overlap with those of *cis*-SC_a and *cis*-SC_b. Moreover, the unfolded nature of *trans*-SC prohibits the assignment due to overlap of intramolecular proton signals and resulting equivocal inter-residual NOEs. Despite these difficulties it was possible to determine the folding state of *trans*-SC.

A first evidence, that *trans*-SC is unfolded and assumes a random coil conformation is provided by the chemical shift of its Trp6 indole NH proton ($H^{\varepsilon 1}$) at 10.089 ppm (Fig. 5, bottom). This is very close to the random coil shift (~10.2 ppm (ref. 51 and 52)) indicating the absence of the hydrophobic cluster of the folded state. Moreover, at 298 K the Trp6 $H^{\varepsilon 1}$ of *cis*-SC_a shows coupling through space to $H^{\beta 2}$, $H^{\beta 3}$, H^{γ} and the backbone H^{N} of Arg16 as well as H^{α} and H^{δ} of Pro18 and $H^{\delta 2/\delta 3}$ of Pro19 (Fig. 7). In contrast, the Trp6 $H^{\varepsilon 1}$ of *trans*-SC displays only one extremely weak NOE cross-peak (3.498 ppm). Even at 278 K, a temperature that favours folding and which enables long measurements due to slow *trans* → *cis* isomerization, no further NOE cross-peaks are observable in the *trans*-SC NOE spectrum.

In addition to NMR spectroscopy, CD spectroscopy also provides evidence that *trans*-SC is completely unfolded. The mean residue molar ellipticity [θMR] at 222 nm in the dark-adapted state amounts to −12 017° M^{-1} m^{-1}, which is reduced to −6725° M^{-1} m^{-1} in the PSS at 385 nm (Fig. 4b). This corresponds to a reduction by 44% which is in the same range as the *cis* → *trans*-conversion ratio in the PSS indicating complete unfolding of the α-helix and thus absence of secondary and tertiary structure in *trans*-SC.

The lack of α-helicity as evidenced by CD-spectroscopy, the Trp6 $H^{\varepsilon 1}$ chemical shift and the disappearance of inter-residual NOE cross-peaks upon switching to the *trans*-state unambiguously demonstrate that the switch cage is entirely unfolded in its *trans*-state. Conversely, the switch cage is nearly

§The recently developed N-bridged diazocines are a remarkable exception to that rule because of their nitrogen-atom incorporated into the bridge. This feature distinguishes them from 'standard' diazocines bearing an ethylene bridge. The NAc-CH_2-bridged diazocine shows *cis* → *trans* conversion rates of 78% *trans*-isomer in D_2O : MeOH-d_4 (80 : 20) at 405 nm.[24]

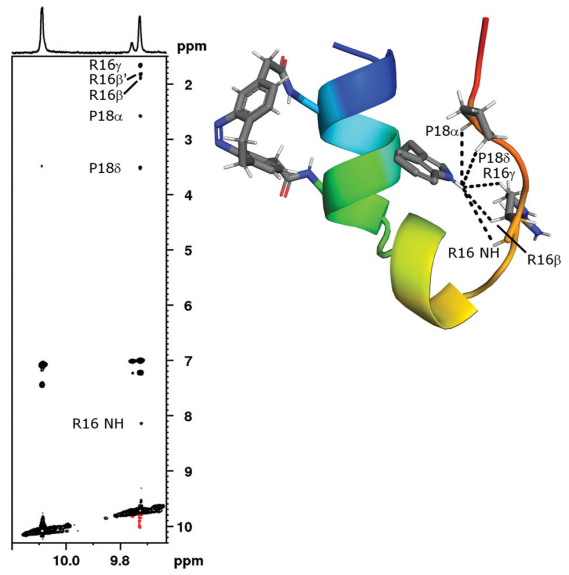

Fig. 7 The ^{1}H,^{1}H-NOESY of the switch cage after irradiation to the PSS at 385 nm was recorded at 298 K. The expansion shows the indole region of *cis*-SC$_a$ (F2: 9.728 ppm), *cis*-SC$_b$ (F2: 9.757 ppm) and *trans*-SC (F2: 10.089 ppm). The six inter-residual cross-peaks in the vertical direction of *cis*-SC$_a$ evidence a stable tertiary structure. The NOE signals highlighted in the expansion are depicted in the model structure of *cis*-SC$_a$. In contrast to *cis*-SC$_a$, only one unassigned cross-peak is observed for the indole proton of *trans*-SC (F2: 10.098 ppm, F1: 3.485 ppm). The NOEs between 7.0 ppm and 7.5 ppm are intra-residual cross-peaks with the neighbouring aromatic protons. For *cis*-SC$_b$ inter-residual NOEs are not visible in this depiction due to low population.

quantitatively folded in the presence of the *cis*-linker. Thus, the folding state of the protein is completely coupled to the isomeric state of the cross-linker.

Switching from *trans*-SC to *cis*-SC

Irradiation with light at the wavelength of 530 nm provides almost complete conversion to *cis*-SC (Fig. S16†). Moreover, the NMR-spectrum of *cis*-SC recorded immediately after irradiation to its PSS at 530 nm is indistinguishable from that of dark-adapted *cis*-SC.

The thermal *trans* → *cis* relaxation process of the switch cage was observed by ^{1}H-NMR spectroscopy and quantified by integration of selected peaks of the protein or the diazocine moiety (Table S5 and Fig. S14, S15†) after irradiation to the PSS at 385 nm. At 298 K in the dark, this process requires 39 h after which *trans*-SC is not quantifiable anymore (Fig. S16†). It follows first order kinetics with a half-live of (6.2 ± 0.3) h (Table S6†). Within the error of measurement, differences in the determined relaxation rates for diazocine signals and protein signals (Trp6 H$^{\varepsilon 1}$) are insignificant. Further, the relaxation of *trans*-SC to *cis*-SC$_a$ and to *cis*-SC$_b$ is equally fast. Together, this is an additional demonstration of the strict coupling between the isomeric state of the diazocine and the folding state of the Trp-cage.

Throughout the entire study, the same sample was used for all spectroscopic measurements. In consequence, it was subjected to multiple switching cycles without showing any sign of photobleaching or other material fatigue. Furthermore, aggregation was never observed, not even in the PSS at 385 nm, when approximately half of the population of the switch cage was unfolded exposing the hydrophobic core and the *trans*-diazocine to the solvent. This emphasizes the reversibility of the switching process and the photochemical stability of the switch cage.

The relationship between *cis*-SC$_a$ and *cis*-SC$_b$

Regardless of the wavelength or intensity of incident light (day-light-adapted, dark-adapted, PSS at 385 nm, PSS at 530 nm), the two diastereomers *cis*-SC$_a$ and *cis*-SC$_b$ have always been observed in a ratio of 3 : 1. While often indicative of a thermodynamic reaction control, the apparently constant ratio of *cis*-SC$_a$ to *cis*-SC$_b$ in photoreactions appears surprising at first. The parent *cis*-diazocine **1** is prochiral and converts upon radiation at 385 nm equally fast into two enantiomeric *trans*-forms, that are believed to comprise an equilibrium of twist- and chair-conformations.[57] These forms convert back to *cis*-diazocine equally well.

In the chiral context of the protein, however, irradiation results in multiple possible *cis*–*trans*-isomerizations (Scheme S1†) between diastereomeric states. Unhindered interconversion would lead to the expectation of a 1 : 1 product ratio of *cis*-SC$_a$ and *cis*-SC$_b$. The observed uneven *cis*-SC$_a$/*cis*-SC$_b$ ratio thus suggest that the conversion rates between the states differ between diastereomers implying a form of chiral induction by the protein moiety.

Although it is possible that the conversion from either *trans*-diastereomer occurs faster to the *cis*-SC$_a$ diastereomer, a chiral induction in the *trans*-state appears unlikely since the protein moiety is unfolded and should have very limited influence on the conversion kinetics. In the *cis*-states, however, the environment of the chromophore differs significantly for example with closer protein-diazocine contacts in *cis*-SC$_a$. These structural differences might slow the photoconversion of *cis*-SC$_a$ sterically or energetically whereas *cis*-SC$_b$ more rapidly isomerizes to either *trans*-isomer. Accordingly, this chiral induction could lead to the observed bias in the photostationary states.

Conclusions

The present study aimed to reversibly fold and unfold the Trp-cage upon irradiation with visible light of different wavelengths. Since the elongation of the diazocine during *cis* → *trans*-isomerization induces unfolding, the switching approach presented in this work is described as "unfolding-upon-extension/folding-upon-contraction". This goal was achieved through the conjugation of an N-terminally acetylated Trp-cage mutant 'TC(4,8)' bearing L-2,3-diaminopropionic acid (Dpr, Γ)‡ in positions 4 and 8. A diazocine-based, primary amine-selec-

tive cross-linker (**1**) was designed to match the distance between the N^{γ} of both Dpr-residues in its *cis*-state. Upon cross-linking, the fold of the resulting photoswitchable Tpr-cage (switch cage, SC) is stabilized significantly compared to the uncross-linked peptide. Irradiation with light of the wavelength 385 nm produces a PSS of approximately 46% *trans*-SC. This isomerization is completely reversed upon irradiation with light at 530 nm or through thermal relaxation. Most importantly, in the *trans*-state, secondary and tertiary structuring is completely abolished. As predicted, pulling apart only one helical turn between residues 4 and 8 destroys the entire helical structure and in consequence unfolds the hydrophobic cluster.

With these features, the switch cage may serve as a valuable tool for the analysis of the Trp-cage folding pathway adding visible light as an alternative trigger to the previously used T-jump[39,41] in IR or fluorescence spectroscopy. The reversibility of the switching process enables multiple switching cycles and thus facilitates multiple and repeated observations of folding and unfolding kinetics.

In this study, a dicarboxy-functionalized diazocine was furbished with selective reactivity towards primary amines by introduction of NHS-active ester moieties. This cross-linking strategy adds a valuable alternative to current methods to conjugate the chromophore with the protein. The NHS-ester cross-linking chemistry is orthogonal to the common cysteine-based chemistry.[58] When incorporated into the protein (*cf.* Scheme 1), the presented diazocine cross-linker is shorter and more rigid than the chloroacetamide-functionalized diazocine.[28]

The active ester cross-linking strategy is especially interesting for synthetic peptides and proteins, as next to lysine several amino group-bearing homologues exist that can be used to tailor length and flexibility of the cyclized product. Particularly short and rigid cross-linkages are obtained when the shortest lysine-homologue Dpr is utilized. The cross-linker **1** may also be incorporated *via* naturally occurring lysine residues or a free N-terminus, but this would limit its application to "folding-upon-extension/unfolding-upon-contraction"-approaches due to the high flexibility of the lysine side chains.

In conclusion, we were able to reversibly fold and unfold the secondary and tertiary structure of the Trp-cage miniprotein upon irradiation with visible light. Most importantly the present study shows that it is generally possible to reversibly fold and unfold a single, solvent-exposed α-helix in a small, but stable protein resulting in photocontrol of the entire fold. This strengthens our beliefs that this approach is applicable to larger proteins or protein domains.

Experimental

Trp-cage synthesis

TC(4,8) (Ac-DAYΓQWLΓDGGPSSGRPPPS)‡ was synthesized using Fmoc-based solid phase peptide synthesis with a microwave-assisted, semi-automated peptide synthesizer Initiator^{+} SP Wave (Biotage, Uppsala, Sweden) on Wang-resin (200–400 mesh, 0.86 mmol g^{-1}; 200 mg, 1 eq.; ChemPep, Wellington, FL, USA) at a 0.172 mmol scale. To avoid aspartimide formation during synthesis the dipeptide Fmoc-Asp(O*t*Bu)-(DMB)Gly-OH (Novabiochem, Merck, Darmstadt, Germany) was used. Moreover, the two consecutive serines were coupled as the pseudo-proline dipeptide Fmoc-Ser(*t*Bu)-Ser(psiMe,Mepro)-OH (Novabiochem, Merck, Darmstadt, Germany). In general, the peptide was synthesised using repetitive cycles of coupling, capping (*i.e.* acetylating unreacted peptide chains) and deprotection. Each coupling, capping or deprotection step was followed by draining the liquid and washing the resin with *N*,*N*-dimethylformamide (DMF; 2 ml) four times. Coupling of amino acids was achieved using the corresponding amino acid (860 μmol, 5 eq.), hexafluorophosphate azabenzotriazole tetramethyl uronium (HATU; 320 mg, 843 μmol 4.9 eq.) and *N*,*N*-diisopropylethylamine (DIPEA; 300 μl, 1.72 mmol, 10 eq.) dissolved in DMF (2 ml). The reaction solution was heated to 75 °C and vortexed at 600 rpm for 5 min. The coupling step was performed twice (double coupling) for the following amino acids: Fmoc-Ser(*t*Bu)-OH, Fmoc-Arg(Pbf)-OH, Fmoc-Gly-OH, Fmoc-Dpr(Boc)-OH, Fmoc-Gln(Trt)-OH and Fmoc-Ala-OH. (Double) coupling was followed by a capping step using a solution (2 ml) of pyridine (25% v/v), and acetic anhydride (25% v/v) in DMF at 75 °C at 600 rpm for 5 min. Removal of the Fmoc-group was achieved in three consecutive steps (1 min, 4 min, 4 min). Each step used a solution (2 ml) of piperidine (25% v/v) in DMF at 75 °C at 600 rpm which was drained afterwards. After the final deprotection, the peptide was N-terminally acetylated using the capping reagents and conditions. The peptide was cleaved off the resin using a mixture of trifluoroacetic acid (TFA; 90% v/v), *m*-dimethoxybenzene (DMB; 5% v/v), triisopropylsilane (TIPS; 2.5% v/v) and water (2.5% v/v). The cleavage reaction was completed after gently agitating it for 3 h at room temperature. The peptide was precipitated using cold diethyl ether and centrifuged. The supernatant was decanted. The pellet was dissolved in water and lyophilized.

Trp-cage purification

The peptide was purified in four batches by high performance liquid chromatography (HPLC) on a VWR-Hitachi LaChrom Elite instrument (VWR, Darmstadt, Germany) equipped with a semi-preparative PLRP-S column (325 mm × 30 mm, 30 nm pore diameter, 8 μm particle size; Agilent, Santa Clara, CA, USA), a VWR-Hitachi L2400 UV detector (VWR, Darmstadt, Germany) and a Foxy R1 fraction collector (Teledyne ISCO, Lincoln, NE, USA). A flow rate of 6 mL min^{-1} and the following gradient (solvent A: water, 0.1% formic acid (FA), solvent B: acetonitrile, 0.1% FA) was applied: 0 min: 5% B, 5 min: 5% B, 25 min: 15% B, 55 min: 25% B, 65 min: 95% B, 75 min: 95% B, 80 min: 5% B, 90 min: 5% B. Fractions of 3 ml were collected between 45 min and 75 min. TC(4,8) eluted after retention time of t_R = 55.5 min. A dead time of 20 min was observed.

Collected fractions were analysed by HPLC-mass spectrometry (HPLC-MS) using the same VWR-Hitachi LaChrom

Elite instrument (VWR, Darmstadt, Germany) equipped with a 717 plus autosampler (Waters, Milford, MA, USA), an analytical PLRP-S column (150 mm × 4.6 mm, 30 nm pore diameter, 8 μm particle size; Agilent, Santa Clara, CA, USA), a VWR-Hitachi L2400 UV detector (VWR, Darmstadt, Germany) and an expressionL cms MS device (Advion, Harlow, UK). A flow rate of 1 mL min^{-1} and the following gradient (solvent A: water, 0.1% FA, solvent B: acetonitrile, 0.1% FA) was applied: 0.0 min: 5% B, 2.5 min: 5% B, 12.5 min: 60% B, 13.5 min: 95% B, 16.0 min: 95% B, 17.0 min: 5% B, 18.5 min: 5% B. A dead time of 2.0 min was observed. TC(4,8) eluted after retention time of t_R = 9.8 min. Fractions deemed sufficiently pure were combined and lyophilized. The peptide was obtained as a white fluffy solid (17.8 mg, 8.65 μmol, 5%).

Cross-linker synthesis and purification

Details regarding the cross-linker synthesis, purification and characterization can be found in the ESI.†

Cross-linking reaction and purification

DIPEA (33 μL, 190 μmol, 100 eq.) and DMSO (1.5 ml) were added to a 50 ml polypropylene (PP) centrifuge tube equipped with a magnetic stir bar. A solution of TC(4,8) (4.0 mg, 1.9 μmol, 1 eq.) in DMSO (1.5 mL) supplemented with DIPEA (33 μL, 190 μmol, 100 eq.) was transferred into a 2 mL syringe. A second 2 ml syringe was filled with a solution of the NHS-functionalized cross-linker **1** (1 mg, 2.1 μmol, 1.1 eq.) in DMSO (1.81 ml). The two reactants were slowly added to the centrifuge tube, each at a speed of 2 μl min^{-1} under continuous stirring at room temperature. After complete addition, the reaction was stirred for 2 d. Subsequently, the solution was flash-frozen with liquid nitrogen and lyophilized. The crude product was dissolved in 2.5 ml of water by briefly sonicating it in the centrifuge tube using an ultrasonic bath. The switch cage was purified in ten small batches *via* HPLC using the VWR-Hitachi LaChrom Elite instrument (VWR, Darmstadt, Germany) equipped with a 717 plus autosampler (Waters, Milford, MA, USA), an analytical PLRP-S column (150 mm × 4.6 mm, 30 nm pore diameter, 8 μm particle size; Agilent, Santa Clara, CA, USA), a VWR-Hitachi L2400 UV detector (VWR, Darmstadt, Germany) and a Foxy R1 fraction collector (Teledyne ISCO, Lincoln, NE, USA). A flow rate of 1 mL min^{-1} and the following gradient (solvent A: water, 0.1% FA, solvent B: acetonitrile, 0.1% FA) was applied: 0.0 min: 5% B, 2.5 min: 5% B, 10 min: 27% B, 20 min: 29% B, 25 min: 95%B, 29 min: 95% B, 31 min: 5% B, 35 min: 5% B. The switch cage eluted after a retention time of t_R = 18.2 min. A dead time of 2.0 min was observed. Fractions of the ten different batches with identical retention times were collected into the same containers. Fractions were analysed using the same HPLC-MS set-up as described in the chapter Trp-cage purification. The switch cage eluted after a retention time of t_R = 12.0 min. Fractions deemed sufficiently pure were combined and lyophilized which afforded the switch cage as a yellowish solid (0.8 mg, 330 nmol, 17%).

Ultrahigh performance liquid chromatography – high resolution mass spectrometry

TC(4,8) and the switch cage analysed by ultrahigh performance liquid chromatography – high resolution mass spectrometry (UHPLC-HRMS) using an Ultimate 3000 RS instrument coupled to a QExactive Plus Hybrid Quadrupol-Orbitrap MS device (both Thermo Fisher Scientific, Waltham, MA, USA). A Zorbax RRHD Eclipse Plus C18 column with a length of 100 mm and a diameter of 3 mm (Agilent, Santa Clara, CA, USA) was used. The MS was set to detect positive ions and the resolution was set to FWHM = 70 000 at m/z = 200. The Full MS method was applied covering an m/z range between 200 and 3000. A flow rate of 0.4 mL min^{-1} and the following gradient (solvent A: water, 0.1% FA, solvent B: acetonitrile, 0.1% FA) was applied: 0.0 min: 5% B, 1.0 min: 5% B, 9.0 min: 80% B, 9.5 min: 95% B, 11.0 min: 95% B, 11.5 min: 5% B, 13.2 min: 5% B. A dead time of 1.23 min was observed. The TC(4,8) eluted after retention time of t_R = 4.92 min. Chromatograms and the corresponding mass spectra of TC(4,8) can be found in the ESI (Fig. S1–S3†). The switch cage eluted after retention time of t_R = 6.19 min. Chromatograms and the corresponding mass spectra of the switch cage can be found in the ESI (Fig. S5–S8†).

Molecular modelling and molecular dynamics simulations

All computational studies were performed using the Schrödinger Suite Release 2017-4 (Schrödinger LLC, New York, NY, USA). The amidated cross-linkers *cis*-**5** and *trans*-**5** were built *in silico* using Maestro (Schrödinger LLC, New York, NY, USA). The structures were geometrically relaxed using MacroModel (Schrödinger LLC, New York, NY, USA) by applying the OPLS3 force field with implicit water. Charges were compensated by the addition of Na^+ or Cl^-. To avoid isomerization during conformational energy minimization, constraints were applied to the CNNC torsion angle (*cis*-**5**: 0°, force constant (FC) = 200 kJ mol^{-1} $Å^{-2}$; *trans*-**5**: 147°, FC = 300 kJ mol^{-1} $Å^{-2}$) and to the NNC bond angles (*cis*-**5**: 121°, FC = 200 kJ mol^{-1} $Å^{-2}$; *trans*-**5**: 112°, FC = 200 kJ mol^{-1} $Å^{-2}$).

The model of TC(4,8) was built from the first structure of the NMR-derived structure ensemble of TC10b (RCSB PDB accession code 2JOF) using Maestro. Energy minimization was achieved in the same way as for *cis*-**5** and *trans*-**5**, but without any constraints.

The model of *cis*-SC was built from the relaxed model of TC(4,8). The relaxed *cis*-**5** cross-linker was incorporated into the peptide using Maestro resulting in the diastereomer *cis*-SC_a. Relaxation was achieved in the same way as for *cis*-**5** applying the same constraints to the cross-linker.

MD simulations were performed using the Desmond Molecular Dynamics System (D. E. Shaw Research, New York, NY, USA) and set up with the Maestro-Desmond Interoperability Tools (Schrödinger LLC, New York, NY, USA). The molecule was submerged in an orthorhombic box of explicit water complying with the SPC water model using the OPLS3 force field. The size of the box was adjusted to a minimal

volume with at least 10 Å distance between the molecule and each side of the box. The temperature was set to 300 K and the pressure was set to 1.01325 bar. MD simulations covered a period of 100 ns with recording intervals of 100 ps (trajectory) and 1.2 ps (energy). The starting geometry of each molecule was the result of the previous minimization using MacroModel. In order to avoid isomerization of the cross-linkers during MD simulations, the central eight-membered ring of the cross-linker was restrained to its starting geometry with a FC of 300 kJ mol^{-1} $Å^{-2}$. Distances between atoms were measured and exported using the simulation event analysis panel of the Schrödinger Suite. The structures created with the Schrödinger Suite were exported as PDB files to create the molecule depictions for the figures using the PyMOL Molecular Graphics System Version 1.9.0.0. (Schrödinger LLC, New York, NY, USA).

CD spectroscopy

CD spectra were recorded on a Jasco J-720 spectropolarimeter (Jasco, Pfungstadt, Germany) equipped with a Haake WKL 26 thermostat (Thermo Electron Corporation, now Thermo Fisher Scientific, Waltham, MA, USA) and a Jasco PTC-423S peltier element (Jasco, Pfungstadt, Germany). For all measurements the same Quartz glass cuvette with an optical path length of 1.00 mm was used. All spectra were obtained in water at concentrations of 36 μM. The pH was adjusted to 5.4 ± 0.2 using 0.1 M solutions of NaOH and/or HCl. The concentration of TC (4,8) was determined by the UV absorption of Tyr and Trp according to Gill and von Hippel.[59] This method was not applicable to the switch cage because of the unknown extinction coefficient of the diazocine in water. Therefore, the concentration of the switch cage was determined by recording a 1D-^{1}H-NMR spectrum of the sample with a known amount of DSS and correlating the integrals of the DSS signal and the Leu7δ-methyl groups of *cis*-SC_a and *cis*-SC_b, which do not exchange and are not overlapping with other signals.

Full spectra are averaged over six measurements and were recorded at 25 °C. In order to obtain the spectra of the switch cage in its PSS, the sample was irradiated at 385 nm for 10 s prior to each of the six measurements.

Thermal unfolding and folding was observed between 5 °C and 90 °C at a wavelength of 222 nm. A heating and cooling rate of 1 °C min^{-1} was applied. Before starting the temperature gradient, the sample was equilibrated for 5 min at the starting temperature. Two consecutive heating and cooling cycles were averaged for each spectrum. This repetition indicated full reversibility of thermal unfolding and folding of *cis*-SC and TC (4,8). For determination of the melting point the spectra were fitted with a sigmoidal Boltzmann fit. The fitting results are given in the ESI.†

NMR spectroscopy

The NMR spectra of TC(4,8) and of the switch cage were obtained on a AV III 600 Fourier transform-NMR spectrometer (Bruker, Billerica, MA, USA) at frequencies of 600.1 MHz for ^{1}H-nuclei. The spectrometer was equipped with a triple resonance cryo probe. All samples were dissolved in a solution of 90% H_2O and 10% D_2O. 4,4-Dimethyl-4-silapentane-1-sulfonic acid (DSS) served as the internal standard for referencing. Water suppression was achieved by excitation sculpting[60] using standard bruker pulse sequences.

Chemical shifts were assigned using 2D-NMR techniques including ^{1}H,^{1}H-correlated spectroscopy (COSY), ^{1}H,^{1}H-total correlation spectroscopy (TOCSY) and ^{1}H,^{1}H-nuclear Overhauser enhancement spectroscopy (NOESY). Except for the spectra of the switch cage after having reached the PSS at 385 nm, all 2D-NMR spectra were recorded with the following parameters: COSY spectra were recorded with a size of free induction decay (FID) of 4096 (F2) by 1024 (F1) data points and a spectral width of 14.0261 ppm (F2) by 14.0000 ppm (F1). TOCSY data were acquired with a size of FID of 4096 (F2) by 512 (F1), a spectral width of 14.0261 ppm (F2) by 14.0261 ppm (F1) and a mixing time of 60 ms. NOESY data were recorded with a size of FID of 4096 (F2) by 512 (F1), a spectral width of 14.0261 ppm (F2) by 14.0261 ppm (F1) and using a mixing time of 200 ms.

All measurements were performed at 298 K if not stated otherwise. Spectra of TC(4,8) were recorded at concentrations of 3.3 mg ml^{-1} (1.6 mM) at pH = 5.3 ± 0.1. Each data point of each spectrum was an accumulation of 8 scans. Spectra of the switch cage were recorded at concentrations of 1.2 mg ml^{-1} (0.5 mM) at pH = 5.5 ± 0.1. Each data point of each spectrum was an accumulation of 16 scans.

In order to obtain spectra of the Trp-cage after having reached its PSS at 385 nm the sample was irradiated for 10 s immediately before each experiment. Due to the relatively fast *trans* → *cis* relaxation the 2D-NMR experiments were recorded with a reduced amount of scans and a reduced size of FID in the F1 dimension but otherwise identical parameters as stated above. The COSY, TOCSY and NOESY were recorded with an F1 FID of 512 and 8 scans per data point.

Irradiation

Irradiation was performed immediately prior to the measurements outside the spectrometer (NMR, CD, UV/vis) with samples already inside their container for the respective spectroscopic measurement. Samples were irradiated using light emitting diodes (LEDs) emitting at 385 nm or 530 nm (Sahlmann Photochemical Solutions, Kiel, Germany). Irradiation at 385 nm was performed from four sides by a total of twelve Nichia NCSU034A LEDs with the following specifications: FWHM = 9 nm, *P*(opt) = 12 × 340 mW. Irradiation at 530 nm was performed from four sides by a total of 16 Luxeon LXML-PM01-0080 LEDs with the following specifications: FWHM = 33 nm, *P*(opt) = 16 × 200 mW. Regardless of the container and the wavelength the PSS was reached within 10 s of irradiation.

Author contributions

F. D. S., M. L., N. P. and W. M. developed the concept. N. P. planned and performed all MD simulations as well as the syn-

thesis and characterization of the Trp-cage and the switch-cage. For his PhD thesis in organic chemistry, W. M. planned and performed the synthesis and characterization of the cross-linker. For his bachelor thesis in biochemistry, W. M. performed the MD-simulations as well as the synthesis and characterization of the Trp-cage and the switch-cage under the guidance of N. P., M. L. and K. B. optimized the cross-linking reaction conditions. N. P. and W. M. prepared the original draft. N. P., W. M., F. D. S. and R. H. revised the manuscript. F. D. S. and R. H. supervised the work. N. P., F. D. S., R. H. and K. B. acquired the funding.

Conflicts of interest

There are no conflicts to declare.

Acknowledgements

The authors gratefully acknowledge financial support by the Deutsche Forschungsgesellschaft (DFG) within the Collaborative Research Center SFB 677, "Function by Switching". N. P. thanks the Deutsche Bundesstiftung Umwelt (German Federal Environmental Foundation) for a predoctoral fellowship. K. B. thanks the Studienstiftung des deutschen Volkes (German Academic Scholarship Foundation) for a predoctoral fellowship. The authors thank Prof. Joachim Grötzinger for granting access to and use of his CD spectrometer.

Notes and references

1 A. A. Beharry and G. A. Woolley, *Chem. Soc. Rev.*, 2011, **40**(8), 4422.
2 W. Szymański, J. M. Beierle, H. A. V. Kistemaker, W. A. Velema and B. L. Feringa, *Chem. Rev.*, 2013, **113**(8), 6114.
3 R. J. Mart and R. K. Allemann, *Chem. Commun.*, 2016, **52**(83), 12262.
4 L. Albert and O. Vázquez, *Chem. Commun.*, 2019, **55**(69), 10192.
5 J. R. Kumita, D. G. Flint, G. A. Woolley and O. S. Smart, *Faraday Discuss.*, 2002, **122**, 89–103; discussion 171–190.
6 A. M. Ali, M. W. Forbes and G. A. Woolley, *ChemBioChem*, 2015, **16**(12), 1757.
7 A. Bergen, S. Rudiuk, M. Morel, T. Le Saux, H. Ihmels and D. Baigl, *Nano Lett.*, 2016, **16**(1), 773.
8 A. Estévez-Torres, C. Crozatier, A. Diguet, T. Hara, H. Saito, K. Yoshikawa and D. Baigl, *Proc. Natl. Acad. Sci. U. S. A.*, 2009, **106**(30), 12219.
9 A.-L. M. Le Ny and C. T. Lee Jr., *J. Am. Chem. Soc.*, 2006, **128**(19), 6400.
10 L. Guerrero, O. S. Smart, C. J. Weston, D. C. Burns, G. A. Woolley and R. K. Allemann, *Angew. Chem., Int. Ed.*, 2005, **44**(47), 7778.
11 L. Guerrero, O. S. Smart, G. A. Woolley and R. K. Allemann, *J. Am. Chem. Soc.*, 2005, **127**(44), 15624.
12 G. A. Woolley, A. S. I. Jaikaran, M. Berezovski, J. P. Calarco, S. N. Krylov, O. S. Smart and J. R. Kumita, *Biochemistry*, 2006, **45**(19), 6075.
13 S. Kneissl, E. J. Loveridge, C. Williams, M. P. Crump and R. K. Allemann, *ChemBioChem*, 2008, **9**(18), 3046.
14 F. Zhang, K. A. Timm, K. M. Arndt and G. A. Woolley, *Angew. Chem., Int. Ed.*, 2010, **49**(23), 3943.
15 R. J. Mart, P. Wysoczański, S. Kneissl, A. Ricci, A. Brancale and R. K. Allemann, *ChemBioChem*, 2012, **13**(4), 515.
16 R. J. Mart, R. J. Errington, C. L. Watkins, S. C. Chappell, M. Wiltshire, A. T. Jones, P. J. Smith and R. K. Allemann, *Mol. BioSyst.*, 2013, **9**(11), 2597.
17 L. Nevola, A. Martín-Quirós, K. Eckelt, N. Camarero, S. Tosi, A. Llobet, E. Giralt and P. Gorostiza, *Angew. Chem., Int. Ed.*, 2013, **52**(30), 7704.
18 A. Martín-Quirós, L. Nevola, K. Eckelt, S. Madurga, P. Gorostiza and E. Giralt, *Chem. Biol.*, 2015, **22**(1), 31.
19 B. Jankovic, A. Gulzar, C. Zanobini, O. Bozovic, S. Wolf, G. Stock and P. Hamm, *J. Am. Chem. Soc.*, 2019, **141**(27), 10702.
20 Z. Zhang, D. C. Burns, J. R. Kumita, O. S. Smart and G. A. Woolley, *Bioconjugate Chem.*, 2003, **14**(4), 824.
21 R. Siewertsen, H. Neumann, B. Buchheim-Stehn, R. Herges, C. Näther, F. Renth and F. Temps, *J. Am. Chem. Soc.*, 2009, **131**(43), 15594.
22 R. Siewertsen, J. B. Schönborn, B. Hartke, F. Renth and F. Temps, *Phys. Chem. Chem. Phys.*, 2011, **13**(3), 1054.
23 M. Hammerich, C. Schütt, C. Stähler, P. Lentes, F. Röhricht, R. Höppner and R. Herges, *J. Am. Chem. Soc.*, 2016, **138**(40), 13111.
24 P. Lentes, E. Stadler, F. Röhricht, A. Brahms, J. Gröbner, F. D. Sönnichsen, G. Gescheidt and R. Herges, *J. Am. Chem. Soc.*, 2019, **141**(34), 13592.
25 W. Moormann, D. Langbehn and R. Herges, *Beilstein J. Org. Chem.*, 2019, **15**, 727.
26 W. Moormann, D. Langbehn and R. Herges, *Synthesis*, 2017, (15), 3471.
27 M. S. Maier, K. Hüll, M. Reynders, B. S. Matsuura, P. Leippe, T. Ko, L. Schäffer and D. Trauner, *J. Am. Chem. Soc.*, 2019, **141**(43), 17295.
28 S. Samanta, C. Qin, A. J. Lough and G. A. Woolley, *Angew. Chem., Int. Ed.*, 2012, **51**(26), 6452.
29 A. M. Petros, A. Medek, D. G. Nettesheim, D. H. Kim, H. S. Yoon, K. Swift, E. D. Matayoshi, T. Oltersdorf and S. W. Fesik, *Proc. Natl. Acad. Sci. U. S. A.*, 2001, **98**(6), 3012.
30 S. W. Muchmore, M. Sattler, H. Liang, R. P. Meadows, J. E. Harlan, H. S. Yoon, D. Nettesheim, B. S. Chang, C. B. Thompson, S.-L. Wong, S.-C. Ng and S. W. Fesik, *Nature*, 1996, **381**(6580), 335.
31 C. R. Kissinger, B. Liu, E. Martin-Blanco, T. B. Kornberg and C. O. Pabo, *Cell*, 1990, **63**(3), 579.
32 N. D. Clarke, C. R. Kissinger, J. Desjarlais, G. L. Gilliland and C. O. Pabo, *Protein Sci.*, 1994, **3**(10), 1779.

33 I. Radhakrishnan, G. C. Pérez-Alvarado, D. Parker, H. J. Dyson, M. R. Montminy and P. E. Wright, *Cell*, 1997, **91**(6), 741.

34 J. Martinez-Oyanedel, H.-W. Choe, U. Heinemann and W. Saenger, *J. Mol. Biol.*, 1991, **222**(2), 335.

35 C. J. McKnight, P. T. Matsudaira and P. S. Kim, *Nat. Struct. Biol.*, 1997, **4**(3), 180.

36 J. W. Neidigh, R. M. Fesinmeyer and N. H. Andersen, *Nat. Struct. Biol.*, 2002, **9**(6), 425.

37 B. Barua, J. C. Lin, V. D. Williams, P. Kummler, J. W. Neidigh and N. H. Andersen, *Protein Eng., Des. Sel.*, 2008, **21**(3), 171.

38 S. H. Gellman and D. N. Woolfson, *Nat. Struct. Biol.*, 2002, **9**(6), 408.

39 H. Meuzelaar, K. A. Marino, A. Huerta-Viga, M. R. Panman, L. E. J. Smeenk, A. J. Kettelarij, J. H. van Maarseveen, P. Timmerman, P. G. Bolhuis and S. Woutersen, *J. Phys. Chem. B*, 2013, **117**(39), 11490.

40 B. N. Markiewicz, H. Jo, R. M. Culik, W. F. DeGrado and F. Gai, *J. Phys. Chem. B*, 2013, **117**(47), 14688.

41 L. Qiu, S. A. Pabit, A. E. Roitberg and S. J. Hagen, *J. Am. Chem. Soc.*, 2002, **124**(44), 12952.

42 A. Byrne, D. V. Williams, B. Barua, S. J. Hagen, B. L. Kier and N. H. Andersen, *Biochemistry*, 2014, **53**(38), 6011.

43 M. Scian, J. C. Lin, I. Le Trong, G. I. Makhatadze, R. E. Stenkamp and N. H. Andersen, *Proc. Natl. Acad. Sci. U. S. A.*, 2012, **109**(31), 12521.

44 W. W. Streicher and G. I. Makhatadze, *Biochemistry*, 2007, **46**(10), 2876.

45 C. Simmerling, B. Strockbine and A. E. Roitberg, *J. Am. Chem. Soc.*, 2002, **124**(38), 11258.

46 S. Kannan and M. Zacharias, *PLoS One*, 2014, **9**(2), e88383.

47 J. Juraszek and P. G. Bolhuis, *Proc. Natl. Acad. Sci. U. S. A.*, 2006, **103**(43), 15859.

48 R. Day, D. Paschek and A. E. Garcia, *Proteins*, 2010, **78**(8), 1889.

49 Matthias Lipfert, *Design of a Stabilizing and Switching Module for α-Helical Peptides*, Dissertation, Kiel, 2017.

50 E. J. Corey and N. Raju, *Tetrahedron Lett.*, 1983, **24**(50), 5571.

51 A. Bundi and K. Wüthrich, *Biopolymers*, 1979, **18**(2), 285.

52 G. Merutka, H. J. Dyson and P. E. Wright, *J. Biomol. NMR*, 1995, **5**(1), 14.

53 G. Cabré, A. Garrido-Charles, À. González-Lafont, W. Moormann, D. Langbehn, D. Egea, J. M. Lluch, R. Herges, R. Alibés, F. Busqué, P. Gorostiza and J. Hernando, *Org. Lett.*, 2019, **21**(10), 3780.

54 E. R. Thapaliya, J. Zhao and G. C. R. Ellis-Davies, *ACS Chem. Neurosci.*, 2019, **10**(5), 2481.

55 J. B. Trads, K. Hüll, B. S. Matsuura, L. Laprell, T. Fehrentz, N. Görldt, K. A. Kozek, C. D. Weaver, N. Klöcker, D. M. Barber and D. Trauner, *Angew. Chem., Int. Ed.*, 2019, **58**(43), 15421.

56 L. Albert, A. Peñalver, N. Djokovic, L. Werel, M. Hoffarth, D. Ruzic, J. Xu, L.-O. Essen, K. Nikolic, Y. Dou and O. Vázquez, *ChemBioChem*, 2019, **20**(11), 1417.

57 H. Sell, C. Näther and R. Herges, *Beilstein J. Org. Chem.*, 2013, **9**, 1.

58 S. S. Wong, *Chemistry of protein conjugation and cross-linking*, CRC Press, Boca Raton, FL, USA, 1991.

59 S. C. Gill and P. H. von Hippel, *Anal. Biochem.*, 1989, **182**(2), 319.

60 T.-L. Hwang and A. J. Shaka, *J. Magn. Reson., Ser. A*, 1995, **112**(2), 275.

3.4 Synthetic Photoswitchable Neurotransmitters

Arguably, the most important requirement for a drug is selectivity. Therapeutics have to interact with one specific target thereby avoiding side effects.[10, 17] Small molecules are known to be less selective than peptide and protein-based therapeutics.[69] However, peptide and protein therapeutics have short lifetimes in blood plasma and their bioavailability is comparatively low. To the discomfort of the patients, peptide and protein-based therapeutics have to be injected, often on a daily basis.[69] Especially in continuous treatment, the oral administration of tablets is favored and gives the small molecules an advantage in the highly competitive pharmaceutical market. For this reason, it would be all the more important to increase the selectivity of small molecule therapeutics. Photopharmacology tries to achieve this through the implementation of photoswitchable molecules into therapeutically active compounds.[10, 17] This concept is aiming to change the affinity of the photo drug towards the target through a light induced configurational change. Diazocines allow the administration of diazocine-based therapeutics in their inactive dark-adapted state and enable reversible activation upon irradiation, thereby living up to the full potential of photopharmacology. To prove this concept, ionotropic glutamate receptors appeared to be a suitable target as they have been extensively investigated in previous studies in photopharmacology, allowing standardized testing *in vitro* and *in vivo*.

3.4.1 Summary of Synthetic Photoswitchable Neurotransmitters Based on Bridged Azobenzenes

This research is aiming to demonstrate that diazocines have an inverse activity in comparison to azobenzenes.[70] Two photoswitchable neurotransmitters were derived from a novel dibromo-substituted diazocine derivative, which was synthesized in an oxidative azo cyclization using oxone as oxidant. The glutamate moiety containing compounds were characterized and tested regarding their activity towards ionotropic kainate receptors (GluK). Whole-cell voltage clamp recordings were accomplished on HEK293 cells expressing GluK. Upon irradiation with 405 nm, the diazocine neurotransmitters were isomerized to the twisted *trans*-isomer. The higher affinity towards GluK of the *trans*-isomer was detected in the voltage clamp recordings. This proof of concept was subsequently tested *in vivo* on GluK-expressing rat hippocampal neurons. No activity was observed in the dark as expected. However, upon irradiation Glu_brAzo **2** showed activity (**Figure 3.4.1**).

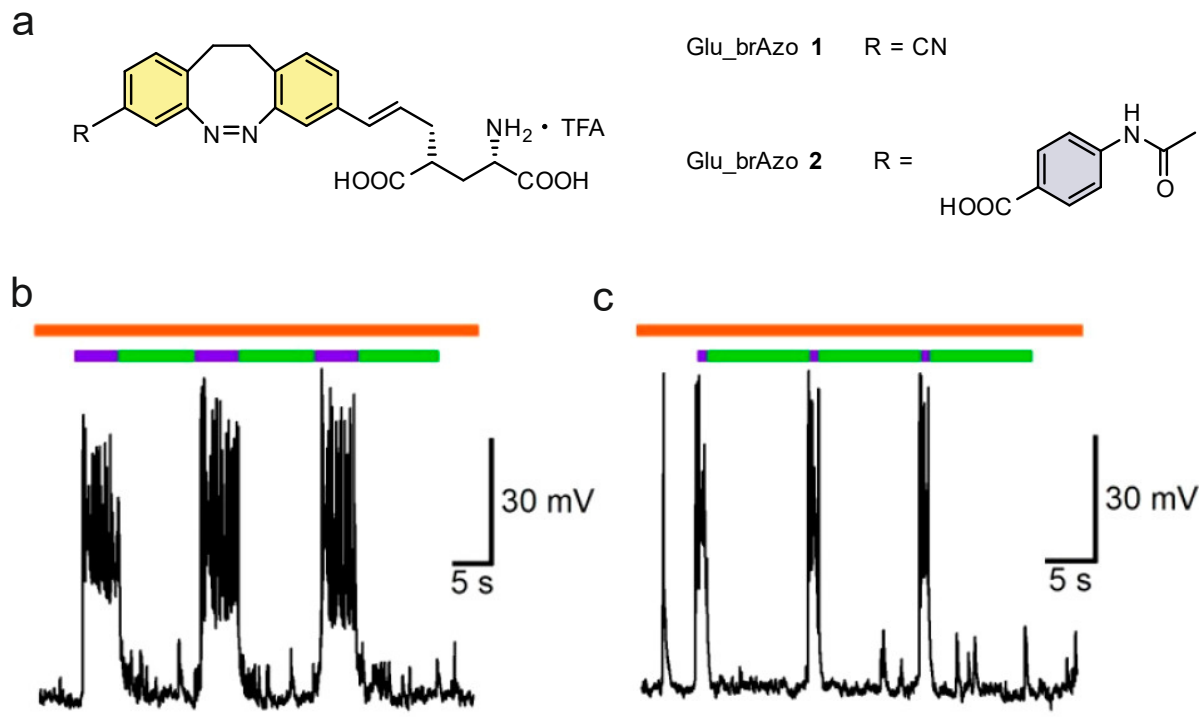

Figure 3.4.1: a) Glu_brAzo**2** not only showed activity *in vitro* but also *in vivo.* b) and c) Whole-cell current clamp recordings of rat hippocampal neurons in culture after perfusion of Glu_brAzo**2** (30 µM). Irradiation at 390 nm (purple) and 530 nm (green) with light pulses of b) 5s and c) 1s resulted in a reversible change of current.

Voltage clamp recordings could demonstrate that the activation was reversible upon irradiation with 530 nm and no fatigue in activation was observed (**Figure 3.4.1 b-c**). However, the activation upon irradiation with 405 nm was hampered by decreased photostationary states of Glu_brAzo **1** (47%) *trans*-isomer and Glu_brAzo **2** (60%) *trans*-isomer in PBS:DMSO 1:1. As expected the deactivation of both Glu_brAzo **1** and Glu_brAzo **2** upon irradiation with 532 nm was quantitative. This change in switching behavior of diazocines in water has been observed in earlier publications on diazocine peptide cross-linkers and was confirmed by the work of both Ellis and Trauner who separately presented similar results on diazocine-based neuron activation.[23, 59]

3.4.2 Synthetic Photoswitchable Neurotransmitters Based on Bridged Azobenzenes

G. Cabré, A. Garrido-Charles, À. González-Lafont, W. Moormann, D. Langbehn, D. Egea, J. M. Lluch, R. Herges, R. Alibés, F. Busqué, P. Gorostiza, and J. Hernando

Org. Lett. **2019**, *21, 10*, 3780-3784.
doi: 10.1021/acs.orglett.9b01222

Scientific contribution to this paper

The syntheses of *(Z)*-8-bromo-11,12-dihydrodibenzo[c,g][1,2]diazocine-3-carbonitrile was developed by me. Based on this intermediate Gisela Cabré and I evolved the synthesis route. Further synthesis and biological testing was carried out by Cabré and co-workers.

OL | Organic Letters

Letter

Cite This: Org. Lett. 2019, 21, 3780−3784

pubs.acs.org/OrgLett

Synthetic Photoswitchable Neurotransmitters Based on Bridged Azobenzenes

Gisela Cabré,[†,▽] Aida Garrido-Charles,[‡,▽] Àngels González-Lafont,[†,§] Widukind Moormann,[∥] Daniel Langbehn,[∥] David Egea,[†] José M. Lluch,[†,§] Rainer Herges,[∥] Ramon Alibés,[†] Félix Busqué,[†] Pau Gorostiza,[*,‡,⊥,#] and Jordi Hernando[*,†]

[†]Departament de Química, Universitat Autònoma de Barcelona (UAB), Cerdanyola del Vallès 08193, Spain

[‡]Institut de Bioenginyeria de Catalunya (IBEC), Barcelona Institute of Science and Technology (BIST), Barcelona 08036, Spain

[§]Institut de Biotecnologia i de Biomedicina (IBB), UAB, Cerdanyola del Vallès 08193, Spain

[∥]Otto Diels-Institute of Organic Chemistry, Christian Albrechts University Kiel, Kiel 24118, Germany

[⊥]Institució Catalana de Recerca i Estudis Avançats (ICREA), Barcelona 08010, Spain

[#]Centro de Investigación Biomédica en Red en Bioingeniería, Biomateriales y Nanomedicina, Zaragoza 50018, Spain

Supporting Information

ABSTRACT: Photoswitchable neurotransmitters of ionotropic kainate receptors were synthesized by tethering a glutamate moiety to disubstituted C2-bridged azobenzenes, which were prepared through a novel methodology that allows access to diazocines with higher yields and versatility. Because of the singular properties of these photochromes, photoisomerizable compounds were obtained with larger thermal stability for their inert *cis* isomer than for their biologically activity *trans* state. This enabled selective neuronal firing upon irradiation without background activity in the dark.

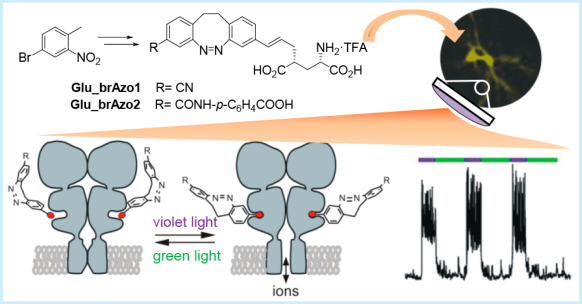

By enabling remote manipulation of neuronal signaling with light, optogenetics[1] and photopharmacology[2] have revolutionized neuroscience and neurobiology. Neural receptors responding to glutamate (GluRs), the primary excitatory neurotransmitter, are one of the major targets in these fields, since they regulate several key processes in the nervous system and are related to numerous diseases.[3] As such, a plethora of photopharmacological tools have been developed for light-gating GluRs,[4] among which photochromic ligands (PCLs)[5−12] are often preferred because they combine (a) the advantages of small-molecule, freely diffusing drugs with (b) the capacity for reversibly photoswitching their activity without byproduct generation nor modification of native receptors.[2,4]

The major strategy employed to derive PCLs relies on introducing an azoaromatic photoswitch into the structure of well-known, biologically active ligands.[2,4] Upon *trans*−*cis* photoisomerization,[13] a geometrical change is induced in these compounds that alters their interaction with the receptor. Typically, the more extended configuration of the *trans* isomer favors such interaction, while affinity is reduced for the folded *cis* state due to steric effects (i.e., *trans*-active PCLs).[2,4] Because of the inherent photochemical properties of azoaromatic compounds,[13] this imposes a severe limitation to most PCLs developed to date for GluRs[5−11] (and other receptors[2]): they are active in the dark, where they lie in the more stable *trans* state. Consequently, these compounds elicit strong tonic responses in the absence of illumination (e.g., when acting as receptor agonists), which drastically hampers their use. This is the case of **GluAzo** (Figure 1a), which is a *trans*-active, *trans*-stable partial agonist of ionotropic kainate receptors GluK1 and GluK2,[5,14,15] two of the principal GluRs mediating excitatory neurotransmission in the central nervous system.[3]

To overcome this obstacle while preserving the main design principles behind azo-based PCLs, bridged azobenzenes (brAzo) such as diazocines (C2 bridge, Figure 1b) could be used as photochromes, since they (a) should also favor *trans*-active behavior by switching between extended *trans* and bent *cis* configurations but (b) exhibit *cis* thermal stability.[16−23] This combination of properties should therefore allow direct administration of the inert *cis* form of the PCL, which could then be selectively photoactivated. In addition, diazocines isomerize with visible light,[16−23] which is a further advantage with respect to common UV-responding azoaromatic compounds.[13] However, the limited synthetic accessibility and versatility of these photochromes have so far limited their application to the photocontrol of biological systems.[22,23b]

Received: April 8, 2019
Published: May 9, 2019

DOI: 10.1021/acs.orglett.9b01222
Org. Lett. 2019, 21, 3780−3784

Organic Letters Letter

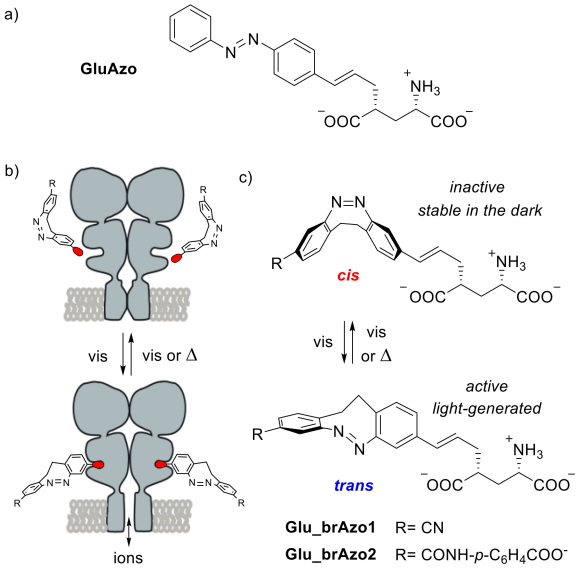

Figure 1. (a) Structure of **GluAzo**.[5] (b) Strategy proposed to prepare *trans*-active, *cis*-stable PCLs based on C2-bridged azobenzenes for the light-control of neuronal membrane receptors GluK1 and GluK2. (c) Photoisomerization of **Glu_brAzo1-2**.

Actually, their use in photopharmacology to modulate the activity of *N*-methyl-D-aspartate (NMDA) receptors and potassium ion channels has only been reported very recently,[24] for which a low-yield 4-monosubstituted diazocine previously described was employed.[23]

In this work we aim to apply this strategy to photocontrol GluK1 and GluK2, while broadening its scope by developing diazocine-based PCLs with larger yields and multiple functionalization sites to favor chemical versatility. To reach this goal our attention focused on 3,3′-disubstituted diazocines,[17,18,21] because very inefficient syntheses have been reported to date for 4,4′-disubstituted analogues (<1% yield[22]). On the basis of these photochromes and the structure of **GluAzo**,[5] we designed **Glu_brAzo2** as the first *trans*-active, *cis*-stable agonist of GluK1 and GluK2 by tethering a diazocine unit to a biologically active glutamate moiety through a vinyl linker (Figure 1c). In addition, we took advantage of the disubstitution pattern of the photochrome to introduce a lateral ionic, bulky group for (a) enhancing solubility in aqueous media and (b) further hindering the interaction of the *cis* isomer with the receptor by increasing the steric congestion around the glutamate moiety. The latter should boost the difference in activity between the two states of the PCL, a required feature given the moderate photoconversions of most functionalized diazocines.[17,18,20−23] To evaluate this effect, **Glu_brAzo1** lacking the additional bulky substituent was also synthesized (Figure 1c).

To validate our design principles, we conducted molecular docking simulations for the two isomers of **Glu_brAzo1-2** on kainate receptors. Our attention particularly focused on GluK2, since (a) it presents a narrower binding cavity that imposes larger steric constraints to ligands,[25] and (b) the crystallographic structure of its ligand-binding domain after complexation with *trans*-**GluAzo** is available.[15] Dockings were computed on this structure keeping the protein rigid, while the initial geometries of the PCLs were optimized at the B3LYP/6-31G(d) level. In all the cases, the best docking solutions placed the glutamate moiety of the ligands in a very similar position as with *trans*-**GluAzo**,[26] thus suggesting analogous interaction with the receptor via hydrogen bonds. However, clear differences were observed for the binding arrangement of each ligand (Figure 2 and Figure S1), which

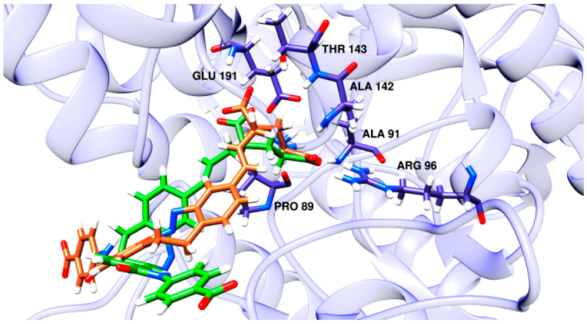

Figure 2. Best docking solutions for *trans*-**Glu_brAzo2** (orange) and *cis*-**Glu_brAzo2** (green) in GluK2. The protein residues interacting with the glutamate group of both ligands are also indicated. Oxygen, nitrogen, and hydrogen atoms are depicted in red, blue, and white, respectively.

led to different complexation energies (in Chemscore units[27]): 41.2, 37.0, 48.0, and 37.3 for *trans*-**Glu_brAzo1**, *cis*-**Glu_brAzo1**, *trans*-**Glu_brAzo2**, and *cis*-**Glu_brAzo2**, respectively. Importantly, these figures indicate larger affinity of the *trans* isomers of **Glu_brAzo1-2** to GluK2, thus preserving the targeted *trans*-active behavior of **GluAzo**. By contrast, they do not support our hypothesis that the introduction of an ionic, bulky group in **Glu_brAzo2** should decrease the binding efficiency of the *cis* isomer with respect to less hindered **Glu_brAzo1**. It must be noted, however, that this is compensated by the higher complexation energy calculated for *trans*-**Glu_brAzo2** relative to *trans*-**Glu_brAzo1**, which arises from the additional attractive hydrogen bonding and lipophilic interactions formed between its bulky group and the receptor. Therefore, an enhanced contrast in biological activity is indeed to be expected between the two states of **Glu_brAzo2**, as originally designed.

On the basis of our experience in the synthesis of C2-bridged azobenzenes[16−21] and light-responsive glutamate ligands,[28−30] we devised a linear sequence to prepare **Glu_brAzo1-2** by Heck coupling reaction between their constituting units: a 3,3′-disubstituted diazocine and previously reported, protected glutamate derivative **1**[29] (Scheme 1). The preparation of the photochromic unit started from commercially available 4-bromo-2-nitrotoluene, **3**, which was subjected to deprotonation with potassium *tert*-butoxide and further oxidation with bromine to afford dinitro derivative **4**. When attempting common reductive ring-closing conditions on this intermediate that had been previously reported for the synthesis of diazocines (e.g., Zn, $Ba(OH)_2$),[16−21] formation of the desired bridged azobenzene was only observed with very low yields (<14%). This prompted us to develop a new methodology for the azocyclization process, for which we explored the Mills coupling reaction. With this aim, we first reduced the nitro groups of **4** using sodium sulfide,[31] which delivered diamine **5** in 90% yield. Then, the oxidative coupling of **5** was undertaken in the presence of Oxone[32] in glacial

DOI: 10.1021/acs.orglett.9b01222
Org. Lett. 2019, 21, 3780−3784

Scheme 1. Synthesis of Glu_brAzo1 and Glu_brAzo2

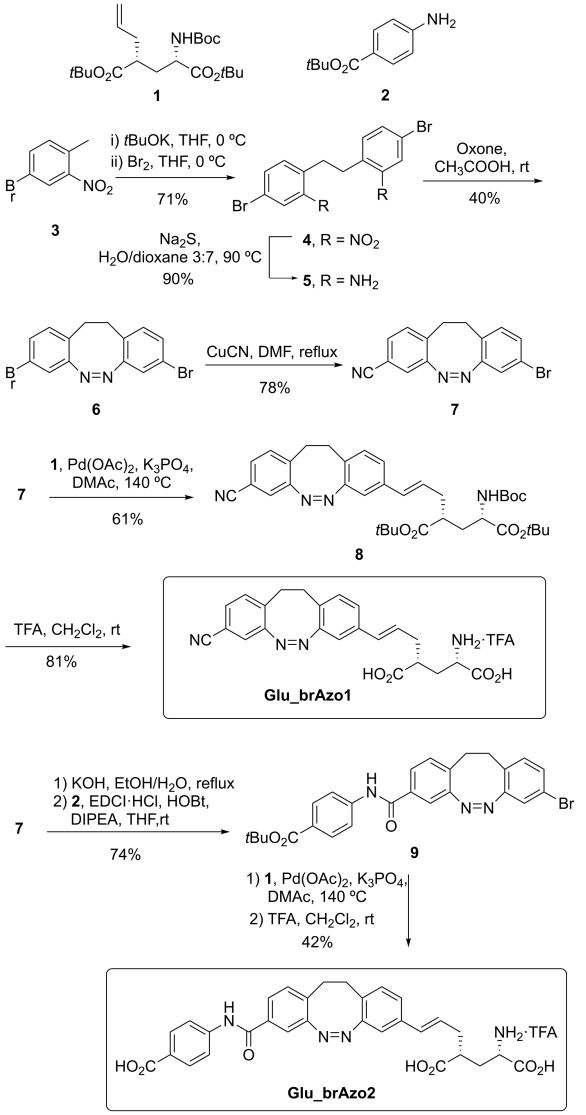

acetic acid[33] at room temperature for 1 h, which nicely furnished dibromosubstituted diazocine **6** in good yield (40%). According to this result, Oxone-mediated oxidation of one of the aniline moieties to provide the corresponding nitrosoarene followed by condensation with the other, unaltered aniline emerges as a novel one-pot synthesis of diazocines with reproducible yields.

Azobenzene **6** was next monocyanated under standard Rosenmund–von Braun conditions[34] to obtain common asymmetric diazocine **7** in 78% yield (based on recovered **6**). This compound was directly coupled to glutamate **1** under palladium catalysis, for which proper selection of the base and the solvent was found to be fundamental. After several tests, the reaction was performed with K_3PO_4 and *N*,*N*-dimethylacetamide[35] at 140 °C under argon in the presence of 0.1 mol % $Pd(OAc)_2$, which delivered **8** in 61% yield. Finally, acid removal of the protecting groups gave the target compound **Glu_brAzo1** as its monotrifluoroacetate salt in good yield. For **Glu_brAzo2**, intermediate **7** was hydrolyzed in basic medium to give the corresponding acid, which was then tethered to previously prepared amine **2** using carbodiimide coupling reagent EDCI·HCl along with HOBt to afford **9** in 74% yield for the two steps. The Heck reaction of this compound with **1** under the aforementioned conditions and subsequent removal of the protecting groups finally delivered the target PCL. It must be noted that, despite its larger structural complexity, **Glu_brAzo2** was obtained with an overall yield that is ca. 2- to 10-fold larger than those recently reported for diazocine-based PCLs,[24] thus paving the way for the general application of this strategy in photopharmacology.

By comparison with previous data reported for diazocines,[16−21] NMR and UV–vis absorption analysis confirmed the formation of the *cis* isomer of **Glu_brAzo1**-**2** due to their larger stability. In addition, upon irradiation of their n–π^* absorption band with violet light ($\lambda_{abs,max}$ ∼ 395 nm, λ_{exc} = 405 nm), spectral changes were observed indicative of *cis*–*trans* isomerization (Figure 3a and Figures S2–S4). This is the case

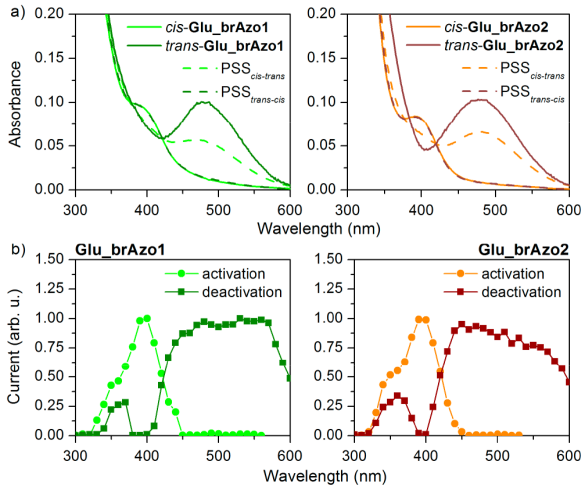

Figure 3. (a) Absorption spectra of both isomers of **Glu_brAzo1** and **Glu_brAzo2** in PBS:DMSO 1:1, as well as of the PSS mixtures obtained under *cis*–*trans* (λ_{exc} = 405 nm) and *trans*–*cis* (λ_{exc} = 532 nm) photoisomerization. (b) Activation and deactivation spectra of GluK2 in HEK293 cells after perfusion of **Glu_brAzo1** or **Glu_brAzo2** and irradiation to induce *cis*–*trans* (for activation) and *trans*–*cis* (for deactivation) photoisomerization.

of the new red-shifted absorption band found at $\lambda_{abs,max}$ ∼ 480 nm, which is distinctive of the *trans* isomer of diazocines[16−18,20−23] and allowed the isomerization process to be reverted by green light illumination (λ_{exc} = 532 nm, Figure 3a and Figures S2, S3, and S5). Further characterization of **Glu_brAzo1**-**2** revealed that they undergo *cis*–*trans* photoisomerization with moderate quantum yields ($\Phi_{cis-trans}$ ∼ 0.1) and efficiencies in aqueous media (Table S1), which resulted in photostationary state mixtures ($PSS_{cis-trans}$) containing 47% and 60% of their *trans* isomer, respectively. By contrast, *trans*–*cis* photoconversion proceeded quantitatively with high quantum yields ($\Phi_{trans-cis}$ ∼ 0.9), thus ensuring fast light-induced recovery of *cis*-**Glu_brAzo1**-**2** (Table S1) and repetitive photoswitching without degradation (Figure S6). Back-isomerization of the *trans* state of these compounds was also found to occur in the dark, though at a much longer time

DOI: 10.1021/acs.orglett.9b01222
Org. Lett. 2019, 21, 3780–3784

scale ($t_{1/2}$ ~ 4 h at 298 K in aqueous media, Figure S7 and Table S1).

To assess the capacity of **Glu_brAzo1-2** to light-gate GluRs, whole-cell voltage clamp recordings were conducted on HEK293 cells expressing GluK1 or GluK2, whose activation causes channel opening and ion flux across the membrane (Figure 1b).[3,5] After perfusion of **Glu_brAzo1-2**, clear changes in the currents evoked in these cells were observed upon irradiation, which were consistent with the different absorption properties of their *cis* and *trans* isomers (Figure 3b and Figures S8–S10). In particular, maximal inward currents arising from receptor activation were measured at λ_{exc} = 390–400 nm (i.e., when inducing *cis*–*trans* photoisomerization of the PCLs). Minimal signals due to receptor deactivation were instead detected in the dark (i.e., for *cis*-**Glu_brAzo1-2**) and at λ_{exc} > 450 nm (i.e., upon *trans*–*cis* photoisomerization). As predicted by our molecular docking calculations, preferential interaction between the glutamate agonist ligand and GluK1/GluK2 was therefore observed for the *trans* state of **Glu_brAzo1-2**, which allowed light-induced manipulation of these receptors.

The *trans*-active behavior of **Glu_brAzo1-2** was further demonstrated when measuring their dose–response curves with GluK1 and GluK2 in the dark and at λ_{exc} = 390 (10–300 μM, Figure S11). In all the cases, larger inward current signals were retrieved for the $PSS_{cis-trans}$ mixture generated upon irradiation of the initial *cis* isomer, though with (a) low-to-moderate photoinduced modulation (ca. 10–35% current increase with respect to the dark) and (b) maximal values that were only about 20–40% of those evoked by free glutamate at 300 μM. Three main factors should account for these results: incomplete photoconversion into the active *trans* isomer, as observed in solution (<60%, Table S1); limited modification of the glutamate-binding site affinity upon *cis*–*trans* isomerization; and the steric effects imparted by the appended diazocine group with respect to free glutamate even in its less hindered *trans* configuration, which are of especial importance for GluK2 interaction because of its narrower ligand-binding cavity.[25] Actually, the latter accounts for the lower inward current signals with higher light-induced selectivity obtained for this receptor. However, it did not prevent **Glu_brAzo2** that bears a bulkier terminal group from (a) showing higher activity (ca. 2-fold increase with respect to **Glu_brAzo1** for GluK2), as anticipated by our molecular docking simulations, which (b) is further modulated upon photoisomerization, as pursued in our initial design.

Glu_brAzo1-2 were finally tested as photoswitchable neurotransmitters in hippocampal neurons where GluK2 is highly expressed.[36] Because of their *trans*-active, *cis*-stable behavior, physiological behavior was not altered upon perfusion of **Glu_brAzo1-2** in the dark, a clear advantage over most PCLs reported for GluRs to date such as **GluAzo**.[5–11] Neuronal firing was instead selectively induced upon *cis*–*trans* photoisomerization of **Glu_brAzo2** at relatively low concentrations (30 μM, Figure 4a–c) and weak light intensities (22.0 and 47.4 μW mm^{-2} at λ_{exc} = 390 and 530 nm, respectively). As a result, sequential and sustained trains of action potentials could be triggered with **Glu_brAzo2** by consecutively switching between violet and green light illumination, even at low irradiation powers and high excitation frequencies (up to 1 Hz, Figure 4c). Interestingly, this photoinduced behavior was inhibited by addition of DNQX,[37] a well-known antagonist of kainate and AMPA GluRs (Figure 4d), which further demonstrates that the efficient photoactivation of hippocampal neurons accomplished with **Glu_brAzo2** arose from its light-dependent interaction with those glutamate receptors. Noticeably, this clean physiological effect was achieved despite the limited activity modulation measured upon **Glu_brAzo2** photoisomerization in GluK2-expressing HEK293 cells (ca. 20% at 30 μM concentration), while it could not be reproduced with the slightly less efficient **Glu_brAzo1** agonist (Figure S12). We ascribe this situation to the well-known nonlinear behavior of neuronal signaling, since ligand interaction with a minimum fraction of glutamate receptors is needed to overcome the depolarization threshold required to initiate an action potential.[5] In our case, such a threshold was only surpassed with *trans*-**Glu_brAzo2**, probably due to its larger affinity for GluK2, as suggested by our measurements in cultured cells.

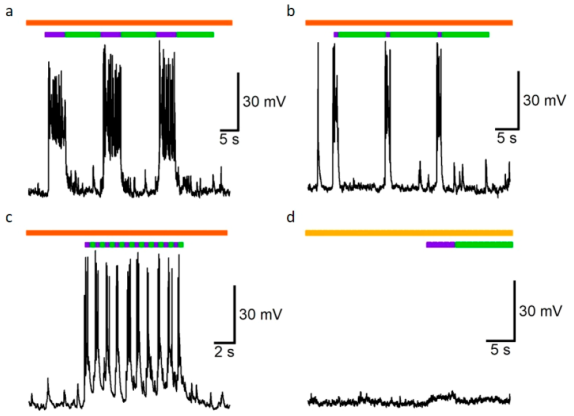

Figure 4. Whole-cell current clamp recordings of rat hippocampal neurons in culture after perfusion of **Glu_brAzo2** (30 μM) and irradiation at λ_{exc} = 390 (purple) and 530 (green) nm. Successful neuron activation was observed with 390 nm light pulses of (a) 5 s, (b) 1s, and (c) 0.5 s (1 Hz stimulation), while it was inhibited upon perfusion of DNQX (10 μM). Neurons were current clamped at −60 mV, and to truly report on their GluK2-mediated gating and connectivity, no concanavalin A was used to prevent receptor desensitization after activation.

In conclusion, we demonstrated in this work the potential of C2-bridged azobenzenes for the preparation of azo-based photochromic ligands capable of light-controlling neural receptors, which preserve the larger activity typically observed for their *trans* state while ensuring larger stability for the inert *cis* isomer. By introducing a novel synthetic methodology for the preparation of 3,3′-disubstituted diazocines based on an Oxone-mediated intramolecular azocyclization reaction, the desired ligands could be obtained with higher yields and larger versatility, thus enabling fine-tuning of their light-dependent biological response. As a proof of concept, this strategy was applied to the preparation of new photoswitchable neurotransmitters for the light-induced operation of kainate glutamate receptors, with which we achieved selective neural firing upon irradiation without background activity in the dark.

■ ASSOCIATED CONTENT

Supporting Information

The Supporting Information is available free of charge on the ACS Publications website at DOI: 10.1021/acs.orglett.9b01222.

DOI: 10.1021/acs.orglett.9b01222
Org. Lett. 2019, 21, 3780–3784

Organic Letters Letter

General methods and materials, synthetic procedures, and additional computational, photochemical, and electrophysiological data (PDF)

AUTHOR INFORMATION

Corresponding Authors

*E-mail: pau@icrea.cat.
*E-mail: jordi.hernando@uab.cat.

ORCID

Àngels González-Lafont: 0000-0003-0729-2483
José M. Lluch: 0000-0002-7536-1869
Rainer Herges: 0000-0002-6396-6991
Ramon Alibés: 0000-0002-7997-2691
Pau Gorostiza: 0000-0002-7268-5577
Jordi Hernando: 0000-0002-1126-4138

Author Contributions

▽G.C. and A.G-.C. contributed equally.

Notes

The authors declare no competing financial interest.

ACKNOWLEDGMENTS

We acknowledge financial support from MINECO/FEDER (Projects CTQ2015-65439-R, CTQ2016-80066-R, CTQ2016-75363-R, and CTQ2017-83745-P), AGAUR/Generalitat de Catalunya (CERCA Programme and Projects 2017-SGR-00465 and 2017-SGR-1442), Human Brain Project WAVE-SCALES projects, Fundaluce foundation, and Deutsche Forschungsgemeinschaft (SFB677). G.C. acknowledges the Generalitat de Catalunya for her predoctoral FI grant. A.G.-C. was supported by fellowship BES-2014-068169.

REFERENCES

(1) (a) Deisseroth, K. *Nat. Methods* **2011**, *8*, 26−29. (b) Deisseroth, K. *Nat. Neurosci.* **2015**, *18*, 1213−1225.
(2) (a) Gorostiza, P.; Isacoff, E. Y. *Science* **2008**, *322*, 395−399. (b) Fehrentz, T.; Schonberger, M.; Trauner, D. *Angew. Chem., Int. Ed.* **2011**, *50*, 12156−12182. (c) Kramer, R. H.; Mourot, A.; Adesnik, H. *Nat. Neurosci.* **2013**, *16*, 816−823. (d) Velema, W. A.; Szymanski, W.; Feringa, B. L. *J. Am. Chem. Soc.* **2014**, *136*, 2178−2191. (e) Berlin, S.; Isacoff, E. Y. *EMBO Rep.* **2017**, *18*, 677−692. (f) Hüll, K.; Morstein, J.; Trauner, D. *Chem. Rev.* **2018**, *118*, 10710−10747.
(3) (a) Traynelis, S. F.; Wollmuth, L. P.; McBain, C. J.; Menniti, F. S.; Vance, K. M.; Ogden, K. K.; Hansen, K. B.; Yuan, H.; Myers, S. J.; Dingledine, R. *Pharmacol. Rev.* **2010**, *62*, 405−496. (b) Niswender, C. M.; Conn, P. J. *Annu. Rev. Pharmacol. Toxicol.* **2010**, *50*, 295−322. (c) Bowie, D. *CNS Neurol. Disord.: Drug Targets* **2008**, *7*, 129−143.
(4) Reiner, A.; Levitz, J.; Isacoff, E. Y. *Curr. Opin. Pharmacol.* **2015**, *20*, 135−143.
(5) Volgraf, M.; Gorostiza, P.; Szobota, S.; Helix, M. R.; Isacoff, E. Y.; Trauner, D. *J. Am. Chem. Soc.* **2007**, *129*, 260−261.
(6) Stawski, P.; Sumser, M.; Trauner, D. *Angew. Chem., Int. Ed.* **2012**, *51*, 5748−5751.
(7) Pittolo, S.; Gómez-Santacana, X.; Eckelt, K.; Rovira, X.; Dalton, J.; Goudet, C.; Pin, J. P.; Llobet, A.; Giraldo, J.; Llebaria, A.; Gorostiza, P. *Nat. Chem. Biol.* **2014**, *10*, 813−815.
(8) Rovira, X.; Trapero, A.; Pittolo, S.; Zussy, C.; Faucherre, A.; Jopling, C.; Giraldo, J.; Pin, J.-P.; Gorostiza, P.; Goudet, C.; Llebaria, A. *Cell Chem. Biol.* **2016**, *23*, 929−934.
(9) Barber, D. M.; Liu, S. A.; Gottschling, K.; Sumser, M.; Hollmann, M.; Trauner, D. *Chem. Sci.* **2017**, *8*, 611−615.
(10) Gómez-Santacana, X.; Pittolo, S.; Rovira, X.; Lopez, M.; Zussy, C.; Dalton, J. A. R.; Faucherre, A.; Jopling, C.; Pin, J.-P.; Ciruela, F.; Goudet, C.; Giraldo, J.; Gorostiza, P.; Llebaria, A. *ACS Cent. Sci.* **2017**, *3*, 81−91.
(11) Hartrampf, F. W. W.; Barber, D. M.; Gottshcling, K.; Leippe, P.; Hollmann, M.; Trauner, D. *Tetrahedron* **2017**, *73*, 4905−4912.
(12) Laprell, L.; Repak, E.; Franckevicius, V.; Hartrampf, F.; Terhag, J.; Hollmann, M.; Sumser, M.; Rebola, N.; DiGregorio, D. A.; Trauner, D. *Nat. Commun.* **2015**, *6*, 8076.
(13) Bandara, H. M. D.; Burdette, S. C. *Chem. Soc. Rev.* **2012**, *41*, 1809−1825.
(14) Abrams, Z. R.; Warrier, A.; Trauner, D.; Zhang, X. *Front. Neural Circuits* **2010**, *4*, 13.
(15) Reiter, A.; Skerra, A.; Trauner, D.; Schiefner, A. *Biochemistry* **2013**, *52*, 8972−8974.
(16) Siewertsen, R.; Neumann, H.; Buchheim-Stehn, B.; Herges, R.; Nather, C.; Renth, F.; Temps, F. *J. Am. Chem. Soc.* **2009**, *131*, 15594−15595.
(17) Sell, H.; Nather, C.; Herges, R. *Beilstein J. Org. Chem.* **2013**, *9*, 1−7.
(18) Tellkamp, T.; Shen, J.; Okamoto, Y.; Herges, R. *Eur. J. Org. Chem.* **2014**, *2014*, 5456−5461.
(19) Hammerich, M.; Schütt, C.; Stahler, C.; Lentes, P.; Rohricht, F.; Höppner, R.; Herges, R. *J. Am. Chem. Soc.* **2016**, *138*, 13111−13114.
(20) Moormann, W.; Langbehn, D.; Herges, R. *Synthesis* **2017**, *49*, 3471−3475.
(21) Moormann, W.; Langbehn, D.; Herges, R. *Beilstein J. Org. Chem.* **2019**, *15*, 727−732.
(22) Samanta, S.; Qin, C. G.; Lough, A. J.; Woolley, G. A. *Angew. Chem., Int. Ed.* **2012**, *51*, 6452−6455.
(23) (a) Joshi, D. K.; Mitchell, M. J.; Bruce, D.; Lough, A. J.; Yan, H. *Tetrahedron* **2012**, *68*, 8670−8676. (b) Eljabu, F.; Dhruval, J.; Yan, H. *Bioorg. Med. Chem. Lett.* **2015**, *25*, 5594−5596. (c) Jun, M.; Joshi, D. K.; Yalagala, R. S.; Vanloon, J.; Simionescu, R.; Lough, A. J.; Gordon, H. L.; Yan, H. *ChemistrySelect* **2018**, *3*, 2697−2701.
(24) Thapaliya, E. R.; Zhao, J.; Ellis-Davies, G. C. R. *ACS Chem. Neurosci.* **2019**, in press. DOI: 10.1021/acschemneuro.8b00734
(25) Mayer, M. L. *Neuron* **2005**, *45*, 539−552.
(26) Guo, Y.; Wolter, T.; Kubar, T.; Sumser, M.; Trauner, D.; Elstner, M. *PLoS One* **2015**, *10*, No. e0135399.
(27) Eldridge, M. D.; Murray, C. W.; Auton, T. R.; Paolini, G. V.; Mee, R. P. *J. Comput.-Aided Mol. Des.* **1997**, *11*, 425−445.
(28) Izquierdo-Serra, M.; Gascón-Moya, M.; Hirtz, J. J.; Pittolo, S.; Poskanzer, K. E.; Ferrer, È.; Alibés, R.; Busqué, F.; Yuste, R.; Hernando, J.; Gorostiza, P. *J. Am. Chem. Soc.* **2014**, *136*, 8693−8701.
(29) Gascón-Moya, M.; Pejoan, A.; Izquierdo-Serra, M.; Pittolo, S.; Cabré, G.; Hernando, J.; Alibés, R.; Gorostiza, P.; Busqué, F. *J. Org. Chem.* **2015**, *80*, 9915−9925.
(30) Cabré, G.; Garrido-Charles, A.; Moreno, M.; Bosch, M.; Porta-de-la-Riva, M.; Krieg, M.; Gascón-Moya, M.; Camarero, N.; Gelabert, R.; Lluch, J. M.; Busqué, F.; Hernando, J.; Gorostiza, P.; Alibés, R. *Nat. Commun.* **2019**, *10*, 907.
(31) Mourot, A.; Kienzler, M. A.; Banghart, M. R.; Fehrentz, T.; Huber, F. M. E.; Stein, M.; Kramer, R. H.; Trauner, D. *ACS Chem. Neurosci.* **2011**, *2*, 536−543.
(32) Yu, B. C.; Shirai, Y.; Tour, J. M. *Tetrahedron* **2006**, *62*, 10303−10310.
(33) Davey, H. H.; Lee, V. Y.; Miller, R. D.; Marks, T. J. *J. Org. Chem.* **1999**, *64*, 4976−4979.
(34) Friedman, L.; Shechter, H. *J. Org. Chem.* **1961**, *26*, 2522−2524.
(35) Yao, Q.; Kinney, E. P.; Yang, Z. *J. Org. Chem.* **2003**, *68*, 7528−7531.
(36) Carta, M.; Fièvre, S.; Gorlewicz, A.; Mulle, C. *Eur. J. Neurosci.* **2014**, *39*, 1835−1844.
(37) Honore, T.; Davies, S. N.; Drejer, J.; Fletcher, E. J.; Jacobsen, P.; Lodge, D.; Nielsen, F. E. *Science* **1988**, *241*, 701−703.

DOI: 10.1021/acs.orglett.9b01222
Org. Lett. 2019, 21, 3780−3784

3.5 Co-Polymerization of Diazocines

Stress indication is one of many interesting applications, which can be envisioned by the incorporation of mechanochromic mechanophores into materials. These mechanophores change their color upon the application of stress. When incorporated into a material in a corresponding ratio, this color change should be visible to the eye and could possibly prevent accidents caused by material exhaustion. To achieve this, thin stress indicating films need to be deposited on the chosen material. Common wetchemistry polymerization is limited in precision and reproducibility with respect to film thickness and the use of solvents prevents the applicability on chemically sensitive materials.[71, 72]

Thin film fabrication *via* initiated chemical vapor deposition (iCVD) is a promising solvent-free method, allowing the production of well-defined thin films on 3D structures from the gas phase (**Figure 3.5.1**).[73, 74] A number of functional coatings have been achieved,[75–78] raising the question if suitable photo- and/or mechanoswitchable molecules can be polymerized from the gas phase using iCVD.

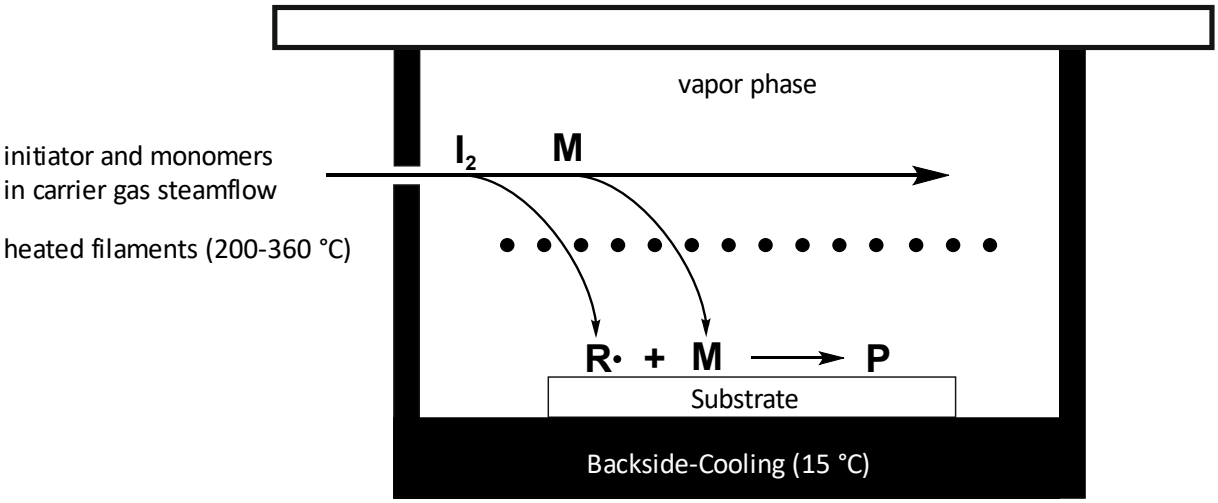

Figure 3.5.1: Preheated N_2 is used as carrier gas to transport both initiator and monomers into the iCVD reactor. The initiator is thermally decomposed by the high temperatures of the heated filaments (200-360 °C). Formed radicals and monomers are adsorbed from the vapor phase onto the surface and thus enable polymerization upon the substrate.[75, 79]

3.5.1 Summary of Fabrication of Diazocine-based photochromic organic thin films *via* initiated Chemical Vapor Deposition

The bifunctional styrenediazocine was used for the synthesis of photoswitchable co-polymer thin films *via* initiated chemical vapor deposition (iCVD). This was possible because the styrenediazocine has a relatively low melting point of 98 °C allowing the use in iCVD as tested prior to the polymerization by sublimation. After initiation with di-*tert*-butylperoxide (DTPO), the styrenediazocine was co-polymerized, using 1,3,5-trivinyl-1,3,5-trimethylcyclotrisiloxane (V_3D_3), a commonly used monomer for the synthesis of highly cross-linked organosilicon thin films (**Figure 3.5.2 a**). The customized reactor enabled the synthesis of co-polymer thin films with an average roughness of 2.57 nm (+/- 0.06 nm), showing the homogeneity of the deposition. The composition of V_3D_3 and styrenediazocine at a ratio of 2.4:1 was confirmed in XPS and FT-IR measurements. The photochemical properties of the polymerized diazocine was investigated by UV-vis spectroscopy. Reversible isomerization was applicable and visible to the bare eye (**Figure 3.5.2 b**). This work has proven that diazocines can be used to produce thin films by the use of iCVD and switching inside the polymer is possible.

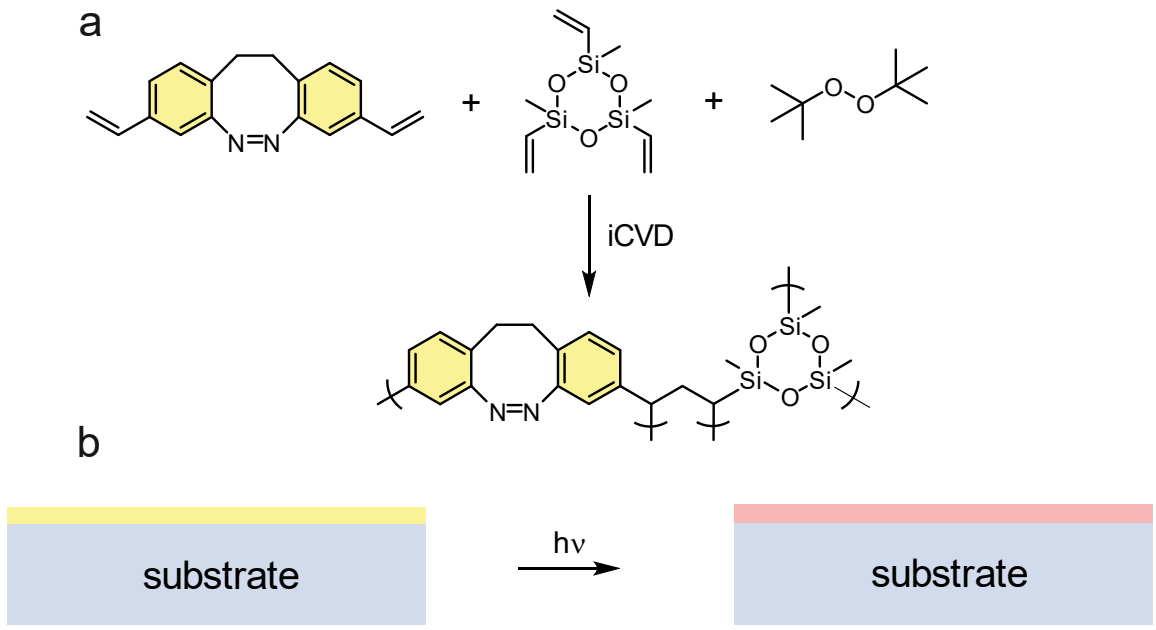

Figure 3.5.2: a) The polymerization of V_3D_3 and bifunctional styrenediazocine was initiated through DTPO, resulting in a highly cross-linked co-polymer. b) The diazocine-containing co-polymer appears yellow and changes its color upon irradiation, confirming successful switching of the diazocine inside the polymer.

3.5.2 Fabrication of Diazocine-based photochromic organic thin films *via* initiated Chemical Vapor Deposition

Maximilian Heiko Burk, Stefan Schröder, Widukind Moormann, Daniel Langbehn, Thomas Strunskus, Stefan Rehders, Rainer Herges and Franz Faupel

Accepted at Macromolecules

Scientific contribution to this paper

The synthesis of bifunctional styrenediazocine was performed by me. Polymer synthesis and the iCVD setup was developed and carried out by Burk and co-workers.

* Unknown * | ACSJCA | JCA11.2.5208/W Library-x64 | manuscript.3f (R5.0.i2:5002 | 2.1) 2020/01/15 13:43:00 | PROD-WS-120 | rq_2261812 | 2/05/2020 10:23:39 | 7 | JCA-DEFAULT

Macromolecules

pubs.acs.org/Macromolecules Article

Fabrication of Diazocine-Based Photochromic Organic Thin Films via Initiated Chemical Vapor Deposition

Maximilian H. Burk, Stefan Schröder, Widukind Moormann, Daniel Langbehn, Thomas Strunskus, Stefan Rehders, Rainer Herges,* and Franz Faupel*

Cite This: https://dx.doi.org/10.1021/acs.macromol.9b02443 Read Online

ACCESS | Metrics & More | Article Recommendations

ABSTRACT: In this work, we demonstrate the first synthesis of photochromic polymer thin films via initiated chemical vapor deposition (iCVD) using bifunctional, crystalline styrenediazocine as a photochromic unit. Since it represents a solid compound, an innovative custom-made sublimation unit is introduced, which allows the sublimation of the chromophore as well as its transport inside the reactor chamber, maintaining the functionality of the photoswitch. Styrenediazocine was co-polymerized with 1,3,5-trivinyl-1,3,5-trimethylcyclotrisiloxane (V_3D_3), a heterocycle with triple vinyl functionality, in a radical polymerization reaction from the gas phase. The structural as well as functional properties of the resulting films were characterized by various methods, including X-ray photoelectron spectroscopy (XPS), Fourier-transform infrared (FT-IR) spectroscopy, and UV−vis spectroscopy. It could be confirmed that, via iCVD, photoswitchable polymer thin films have been obtained. The polymer is based on a copolymer structure where all photoswitchable molecules are covalently bonded in the main polymer chain. Our approach could pave the way for a completely new class of high-quality, photochromic thin films that are basically applicable on almost every kind of substrate for novel, interdisciplinary application fields, where particularly classical wet chemistry methods cannot be applied.

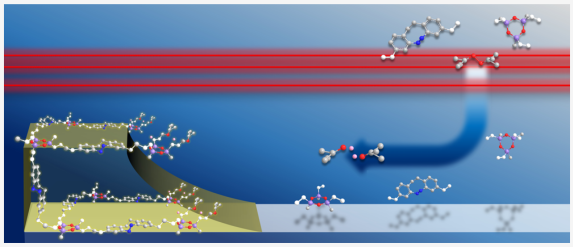

1. INTRODUCTION

Photoswitchable polymer thin films are of high interest because, upon irradiation with monochromatic light, their shape can be reversibly changed between two stable states.[1−5] The process of photoisomerization leads to a substantial change in the physical properties of a chromophoric compound such as absorption, fluorescence, dipole moment, or electric conductivity, which is desirable to be exploited on the macromolecular scale.[5,6] In the context of materials science, one critical prerequisite for a potential photoswitch must be the bistability of properties, meaning that both isomers can be sharply distinguished after interconverting into each other. Based on the fact that light as an external stimulus represents an eco-friendly, sustainable and fast way to power these motions, functional photochromic polymers find implementation in areas such as labeling, electronic displays, or functional membranes, and they are promising candidates for the development of novel devices on the nanoscale.[5−9] Notwithstanding the high potential of photoswitchable polymer thin films, one must consider that photoisomerization of chromophores in solids is far more complicated compared to their switching behavior in solution. Their half-life in the metastable state fundamentally depends on their bonding inside the polymer, either as part of the main chain or as a side-group attached to it, as well as the density of the polymer matrix.[10] Besides chemical synthesis, reproducible deposition of photoswitchable polymers is essential to transfer the unique properties of the thin film to desired substrate materials. Common thin film fabrication methods like drop-casting, spin-coating, or dip-coating offer fast and uncomplicated handling but lack high precision and reproducibility over the resulting film thickness, especially on the nanometer scale. Moreover, they require the additional use of solvents, making the coating of chemically sensitive materials practically impossible.[2,11,12] In recent years, the polyelectrolyte multilayer method (PEM) introduced by Decher et al. has gained increasing interest for the deposition of chromophore-containing polymer thin films. PEM allows the creation of thin films in the nm range but restricts the choice of potential chromophores as well as polymers to only water-soluble components. The poor reproducibility and low quality of the resulting films exclude the PE method when it comes to the coating of surface-sensitive materials whose topography must be kept intact.[13] In contrast to the previously mentioned fabrication methods,

Received: November 22, 2019
Revised: January 17, 2020

https://dx.doi.org/10.1021/acs.macromol.9b02443
Macromolecules XXXX, XXX, XXX−XXX

initiated chemical vapor deposition (iCVD) seems to be a promising, versatile technology for future developments.

iCVD gained a steadily increasing interest in the area of surface engineering due to the fact that it is possible to create well-defined polymer thin films directly from the gas phase with almost complete preservation of the monomer's functionality and without the need for additional solvents.[14] In general, a heated precursor stream consisting of monomer and initiator species is led through a hot metal filament at low pressure, resulting in thermal decomposition of the corresponding initiator. Both monomer and activated initiator impinge on the cooled substrate mounted below the filament plane, resulting in a radical polymerization reaction directly on the material to be coated.[15−17] In contrast to conventional wet chemistry methods, no solvents are needed and the topography of the substrate is fully preserved, enabling the addition of functional polymer layers to three-dimensional (3D) structures without any purification steps after deposition.[17,18] The modification of surfaces with functional polymers, such as pH-responsive hydrogels with swelling properties, ultrahydrophobic fluorocarbon polymers in the context of dielectric layers, or coatings for controlled drug release, in the nano range via iCVD has been intensively investigated so far.[14,19−24] Even though the fabrication of a manifold of different polymers via iCVD has been intensely investigated in the past, deposition of photoswitchable layers has not been reported yet. Coclite et al. demonstrated the deposition of poly(2-hydroxyethyl methacrylate) (pHEMA)-hydrogels via iCVD followed by post-reactional functionalization with common azobenzenes.[25] Their main aim was the synthesis of a multiresponsive polymer thin film reacting on external stimuli, like the change of pH level and irradiation with light, with expansion and contraction of the polymer matrix. Although their work shows in an impressive way the topicality of the approach, one would assume that co-polymerization of the chromophore directly within the iCVD process holds great potential for the development of novel hybrid systems on the nanoscale, whereas the resulting thin films would react to stimuli predefined by the characteristic functional groups of the used components. In our work, the photoswitchable compound of choice is represented by a functional diazocine. Diazocine represents an azobenzene-related compound with an eight-membered heterocyclic ring as the central unit, which results in higher stiffness and more efficient power transmission to the environment, which is an advantage in materials science.[26−28] In contrast to azobenzene, diazocines are thermodynamically more stable in their *Z* configuration, which is a further advantage in actuator and mechanophore applications. Upon irradiation with violet light (385−400 nm), the bent *Z* configuration converts to the extended *E* isomer (Figure 1).

Back-isomerization is very efficiently affected by blue light (500 nm). At room temperature also a slow thermal back-reaction to a more stable *Z* isomer occurs.[27,29]

Moreover, both isomers of diazocine in bulk crystalline form or dissolved in solution can be distinguished by their specific color: The *Z* isomer possesses a yellow color, whereas the *E* isomer exhibits a red color, and the color change can be observed with the bare eye. The absorption bands of the two isomers are well separated from each other, making them excellent candidates for optical and mechanical sensing.[26−28]

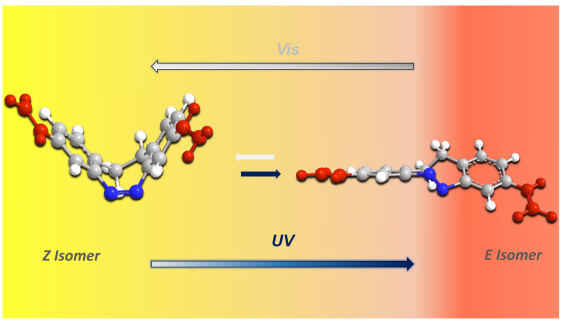

Figure 1. Structure and photoisomerization of the used styrenediazocine upon irradiation with UV light. The functional vinyl groups are marked in red. The absorption spectra of diazocines drastically change after switching compared to common azobenzenes, whereas the *Z* Isomer appears yellow, and the *E* Isomer exhibits a reddish color. Photoinduced motion results in expansion/contraction of the chromophore, making it an interesting candidate for future mechanistic studies.[26−29]

2. EXPERIMENTAL SECTION

A heterocyclic compound with triple vinyl functionality, 1,3,5-trimethylcyclotrisiloxane (V_3D_3) (abcr GmbH), was co-polymerized with a custom-made styrenediazocine, a novel functional chromophore synthesized and published recently by Moormann et al.[30] The radical polymerization reaction was carried out with di-*tert*-butyl peroxide (TBPO) (Tokyo Chemical Industry) as an initiator in a custom-build iCVD reactor similar to a setup as described by Gleason et al.[14] The fluid precursors were preheated in separate jars and delivered inside the reactor chamber under low-pressure conditions, and their flows were maintained using needle valves. Then, 20 mg of the solid chromophore was dissolved in 5 mL of acetone (Sigma-Aldrich) and fed into the sublimation unit using a syringe. All chemicals were used without further purification. For transportation of the photoswitch inside the reactor chamber via an inert carrier gas, a custom-built sublimation unit was implemented (Figure 2).

The flow rates of the used species were set as follows, where the flow used for the chromophore is represented by the N_2 carrier-gas flow: $F_{V_3D_3}$ = 0.80 sccm, F_{TBPO} = 0.40 sccm, F_{N_2} = 15.0 sccm. The substrates to be coated were cooled to 15 °C by backside contact with a cooling table. A process pressure of 50 pa was maintained using a butterfly valve.

The used NiCr filaments (Goodfellow, Ø 0.5 mm, 20 wt % Cr) were mounted parallel to the sample stage and powered by an external power supply, which was set to a voltage of 15.5 V and a current of 1.9 A. ^{1}H NMR spectra were recorded at 300 K with a Bruker AVANCE III HD 400 MHz Pulse Fourier-transform (FT) spectrometer and referenced to the residual solvent signal from acetone. Raman measurements were done on a WiTec RA300 device with a green and red laser, exhibiting excitation wavelengths of 532 and 633 nm, respectively. Ellipsometry measurements for determination of thin film quality, photoswitchability, and thermal relaxation were carried out using a J. A. Woollam M-2000 Spectroscopic Ellipsometer.

To induce photoswitching, a custom-made device with an ultraviolet light-emitting diode (UV-LED) (365 nm, 14 mW/cm^2) was used with an irradiation time of 18 min. Backswitching was done using a Labino Wh Midlight H135 lamp with an irradiation time of 10 min. The distance of the light source to the samples was 10 mm. X-ray photoelectron spectroscopy (XPS) was conducted on an Omicron Nanotechnology GmbH device with a VG Microtech XR3E2 aluminum anode. UV−vis spectroscopy was carried out on a PerkinElmer UV/vis/NIR Lambda 900 device. FT-IR spectra were recorded with a Bruker Vertex 80 V.

https://dx.doi.org/10.1021/acs.macromol.9b02443
Macromolecules XXXX, XXX, XXX−XXX

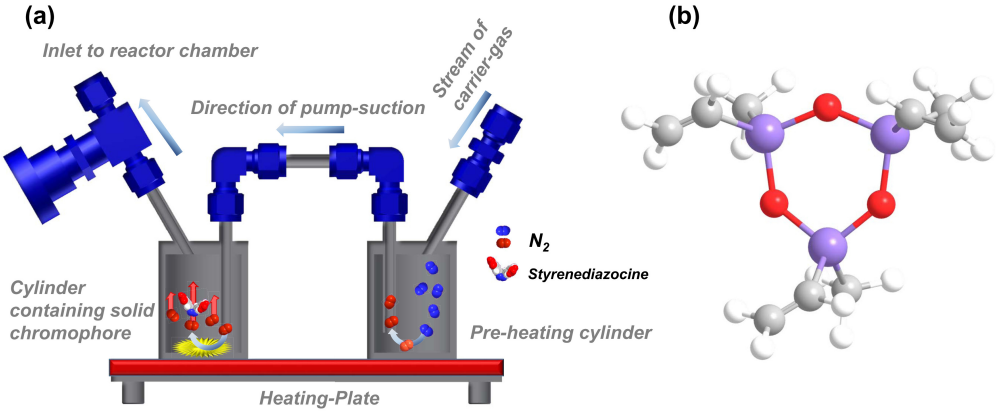

Figure 2. (a) Setup of the introduced sublimation unit for transportation of styrenediazocine inside the reactor chamber. An inert stream of N_2 is used as a carrier gas and preheated in an upstream steel cylinder to prevent unwanted condensation. After heating up, N_2 is led into the downstream cylinder, where it impinges on the solid compound. Due to the low-pressure conditions and direction of the pump suction, styrenediazocine is driven into the reactor chamber. (b) Chemical structure of V_3D_3, exhibiting three functional vinyl groups.

3. RESULTS AND DISCUSSION

3.1. Pre-Deposition: Verification of the Chromophore's Functionality in the Context of iCVD Processing. Before co-polymerization and thin film deposition, it is mandatory to prove that the used chromophore is compatible with the prevailed iCVD process parameters such as temperature, low-pressure environment, and the hot filament. To check this, styrenediazocine was sublimed, making use of the aforementioned sublimation system under iCVD-deposition conditions without an additional monomer or initiator. The compound obtained after condensation deposition on the Si wafers was investigated via ^{1}H NMR spectroscopy (Figure 3) as well as Raman spectroscopy (Figure 4) to verify relevant functional chemical groups that need to be preserved to enable co-polymerization.

The results of ^{1}H NMR spectroscopy show the multiplets of the H-atoms of the C−C double bond, clearly indicating that the vinyl functionality of the chromophore was preserved. In addition to that, Raman spectra of both bulk and condensed styrenediazocine showed a characteristic double peak at around 1620 cm^{-1}, assigned to the N−N double bond of the azo group. The overall results reveal that the used chromophore is stable under iCVD conditions since the relevant vinyl groups, elementary for the radical polymerization reaction, as well as the azo group were maintained after sublimation and recondensation.

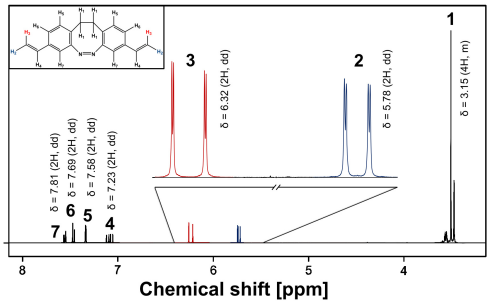

Figure 3. ^{1}H NMR spectrum of condensed styrenediazocine after processing in the sublimation unit, where all peaks are similar to the unprocessed compound. The signals at δ = 5.78 and 6.32 ppm, respectively, can be assigned to the chemical shift of the H-atom bonding to the two symmetric vinyl groups of the photoswitchable compound. This leads to the assumption that all relevant chemical groups present in the solid compound before sublimation are preserved after processing.

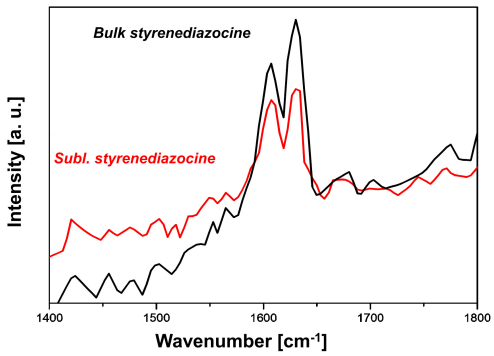

Figure 4. Raman spectra of bulk (crystalline) as well as sublimed styrenediazocine. Both exhibit a double peak at 1620 cm^{-1}, which can be assigned to the N−N double bond, characteristic of the photoactive azo group of the chromophore.

3.2. iCVD of V_3D_3 and Styrenediazocine. Due to the number of functional vinyl groups in both monomers, the overall structure of the expected three-dimensional copolymer was assumed to be highly cross-linked with a free volume above the average and low density of the polymer matrix, facilitating photoswitching in solid thin films (Figure 5).

The resulting layers were investigated in terms of structural as well as chemical composition and tested on their ability to undergo photoisomerization. As determined by ellipsometry, an average deposition rate of 400 nm/h was achieved with an average roughness of 2.57 nm (±0.06 nm), demonstrating the overall homogeneity of the resulting thin film.

Thin films to be investigated exhibited a thickness of 400 nm. By simply putting a mask on a substrate, patterned photochromic coatings, as well as homogeneous thin films on larger substrates, are possible.

https://dx.doi.org/10.1021/acs.macromol.9b02443
Macromolecules XXXX, XXX, XXX−XXX

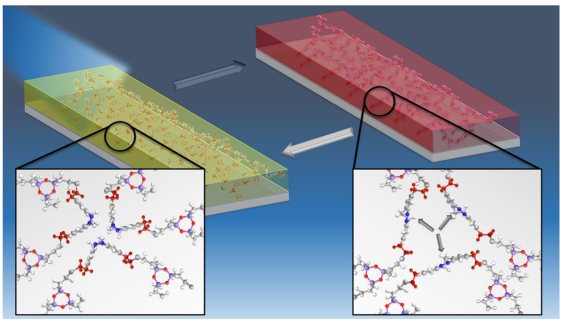

Figure 5. Schematic representation of the resulting polymer thin film on the molecular scale with the incorporated photoswitch. Diazocine experiences reversible expansion/contraction upon irradiation, which can be seen by the bare eye due to the change of the specific color. For better visibility, only a small part of the macromolecule is shown.

Via XPS measurements, specific elements and bonds of the used compounds, as well as their quantitative content in the copolymer layer, were verified (Figure 6).

The results strongly indicate that both the co-monomer and chromophore are present in the deposited layer (Figure 6a,b). A detailed quantitative investigation of the nitrogen peak as well as the silicon peak allowed conclusions about the ratio of the photoswitch compared to V_3D_3 inside the thin film (Figure 6c–e). Given that a homogeneous distribution of the copolymer film in the XPS probing region is expected, quantitative analysis showed that nitrogen, present in styrenediazocine only, made up a proportion of 21.5 au compared with silicon, present in V_3D_3 only, with 78.5 au. The chemical structures of both monomers displayed in Figure 6d show the stoichiometry of silicon and nitrogen in each of the compounds, which can be used to calculate the ratio of the chromophore to the co-monomer inside the polymer matrix. Derived from that assumption, a ratio of styrenediazocine to V_3D_3 of 1:2.4 results.

Since iCVD basically constitutes a radical polymerization from the gas phase, specific vibrations of the vinyl groups must be in the focus of investigation to further determine if a monomer-consuming polymerization with resulting covalent bonding took place. Therefore, high-resolution FT-IR spectroscopy was conducted to characterize the functional chemical groups of the used precursors as well as the copolymer, to compare specific vibrations before and after iCVD-deposition (Figure 7).

The FT-IR spectra of the investigated compounds provide two major insights about the chemical bonds of the precursors and the expected copolymer: first, vibrations of V_3D_3 at 1020 and 2952 cm^{-1}, as well as vibrations of styrenediazocine located at 2850 and 2925 cm^{-1}, are present in the expected copolymer, which are consistent with the findings of the XPS analysis. Second, and most important, stretching vibrations of the vinyl group above 3000 cm^{-1} and bending vibrations in the fingerprint region below 1000 cm^{-1} that can be seen in the spectrum of the unprocessed photoswitch completely dis-

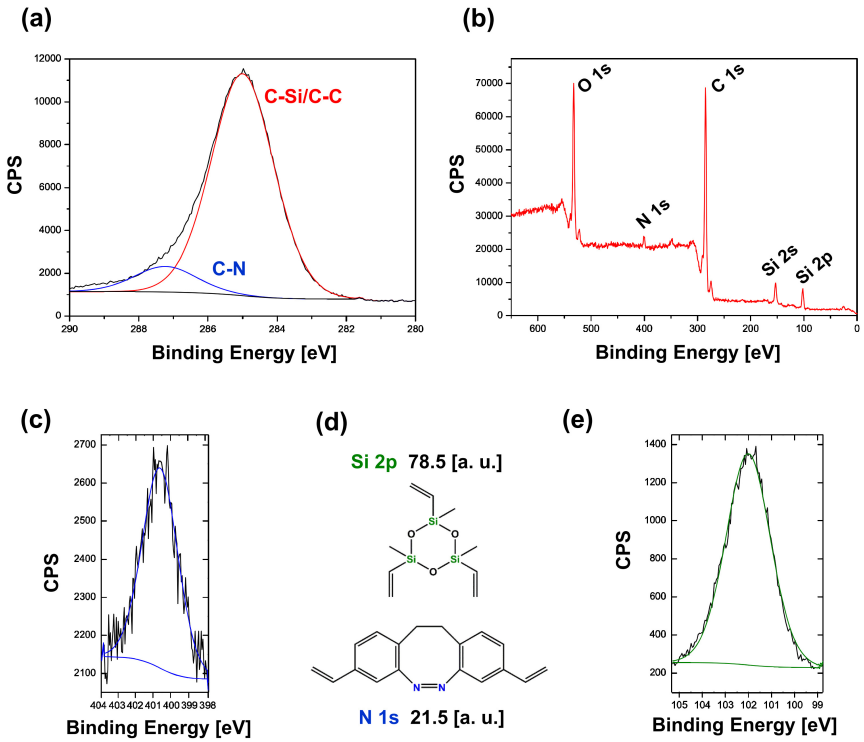

Figure 6. Detailed XPS analysis of the resulting thin film. The wide spectrum (a) and the C 1s spectrum (b) show the presence of nitrogen and silicon, which are both specific for the used monomers, respectively (d). A detailed investigation of the areas below the regions of the N 1s peak (c) and Si 2p peak (e) reveals the quantitative content of both monomers inside the final polymer, allowing conclusions about the composition of the thin film.

https://dx.doi.org/10.1021/acs.macromol.9b02443
Macromolecules XXXX, XXX, XXX−XXX

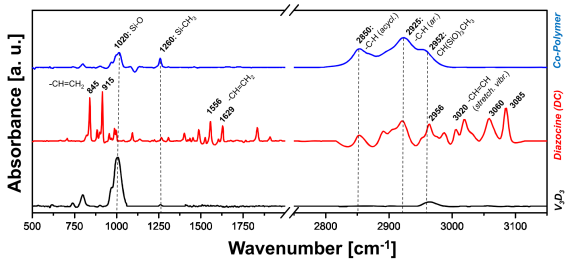

Figure 7. FT-IR spectra of the V_3D_3-homopolymer deposited via iCVD, drop-casted styrenediazocine and the expected copolymer. The copolymer spectrum is composed of specific chemical groups of both V_3D_3 and styrenediazocine. Moreover, −C═C−H vibrations of the vinyl groups completely disappear. This indicates that the co-polymerization was successful.[31]

appear in the expected copolymer spectrum. This allows the conclusion that the used styrenediazocine is completely covalently inside the polymer matrix.

In addition to the analysis of the chemical composition, photoswitchability of the incorporated chromophore was investigated via UV−vis spectroscopy as well as ellipsometry (Figure 8). For a detailed insight into the photoisomerization of the incorporated chromophore, the characteristic n−π^* bands of the photoisomers at 405 nm (Z) and 480 nm (E), respectively, have been investigated.[30]

As shown by UV−vis as well as ellipsometry, the produced thin films are able to undergo reversible switching. The diazocine shows a relatively fast relaxation, which can be attributed to the chromophore's geometry as well as its covalent bonding inside the polymer.

Despite all potential parameters that are able to inhibit photoswitching (covalent bonding, nature of the photoswitch, and the high amount in the copolymer), the results show that the thin film exhibits photoswitching abilities that are visible with the bare eye (Figure 9).

4. CONCLUSIONS

In conclusion, we were able to demonstrate the successful synthesis of the first-ever photoswitchable copolymer thin film via initiated chemical vapor deposition, using a novel functional chromophore as well as an innovative system for implementation of solid compounds in the iCVD process, with decent deposition rates and high homogeneity of the resulting film. Before thin film deposition, the applicability of the photoswitch in terms of iCVD was investigated. ^{1}H NMR spectroscopy showed the retention of the vinyl functionality, whereas Raman spectroscopy verified the presence of the azo group before and after sublimation.

XPS measurements showed that both compounds were present in the expected copolymer and revealed an above-average amount of photoswitch covalently bonded inside the solid polymer layer. Compared to the well-known methods of wet chemistry, no unwanted side effects occur and the chromophore does not undergo any side reactions with potential solvents that could interfere with the polymerization. Via FT-IR spectroscopy, it was possible to see that the vinyl

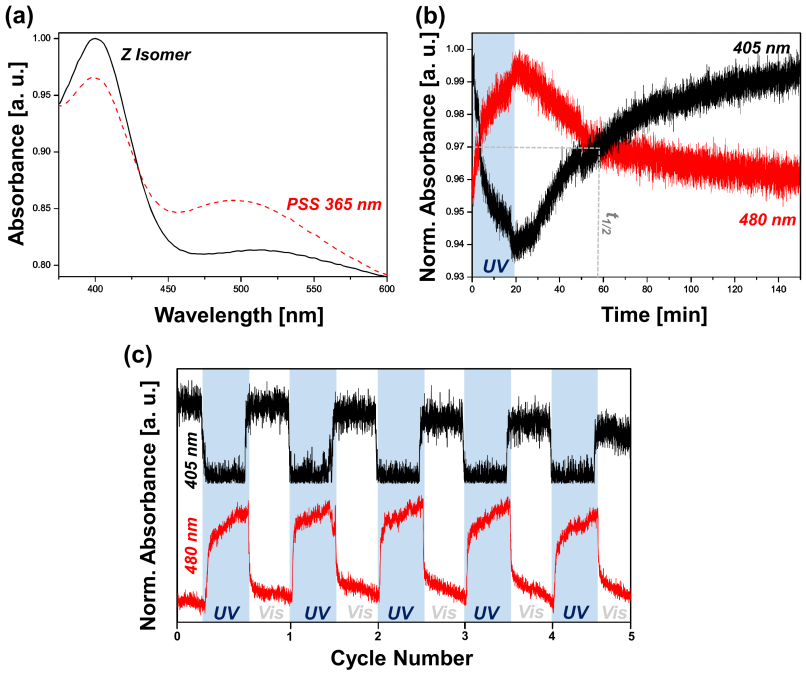

Figure 8. (a) UV−vis spectra of the copolymer in absorbance mode. Although styrenediazocine is covalently bonded inside the polymer matrix, the results show that the chromophore still undergoes reversible photoisomerization. A decrease in absorbance at 405 nm with a simultaneous increase at 480 nm indicates successful photoswitching. (b) Thermal relaxation and backswitching of the diazocine at 293 K after UV irradiation. The normalized absorbance of the 405 nm band (Z) increases, whereas the absorbance of the 480 nm band (E) decreases over time. The half-life time of the incorporated chromophore was determined to be 40 min. (c) Reversible switching of the copolymer upon irradiation with UV and white light.

https://dx.doi.org/10.1021/acs.macromol.9b02443
Macromolecules XXXX, XXX, XXX−XXX

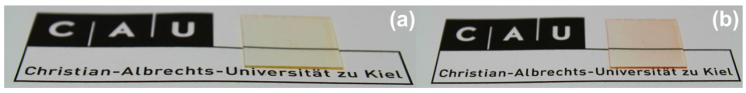

Figure 9. Images of the iCVD-produced thin films on glass substrates. Upon irradiation with UV light for 18 min, the chromophoric copolymer changes its color from yellow (a) to red (b), which demonstrates the photoswitchability of the incorporated diazocine in the solid film.

groups of the functional styrenediazocine were consumed during the radical polymerization, confirming the covalent nature of the resulting polymer. Against previously mentioned potential drawbacks preventing photoisomerization of the used diazocine in the solid phase, photoswitchability was demonstrated via UV−vis spectroscopy as well as by optical change of color from yellow to red. All in all, the above-mentioned findings show that iCVD is a promising technology for the synthesis and deposition of photochromic organic films on various kinds of desired and sensitive substrates. As described in detail by Gleason et al.,[14] a huge library of potential monomers utilizable in iCVD polymerization already exists. It is most desirable to combine the chromophore's photoswitchability, accompanied by its mechanical movement, with different monomers and their chemical traits. This allows us to fully exploit synergistic potentials in the quest of creating multiresponsive sensing layers, paving the way for a new class of interdisciplinary applications on the nanoscale.

■ AUTHOR INFORMATION

Corresponding Authors

Rainer Herges − *Otto-Diels-Institute for Organic Chemistry, Christian-Albrechts-University, 24118 Kiel, Germany;* orcid.org/0000-0002-6396-6991; Email: rherges@oc.uni-kiel.de

Franz Faupel − *Institute for Materials Science, Christian-Albrechts-University, 24143 Kiel, Germany;* orcid.org/0000-0003-3367-1655; Email: ff@tf.uni-kiel.de

Authors

Maximilian H. Burk − *Institute for Materials Science, Christian-Albrechts-University, 24143 Kiel, Germany*

Stefan Schröder − *Institute for Materials Science, Christian-Albrechts-University, 24143 Kiel, Germany*

Widukind Moormann − *Otto-Diels-Institute for Organic Chemistry, Christian-Albrechts-University, 24118 Kiel, Germany*

Daniel Langbehn − *Otto-Diels-Institute for Organic Chemistry, Christian-Albrechts-University, 24118 Kiel, Germany*

Thomas Strunskus − *Institute for Materials Science, Christian-Albrechts-University, 24143 Kiel, Germany;* orcid.org/0000-0003-3931-5635

Stefan Rehders − *Institute for Materials Science, Christian-Albrechts-University, 24143 Kiel, Germany*

Complete contact information is available at: https://pubs.acs.org/10.1021/acs.macromol.9b02443

Notes

The authors declare no competing financial interest.

■ ACKNOWLEDGMENTS

This work was funded by the German Research Foundation (DFG) under SFB1261, Project A2 and SFB677, Project C01 and by the Research Training Group GRK 2154, Project P4.

■ REFERENCES

(1) Kim, D.; Kim, J.; Lee, T. S. Photoswitchable chromic behavior of conjugated polymer films for reversible patterning and construction of a logic gate. *Polym. Chem.* **2017**, *8*, 5539−5545.

(2) Weis, P.; Wang, D.; Wu, S. Visible-Light-Responsive Azopolymers with Inhibited $\pi-\pi$ Stacking Enable Fully Reversible Photopatterning. *Macromolecules* **2016**, *49*, 6368−6373.

(3) Kinoshita, T. Photoresponsive membrane systems. *J. Photochem. Photobiol., B* **1998**, *42*, 12−19.

(4) Russew, M.-M.; Hecht, S. Photoswitches: From Molecules to Materials. *Adv. Mater.* **2010**, *22*, 3348−3360.

(5) Zhang, J.; Zou, Q.; Tian, H. Photochromic Materials: More Than Meets The Eye. *Adv. Mater.* **2013**, *25*, 378−399.

(6) Bertrand, O.; Gohy, J.-F. Photo-responsive polymers: synthesis and applications. *Polym. Chem.* **2017**, *8*, 52−73.

(7) Viswanathan, N.; Kim, D.; Bian, S.; Williams, J.; Liu, W.; Li, L.; Samuelson, L.; Kumar, J.; Tripathy, S. Surface relief structures on azo polymer films. *J. Mater. Chem.* **1999**, *9*, 1941−1955.

(8) Schneider, V.; Polonskyi, O.; Strunskus, T.; Elbahri, M.; Faupel, F. Light-induced Conductance Switching in Photomechanically Active Carbon Nanotube-Polymer Composites. *Sci. Rep.* **2017**, *7*, No. 9648.

(9) Hedayati, M. K.; Javaheri, M.; Zillohu, A. U.; El-Khozondar, H. J.; Bawa'aneh, M. S.; Lavrinenko, A.; Faupel, F.; Elbahri, M. Photo-driven Super Absorber as an Active Metamaterial with a Tunable Molecular-Plasmonic Coupling. *Adv. Opt. Mater.* **2014**, *2*, 705−710.

(10) Bahrenburg, J.; Renth, F.; Plamper, F.; Richtering, W.; Temps, F. Femtosecond spectroscopy reveals huge differences in the photoisomerisation dynamics between azobenzenes linked to polymers and azobenzenes in solution. *Phys. Chem. Chem. Phys.* **2014**, *16*, 11549−11554.

(11) Zhao, Y.; Ikeda, T. *Smart Light-Responsive Materials*; Wiley: New Jersey, 2009.

(12) Seki, T. Smart Photoresponsive Polymer Systems organized in two Dimensions. *Bull. Chem. Soc. Jpn.* **2007**, *80*, 2084−2109.

(13) Decher, G.; Hong, J. D.; Schmitt, J. Buildup of ultrathin multilayer films by a self-assembly process: III. Consecutively alternating adsorption of anionic and cationic polyelectrolytes on charged surfaces. *Thin Solid Films* **1992**, *210/211*, 831−835.

(14) Gleason, K. K. *CVD Polymers*; Wiley: Weinheim, 2015.

(15) Chen, G.; Lau, K. K. S.; Gleason, K. K. iCVD growth of poly(N-vinylimidazole) and poly(N-vinylimidazole-co-N-vinylpyrrolidone). *Thin Solid Films* **2009**, *517*, 3539−3542.

(16) Lau, K. K. S.; Gleason, K. K. Initiated chemical vapor deposition (iCVD) of copolymer thin films. *Thin Solid Films* **2008**, *516*, 678−680.

(17) Bakker, R.; Verlaan, V.; Verkerk, A. D.; van der Werf, C. H. M.; van Dijk, L.; Rudolph, H.; Rath, J. K.; Schropp, R. E. I. Heat transfer model of an iCVD reactor. *Thin Solid Films* **2009**, *517*, 3555−3558.

(18) Alf, M. E.; Asatekin, A.; Barr, M. C.; Baxamusa, S. H.; Chelawat, H.; Ozaydin-Ince, G.; Petruczok, C. D.; Sreenivasan, R.; Tenhaeff, W. E.; Trujillo, N. J.; Vaddiraju, S.; Xu, J.; Gleason, K. K. Chemical Vapor Deposition of Conformal, Functional, and Responsive Polymer Films. *Adv. Mater.* **2010**, *22*, 1993−2027.

(19) Martin, T. P.; Lau, K. K. S.; Chan, K.; Mao, Y.; Gupta, M.; O'Shaughnessy, W. S.; Gleason, K. K. Initiated chemical vapor deposition (iCVD) of polymeric nanocoatings. *Surf. Coat. Technol.* **2007**, *201*, 9400−9405.

(20) Tenhaeff, W. E.; Gleason, K. K. Crosslinking of copolymer thin films by initiated chemical vapor deposition for hydrogel applications. *Thin Solid Films* **2009**, *517*, 3543−3546.

https://dx.doi.org/10.1021/acs.macromol.9b02443
Macromolecules XXXX, XXX, XXX−XXX

(21) Park, S. W.; Lee, D.; Lee, H. R.; Moon, H.-J.; Lee, B. R.; Ko, W.-K.; Song, S.-J.; Lee, S. J.; Shin, K.; Jang, W.; Yi, J.-K.; Im, S. G.; Kwon, I. K. Generation of functionalized polymer nanolayer on implant surface via initiated chemical vapor deposition. *J. Colloid Interface Sci.* **2015**, *439*, 34−41.
(22) Schröder, S.; Strunskus, T.; Rehders, S.; Gleason, K. K.; Faupel, F. Tunable polytetrafluoroethylene electret films with extraordinary charge stability synthesized by initiated chemical vapor deposition for organic electronics applications. *Sci. Rep.* **2019**, *9*, No. 2237.
(23) Aktas, O. C.; Schröder, S.; Veziroglu, S.; Ghori, M. Z.; Haidar, A.; Polonskyi, O.; Strunskus, T.; Gleason, K. K.; Faupel, F. Superhydrophobic 3D Porous PTFE/TiO_2 Hybrid Structures. *Adv. Mater. Interfaces* **2019**, No. 1801967.
(24) Mintken, M.; Schweichel, M.; Schröder, S.; Kaps, S.; Carstensen, J.; Mishra, Y. K.; Strunskus, T.; Faupel, F.; Adelung, R. Nanogenerator and piezotronic inspired concepts for energy efficient magnetic field sensors. *Nano Energy* **2019**, *56*, 420−425.
(25) Unger, K.; Salzmann, P.; Masciullo, C.; Cecchini, M.; Koller, G.; Coclite, A. M. Novel Light-Responsive Biocompatible Hydrogels produced by Initiated Chemical Vapor Deposition. *ACS Appl. Mater. Interfaces* **2017**, *9*, 17408−17416.
(26) Siewertsen, R.; Schönborn, J.; Hartke, B.; Renth, F.; Temps, F. Superior Z→E and E→Z photoswitching dynamics of dihydrodibenzodiazocine, a bridged azobenzene, by S1(nπ^*) excitation at λ= 387 and 490 nm. *Phys. Chem. Chem. Phys.* **2011**, *13*, 1054−1063.
(27) Sell, H.; Näther, C.; Herges, R. Amino-substituted diazocines as pincer-type photochromic switches. *Beilstein J. Org. Chem.* **2013**, *9*, 1−7.
(28) Krämer, R.; Nöthling, N.; Lehmann, C. W.; Mohr, F.; Tausch, M. E-Diazocine in Chemical Education: Synthesis, Structure, Photochromism and Thermal Stability. *ChemPhotoChem* **2018**, *2*, 6−11.
(29) Siewertsen, R.; Neumann, H.; Buchheim-Stehn, B.; Herges, R.; Näther, C.; Renth, F.; Temps, F. Highly Efficient Reversible Z-E Photoisomerization of a bridged Azobenzene with Visible Light through Resolved S1(nπ^*) Absorption Bands. *J. Am. Chem. Soc.* **2009**, *131*, 15594−15595.
(30) Moormann, W.; Langbehn, D.; Herges, R. Synthesis of functionalized diazocines for application as building blocks in photo- and mechanoresponsive materials. *Beilstein J. Org. Chem.* **2019**, *15*, 727−732.
(31) Matsumura, H.; Umemoto, H.; Gleason, K. K.; Schropp, R. *Catalytic Chemical Vapor Deposition: Technology and Applications of Cat-CVD*; Wiley: Weinheim, 2019.

https://dx.doi.org/10.1021/acs.macromol.9b02443
Macromolecules XXXX, XXX, XXX−XXX

4 Oxidative C-C Coupling

Although all relevant details have been mentioned for each of the previously published systems it is helpful for future syntheses to summarize the details of the oxidative C-C coupling using KO^{t}Bu and bromine. Generally, both bromine and iodine were used successfully as oxidants. However, it is more practical to use bromine, as iodine does not dissove in THF sufficiently to perform the reaction in homogeneous solution. The mechanism of this reaction strongly depends on the deprotonation of the α-protons. The use of substrates with other more acidic protons leads to the formation of the constitutional isomer (**Figure 4.1 a**). This is a detrimental side-reaction in diazocine synthesis but shows that the reaction is not limited to 2-nitrotoluene derivatives and can be beneficial in the synthesis of different coupling patterns.

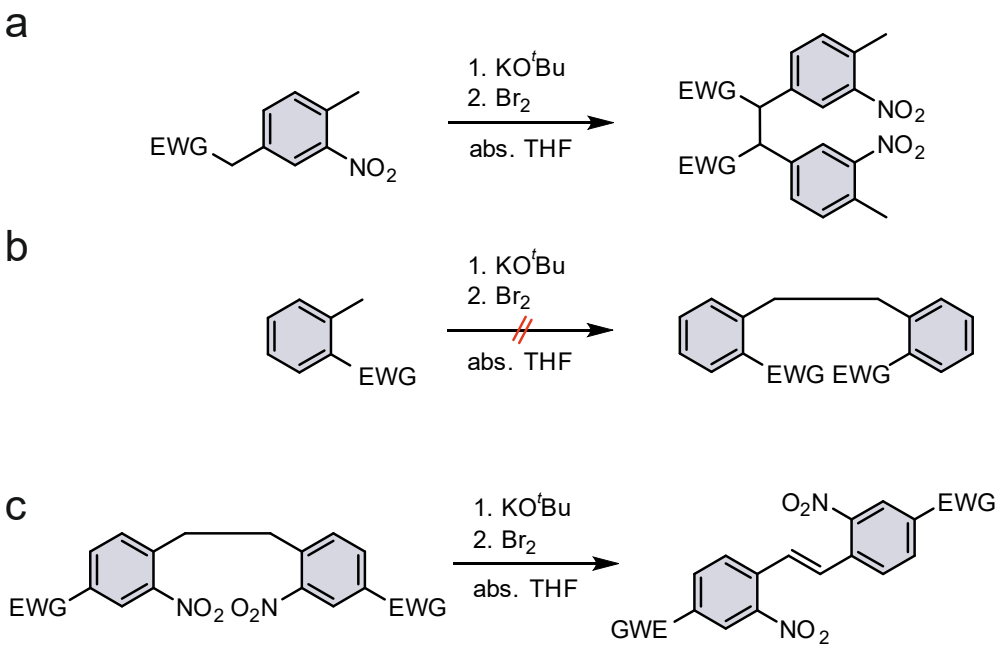

Figure 4.1: a) When coupling (4-methyl-3-nitrophenyl) methane derivatives the CH-acidity of the methyl group in 4-position must always exceed all further CH groups in the molecule. Otherwise, the C-C coupling will form an unwanted stereoisomer. b) Substitution of the nitro group with other EWGs like an ester or nitrile prevented the reaction. c) EWGs will cause the formation of stilbenes as side-products if reaction temperature, excess of KO^{t}Bu and concentration are not adjusted.

The above stated findings seemingly lead to the conclusion that the nitro group could be substituted by another electron-withdrawing group (EWG) like an ester or nitrile. This was not successful suggesting that the nitro group is essential in the reaction mechanism (**Figure 4.1 b**).

In addition to the acidity, the influence of the electronic nature of the substituents on the C-C coupling must be taken into account. Electron-withdrawing substituents like halogens, nitriles or esters can lead to the formation of a double bond (**Figure 4.1 c**). It is conceivable that the formation of a double bond proceeds according to a similar mechanism. However, it is sterically demanding in comparison to the formation of the first C-C bond and thus the temperature of the reaction influences the formation of the stilbene. Furthermore, it is necessary to work under high concentrations in order to favor the intermolecular over the intramolecular reaction. However, this is limited to the solubility of KO^tBu in THF. While the single C-C coupling is completed within several minutes, the formation of the double bond can take place even hours after addition of bromine, requiring the hydrolyzation of the reaction around 10 min after addition of bromine is completed. In general, a higher acidity of the benzylic protons leads to a more exothermic reaction. Thus, consistent cooling and slow addition of bromine is required to prevent stilbene formation. Using substrates with additional EWG requires the use of equivalent amounts of KO^tBu. In contrast, when electron-donating groups are present, the reaction often needs elevated temperatures and an excess of KO^tBu.

5 Conclusion

Because of the difficult synthesis of substituted diazocines, their excellent photochemical properties have rarely been exploited. This work was dedicated to the synthesis of diazocines for applications in photopharmacology, molecular biology and materials science.

To develop a practical synthesis procedure for diazocines, previous approaches were critically evaluated. Several apparently viable approaches notwithstanding, starting the synthesis from 2-nitrotoluene derivatives seemed to be advantageous (**Figure 5.1**). These were often commercially available or synthetically accessible and allow for a two-step synthesis. The 2-nitrotoulene derivatives were dimerized via an optimized oxidative C-C coupling reaction, using KOtBu as a base for the abstraction of the α-toluene protons and bromine for the subsequent oxidation of the carbanions to radicals. C-C bond formation between a radical and a carbanion forming a radical anion, followed by oxidation yielded the dinitro diazocine precursor. The reaction conditions were adjusted to prevent the formation of the stilbene side-product and to achieve high yields for a number of substrates. Not only is this procedure very fast, easy to handle and versatile but it can be scaled from 100 mg to 10 g.

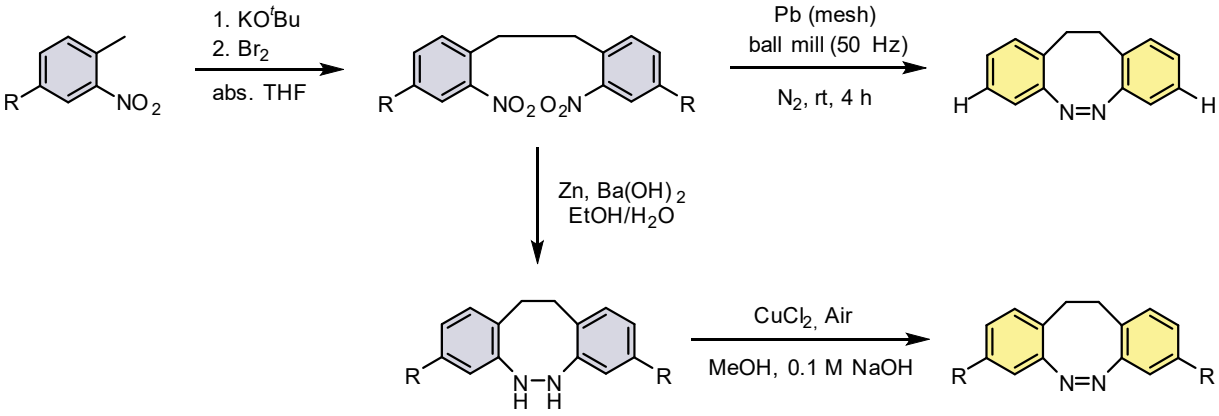

Figure 5.1: Starting from 2-nitrotoluene derivatives an oxidative C-C coupling with KO^{t}Bu and bromine resulted in dimerization in almost quantitative yields. Reduction to the diazocine was achieved in one step, solvent-free in a ball mill with lead or in two-steps by reduction to the hydrazine with Zn/$Ba(OH)_2$ and reoxidation with $CuCl_2$/O_2 to yield the diazocine. The combination of these reactions was successfully tested on a large number of substituted diazocines.

A number of procedures for the azo cyclization of dinitro precursors had been published prior to this work, but none was sufficiently practicable and versatile to form the basis of this work. The procedures of Duval and later of Paudler successfully yielded diazocines, however, they were unreliable and the yields were not reproducible. Therefore, these procedures were investigated in detail to elucidate the problems. Concluding that the reactivity and quality of the zinc has a large influence on the success of the reaction, a procedure was implemented which allows the control of the reaction process. (**Figure 5.1**). At first the dinitro precursor was reduced with Zn and $Ba(OH)_2$ to the hydrazine compound under conditions which did not allow further reduction to the diamine. This is beneficial because the hydrazine can be oxidized easily to the diazocine with $CuCl_2$ and air without prior isolation. This procedure allowed the synthesis of a number of substituted diazocine derivatives. To simplify the synthesis a direct azo cyclization was investigated using lead powder as reducing agent without solvents in a ball mill. (**Figure 5.1**). This solvent-free synthesis of diazocine provided similar yields in one step but is restricted to a very limited number of functionalized diazocines, due to interactions of many relevant functional groups with lead. The reductive azo cyclization of halogen-substituted dinitro diazocine precursors during the synthesis of glutamate neurotransmitters appeared to be hampered and only achieved very low yields. To improve this reaction, an oxidative approach for the azo cyclization was developed starting from a diamino diazocine precursor using oxone® as oxidant. Although the yields were significantly improved, Trauner and co-workers pointed out that the application of a milder peroxide reagent and high dilution conditions during the cyclization could further enhance the yield.[42] Aiming at the implementation of diazocines as cross-linkers for the photo control of macromolecules, it was necessary to achieve a significant change of length during the isomerization. The biggest difference in length can be gained by attaching diazocine substituents in either *para* or *meta* position to the azo group. *Para* substituents affect the photochemical properties more strongly than the *meta* substitution. Thus, this work focused on the synthesis of bifunctional *meta* substituted diazocines (**Figure 5.2**). Nevertheless, the direct functionalization of diazocines particularly with amines impairs that the superior photochemical properties of the diazocine parent system, even when introduced in *meta* position. Electronic decoupling between the aromatic ring and the functional group, through insertion of one or two methylene groups clearly improved the PSS (**Figure 5.2**).

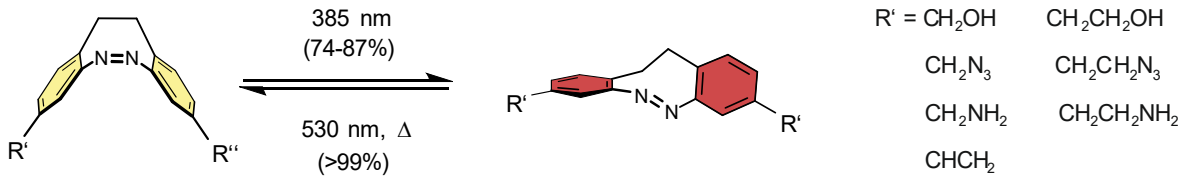

Figure 5.2: Several bifunctional *meta* substituted diazocines were prepared and investigated with regard to their photochemical properties. The insertion of one or two methylene groups between functional groups and aromatic ring significantly improved the photochemical properties in organic solvents.

Following the successful synthesis and optimization of photochemical properties in organic solvents, the application of the substituted diazocine as cross-linker in biological and artificial macromolecules as well as in photopharmacology were investigated in collaboration with expert groups in the these fields.

The Trp-cage miniprotein was an ideal system to investigate the hypothesis, that a single solvent-exposed α-helix with particular importance for the fold of a globular protein can be used to manipulate the entire fold by attaching a diazocine cross-linker to the α-helix. In this work, a diazocine substituted with two carboxylic acids was used to fold and unfold the Trp-cage miniprotein reversibly (**Figure 5.3**). As predicted from computational calculations, the α-helix and the tertiary structure were stabilized upon cross-linkage. Irradiation with light of 385 nm resulted in a *cis* → *trans* isomerization and a complete unfolding of the Trp-cage was observed. The reversibility of this process could be achieved upon irradiation with light of 530 nm or through thermal relaxation.

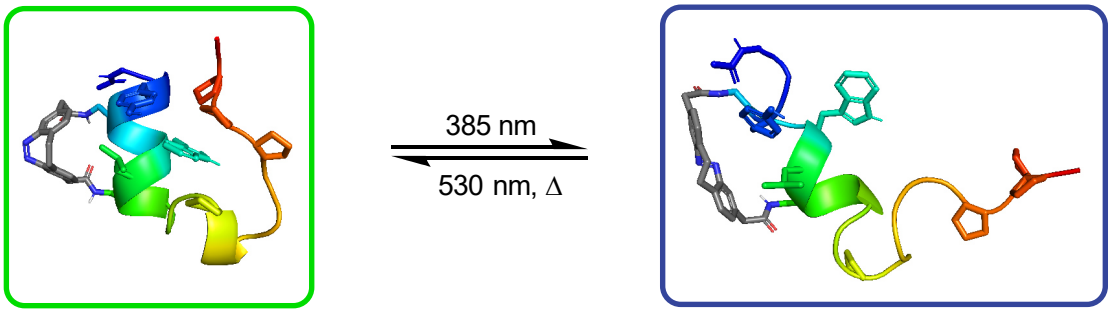

Figure 5.3: Equipped with a diazocine cross-linker the globular fold of the Trp-cage miniprotein was reversibly controlled.

Surprisingly the *cis* → *trans* isomerization upon irradiation with 385 nm was only achieved with 46%. By comparing the conversion rates with those achieved in organic solvents it became clear that aqueous environment deteriorated the photochemical properties of the diazocine. An effect, which was also observed when investigating diazocine-based neurotransmitters on the neuronal signaling of glutamate ionotropic kainate receptors (GluK).

In comparison to azobenzene, diazocines have an inverse configurational stability and are thermally stable in the more bulky *cis* configuration. The vast majority of azobenzene-containing photopharmacophores have shown activity in their dark-adapted *trans* configuration.[10] A diazocine-based drug could be administered in the dark-adapted and inactive *cis* configuration and selectively activated at the site of interest upon irradiation. This strategy would exploit the fundamental advantage of photopharmacology. Glutamate substructure containing diazocine neurotransmitters were synthesized starting from a dibromo diazocine in order to prove the advantage of diazocines over azobenzenes in photopharmacology. Two neurotransmitters with different steric claim were tested *in vitro* and *in vivo*. Voltage clamp recordings on HEK293 cells revealed that both compounds were only active upon isomerization into the *trans* configuration (**Figure 5.4**). This proof of concept was confirmed for one of the compounds *in vivo* on GluK expressing rat hippocampal neurons.

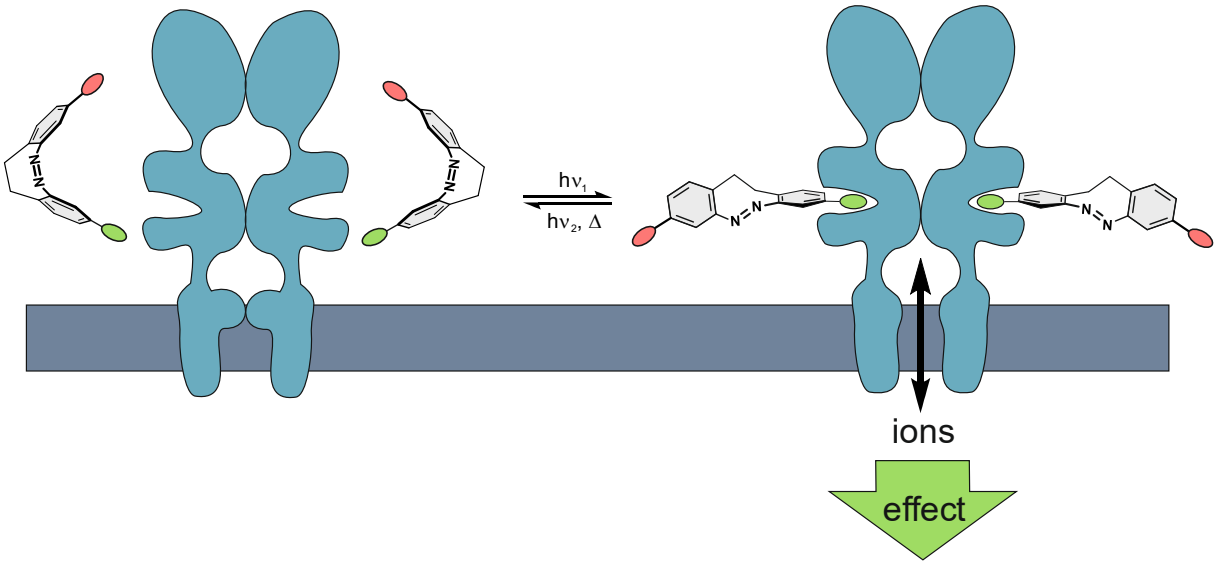

Figure 5.4: In this concept, diazocines equipped with a glutamate moiety were prepared to demonstrate the inverse activity of diazocine-based drugs in comparison to azobenzene and thus applicability in pharmacology.

The PSS of the *cis* → *trans* isomerization of both compounds upon irradiation with 405 nm in a PBS:DMSO 1:1 mixture was relatively low with 47% and 60%, concluding that the switching efficiency is hampered in an aqueous surrounding.

The previously published bifunctional styrenediazocine is an ideal system to investigate the mechanochromic properties of highly cross-linked polymers and thus the possibility to utilize diazocines as mechanophores in stress-sensing applications. Due to its functionalization and low melting point, the styrenediazocine is suitable for initiated chemical vapor deposition (iCVD), a method that allows coating without the use of solvents. The polymerization of the diazocine with 1,3,5-trivinyl-1,3,5-trimethylcyclotrisiloxane (V_3D_3) was initiated with Di-tert-butyl peroxide (DTPO). The resulting polymer film showed reversible switching upon irradiation, confirming iCVD as a successful method for the synthesis of diazocine-based stress indicating thin films.

6 Outlook

The development of the diazocine synthesis in this and other works enables the reconsideration of a number of projects, which had to be stopped due to the difficult synthesis of diazocines.[42, 80] For example, the proposed amine- and carboxyl-functionalized diazocine was a promising target as peptide backbone cross-linker in photopharmacology and structural biology but was never synthesized (**Figure 6.1**). An azobenzene with equivalent functionalization was used amongst others for optical control of insulin secretion and receptor-linked guanylyl cyclase.[81, 82]

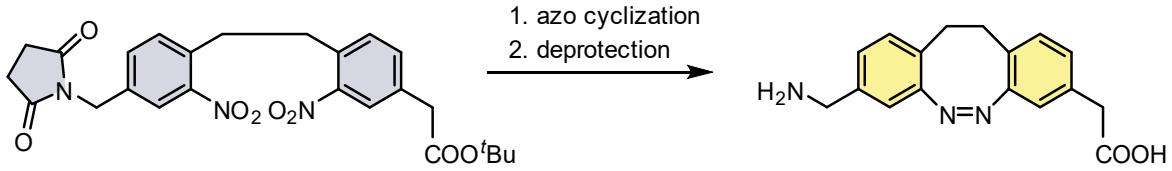

Figure 6.1: The synthesis of the amine- and carboxyl-functionalized diazocine failed in the azo cyclization step. Applying the developed procedure with Zn, $Ba(OH)_2$ should finalize this project after deprotection in the last step.

Having proven the applicability of diazocine in photopharmacology, it is purposeful to determine suitable targets and treatments. Since the penetration depth of wavelength currently needed to activate diazocine-based drugs is smaller than one mm, targets that can be reached by exposure from outside the body are certainly and foremost suitable.[83] Already, investigated problems such as vision restoration or bacteria-caused skin infection appear to be ideal starting points. Previously, photoswitchable anticataract agents have been investigated. Cataract is caused by an over-activated protease called calpain, which cleaves eye lens protein and thereby disturbs vision.[84] Azobenzene-based calpain inhibitors have shown a switchable activity upon irradiation with UV light. Designing a diazocine-based calpain inhibitor would allow to only activate the drug when it reaches its target by irradiation of natural visible daylight (**Figure 6.2**).[85]

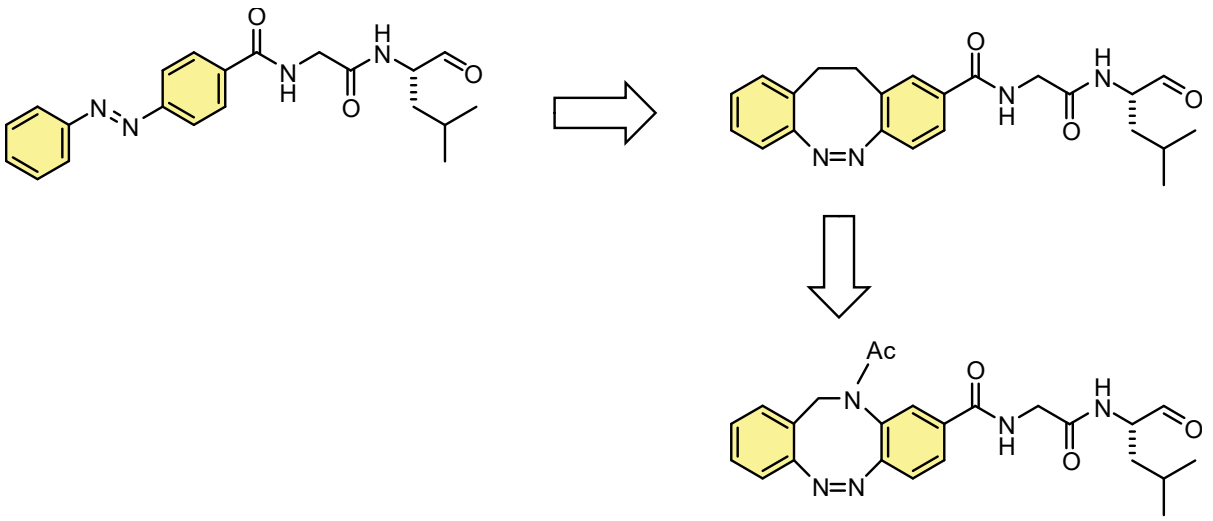

Figure 6.2: Transforming the previously investigated photoswitchable calpain inhibitor to a diazocine-based system would enable to use natural visible light to activate the inhibitor. To enhance the activation of these inhibitors in aqueous solution upon irradiation it appears practical to use N-Acetyl (NAc) bridged systems instead of the parent diazocine.

As experienced in this work, the switching efficiency of diazocines in water is hampered in comparison to organic solvents. However, it is still in the range where activation of a dark-adapted inactive drug is sensible.[23, 59, 68] Although it is possible to deliver light to most organs with small optic fiber through an incision, it is to the unease of the patient and thus not ideal for applied research.[17, 86] To avoid this and to further implement diazocines in photopharmacology the development of the photochemical properties such as switching efficiency in water and switching within the bio optical window should be further investigated. Recently published nitrogen bridged diazocines by Lentes *et al.* show interesting improvements.[51] The *trans* → *cis* isomerization of both NMe and NEt bridged diazocines was achieved upon irradiation in the near infrared region (720 nm), resulting in a bathochromic shift of 64 nm in comparison to the parent diazocine. All previously published diazocine systems have in common that they are insoluble in water without further aromatic substitution. The N-Acetyl (NAc) bridged analogue however is soluble in water and the switching efficiency of back and forth isomerization is not hampered. Since all parent diazocine based systems have a lack of switching efficiency in water, it is practical to focus future investigation on the NAc bridged diazocine (**Figure 6.2**).

In contrast to *in vivo* applications, the parent diazocine appears to be the appropriate system in materials science. The switching efficiency is not hampered when the photoswitch is incorporated into a polymer and functionalized diazocines proved to be just as stable and resistant as the parent system.[35, 68, 87] Hetero-bridged diazocines on the other hand are not as robust.[51, 52] After the successful co-polymerization of a bi functional styrenediazocine with iCVD, it is essential to produce materials, which allow investigations on the mechano-sensitivity of diazocines. Due to the large number of functional diazocines that are now available, an almost unlimited amount of material properties should be designable in order to get closer to the goals of stress sensing and drug release.

7 References

1. Ostrovsky, M. A. *Paleontol. J.* **2017,** *51* (5), 562–572. doi:10.1134/S0031030117050069
2. Polli, D.; Altoè, P.; Weingart, O.; Spillane, K. M.; Manzoni, C.; Brida, D.; Tomasello, G.; Orlandi, G.; Kukura, P.; Mathies, R. A.; Garavelli, M.; Cerullo, G. *Nature* **2010,** *467* (7314), 440–443. doi:10.1038/nature09346
3. Schoenlein, R. W.; Peteanu, L. A.; Mathies, R. A.; Shank, C. V. *Science (New York, N.Y.)* **1991,** *254* (5030), 412–415. doi:10.1126/science.1925597
4. Kandori, H.; Shichida, Y.; Yoshizawa, T. *Biochemistry. Biokhimiia* **2001,** *66* (11), 1197–1209. doi:10.1023/A:1013123016803
5. Weitz, A. J.; Lee, J. H. *Stem cells international* **2016,** *2016*, 8612751. doi:10.1155/2016/8612751
6. Feringa, B. L. *Angewandte Chemie (International ed. in English)* **2017,** *56* (37), 11060–11078. doi:10.1002/anie.201702979
7. Albert, L.; Vázquez, O. *Chemical communications (Cambridge, England)* **2019,** *55* (69), 10192–10213. doi:10.1039/c9cc03346g
8. Broichhagen, J.; Frank, J. A.; Trauner, D. *Accounts of chemical research* **2015,** *48* (7), 1947–1960. doi:10.1021/acs.accounts.5b00129
9. Szymański, W.; Beierle, J. M.; Kistemaker, H. A. V.; Velema, W. A.; Feringa, B. L. *Chemical reviews* **2013,** *113* (8), 6114–6178. doi:10.1021/cr300179f
10. Hüll, K.; Morstein, J.; Trauner, D. *Chemical reviews* **2018,** *118* (21), 10710–10747. doi:10.1021/acs.chemrev.8b00037
11. Merino, E.; Ribagorda, M. *Beilstein journal of organic chemistry* **2012,** *8*, 1071–1090. doi:10.3762/bjoc.8.119
12. Bandara, H. M. D.; Burdette, S. C. *Chemical Society reviews* **2012,** *41* (5), 1809–1825. doi:10.1039/C1CS15179G
13. Ash, C.; Dubec, M.; Donne, K.; Bashford, T. *Lasers in Medical Science* **2017,** *32* (8), 1909–1918. doi:10.1007/s10103-017-2317-4
14. Beharry, A. A.; Sadovski, O.; Woolley, G. A. *Journal of the American Chemical Society* **2011,** *133* (49), 19684–19687. doi:10.1021/ja209239m

15. Bléger, D.; Schwarz, J.; Brouwer, A. M.; Hecht, S. *Journal of the American Chemical Society* **2012,** *134* (51), 20597–20600. doi:10.1021/ja310323y
16. Kienzler, M. A.; Reiner, A.; Trautman, E.; Yoo, S.; Trauner, D.; Isacoff, E. Y. *Journal of the American Chemical Society* **2013,** *135* (47), 17683–17686. doi:10.1021/ja408104w
17. Velema, W. A.; Szymanski, W.; Feringa, B. L. *Journal of the American Chemical Society* **2014,** *136* (6), 2178–2191. doi:10.1021/ja413063e
18. Beharry, A. A.; Woolley, G. A. *Chemical Society reviews* **2011,** *40* (8), 4422–4437. doi:10.1039/C1CS15023E
19. Carlet, J.; Collignon, P.; Goldmann, D.; Goossens, H.; Gyssens, I. C.; Harbarth, S.; Jarlier, V.; Levy, S. B.; N'Doye, B.; Pittet, D.; Richtmann, R.; Seto, W. H.; van der Meer, J. W. M.; Voss, A. *The Lancet* **2011,** *378* (9788), 369–371. doi:10.1016/S0140-6736(11)60401-7
20. Yost, E. E.; Meyer, M. T.; Dietze, J. E.; Meissner, B. M.; Worley-Davis, L.; Williams, C. M.; Lee, B.; Kullman, S. W. *Environmental science & technology* **2013,** *47* (23), 13781–13790. doi:10.1021/es4026408
21. Suri, R. P. S.; Singh, T. S.; Chimchirian, R. F. *Environmental monitoring and assessment* **2012,** *184* (3), 1657–1669. doi:10.1007/s10661-011-2068-9
22. Bonnefille, B.; Gomez, E.; Courant, F.; Escande, A.; Fenet, H. *Marine pollution bulletin* **2018,** *131* (Pt A), 496–506. doi:10.1016/j.marpolbul.2018.04.053
23. Paoletti, P.; Ellis-Davies, G. C. R.; Mourot, A. *Nature Reviews Neuroscience* **2019,** *20* (9), 514–532. doi:10.1038/s41583-019-0197-2
24. Stein, M.; Middendorp, S. J.; Carta, V.; Pejo, E.; Raines, D. E.; Forman, S. A.; Sigel, E.; Trauner, D. *Angewandte Chemie (International ed. in English)* **2012,** *51* (42), 10500–10504. doi:10.1002/anie.201205475
25. Fortin, D. L.; Banghart, M. R.; Dunn, T. W.; Borges, K.; Wagenaar, D. A.; Gaudry, Q.; Karakossian, M. H.; Otis, T. S.; Kristan, W. B.; Trauner, D.; Kramer, R. H. *Nature methods* **2008,** *5* (4), 331–338. doi:10.1038/nmeth.1187
26. Velema, W. A.; van der Berg, J. P.; Hansen, M. J.; Szymanski, W.; Driessen, A. J. M.; Feringa, B. L. *Nature chemistry* **2013,** *5* (11), 924–928. doi:10.1038/nchem.1750
27. *Therapeutic Drug Monitoring;* Elsevier, 2012.

28. Butterfield, J.; Lodise, T. P.; Pai, M. P. Applications of Pharmacokinetic and Pharmacodynamic Principles to Optimize Drug Dosage Selection. *Therapeutic Drug Monitoring*; Elsevier, 2012; pp 175–196.
29. Shen, Y.; Jin, E.; Zhang, B.; Murphy, C. J.; Sui, M.; Zhao, J.; Wang, J.; Tang, J.; Fan, M.; van Kirk, E.; Murdoch, W. J. *Journal of the American Chemical Society* **2010,** *132* (12), 4259–4265. doi:10.1021/ja909475m
30. Alvarez-Lorenzo, C.; Concheiro, A. *Smart materials for drug delivery;* Royal Society Of Chem: Cambridge, 2013.
31. VASHIST, A.; AHMAD, S. *Orientjchem.* **2013,** *29* (03), 861–870. doi:10.13005/ojc/290303
32. Sponchioni, M.; Capasso Palmiero, U.; Moscatelli, D. *Materials science & engineering. C, Materials for biological applications* **2019,** *102*, 589–605. doi:10.1016/j.msec.2019.04.069
33. Wojtecki, R. J.; Meador, M. A.; Rowan, S. J. *Nature Materials* **2010,** *10*, 14 EP -. doi:10.1038/nmat2891
34. Jiang, S.; Zhang, L.; Xie, T.; Lin, Y.; Zhang, H.; Xu, Y.; Weng, W.; Dai, L. *ACS Macro Lett.* **2013,** *2* (8), 705–709. doi:10.1021/mz400198n
35. Li, S.; Han, G.; Zhang, W. *Macromolecules* **2018,** *51* (11), 4290–4297. doi:10.1021/acs.macromol.8b00687
36. Mirfakhrai, T.; Madden, J. D.W.; Baughman, R. H. *Materials Today* **2007,** *10* (4), 30–38. doi:10.1016/S1369-7021(07)70048-2
37. Lee, C. K.; Davis, D. A.; White, S. R.; Moore, J. S.; Sottos, N. R.; Braun, P. V. *Journal of the American Chemical Society* **2010,** *132* (45), 16107–16111. doi:10.1021/ja106332g
38. Esser-Kahn, A. P.; Odom, S. A.; Sottos, N. R.; White, S. R.; Moore, J. S. *Macromolecules* **2011,** *44* (14), 5539–5553. doi:10.1021/ma201014n
39. Beiermann, B. A.; Davis, D. A.; Kramer, S. L. B.; Moore, J. S.; Sottos, N. R.; White, S. R. *J. Mater. Chem.* **2011,** *21* (23), 8443. doi:10.1039/c0jm03967e
40. Klajn, R. *Chemical Society reviews* **2014,** *43* (1), 148–184. doi:10.1039/C3CS60181A
41. Surampudi, S. K.; Patel, H. R.; Nagarjuna, G.; Venkataraman, D. *Chemical communications (Cambridge, England)* **2013,** *49* (68), 7519–7521. doi:10.1039/C3CC43797C
42. Maier, M. S.; Hüll, K.; Reynders, M.; Matsuura, B. S.; Leippe, P.; Ko, T.; Schäffer, L.; Trauner, D. *Journal of the American Chemical Society* **2019. doi:**10.1021/jacs.9b08794

43. Samanta, S.; Beharry, A. A.; Sadovski, O.; McCormick, T. M.; Babalhavaeji, A.; Tropepe, V.; Woolley, G. A. *Journal of the American Chemical Society* **2013,** *135* (26), 9777–9784. doi:10.1021/ja402220t
44. Brown, M. A.; Vito, S. C. de. *Critical Reviews in Environmental Science and Technology* **1993,** *23* (3), 249–324. doi:10.1080/10643389309388453
45. Mori, H.; Mori, Y.; Sugie, S.; Yoshimi, N.; Takahashi, M.; Ni-i, H.; Yamazaki, H.; Toyoshi, K.; Williams, G. *Cancer research* **1986,** *46*, 1654–1658.
46. Neish, W.J.P.; Davies, H. M.; Reeve, P. M. *Biochemical Pharmacology* **1964,** *13* (9), 1291–1303. doi:10.1016/0006-2952(64)90230-8
47. Siewertsen, R.; Neumann, H.; Buchheim-Stehn, B.; Herges, R.; Näther, C.; Renth, F.; Temps, F. *Journal of the American Chemical Society* **2009,** *131* (43), 15594–15595. doi:10.1021/ja906547d
48. Siewertsen, R.; Schönborn, J. B.; Hartke, B.; Renth, F.; Temps, F. *Physical chemistry chemical physics : PCCP* **2011,** *13* (3), 1054–1063. doi:10.1039/C0CP01148G
49. H Duval. *Bull Soc Chim Fr.* **1910**.
50. Böckmann, M.; Doltsinis, N. L.; Marx, D. *Angewandte Chemie (International ed. in English)* **2010,** *49* (19), 3382–3384. doi:10.1002/anie.200907039
51. Lentes, P.; Stadler, E.; Röhricht, F.; Brahms, A.; Gröbner, J.; Sönnichsen, F. D.; Gescheidt, G.; Herges, R. *Journal of the American Chemical Society* **2019,** *141* (34), 13592–13600. doi:10.1021/jacs.9b06104
52. Hammerich, M.; Schütt, C.; Stähler, C.; Lentes, P.; Röhricht, F.; Höppner, R.; Herges, R. *Journal of the American Chemical Society* **2016,** *138* (40), 13111–13114. doi:10.1021/jacs.6b05846
53. Huck, N. P. M.; Jager, W. F.; Lange, B. de; Feringa, B. L. *Science (New York, N.Y.)* **1996,** *273* (5282), 1686–1688. doi:10.1126/science.273.5282.1686
54. Samanta, S.; Qin, C.; Lough, A. J.; Woolley, G. A. *Angewandte Chemie (International ed. in English)* **2012,** *51* (26), 6452–6455. doi:10.1002/anie.201202383
55. Tellkamp, T.; Shen, J.; Okamoto, Y.; Herges, R. *Eur. J. Org. Chem.* **2014,** *2014* (25), 5456–5461. doi:10.1002/ejoc.201402541
56. Sell, H.; Näther, C.; Herges, R. *Beilstein journal of organic chemistry* **2013,** *9*, 1–7. doi:10.3762/bjoc.9.1

57. Joshi, D. K.; Mitchell, M. J.; Bruce, D.; Lough, A. J.; Yan, H. *Tetrahedron* **2012,** *68* (41), 8670–8676. doi:10.1016/j.tet.2012.06.007

58. Eljabu, F.; Dhruval, J.; Yan, H. *Bioorganic & medicinal chemistry letters* **2015,** *25* (23), 5594–5596. doi:10.1016/j.bmcl.2015.10.043

59. Trads, J. B.; Hüll, K.; Matsuura, B. S.; Laprell, L.; Fehrentz, T.; Görldt, N.; Kozek, K. A.; Weaver, C. D.; Klöcker, N.; Barber, D. M.; Trauner, D. *Angewandte Chemie (International ed. in English)* **2019,** *58* (43), 15421–15428. doi:10.1002/anie.201905790

60. Gerson, F.; Heilbronner, E.; van Veen, A.; Wepster, B. M. *HCA* **1960,** *43* (7), 1889–1898. doi:10.1002/hlca.19600430702

61. Gerson, F.; Lamprecht, A.; Scholz, M.; Troxler, H.; Lenoir, D. *HCA* **1996,** *79* (1), 307–318. doi:10.1002/hlca.19960790130

62. Tauer, E.; Machinek, R. *Liebigs Ann./Recl.* **1996,** *1996* (7), 1213–1216. doi:10.1002/jlac.199619960723

63. Wang, J.; He, J.; Zhi, C.; Luo, B.; Li, X.; Pan, Y.; Cao, X.; Gu, H. *RSC Adv.* **2014,** *4* (32), 16607. doi:10.1039/C4RA00749B

64. Chaudhuri, N. K.; Ball, T. J. *J Label Compd Radiopharm* **1981,** *18* (8), 1189–1196. doi:10.1002/jlcr.2580180814

65. Paudler, W. W.; Zeiler, A. G. *J. Org. Chem.* **1969,** *34* (11), 3237–3239. doi:10.1021/jo01263a004

66. Wada, S.; Urano, M.; Suzuki, H. *J. Org. Chem.* **2002,** *67* (23), 8254–8257. doi:10.1021/jo0203645

67. Moormann, W.; Langbehn, D.; Herges, R. *Synthesis* **2017,** *49* (15), 3471–3475. doi:10.1055/s-0036-1590685

68. Cabré, G.; Garrido-Charles, A.; González-Lafont, À.; Moormann, W.; Langbehn, D.; Egea, D.; Lluch, J. M.; Herges, R.; Alibés, R.; Busqué, F.; Gorostiza, P.; Hernando, J. *Organic letters* **2019,** *21* (10), 3780–3784. doi:10.1021/acs.orglett.9b01222

69. Lau, J. L.; Dunn, M. K. *Bioorganic & medicinal chemistry* **2018,** *26* (10), 2700–2707. doi:10.1016/j.bmc.2017.06.052

70. Volgraf, M.; Gorostiza, P.; Szobota, S.; Helix, M. R.; Isacoff, E. Y.; Trauner, D. *Journal of the American Chemical Society* **2007,** *129* (2), 260–261. doi:10.1021/ja067269o

71. Zhao, Y.; Ikeda, T. *Smart light-responsive materials*. *Azobenzene-containing polymers and liquid crystals;* Wiley: Hoboken, N.J, 2009.
72. Seki, T. *BCSJ* **2007,** *80* (11), 2084–2109. doi:10.1246/bcsj.80.2084
73. Alf, M. E.; Asatekin, A.; Barr, M. C.; Baxamusa, S. H.; Chelawat, H.; Ozaydin-Ince, G.; Petruczok, C. D.; Sreenivasan, R.; Tenhaeff, W. E.; Trujillo, N. J.; Vaddiraju, S.; Xu, J.; Gleason, K. K. *Advanced materials (Deerfield Beach, Fla.)* **2010,** *22* (18), 1993–2027. doi:10.1002/adma.200902765
74. Mao, Y.; Gleason, K. K. *Langmuir : the ACS journal of surfaces and colloids* **2004,** *20* (6), 2484–2488. doi:10.1021/la0359427
75. Lau, K. K. S.; Gleason, K. K. *Macromolecules* **2006,** *39* (10), 3688–3694. doi:10.1021/ma0601619
76. Park, S. W.; Lee, D.; Lee, H. R.; Moon, H.-J.; Lee, B. R.; Ko, W.-K.; Song, S.-J.; Lee, S. J.; Shin, K.; Jang, W.; Yi, J.-K.; Im, S. G.; Kwon, I. K. *Journal of colloid and interface science* **2015,** *439*, 34–41. doi:10.1016/j.jcis.2014.10.018
77. Schröder, S.; Strunskus, T.; Rehders, S.; Gleason, K. K.; Faupel, F. *Scientific reports* **2019,** *9* (1), 2237. doi:10.1038/s41598-018-38390-w
78. Tenhaeff, W. E.; Gleason, K. K. *Thin Solid Films* **2009,** *517* (12), 3543–3546. doi:10.1016/j.tsf.2009.01.052
79. Martin, T. P.; Lau, K. K.S.; Chan, K.; Mao, Y.; Gupta, M.; Shannan O'Shaughnessy, W.; Gleason, K. K. *Surface and Coatings Technology* **2007,** *201* (22-23), 9400–9405. doi:10.1016/j.surfcoat.2007.05.003
80. Tom Podewin. Photoswitchable peptides for photopharmacological and structural biology applications. Dissertation; LMU München, München, 2017.
81. Broichhagen, J.; Podewin, T.; Meyer-Berg, H.; Ohlen, Y. von; Johnston, N. R.; Jones, B. J.; Bloom, S. R.; Rutter, G. A.; Hoffmann-Röder, A.; Hodson, D. J.; Trauner, D. *Angewandte Chemie (International ed. in English)* **2015,** *54* (51), 15565–15569. doi:10.1002/anie.201506384
82. Podewin, T.; Broichhagen, J.; Frost, C.; Groneberg, D.; Ast, J.; Meyer-Berg, H.; Fine, N. H. F.; Friebe, A.; Zacharias, M.; Hodson, D. J.; Trauner, D.; Hoffmann-Röder, A. *Chemical science* **2017,** *8* (6), 4644–4653. doi:10.1039/C6SC05044A

83. Avci, P.; Gupta, A.; Sadasivam, M.; Vecchio, D.; Pam, Z.; Pam, N.; Hamblin, M. *Seminars in cutaneous medicine and surgery* **2013,** *32*, 41–52.

84. Biswas, S.; Harris, F.; Dennison, S.; Singh, J.; Phoenix, D. A. *Trends in molecular medicine* **2004,** *10* (2), 78–84. doi:10.1016/j.molmed.2003.12.007

85. Abell, A. D.; Jones, M. A.; Neffe, A. T.; Aitken, S. G.; Cain, T. P.; Payne, R. J.; McNabb, S. B.; Coxon, J. M.; Stuart, B. G.; Pearson, D.; Lee, H. Y.-Y.; Morton, J. D. *Journal of medicinal chemistry* **2007,** *50* (12), 2916–2920. doi:10.1021/jm061455n

86. Agostinis, P.; Berg, K.; Cengel, K. A.; Foster, T. H.; Girotti, A. W.; Gollnick, S. O.; Hahn, S. M.; Hamblin, M. R.; Juzeniene, A.; Kessel, D.; Korbelik, M.; Moan, J.; Mroz, P.; Nowis, D.; Piette, J.; Wilson, B. C.; Golab, J. *CA: a cancer journal for clinicians* **2011,** *61* (4), 250–281. doi:10.3322/caac.20114

87. Moormann, W.; Langbehn, D.; Herges, R. *Beilstein journal of organic chemistry* **2019,** *15*, 727–732. doi:10.3762/bjoc.15.68

8 Supporting Information of the Publications

1. Synthesis of functionalized diazocines for application as building blocks in photo- and mechanoresponsive materials (Page 86 - 126)

2. Visible-Light-Driven Photocontrol of the Trp-cage Protein Fold by a Diazocine Cross-Linker (Page 127 - 156)

3. Synthetic Photoswitchable Neurotransmitters Based on Bridged Azobenzenes (Page 157 - 189)

BEILSTEIN JOURNAL OF ORGANIC CHEMISTRY

Supporting Information

for

Synthesis of functionalized diazocines for application as building blocks in photo- and mechanoresponsive materials

Widukind Moormann, Daniel Langbehn and Rainer Herges

Beilstein J. Org. Chem. **2019,** *15,* 727–732. doi:10.3762/bjoc.15.68

Analytical equipment, experimental procedures, NMR and UV–vis spectra

Table of contents

I. Analytical equipment

NMR spectroscopy

NMR spectra were measured in deuterated solvents (Deutero). To reference the NMR spectra the following solvent signals were used:

solvent	degree of deuteration	^{1}H signal	^{13}C signal
acetone-d_6	99.8 %	2.05 (quintet)	29.84 (septet)
chloroform-d_1	99.8 %	7.26 (s)	77.16 (triplet)
acetonitril-d_3	99.8 %	1.94 (quintet)	118.26 (septet)
D_2O	99.8 %	4.76 (s)	

NMR measurements were performed with a Bruker DRX 500 (^{1}H-NMR: 500 MHz, ^{13}C-NMR: 125 MHz) and a Bruker AV 600 (^{1}H-NMR: 600 MHz, ^{13}C-NMR: 150 MHz).

Melting point

Melting points were measured with a Melting Point B-560 (Büchi) in melting point tubes.

Mass spectrometry

The high resolution (HR-EI) mass spectra were measured with an AccuTOF GCv 4G (Joel) with ionization energy of 70 eV. High resolution (APCI) mass spectra were measured with a Thermo Fischer Q Exactive Plus MS, Hybrid Quadrupol-Orbitrap and ASSY-APCI Probe-USI 4-4.7 kV by Dynamic Integrated Solutions.

IR spectroscopy

Infrared spectra were measured on a Perkin-Elmer 1600 Series FTIR spectrometer with an A531-G Golden-Gate-Diamond-ATR-unit. Signals were abbreviated with w, m, s, vs for weak, medium, strong and very strong signal intensity.

UV–vis spectroscopy

UV–vis spectra were recorded with a Lambda 14 UV/Vis spectrometer, Perkin–Elmer. Quartz cuvettes of 10 mm optical path length were used.

Chromatography stationary phases

Flash column chromatography purfications were performed on a Biotage® type Isolera one with Biotage® Ultra cartridges (Biotage®, HP-Sphere™, particle diameter: 25 µm, cartridges sizes: 10 g, 25 g, 50 g and 100 g) were used. R_f values were determined by thin layer chromatography on Polygram® SilG/UV_{254} (Macherey Nagel, 0.2 mm particle size) and ALUGRAM® Xtra SIL G/UV_{254} (Macherey Nagel, 0.2 mm particle size).

Light sources

The irradiation of the samples was performed with LEDs with a wavelength of 385 and 530 nm from SAHLMANN PHOTOCHEMICAL SOLUTIONS with followed specifications:

- 385 nm: 12 x Nichia NCSU034A, FWHM = 9 nm, P(opt) = 12 x 340 mW,
- 530 nm: 16 x Luxeon LXML-PM01-0080, FWHM = 33 nm, P(opt) = 16 x 200 mW],

II. Syntheses

II.1. Synthesis of 4-(*tert*-butoxymethyl)-2-nitrotoluene (9a)

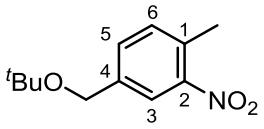

Under a N_2 atmosphere 4-hydroxymethyl-2-nitrotoluene (**8a**, 20.0 g, 120 mmol) was dissolved in 300 mL dry DCM, followed by the addition of isobutylene in DCM (300 mL, 251 mmol) and concentrated sulfuric acid (1.25 mL, 23.3 mmol). The reaction mixture was stirred for 16 h at room temperature and diluted with saturated sodium hydrogen carbonate (250 mL). The organic layer was separated and the aqueous layer was extracted with DCM (200 mL). The combined organic layers were washed with saturated sodium chloride solution, dried over magnesium sulfate and the solvent was removed in vacuo. The crude product was purified on silica flash column chromatography (cyclohexane/ethyl acetate, ethyl acetate 10% → 100%) to obtain a yellow oil (24.9 g, 111 mmol, 93%).

$\mathbf{R}_f$: 0.60 (cyclohexane/ethyl acetate, 1:1).

^{1}H-NMR (500.1 MHz, $CDCl_3$, 300 K): δ = 7.96 (d, ^4J = 1.5 Hz, 1 H, *H*-3), 7.47 (dd, ^3J = 7.8 Hz, ^4J = 1.5 Hz, 1 H, *H*-5), 7.29 (d, ^3J = 7.8 Hz, 1 H, *H*-6), 4.47 (s, 2 H, ^{t}BuO-CH_2), 2.57 (s, 3 H, CH_3), 1.30 (s, 9 H, *H*-^{t}Bu) ppm.

^{13}C-NMR (125.8 MHz, $CDCl_3$, 300 K): δ = 149.1 (*C*-2), 139.5 (*C*-4), 132.6 (*C*-6), 132.1 (*C*-1), 131.7 (*C*-5), 123.3 (*C*-3), 73.9 (*C*-$(CH_3)_3$), 62.8 (*C*H_2), 27.6 (C-(*C*H_3)$_3$), 20.2 (*C*H_3) ppm.

IR (ATR): $\tilde{\upsilon}$ = 2974 (m), 2933 (w), 2870 (w), 1526 (s), 1453 (w), 1389 (w), 1346 (s), 1235 (w), 1192 (s), 1089 (m), 1025 (w), 883 (m), 814 (s), 755 (w), 680 (w) cm^{-1}.

MS (EI, 70 eV): m/z (%) = 150 (100), 208 (16), 104 (6).

MS (EI, HR, 70 eV): $C_{12}H_{17}NO_3$, m/z = calc.: 223.1208, found: 223.1211.

II.2. Synthesis of 1,2-bis(4-(*tert*-butoxymethyl)-2-nitrophenyl)ethane (10a)

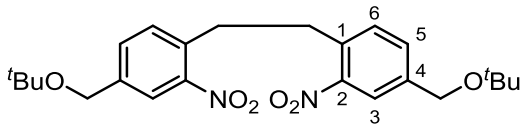

Under a N_2 atmosphere 4-(*tert*-butoxymethyl)-2-nitrophenyl)ethane (**9a**, 1.00 g, 4.48 mmol) was dissolved in 90 mL dry THF, cooled to −5 °C, followed by potassium butoxide addition (653 mg, 5.82 mmol). The reaction mixture was stirred for 30 s before the addition of bromine (274 µL, 5.38 mmol). After further stirring for 10 min the reaction mixture was added to 1 L ice. The precipitate was filtered and recrystallized from ethanol to obtain colourless crystals (816 mg, 1.84 mmol, 82%).

melting point: 131 °C.

R_f: 0.80 (cyclohexane/ethylacetate, 1:1).

^{1}H-NMR (500.1 MHz, $CDCl_3$, 300 K): δ = 7.95 (d, ^4J = 1.5 Hz, 2 H, *H*-3), 7.51 (dd, ^3J = 7.8 Hz, ^4J = 1.5 Hz, 2 H, *H*-5), 7.38 (d, ^3J = 7.8 Hz, 2 H, *H*-6), 4.49 (s, 4 H, ^{t}BuO-CH_2), 3.19 (s, 4 H, C_2H_4), 1.31 (s, 18 H, *H*-^{t}Bu) ppm.

^{13}C-NMR (125.8 MHz, $CDCl_3$, 300 K): δ = 149.1 (*C*-2), 140.2 (*C*-4), 134.7 (*C*-1), 132.4 (*C*-6), 131.9 (*C*-5), 123.3 (*C*-3), 74.8 (*C*-CH_3), 62.7 (^{t}BuO-*C*H_2), 34.2 (C_2H_4), 27.6 (C-(*C*H_3)$_3$) ppm.

IR (ATR): ῡ = 2977 (m), 1569 (w), 1520 (vs), 1390 (m), 1362 (s), 1344 (s), 1195 (vs), 1120 (m), 1063 (s), 1025(m), 888 (s), 833 (s), 814 (s), 750 (m), 677 (m) cm^{-1}.

MS (APCI): m/z (%) = 483 (100) [M+K], 467 (12) [M+Na].

MS (APCI): m/z (%) = [$C_{24}H_{32}O_6N_2{}^{39}$K], m/z = calc.: 483.1892, found: 483.1890.

= [$C_{24}H_{32}O_6N_2{}^{23}$Na], m/z = calc.: 476.2153, found: 476.2152.

II.3. Synthesis of (*Z*)-3,8-bis(*tert*-butoxymethyl)-11,12-dihydrodibenzo[*c*,*g*][1,2]diazocine (11a)

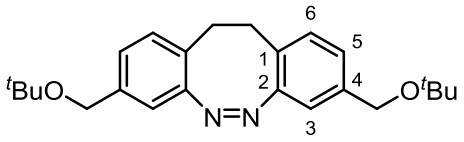

A mixture of 1,2-bis(4-(*tert*-butoxymethyl)-2-nitrophenyl)ethane (**10a**, 193 mg, 434 µmol), $Ba(OH)_2$ $8H_2O$ (411 mg, 1.30 mmol) and zinc powder (454 mg, 6.94 mmol) were dissolved in an ethanol/water mixture (60 mL, 2:1) and stirred for 5 h under reflux. After filtration trough Celite and evaporation of the solvent under reduced pressure, the crude product was dissolved in 0.1 M methanolic NaOH solution (150 mL), $CuCl_2$ (5.00 mg, 37.2 µmol) was added, and air was led trough the solution for 4 h. The reaction mixture was neutralized with 2 M HCl and the aqueous layer was extracted with DCM (3 × 75 mL). The combined organic layers were washed with a saturated sodium chloride solution and dried over magnesium sulfate. The solvent was evaporated in vacuo and the crude product was purified by flash column chromatography (cyclohexane/ethyl acetate, ethyl acetate 10% → 100%) to afford the product as a yellow solid (93.1 mg, 245 µmol, 56%).

melting point: 128 °C.

$\mathbf{R}_f$: 0.59 (cyclohexane/ethyl acetate, 1:1).

^{1}H-NMR (500.1 MHz, $CDCl_3$, 300 K): δ = 6.99 (dd, ^3J = 7.8 Hz, ^4J = 1.7 Hz, 2 H, *H*-5), 6.92 (d, ^3J = 7.8 Hz, 2 H, *H*-6), 6.84 (d, ^4J = 1.7 Hz, 2 H, *H*-3), 4.35 (d, ^4J = 3.6 Hz, 4 H, CH_2), 3.01-2.65 (m, 4 H, C_2H_4), 1.24 (s, 9 H, *H*-^{t}Bu) ppm.

^{13}C-NMR (125.8 MHz, $CDCl_3$, 300 K): δ = 155.2 (*C*-2), 138.7 (*C*-4), 129.5 (*C*-6), 126.6 (*C*-1), 125.8 (*C*-5), 117.9 (*C*-3), 73.5 (*C*-$(CH_3)_3$), 63.4 (*C*H_2), 31.5 (C_2H_4), 27.6 (C-(*C*H_3)$_3$) ppm.

IR (ATR): $\tilde{\upsilon}$ = 2974 (s), 2872 (w), 1458 (w), 1388 (m), 1361 (s), 1192 (s), 1061 (s), 1022 (m), 902 (m), 830 (s), 814 (m), 771 (m) 746 (w) cm^{-1}.

MS (EI, 70 eV): m/z (%) = 380 (37), 323 (1), 307 (7), 279 (100), 193 (72).

MS (EI, HR, 70 eV): $C_{24}H_{32}N_2O_2$, m/z = calc.: 380.2463, found: 380.2463.

II.4. Synthesis of (*Z*)-(11,12-dihydrodibenzo[*c*,*g*][1,2]diazocine-3,8-diyl)dimethanol (4a)

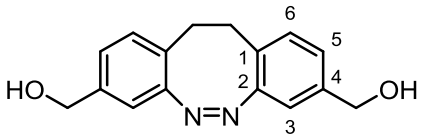

Under a N_2 atmosphere (*Z*)-3,8-bis(*tert*-butoxymethyl)-11,12-dihydrodibenzo[*c*,*g*][1,2]diazocine (**11a**, 100 mg, 260 µmol) was dissolved in 1 mL dry DCM, cooled to 0 °C and $TiCl_4$ (90.0 µL, 789 µmol) was added. After 1 min 20 mL saturated potassium carbonate solution were added. The solution was acidified with 1 M hydrochloric acid solution and extracted with DCM. The combined organic layers were washed with saturated sodium chloride solution 50 mL, dried over magnesium sulfate and the solvent was removed in vacuo. The crude product was purified on silica flash column chromatography (cyclohexane/ethyl acetate) to obtain a yellow solid. (70.0 mg, 260 µmol, 99%).

melting point: 133 °C.

R_f: 0.11 (cyclohexane/ethylacetate, 1:1).

^{1}H-NMR (500.1 MHz, $CDCl_3$, 300 K): δ = 7.00 (dd, ^3J = 8.0 Hz, ^4J = 1.6 Hz, 2 H, *H*-5), 6.96 (d, ^3J = 7.9 Hz, 2 H, *H*-6), 6.83 (d, ^4J = 1.1 Hz, 2 H, *H*-3), 4.56 (s, 4 H, CH_2-OH, 2.95 (s, 2 H, C_2H_4), 2.77 (s, 2 H, C_2H_4) ppm.

^{13}C-NMR (125.8 MHz, $CDCl_3$, 300 K): δ = 155.4 (*C*-2), 139.6 (*C*-1), 129.9 (*C*-6), 127.3 (*C*-4), 125.6 (*C*-5), 117.4 (*C*-3), 64.5 (*C*H_2-OH), 31.4 (C_2H_4) ppm.

IR (ATR): ϑ = 3258 (m), 2939(w), 2884 (w), 1525 (w), 1459 (w), 1405 (m), 1353 (w), 1276 (w), 1225 (w), 1092 (w), 1019 (vs), 996 (vs), 889 (m), 833 (s), 818 (s), 751 (s), 724 (m), 701 (m), 620 (m) cm^{-1}.

MS (EI, 70 eV): m/z (%) = 268 (100), 236 (83), 207 (56).

MS (EI, HR, 70 eV): $C_{16}H_{16}N_2O_2$, m/z = calc.: 268.1212, found: 268.1199.

II.5. Synthesis of (*Z*)-3,8-bis(azidomethyl)-11,12-dihydrodibenzo[*c*,*g*][1,2]diazocine (5a)

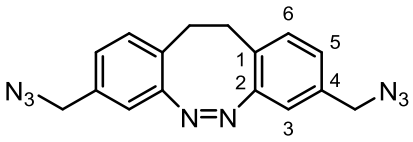

Under a N_2 atmosphere (*Z*)-(11,12-dihydrodibenzo[*c*,*g*][1,2]diazocine-3,8-diyl)dimethanol (**4a**, 1.00 g, 3.73 mmol) was dissolved in dry THF (20 mL). 2-Azido-1,3-dimethylimidazolinium hexafluorophosphate (2.65 g, 9.29 mmol)) and DBU (1.71 g, 11.2 mmol) were added slowly. After stirring for 30 min at room temperature the reaction mixture was diluted with saturated potassium carbonate solution. The organic layer was separated and the aqueous layer was extracted with DCM (3 × 50 mL), washed with saturated sodium chloride solution and dried over magnesium sulfate. The solvent was evaporated in vacuo and the crude product was then purified by flash column chromatography (cyclohexane/ethyl acetate, ethyl acetate 10% → 100%) to obtain a yellow solid (956 mg, 3.00 mmol, 81%).

melting point: 62 °C.

R_f: 0.50 (cyclohexane/ethyl acetate, 1:1).

^{1}H-NMR (600.1 MHz, $CDCl_3$, 300 K): δ = 7.01-6.95 (m, 4 H, *H*-5, *H*-6), 6.76 (d, ^4J = 1.2 Hz, 2 H, *H*-3), 4.22 (m, 4 H, CH_2), 3.04-2.72 (m, 4 H, C_2H_4) ppm.

^{13}C-NMR (150.9, $CDCl_3$, 300 K): δ = 155.6 (*C*-4), 134.2 (*C*-2), 130.3 (*C*-6), 128.2 (*C*-1), 126.7 (*C*-5), 118.3 (*C*-3), 53.9 (*C*H_2), 31.3 (C_2H_4) ppm.

IR (ATR): $\tilde{\upsilon}$ = 2931 (w), 2093 (s), 1451 (w), 1338 (m), 1247 (s), 1092 (w), 874 (m), 826 (s), 807 (m), 750 (m), 630 (w), 611 (w) cm^{-1}.

MS (EI, 70 eV): m/z (%) = 318 (15), 262 (4), 248 (13), 233 (15), 178 (100).

MS (EI, HR, 70 eV): $C_{16}H_{14}N_8$, m/z = calc.: 318.1341, found: 318.1339.

II.6. Synthesis of (*Z*)-(11,12-dihydrodibenzo[1,2]diazocin-3,8-diyl)dimethanamine (6a)

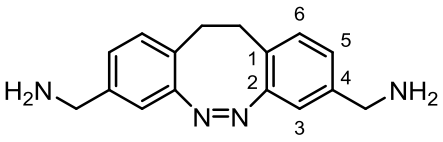

(*Z*)-(11,12-dihydrodibenzo[*c*,*g*][1,2]diazocine-3,8-diyl)dimethanol (**5a**, 78 mg, 245 µmol) and triphenylphosphine (141 mg, 540 µmol) were dissolved in dry THF. After the addition of water (88 µL, 490 µmol) the reaction mixture was stirred for 1 h at room temperature and afterwards diluted with water. The solution was acidified with 1 M hydrochloric acid solution and washed with DCM (3 × 50 mL). The aqueous solution was neutralized with 1 M sodium hydroxide solution and extracted at pH > 7 with DCM. The combined organic layers were washed with saturated sodium chloride solution, dried over magnesium sulfate and the solvent was removed in vacuo to obtain a yellow solid. (62.9 mg, 236 µmol, 96%).

melting point: 118 °C.

R_f: 0.01 (cyclohexane/ethylacetate, 1:1).

^{1}H-NMR (500.1 MHz, $CDCl_3$, 300 K): δ = 6.97 (dd, ^3J = 7.7 Hz, ^4J = 2.1 Hz, 2 H, *H*-5), 6.95 (d, ^3J = 7.7 Hz, 2 H, *H*-6), 6.81 (d, ^4J = 1.1 Hz, 2 H, *H*-3), 3.78 (s, 4 H, C*H*$_2$-NH$_2$), 3.02-2.70 (m, 4 H, C$_2$*H*$_4$) ppm.

^{13}C-NMR (125.8 MHz, $CDCl_3$, 300 K): δ = 155.4 (*C*-2), 141.9 (*C*-4), 129.8 (*C*-6), 126.4 (*C*-1), 125.8 (*C*-5), 117.5 (*C*-3), 45.8 (*C*H$_2$-NH$_2$), 31.4(*C*$_2$H$_4$) ppm.

IR (ATR): ϋ = 2871 (m), 1556 (s), 1455 (vs), 1372 (s), 1297 (vs), 911 (m), 811 (vs), 695 (m) cm^{-1}.

MS (EI, 70 eV): m/z (%) = 266 (59), 237 (100) 220 (82).

MS (EI, HR, 70 eV): $C_{16}H_{18}N_4$, m/z = calc.: 266.1532, found: 266.1543.

II.7. Synthesis of 4-(2-(*tert*-butoxy)ethyl)-2-nitrotoluene (9b)

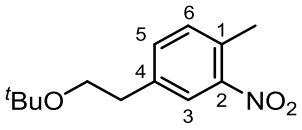

Under a N_2 atmoshere 4-(2-(hydroxy)ethyl)-2-nitrotoluene (**8b**, 2.63 g, 14.5 mmol) was dissolved in 150 mL dry DCM, followed by the addition of isobutylene in DCM (150 mL, 126 mmol) and concentrated sulfuric acid (700 µL, 13.1 mmol). The reaction mixture was stirred for 15 h at room temperature and afterwards diluted with saturated sodium hydrogen carbonate (50 mL). The organic layer was separated and the aqueous layer was extracted with DCM (3 × 50 mL). The combined organic layers were washed with saturated sodium chloride solution, dried over magnesium sulfate and the solvent was removed in vacuo. The crude product was purified on silica flash column chromatography (cyclohexane/ethyl acetate, ethyl acetate 10% → 100%) to obtain a yellow oil (3.28 g, 13.6 mmol, 95%).

$\mathbf{R}_f$: 0.63 (cyclohexane/ethyl acetate, 1:1).

^{1}H-NMR (500.1 MHz, $CDCl_3$, 300 K): δ = 7.87 (d, ^4J = 1.7 Hz, 1 H, *H*-3), 7.37 (dd, ^3J = 7.8 Hz, ^4J = 1.7 Hz, 1 H, *H*-5), 7.23 (d, ^3J = 7.8 Hz, 1 H, *H*-6), 3.56 (t, ^3J = 6.8 Hz, 2 H, ^{t}BuO-CH_2), 2.85 (t, ^3J = 6.8 Hz, 2 H, ^{t}BuO-CH2-C*H*2), 3.22 (s, 3 H, CH_3), 1.15 (s, 9 H, *H*-^{t}Bu) ppm.

^{13}C-NMR (125.8 MHz, $CDCl_3$, 300 K): δ = 149.0 (*C*-2), 139.1 (*C*-4), 133.9 (*C*-5), 132.5 (*C*-6), 131.1 (*C*-1), 125.0 (*C*-3), 73.0 (*C*-(CH_3)$_3$), 62.0 (^{t}BuO-*C*H$_2$), 36.3 (^{t}BuO-CH$_2$-*C*H$_2$), 27.5 (C-(*C*H$_3$)$_3$), 20.1 (*C*H$_3$) ppm.

IR (ATR): $\tilde{\upsilon}$ = 2973 (m), 2933 (m), 2870 (w), 1526 (s), 1498 (w), 1453 (w), 1362 (m), 1345 (m), 1193 (m), 1079 (m), 1022 (w), 940 (w), 889 (w), 807 (m), 738 (m), 679 (w) cm^{-1}.

MS (EI, 70 eV): m/z (%) = 238 (8), 207 (52), 182 (42), 151 (100), 134 (88).

MS (EI, HR, 70 eV): $C_{13}H_{20}NO_2$, m/z = calc.: 238.1443, found: 238.1445.

II.8. Synthesis of 1,2-bis(4-(2-(*tert*-butoxy)ethyl)-2-nitrophenyl)ethane (10b)

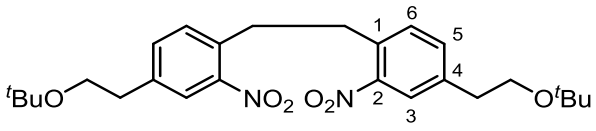

Under a N_2 atmosphere 4-(*tert*-butoxyethyl)-2-nitrophenyl)ethane (**9b**, 4.00 g, 16.9 mmol) was dissolved in 80 mL dry THF, cooled to −5 °C, followed by potassium butoxide addition (2.65 g, 23.6 mmol). The reaction mixture was stirred for 30 s before the addition of bromine (1.12 mL, 21.9 mmol). After further stirring for 20 min the reaction mixture was added to 1 L ice. The precipitate was filtered and recrystallized from ethanol to obtain colourless crystals (2.97 g, 6.29 mmol, 75%).

melting point: 72 °C.

R_f: 0.51 (cyclohexane/ethylacetate, 3:1).

^{1}H-NMR (500.1 MHz, $CDCl_3$, 300 K): δ = 7.85 (d, ^4J = 1.7 Hz, 2 H, *H*-3), 7.40 (dd, ^3J = 7.8 Hz, ^4J = 1.7 Hz, 2 H, *H*-5), 7.30 (d, ^3J = 7.8 Hz, 2 H, *H*-6), 3.57 (t, ^3J = 6.8 Hz, 2 H, (^{t}BuO-CH_2), 3.19 (s, 4 H, C_2H_4), 2.87 (t, ^3J = 6.7 Hz, 2 H, (^{t}BuO-CH$_2$-CH_2), 1.16 (s, 18 H, *H*-^{t}Bu) ppm.

^{13}C-NMR (125.8 MHz, $CDCl_3$, 300 K): δ = 149.2 (*C*-2), 140.0 (*C*-1), 134.7 (*C*-4), 134.1 (*C*-5), 132.1 (*C*-6), 125.09 (*C*-3), 73.1 (*C*-CH_3), 62.0 (^{t}BuO-*C*H_2), 36.6 (^{t}BuO-CH$_2$-*C*H_2) 34.2 (C_2H_4), 27.3 (C-(*C*H_3)$_3$) ppm.

IR (ATR): ϑ = 2974 (m), 2872 (w), 1566 (w), 1526 (vs), (1463 (w), 1392 (w), 1362 (s), 1348 (s), 1266 (m), 1196 (s), 1079 (s), 1029 (w), 939 (w), 894 (w), 843 (m), 830 (w), 806 (m), 766 (w), 736 (w), 677 (w) cm^{-1}.

MS (APCI): m/z (%) = 511 (100) [M+K].

MS (HR-APCI): m/z (%) = [$C_{26}H_{36}O_6N_2{}^{39}K$], m/z = calc.: 511.2205, found: 511.2204.

II.9. Synthesis of (*Z*)-3,8-bis(2-(*tert*-butoxy)ethyl)-11,12-dihydrodibenzo[*c*,*g*][1,2]diazocine (11b)

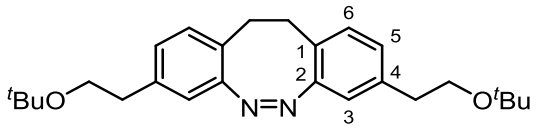

To a solution of 1,2-bis(4-(2-(*tert*-butoxy)ethyl)-2-nitrophenyl)ethane (**10b**, 900 mg, 1.90 mmol) in 105 mL of ethanol, $Ba(OH)_2 \cdot 8H_2O$ (1.80 g, 5.71 mmol) in 50 mL of H_2O and zinc powder (1.99 g, 30.5 mmol) were added, and the mixture was stirred for 5 h under reflux. The reaction mixture was filtered through Celite, and the solvent was removed under reduced pressure. The crude product was dissolved in DCM, filtered through Celite, and the solvent was removed under reduced pressure. The crude product was dissolved in 120 mL 0.1 M methanolic sodium hydroxide solution, $CuCl_2$ (20 mg, 149 µmol) was added and air was led through the solution until completion of the reaction. The reaction mixture was neutralized with 6 M HCl solution. After the addition of saturated sodium bicarbonate solution the aqueous layers were extracted with DCM. The combined organic layers were dried over $MgSO_4$ and the solvent was reduced under reduced pressure. The crude product was purified by flash column chromatography (cyclohexane/ethyl acetate, 3:1) to obtain a yellow oil (466 mg, 1.14 mmol, 60%).

R_f : 0.44 (cyclohexane/ethyl acetate, 3:1).

^{1}H-NMR (500.1 MHz, $CDCl_3$, 300 K): δ = 6.88 (m, 4 H, *H*-5, *H*-6), 6.67 (s, 2 H, *H*-3), 3.45 (t, ^3J = 7.1 Hz, 4 H, ^{t}BuO-C*H*$_2$-CH$_2$), 2.82 (m, 4 H, C$_2$*H*$_4$), 2.70 (t, ^3J = 7.1 Hz, 4 H, ^{t}BuO-CH$_2$-C*H*$_2$), 1.08 (s, 18 H, *H*-^{t}Bu) ppm.

^{13}C-NMR (125.8 MHz, $CDCl_3$, 300 K): δ = 155.2 (*C*-2), 138.2 (*C*-4), 129.4 (*C*-6), 127.8 (*C*-1), 125.7 (*C*-5), 119.4 (*C*-3), 72.8 (*C*-(CH$_3$)$_3$), 62.5 (^{t}BuO-*C*H$_2$), 36.7 (^{t}BuO-CH$_2$-*C*H$_2$), 31.4 (*C*$_2$H$_4$), 27.4 (C-(*C*H$_3$)$_3$) ppm.

IR (ATR): ῡ = 2972 (m), 2866 (w), 1611 (w), 1566 (w), 1491 (w), 1390 (m), 1362 (s), 1233 (w), 1194 (s), 1078 (vs), 1020 (w), 939 (w), 879 (m), 811 (m), 740 (m), 628 (w) cm^{-1}.

MS (EI, 70 eV): m/z (%) = 408 (40), 321 (18), 293 (82), 279 (28), 264 (16), 208 (100).

MS (EI, HR, 70 eV): $C_{26}H_{36}N_2O_2$, m/z = calc.: 408.2777, found: 408.2771.

II.10. Synthesis of (*Z*)-2,2'-(11,12-dihydrodibenzo[*c*,*g*][1,2]diazocine-3,8-diyl)bis(ethan-1-ol) (4b)

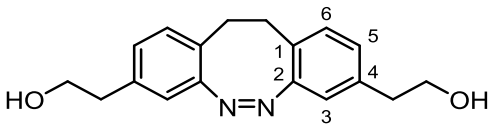

Under a N_2 atmosphere (*Z*)-3,8-bis(2-(*tert*-butoxy)ethyl)-11,12-dihydrodibenzo[*c*,*g*][1,2]diazocine (**11b**, 340 mg, 833 µmol) was dissolved in 3 mL dry DCM, cooled to 0 °C and $TiCl_4$ (90.0 µL, 789 µmol) was added. After 30 s 20 mL saturated potassium carbonate solution were added. The solution was acidified with 1 M hydrochloric acid solution and extracted with DCM. The combined organic layers were washed with saturated sodium chloride solution (50 mL), dried over magnesium sulfate and the solvent was removed in vacuo. The crude product was purified on silica flash column chromatography (cyclohexane/ethyl acetate, 1:1) to obtain a yellow solid. (221 mg, 746 µmol, 90%).

melting point: 94 °C.

R_f : 0.09 (cyclohexane/ethyl acetate, 1:1).

^{1}H-NMR (500.1 MHz, $CDCl_3$, 300 K): δ = 6.90 (d, ^3J = 7.8 Hz, 2 H, *H*-6), 6.96 (dd, ^3J = 7.5 Hz, ^4J = 1.6 Hz 2 H, *H*-5), 6.67 (d, ^4J = 1.6 Hz, 2 H, *H*-3), 3.72 (t, ^3J = 6.2 Hz, 4 H, HO-CH_2), 2.82 (s, 4 H, C_2H_4), 2.73 (t, ^3J = 6.4 Hz, 4 H, HO-CH_2-CH_2) ppm.

^{13}C-NMR (125.8 MHz, $CDCl_3$, 300 K): δ = 155.7 (*C*-2), 137.7 (*C*-4), 130.0 (*C*-6), 126.4 (*C*-1), 127.8 (*C*-5), 118.9 (*C*-3), 63.7 (HO-*C*H_2), 38.8 (HO-CH_2-*C*H_2), 31.4 (C_2H_4) ppm.

IR (ATR): ϑ = 3294 (m), 2918 (m), 1402 (m), 1329 (m), 1068 (s), 1030 (vs), 886 (w), 860 (w), 797 (s), 618 (s) cm^{-1}.

MS (EI, 70 eV): m/z (%) = 296 (32), 265 (10), 237 (100), 219 (32), 204 (55).

MS (EI, HR, 70 eV): $C_{18}H_{18}N_2O_2$, m/z = calc.: 296.1525, found: 296.1509.

II.11. Synthesis of (*Z*)-3,8-bis(2-azidoethyl)-11,12-dihydrodibenzo[*c*,*g*][1,2]diazocine (5b)

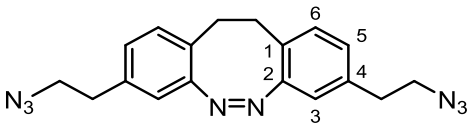

Under a N_2 atmosphere (*Z*)-2,2'-(11,12-dihydrodibenzo[*c*,*g*][1,2]diazocine-3,8-diyl)bis(ethan-1-ol) (**4b**, 132 mg, 445 µmol) was dissolved in 2 mL dry THF. 2-Azido-1,3-dimethylimidazolinium hexafluorophosphate (316 mg, 1.11 mmol) and DBU (199 µL, 1.34 mmol) were added, the reaction was stirred for 2 h at room temperature and stopped by the addition of 20 mL saturated potassium solution. After extraction with DCM the combined organic layers were washed with saturated sodium chloride solution, dried over magnesium sulfate and the solvent was removed in vacuo. The crude product was purified on silica flash column chromatography (cyclohexane/ethyl acetate, 1:1) to obtain a yellow oil. (121 mg, 350 µmol, 79%).

R_f: 0.8 (cyclohexane/ethyl acetate, 1:1).

^{1}H-NMR (500.1 MHz, $CDCl_3$, 300 K): δ = 6.93 (d, ^3J = 7.8 Hz, 2 H, *H*-6), 6.87 (dd, ^3J = 7.8 Hz, ^4J = 1.7 Hz 2 H, *H*-5), 6.70 (d, ^4J = 1.6 Hz, 2 H, *H*-3), 3.41 (t, ^3J = 5.8 Hz, 4 H, N_3-CH_2), 2.94 (s, 4 H, C_2H_4), 2.78 (t, ^3J = 7.1 Hz, 4 H, N_3-CH_2-CH_2) ppm.

^{13}C-NMR (125.8 MHz, $CDCl_3$, 300 K): δ = 155.5 (*C*-2), 136.8 (*C*-4), 129.6 (*C*-6), 127.5 (*C*-1), 126.6 (*C*-5), 119.0 (*C*-3), 52.1 (N_3-*C*H_2), 34.8 (N_3-CH_2-*C*H_2), 31.4 (C_2H_4) ppm.

IR (ATR): ῡ = 2928 (w), 2087 (vs), 1685 (w), 1610 (w), 1566 (m), 1492 (m), 1485 (m), 1437 (m), 1346 (m), 1252 (s), 1137 (w), 1091 (w), 1043 (w), 979 (w), 948 (w), 887 (m), 809 (m) cm^{-1}.

MS (EI, 70 eV): m/z (%) = 346 (34), 262 (18), 234 (22), 218 (30), 202 (67), 191 (100).

MS (EI, HR, 70 eV): $C_{18}H_{18}N_8$, m/z = calc.: 346.1654, found: 346.1650.

II.12. Synthesis of (*Z*)-2,2'-(11,12-dihydrodibenzo[*c*,*g*][1,2]diazocine-3,8-diyl)bis(ethan-1-amine) (6b)

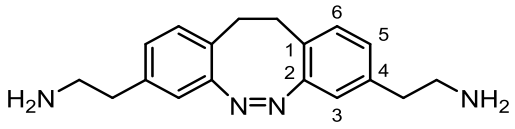

(*Z*)-3,8-Bis(2-azidoethyl)-11,12-dihydrodibenzo[*c*,*g*][1,2]diazocine (**5b**, 68 mg, 196 µmol) and triphenylphosphine (113 mg, 431 µmol) were dissolved in dry THF. After the addition of water (71.0 µL, 392 µmol) the reaction mixture was stirred for 4 h at room temperature and afterwards diluted with water. The solution was acidified with 1 M hydrochloric acid solution and washed with DCM (3 × 50 mL). The aqueous solution was neutralized with 1 M sodium hydroxide solution and extracted at pH > 7 with DCM. The combined organic layers were washed with saturated sodium chloride solution, dried over magnesium sulfate and the solvent was removed in vacuo to obtain a yellow solid. (55.0 mg, 187 µmol, 95%).

R_f: 0.01 (cyclohexane/ethyl acetate, 1:1).

^{1}H-NMR (500.1 MHz, D_2O, 300 K): δ = 7.11 (d, ^3J = 7.9 Hz, 2 H, *H*-6), 7.03 (dd, ^3J = 7.9 Hz, ^4J = 1.7 Hz, 2 H, *H*-5), 6.83 (d, ^4J = 1.6 Hz, 2 H, *H*-3), 3.17 (t, ^3J = 6.2 Hz, 4 H, H_2N-CH_2), 2.87 (s, 4 H, C_2H_4), 2.86 (m, 4 H, H_2N-CH_2-CH_2) ppm.

^{13}C-NMR (125.8 MHz, D_2O, 300 K): δ = 154.1 (*C*-2), 136.7 (*C*-4), 130.7 (*C*-6), 128.5 (*C*-1), 128.1 (*C*-5), 119.0 (*C*-3), 40.1 (N_3-*C*H_2), 32.1 (N_3-CH_2-*C*H_2), 30.5 (C_2H_4) ppm.

IR (ATR): ϑ̃ = 2944 (w), 1777 (w), 1671 (s), 1520 (w), 1469 (w), 1434 (w), 1135 (vs), 962 (m), 839 (m), 812 (s), 797 (s), 750 (w), 723 (s), 704 (s) cm^{-1}.

MS (EI, 70 eV): m/z (%) = 294 (1), 265 (100), 236 (11), 220 (35), 205 (54).

MS (EI, HR, 70 eV): $C_{18}H_{22}N_4$, m/z = calc.: 294.1845, found: 294.1839.

II.13. Synthesis of (*Z*)-3,8-divinyl-11,12-dihydrodibenzo[*c*,*g*][1,2]diazocine (7)

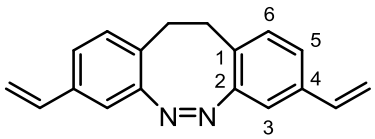

Under a N_2 atmosphere tosylchloride (325 mg, 1.71 mmol) and DMAP (27 mg, 223 µmol) were dissolved in 4 mL dry DCM and TEA (414 mL, 2.97 mmol) was added. (*Z*)-2,2'-(11,12-Dihydrodibenzo[*c*,*g*][1,2]diazocine-3,8-diyl)bis(ethan-1-ol) (**4b**, 220 mg, 742 µmol) was dissolved in 7 mL dry DCM and added dropwise over a period of 10 min. The reaction mixture was stirred for 5 h at room temperature, followed by the addition of saturated sodium carbonate solution. After extraction with DCM the combined organic layers were washed with water and saturated sodium chloride solution and dried over magnesium sulfate. The solvent was removed in vacuo and the crude product was purified on silica flash column chromatography (cyclohexane/ethyl acetate, 1:1). The isolated product from step one was dissolved under N_2 atmosphere in dry THF and potassium butoxide (151 mg, 1.35 mmol) was dissolved in dry THF and added dropwise at 0 °C. The reaction mixture was stirred at 0 °C for 30 min and diluted in ethyl acetate and water. After separation, the aqueous phase was extracted with ethyl acetate twice, washed with saturated sodium chloride solution twice, and dried over magnesium sulfate. The solvent was removed under reduced pressure and the residue purified by silica flash column chromatography (cyclohexane/ethyl acetate, 1:1) to obtain yellow crystals. (139 mg, 534 µmol, 72%).

melting point: 98 °C.

R_f : 0.65 (cyclohexane/ethyl acetate, 2:1).

^{1}H-NMR (500.1 MHz, $CDCl_3$, 300 K): δ = 7.06 (dd, ^3J = 7.8 Hz, ^4J = 1.7 Hz 2 H, *H*-5), 6.94 (d, ^3J = 7.9 Hz, 2 H, *H*-6), 6.87 (d, ^4J = 1.7 Hz, 2 H, *H*-3), 6.59 (dd, ^2J = 17.6 Hz, ^3J = 10.9 Hz, 2 H, C*H*-CH_2), 5.66 (dd, ^3J = 17.6 Hz, ^4J = 0.7 Hz, 2 H, CH-C$H_{2\ trans}$), 5.21 (dd, ^3J = 10.9 Hz, ^4J = 0.6 Hz, 2 H, CH-C$H_{2\ cis}$), 2.86 (m, 4 H, C_2H_4) ppm.

^{13}C-NMR (125.8 MHz, $CDCl_3$, 300 K): δ = 155.4 (*C*-2), 136.2 (*C*-4), 135.8 (*C*H-CH_2), 129.9 (*C*-6), 127.6 (*C*-1), 124.9 (*C*-5), 116.7 (*C*-3), 114.5 (CH-*C*H_2), 31.5 (C_2H_4), ppm.

IR (ATR): $\tilde{\upsilon}$ = 2021 (w), 1836 (w), 1556 (w), 1487 (w), 1434 (w), 1267 (w), 1093 (w), 997 (m), 986 (m), 956 (m), 914 (vs), 900 (s), 884 (m), 819 (s), 749 (m), 707 (w) cm^{-1}.

MS (EI, 70 eV): m/z (%) = 260 (78), 215 (53), 202 (100).

MS (EI, HR, 70 eV): $C_{18}H_{16}N_2$, m/z = calc.: 260.1313, found: 260.1317.

III. NMR spectra

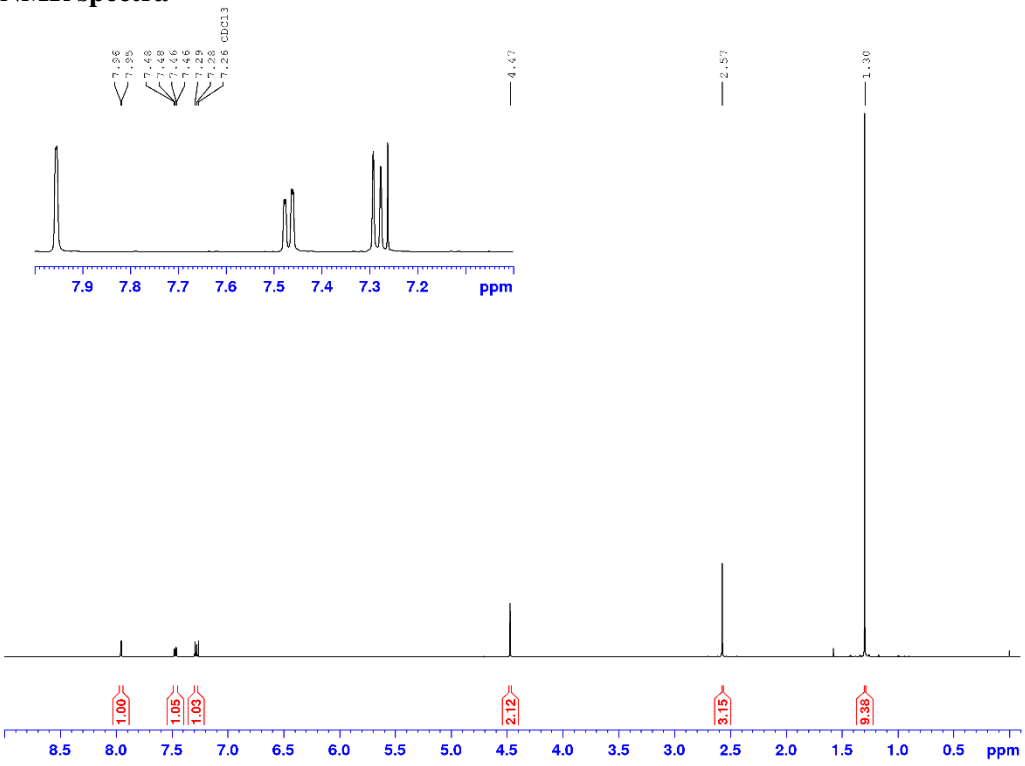

Figure S1: ^{1}H-NMR spectrum of compound **9a** measured in deuterated chloroform.

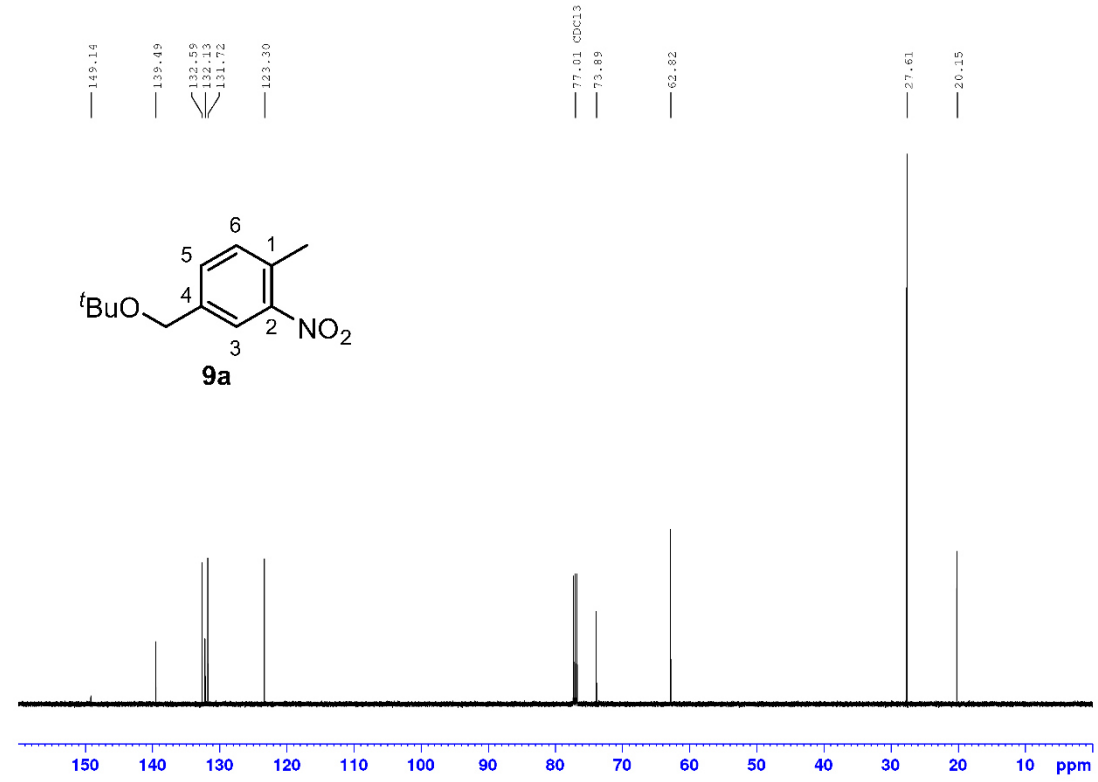

Figure S2: ^{13}C-NMR spectrum of compound **9a** measured in deuterated chloroform.

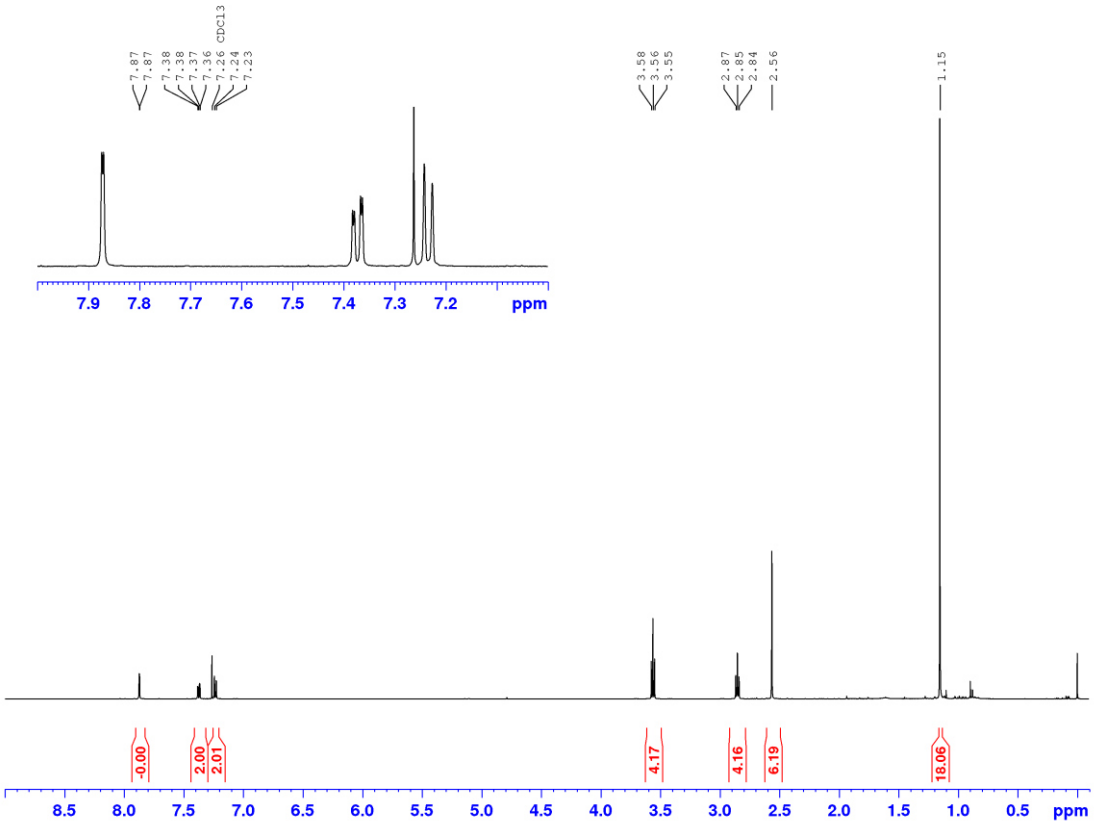

Figure S3: [1]H-NMR spectrum of compound **9b** measured in deuterated chloroform.

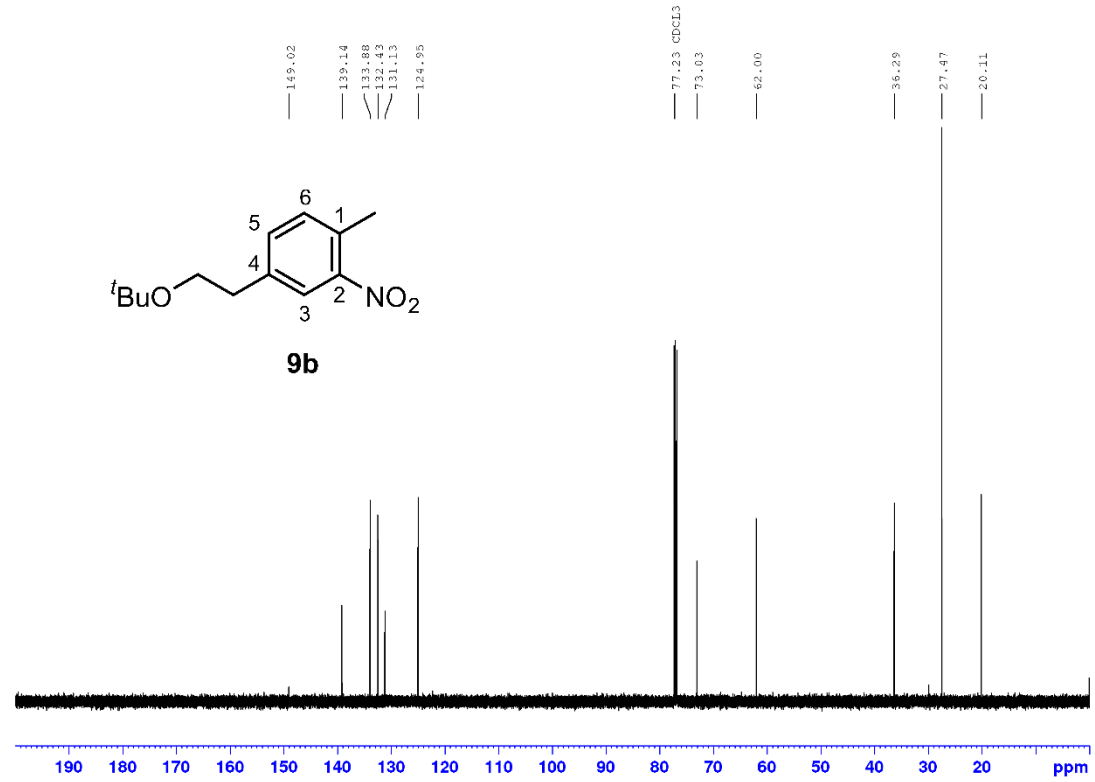

Figure S4: [13]C-NMR spectrum of compound **9b** measured in deuterated chloroform.

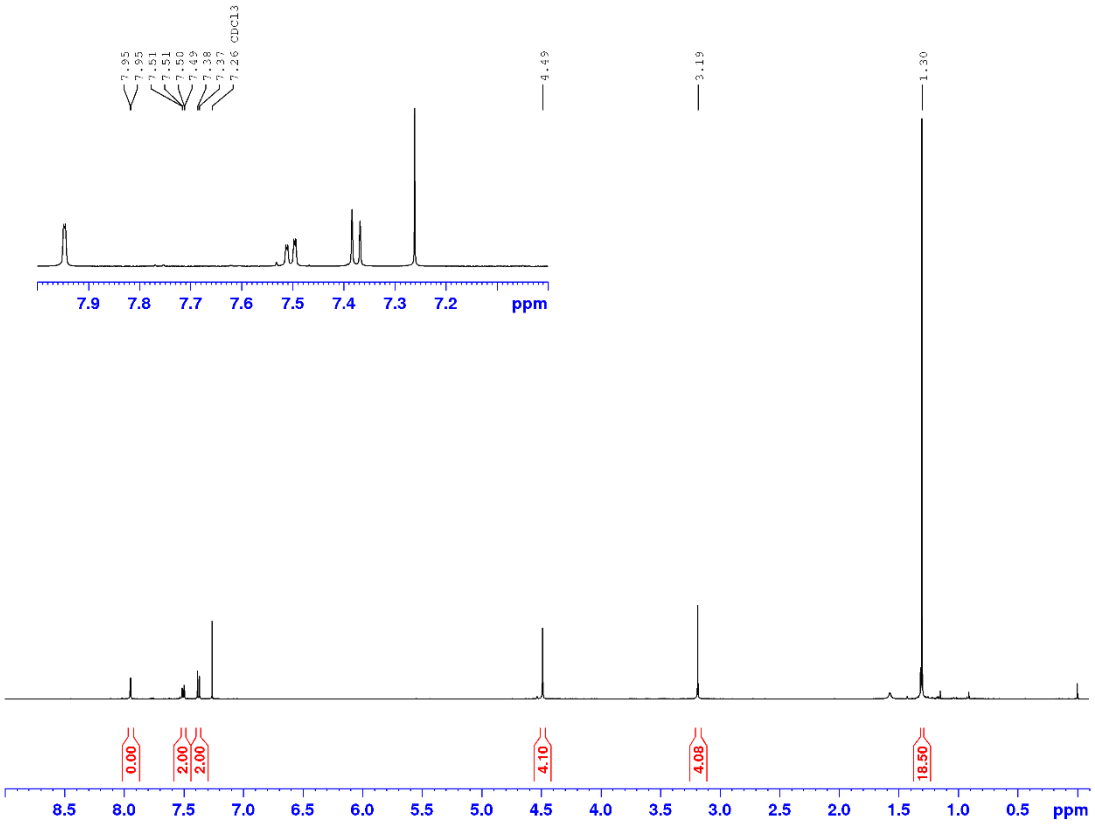

Figure S5: ^{1}H-NMR spectrum of compound **10a** measured in deuterated chloroform.

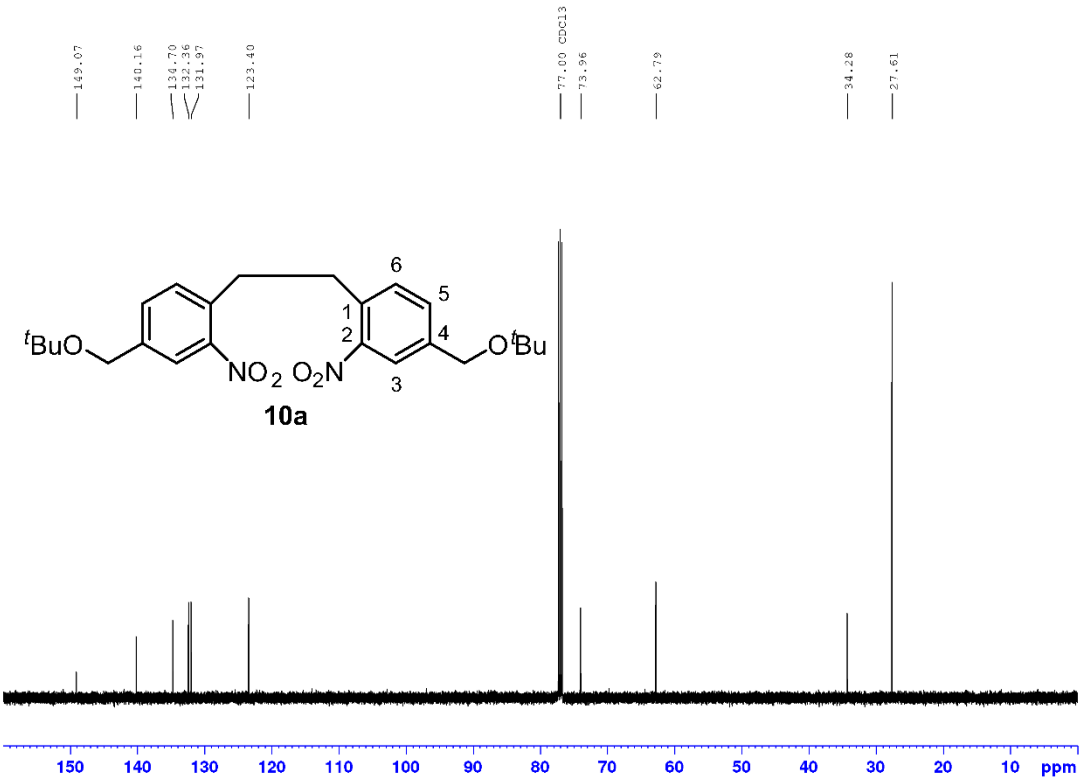

Figure S6: ^{13}C-NMR spectrum of compound **10a** measured in deuterated chloroform.

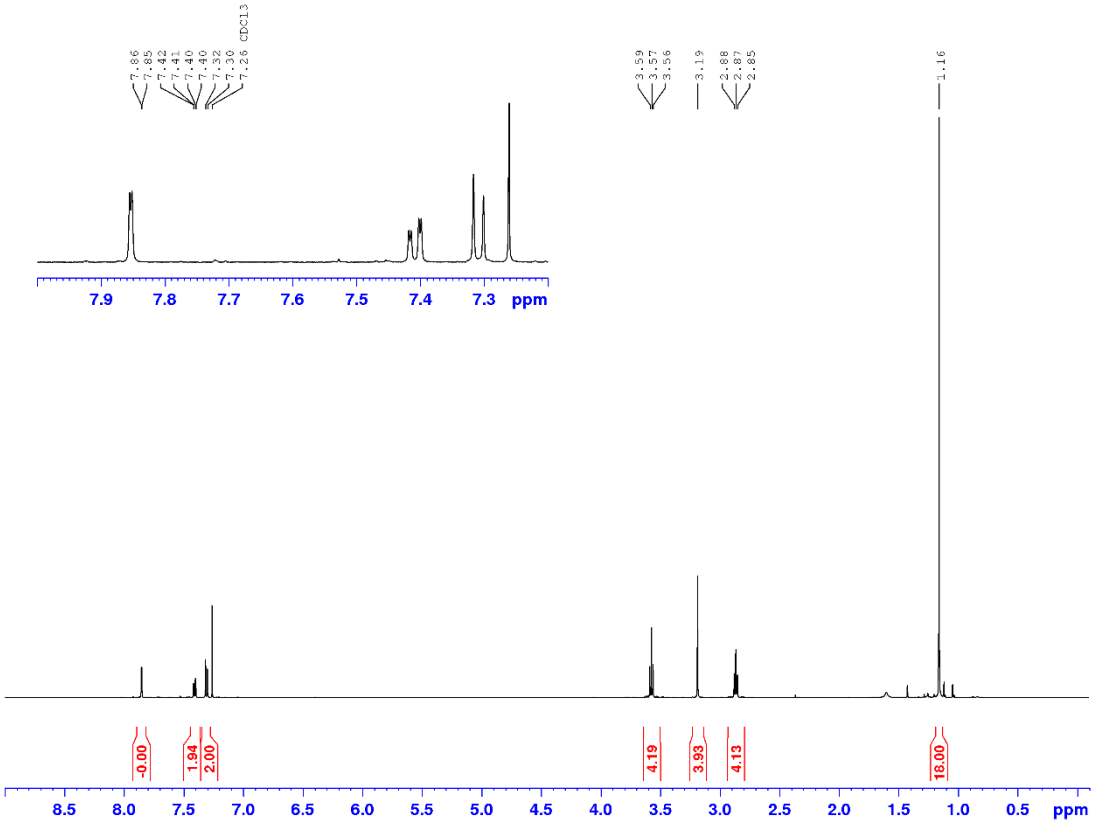

Figure S7: ^{1}H-NMR spectrum of compound **10b** measured in deuterated chloroform.

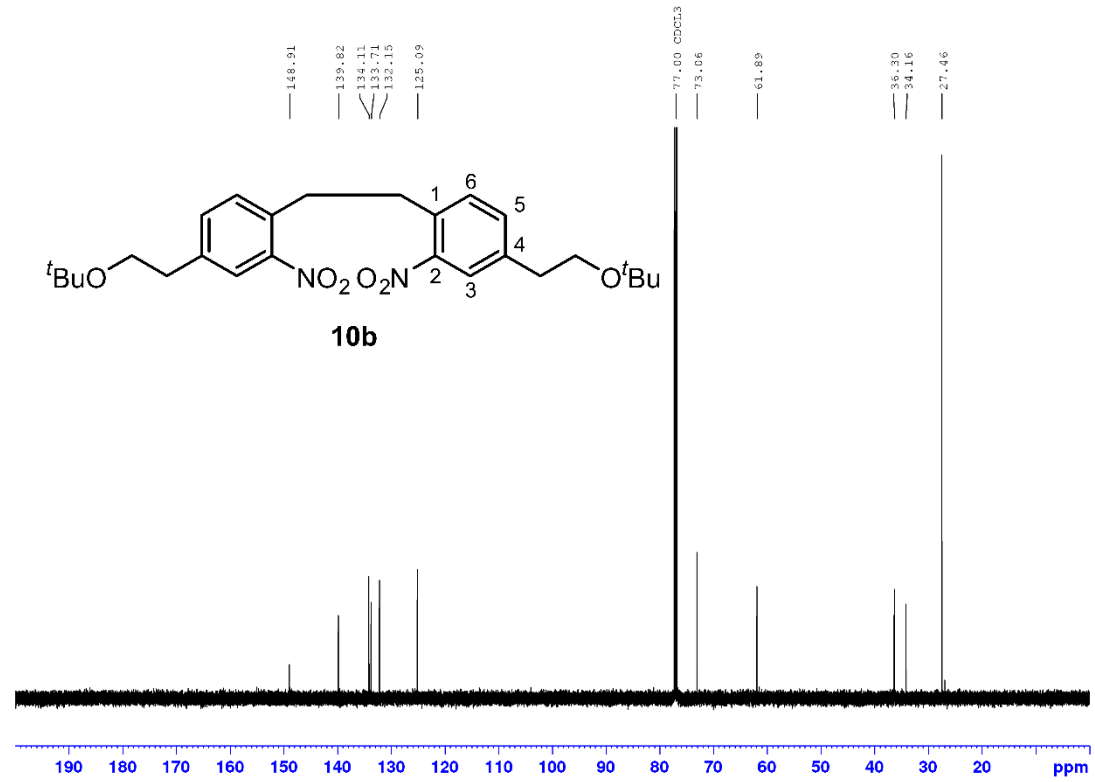

Figure S8: ^{13}C-NMR spectrum of compound **10b** measured in deuterated chloroform.

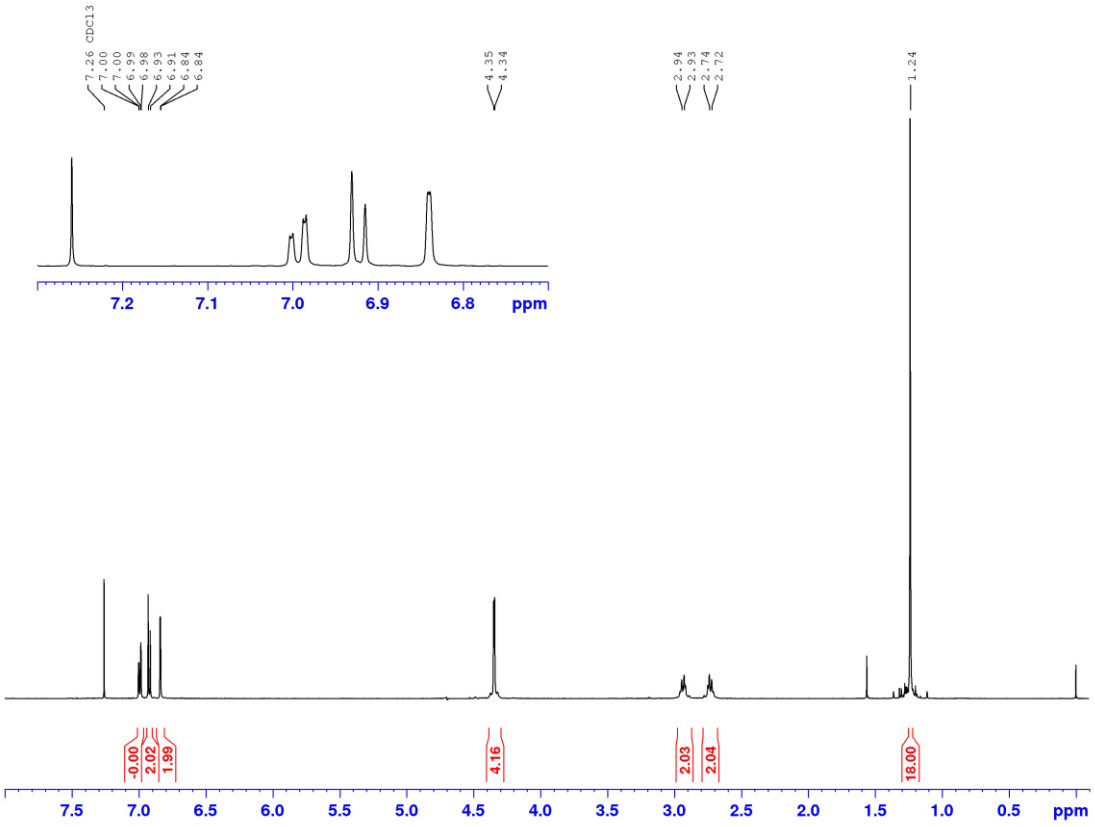

Figure S9: ^{1}H-NMR spectrum of compound **11a** measured in deuterated chloroform.

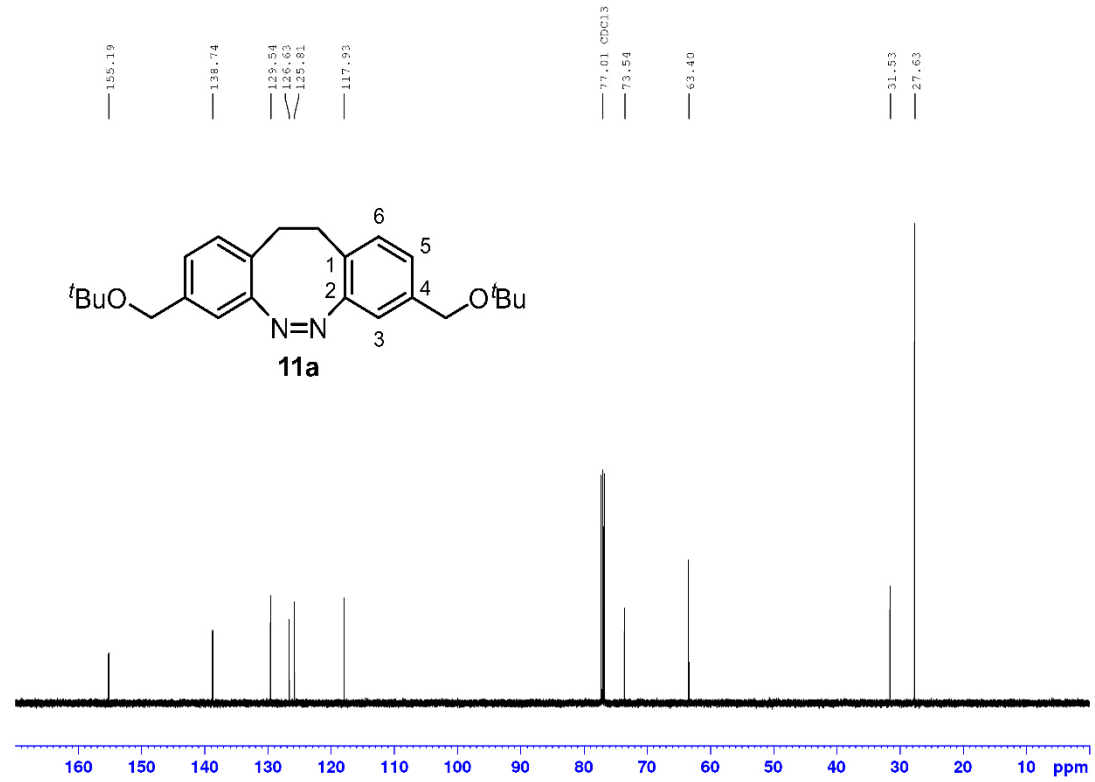

Figure S10: ^{13}C-NMR spectrum of compound **11a** measured in deuterated chloroform.

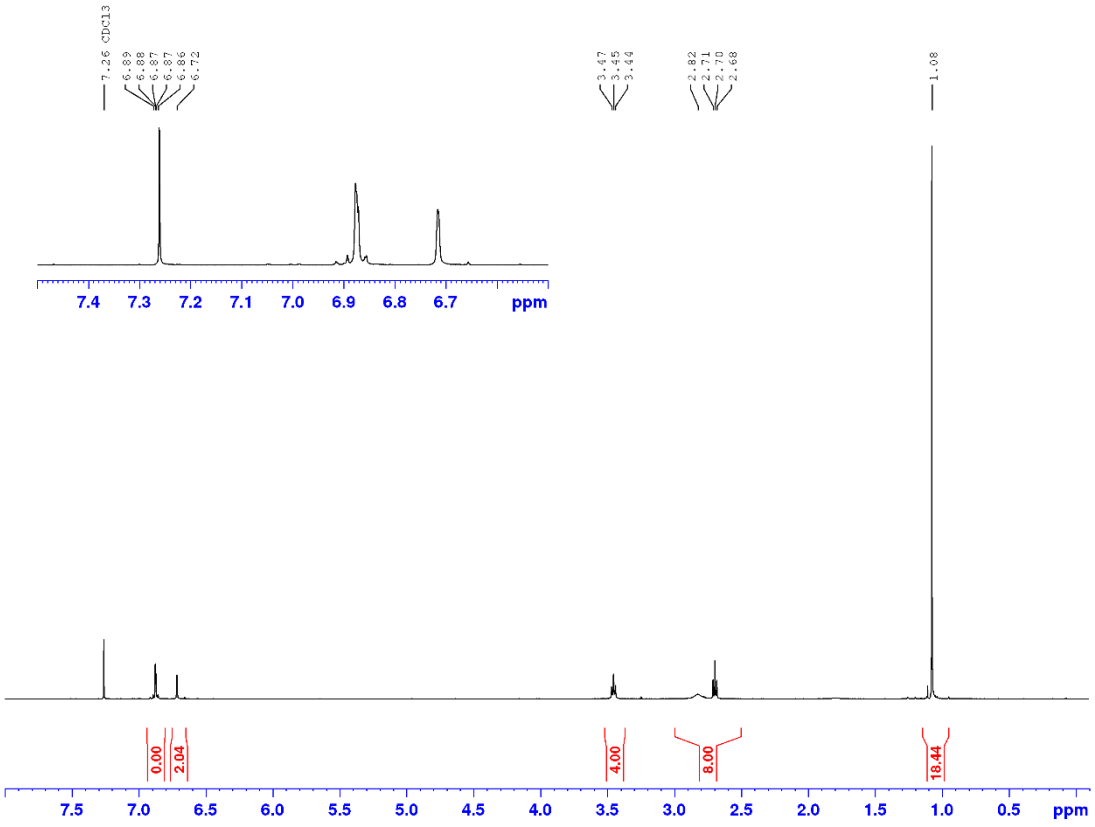

Figure S11: ^{1}H-NMR spectrum of compound **11b** measured in deuterated chloroform.

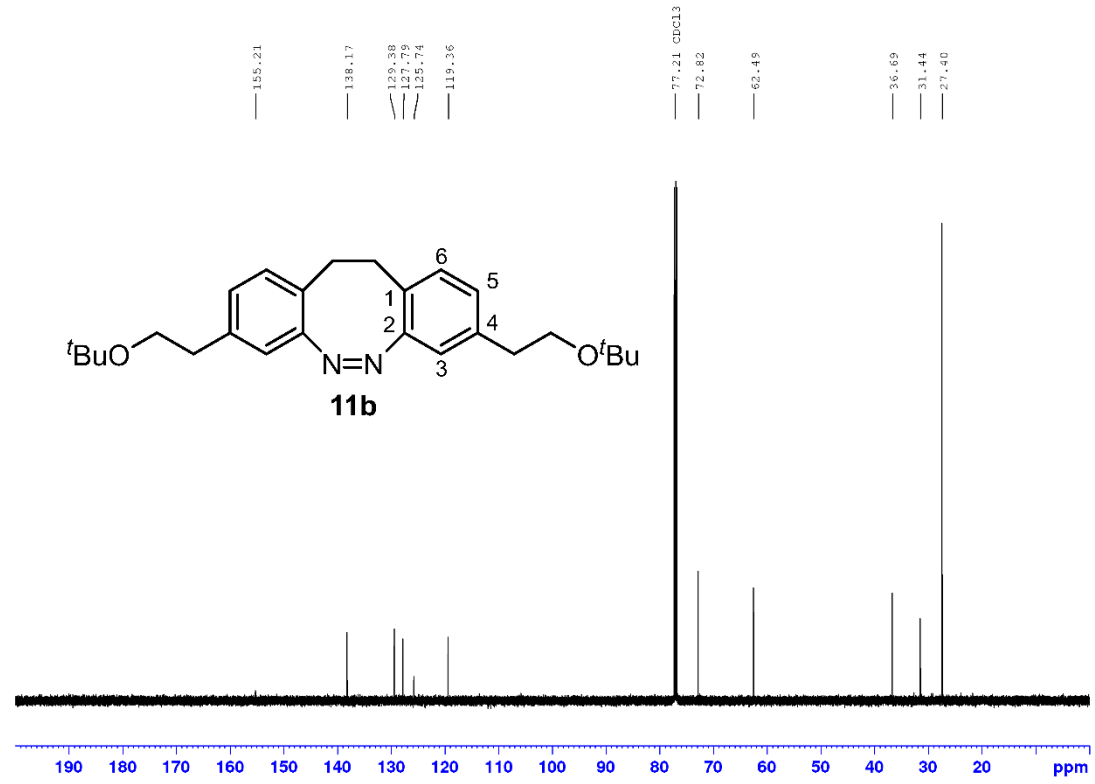

Figure S12: ^{13}C-NMR spectrum of compound **11b** measured in deuterated chloroform.

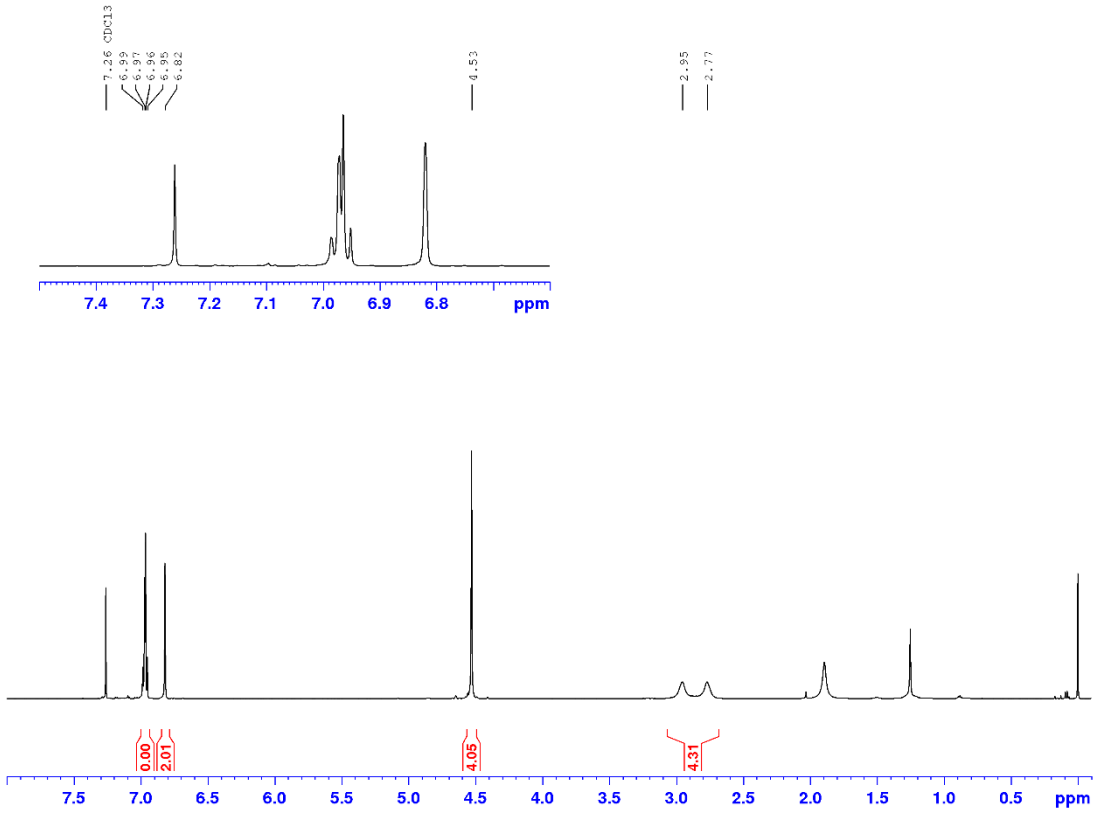

Figure S13: ^{1}H-NMR spectrum of compound **4a** measured in deuterated chloroform.

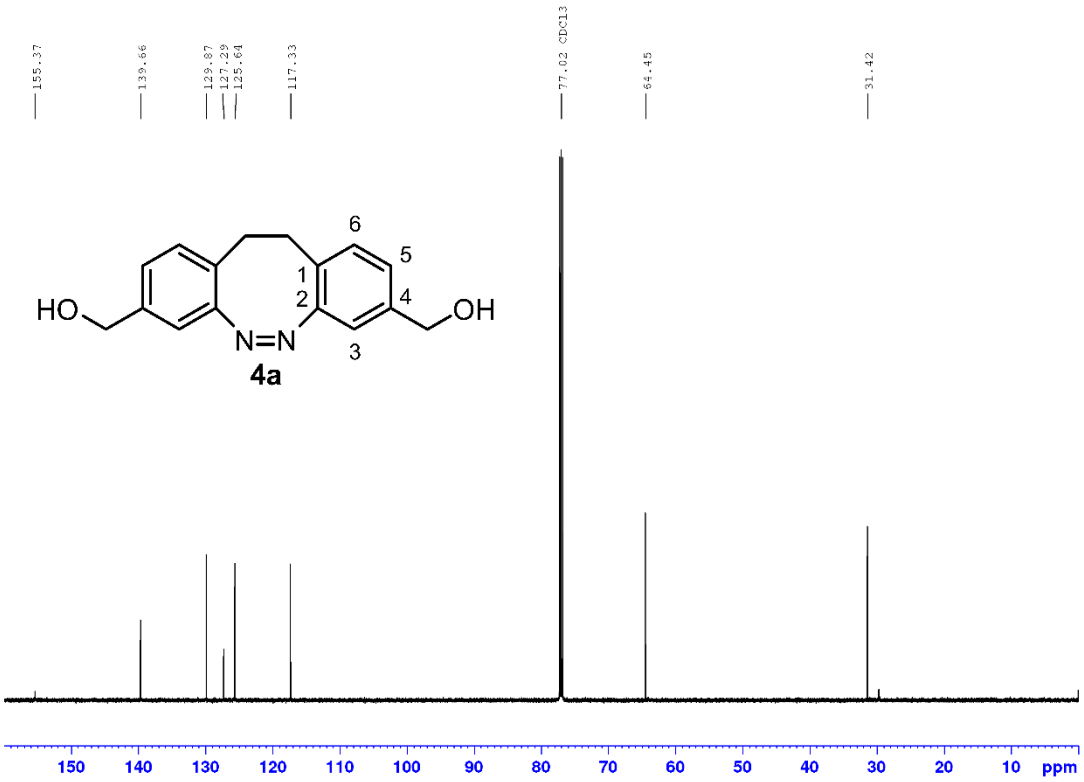

Figure S14: ^{13}C-NMR spectrum of compound **4a** measured in deuterated chloroform.

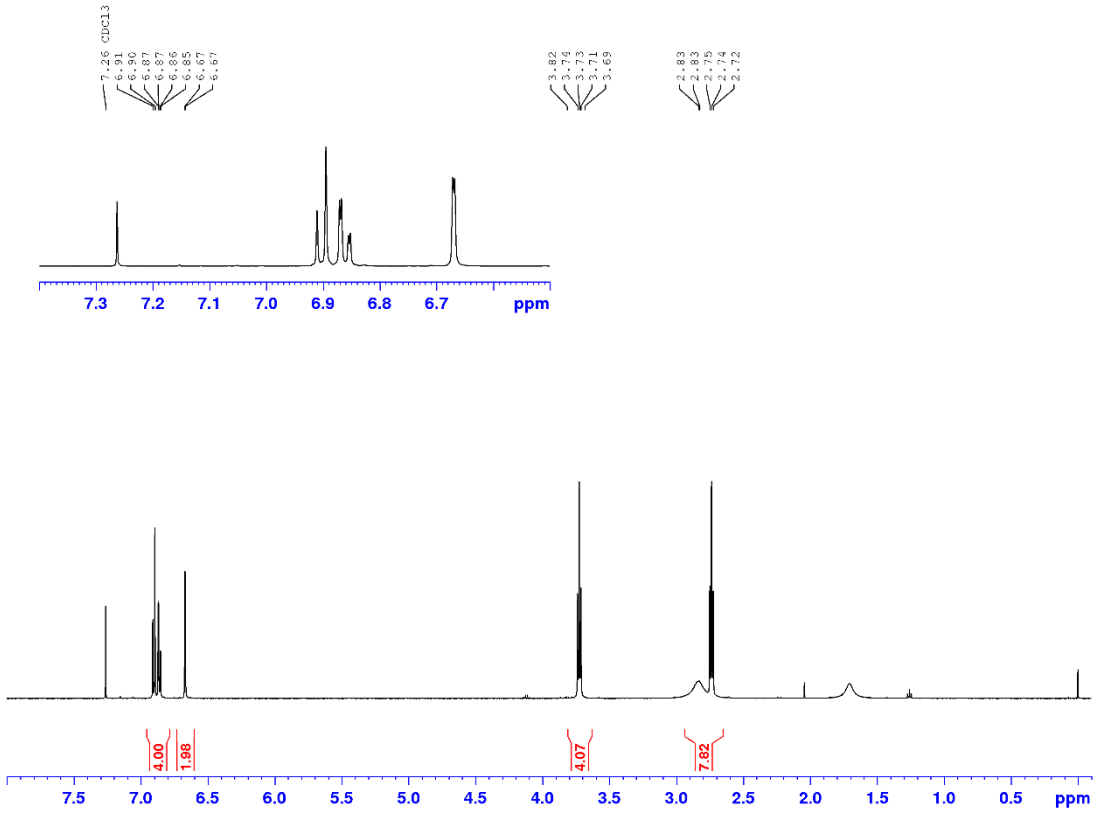

Figure S15: [1]H-NMR spectrum of compound **4b** measured in deuterated chloroform.

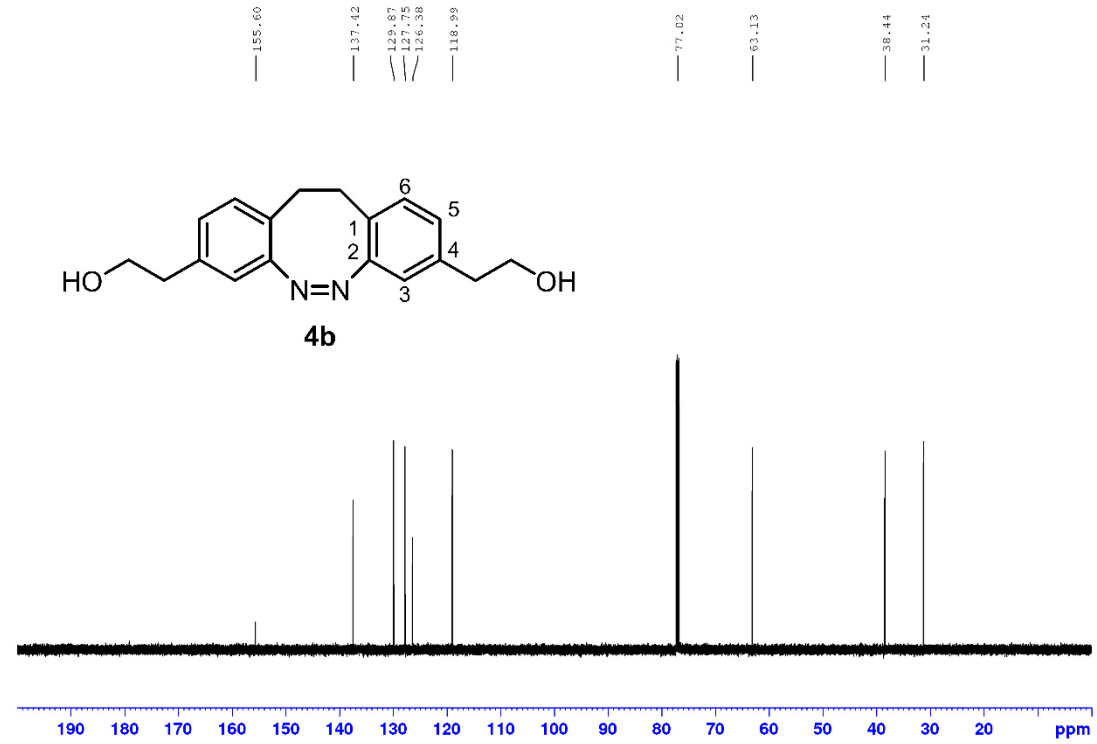

Figure S16: [13]C-NMR spectrum of compound **4b** measured in deuterated chloroform.

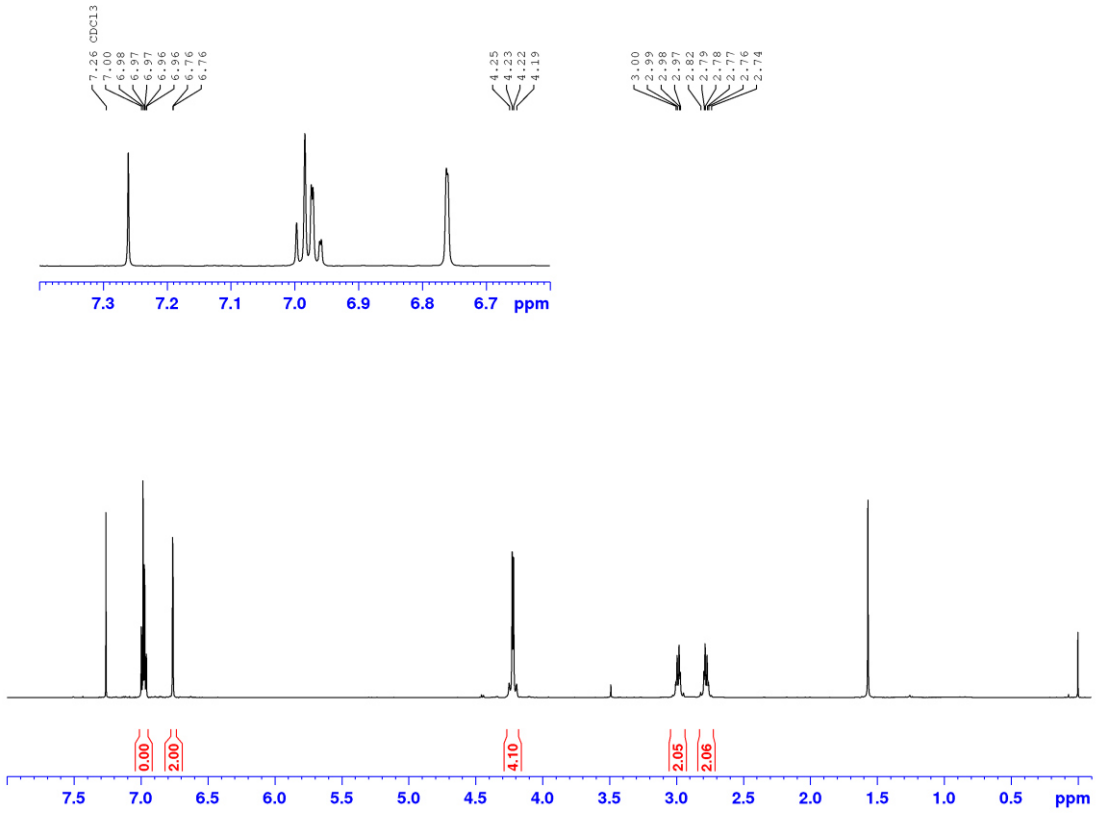

Figure S17: ^{1}H-NMR spectrum of compound **5a** measured in deuterated chloroform.

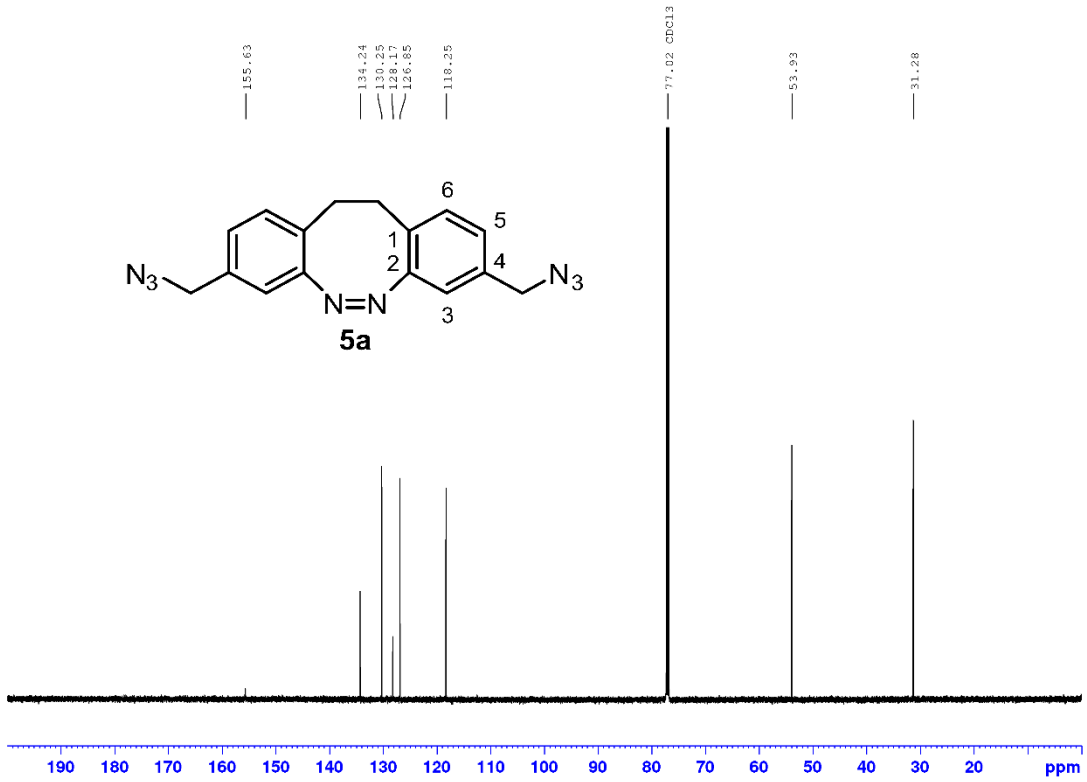

Figure S18: ^{13}C-NMR spectrum of compound **5a** measured in deuterated chloroform.

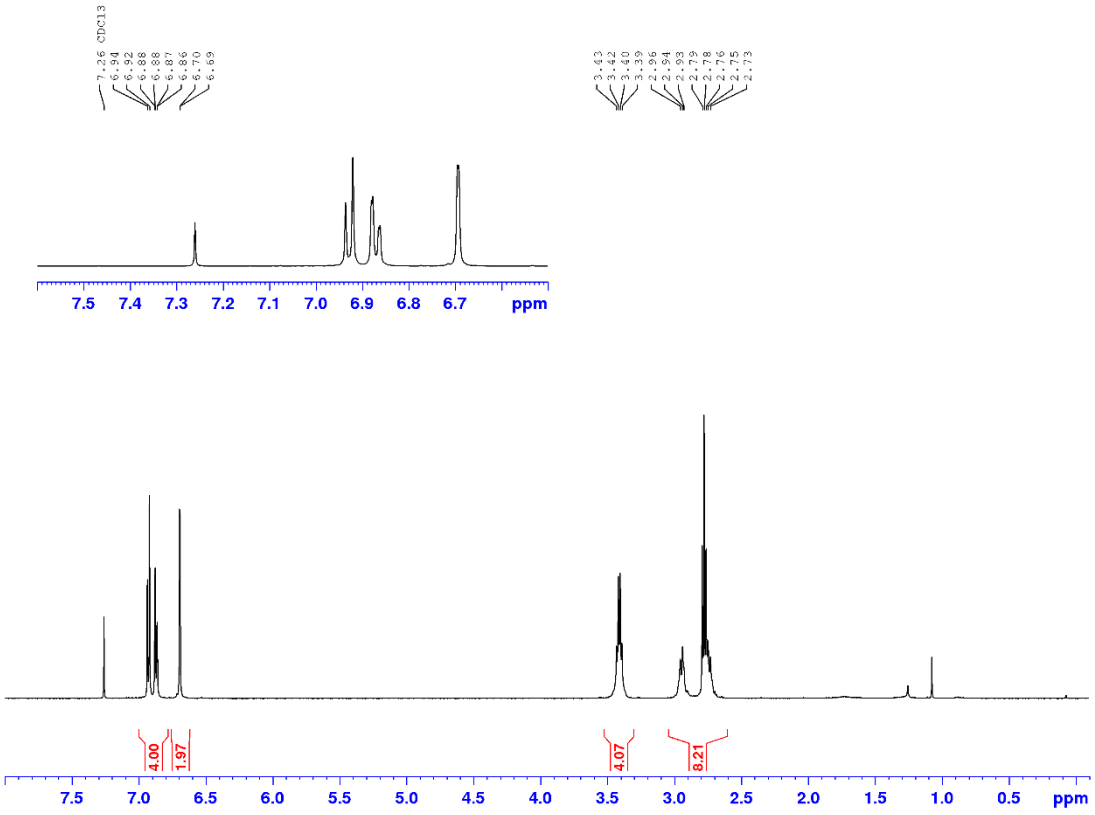

Figure S19: ^{1}H-NMR spectrum of compound **5b** measured in deuterated chloroform.

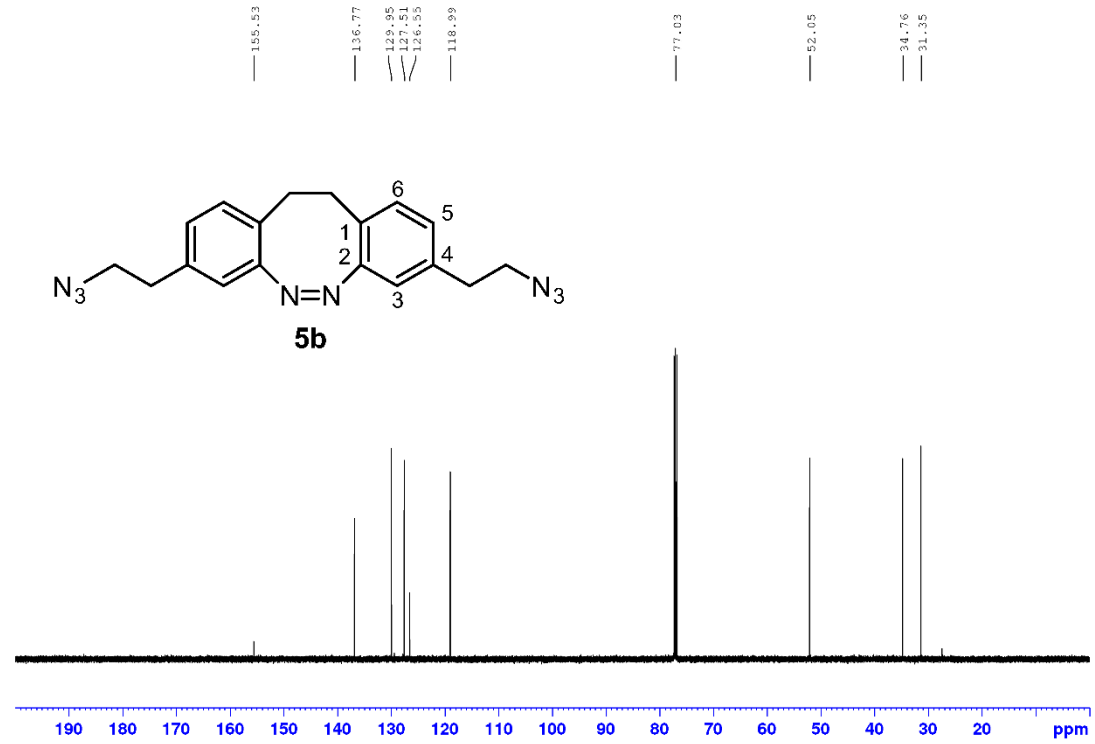

Figure S20: ^{13}C-NMR spectrum of compound **5b** measured in deuterated chloroform.

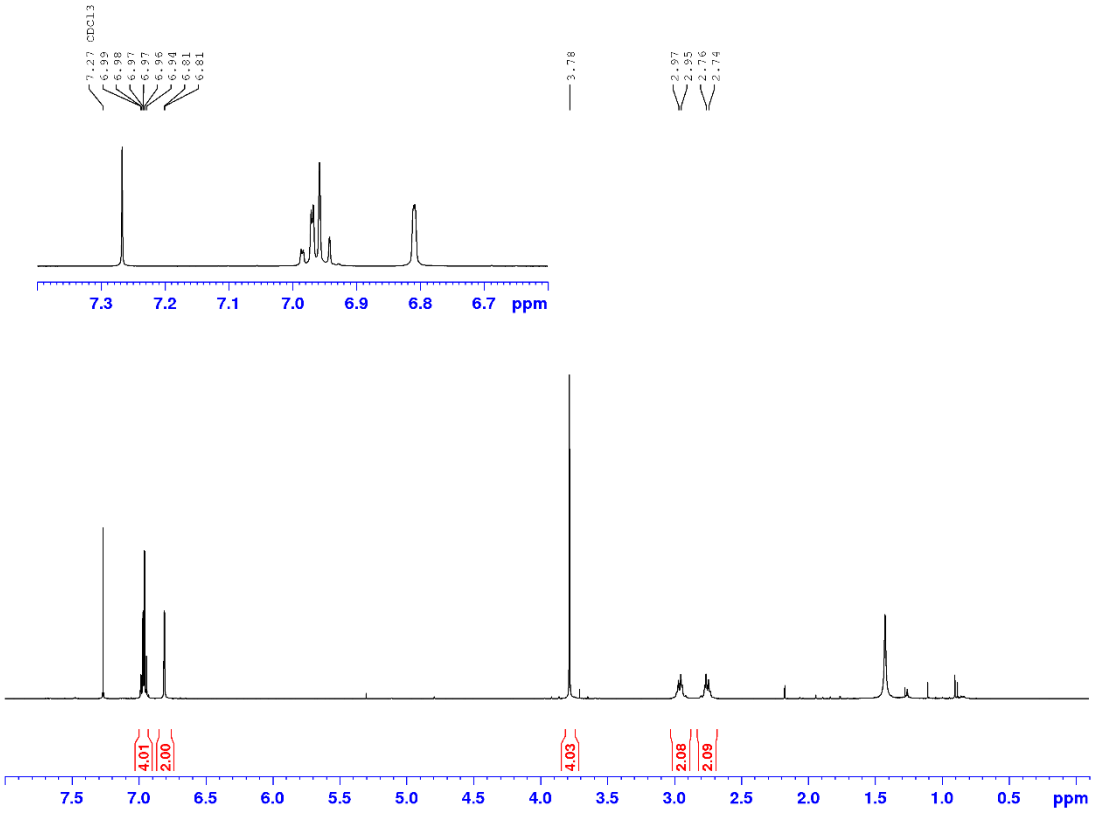

Figure S21: ^{1}H-NMR spectrum of compound **6a** measured in deuterated chloroform.

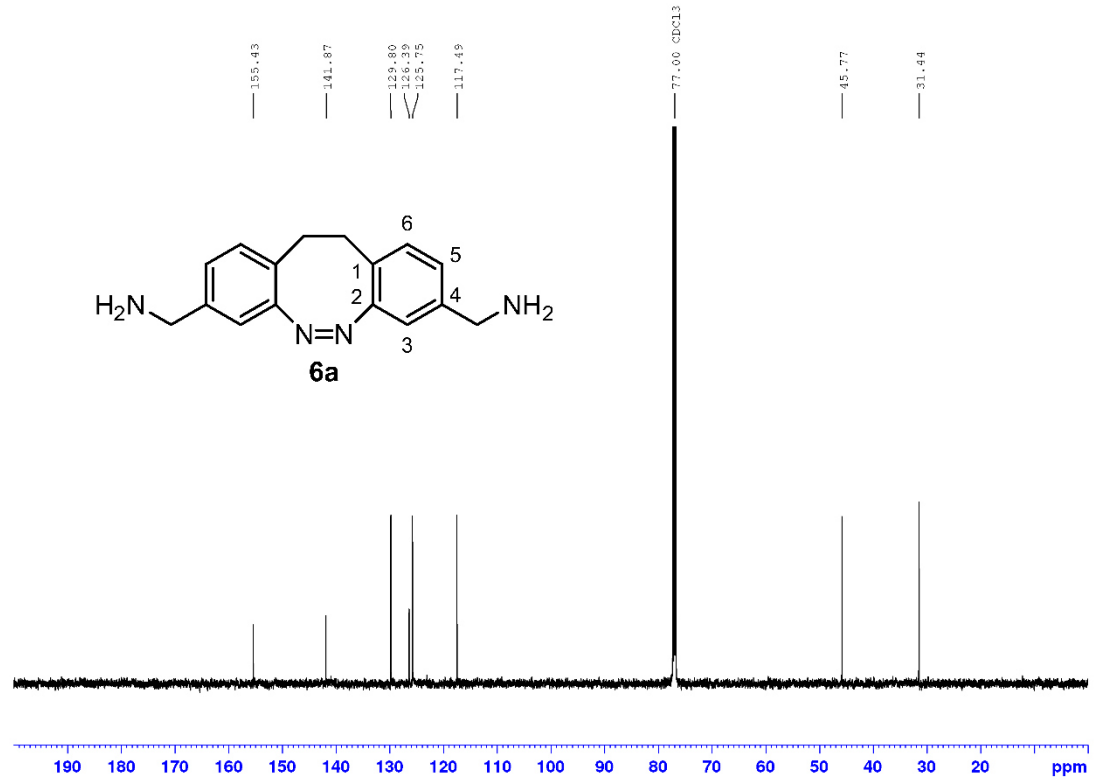

Figure S22: ^{13}C-NMR spectrum of compound **6a** measured in deuterated chloroform.

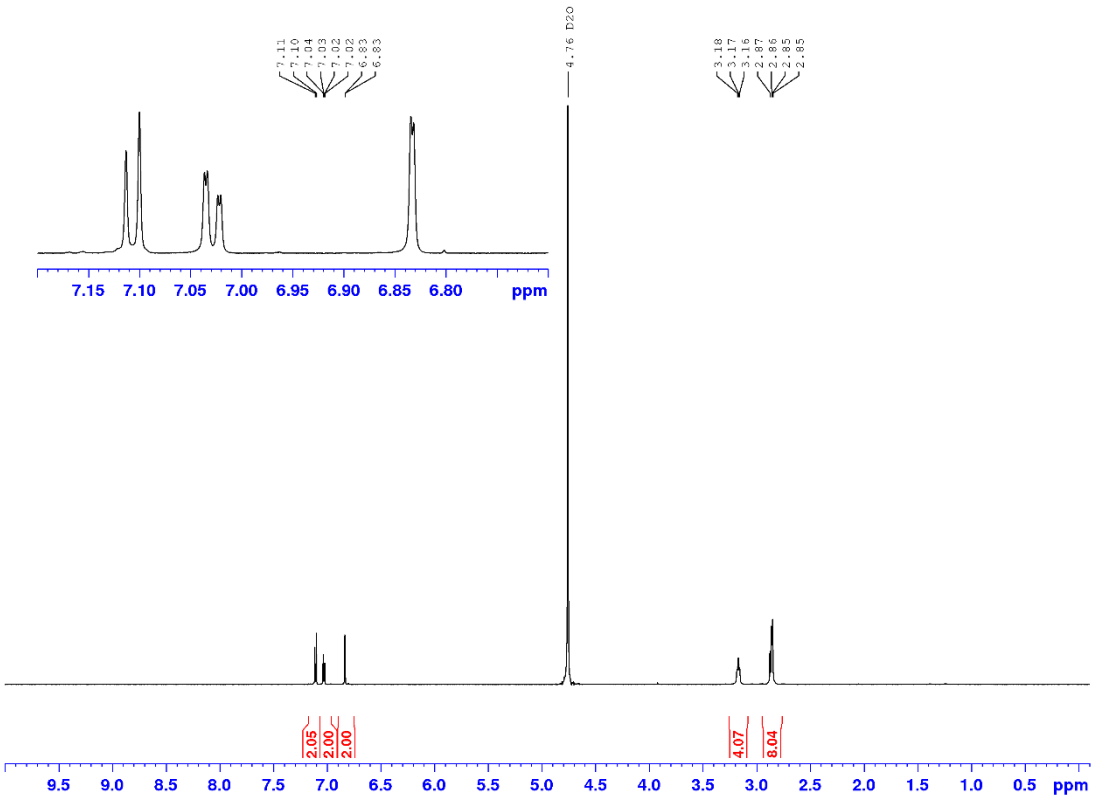

Figure S23: ^{1}H-NMR spectrum of compound **6b** measured in deuterated water.

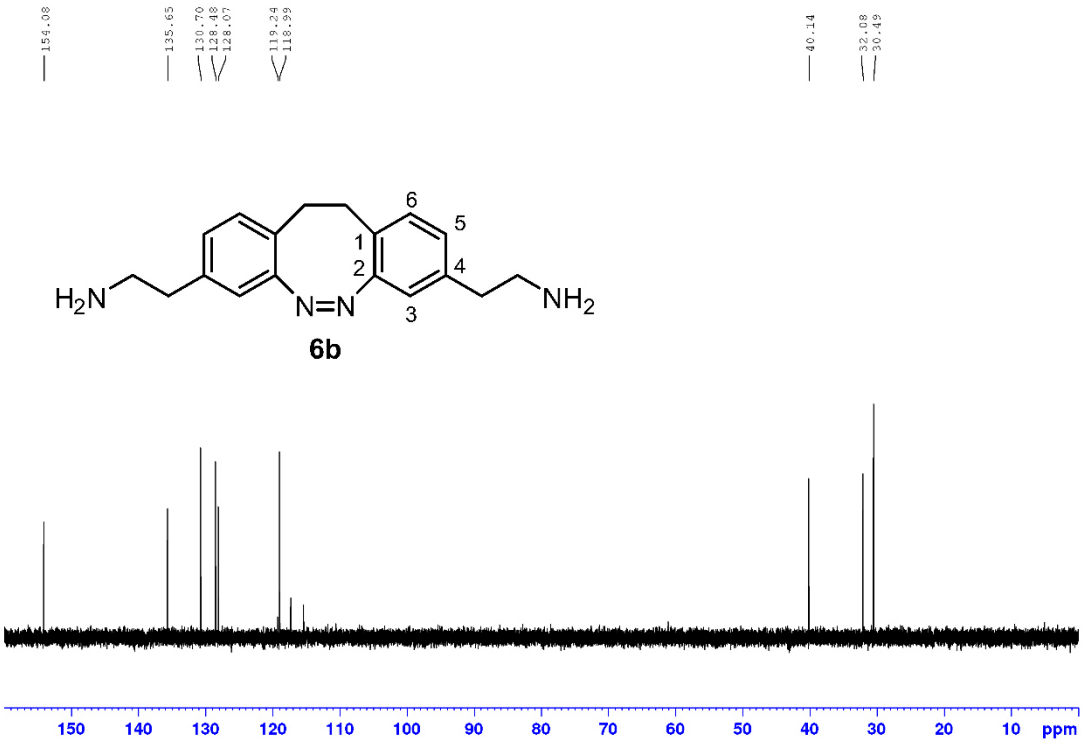

Figure S24: ^{13}C-NMR spectrum of compound **6b** measured in deuterated water.

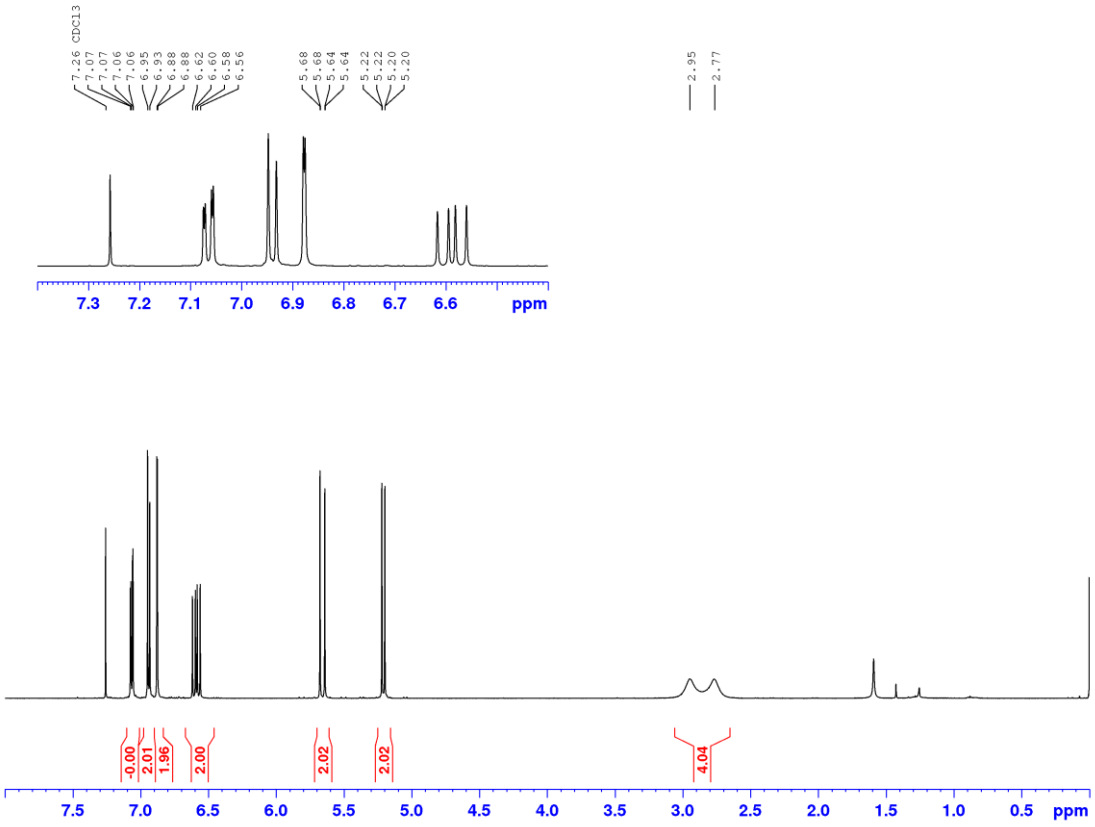

Figure S25: [1]H-NMR spectrum of compound **7** measured in deuterated chloroform.

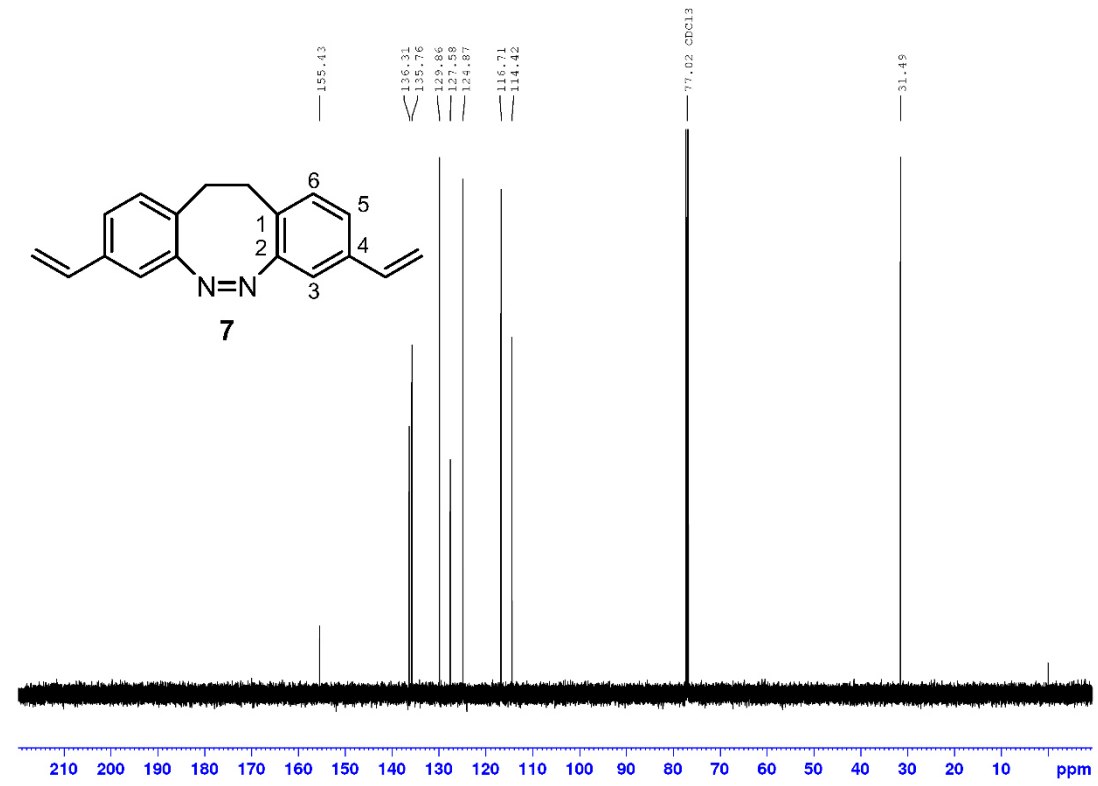

Figure S26: [13]C-NMR spectrum of compound **7** measured in deuterated chloroform.

IV. UV–vis spectra

The functionalized diazocines **1**–**7**,**11a** and **11b** were dissolved in acetonitrile (0.05 mM) under exclusion of light and UV–vis *cis* spectra (black) were recorded. Then the solutions were irradiated at 385 nm for 2 min and the UV–vis PSS spectra (red) were measured.

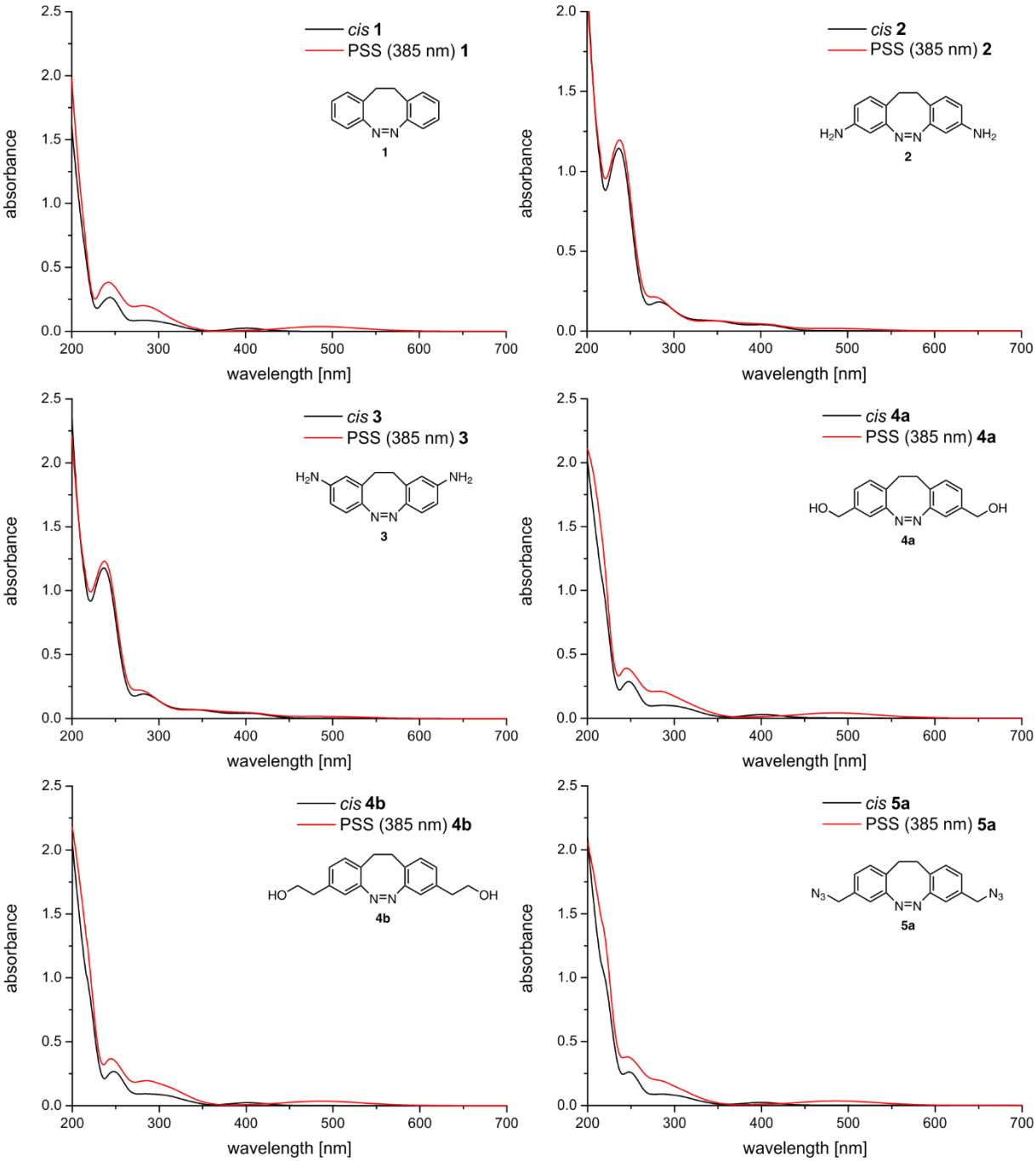

Figure S27: UV–vis spectra of functionalized diazocines **1**, **2**, **3**, **4a**, **4b** and **5a** spectra measured at 25 °C in acetonitrile (0.05 mM). The black line is the spectrum of the pure *cis* compound and in red the PSS after irradiation at 385 nm.

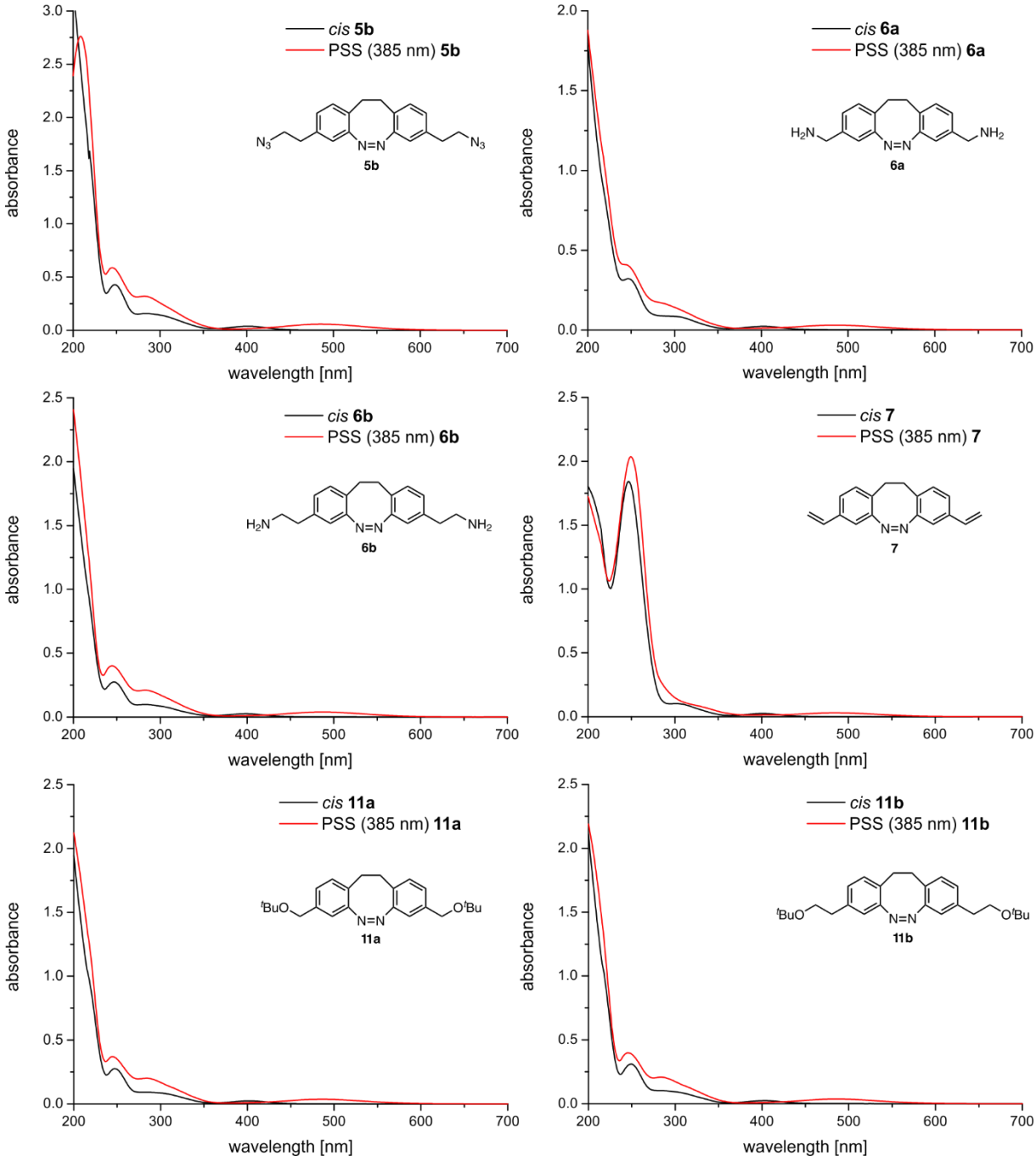

Figure S28: UV–vis of functionalized diazocines **5b**, **6a**, **6b**, **7**, **11a** and **11b** spectra measured at 25 °C in acetonitrile 0.05mM. The black line is the spectrum of the pure *cis* compound and in red the PSS after irradiation at 385 nm.

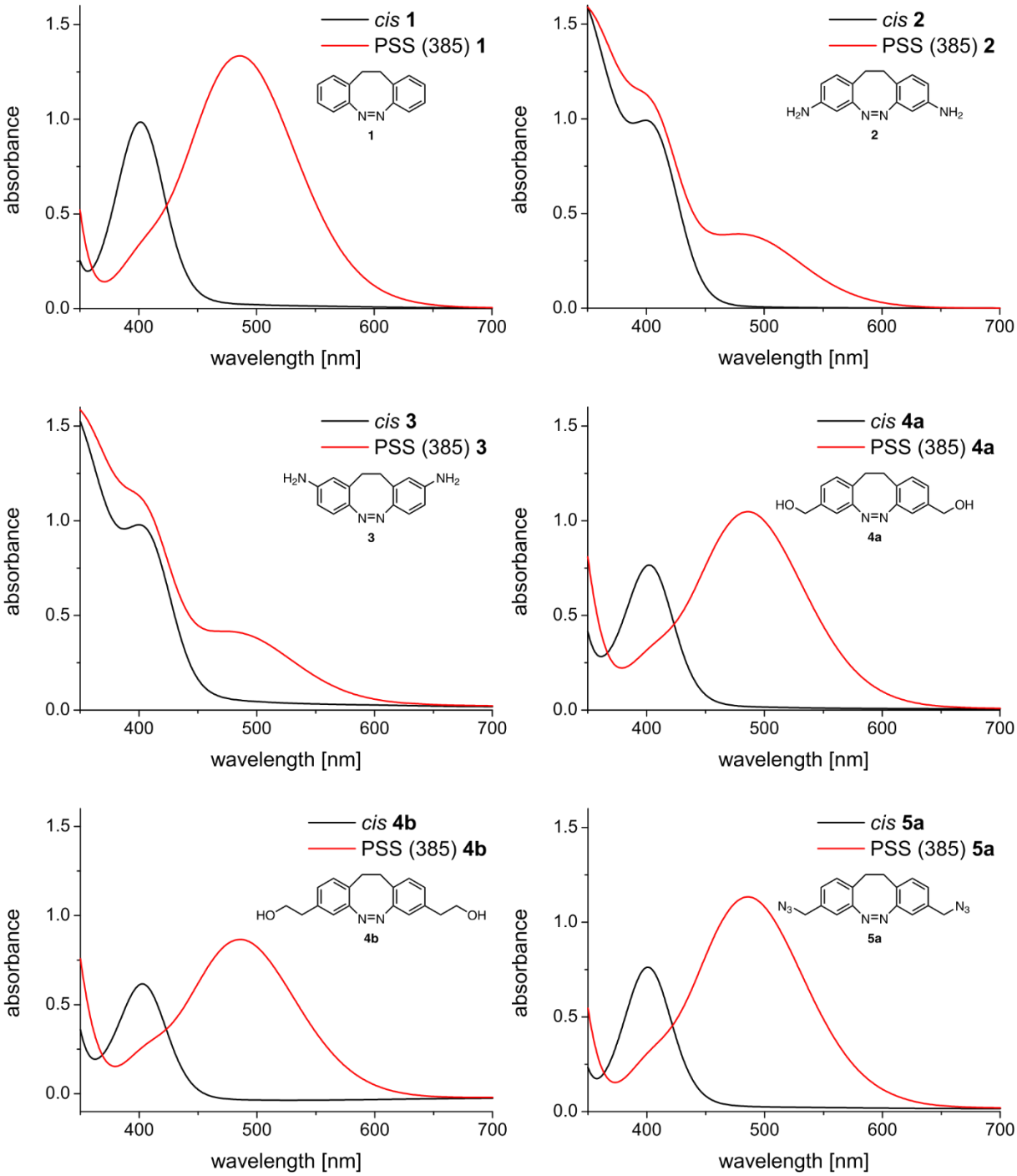

Figure S29: UV–vis spectra of functionalized diazocines **1** (2.0 mM), **2** (1.3 mM), **3** (1.3 mM), **4a** (1.5 mM), **4b** (1.5 mM) and **5a** (1.0 mM) spectra measured at 25 °C in acetonitrile. The black line is the spectrum of the pure *cis* compound and the red the PSS after irradiation at 385 nm.

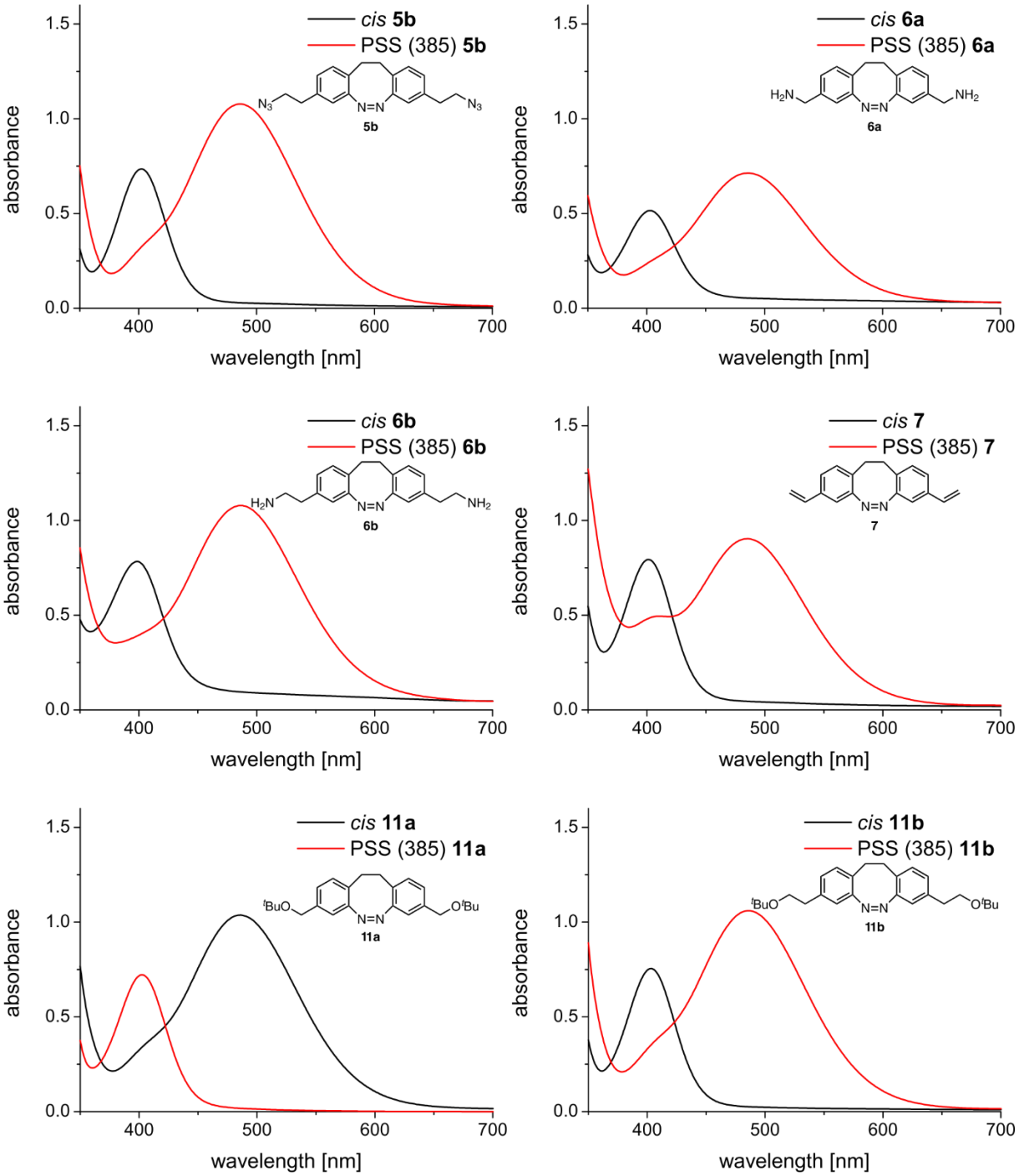

Figure S30: UV–vis of functionalized diazocines **5b** (1.7 mM), **6a** (1.2 mM), **6b** (1.6 mM), **7** (1.6 mM), **11a** (1.5 mM) and **11b** (1.5 mM) spectra measured at 25 °C in acetonitrile. The black line is the spectrum of the pure *cis* compound and in red the PSS after irradiation at 385 nm.

V. Photochemical experiments

Photostationary states (PSS 385 nm)

Photostationary states (PSS) were investigated by ^{1}H-NMR spectroscopy and measured in acetonitrile-d_3 at 300 K. Samples of 10 mM were prepared under exclusion of light and measured without irradiation. Afterwards the samples were irradiated for 5 min at 385 nm outside the NMR spectrometer and under ventilation. After recording the samples were irradiated again under the same conditions to guarantee no further isomerization and recorded a second time. Integration of the relevant signals in the ^{1}H-NMR spectra leads to the PSS at 385 nm.

NMR spectra at PSS (385 nm)

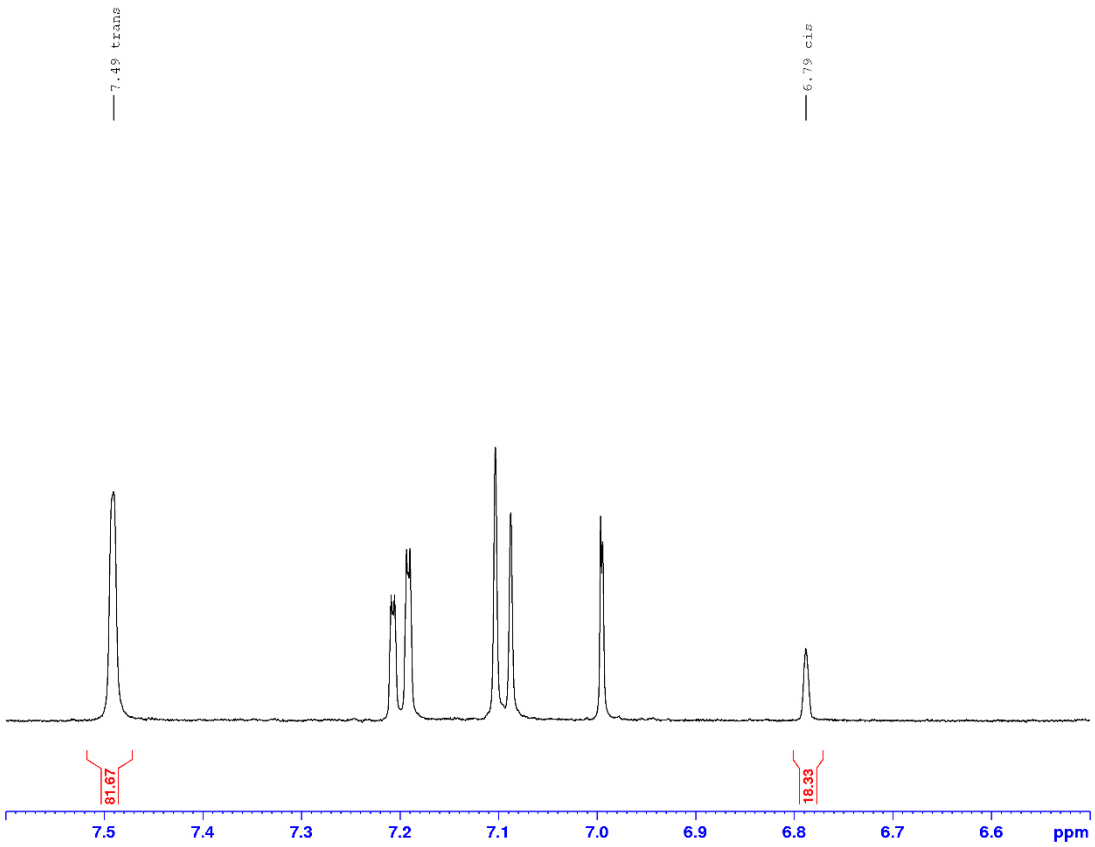

Figure S31: ^{1}H-NMR spectrum of compound **11a** at PSS (385 nm).

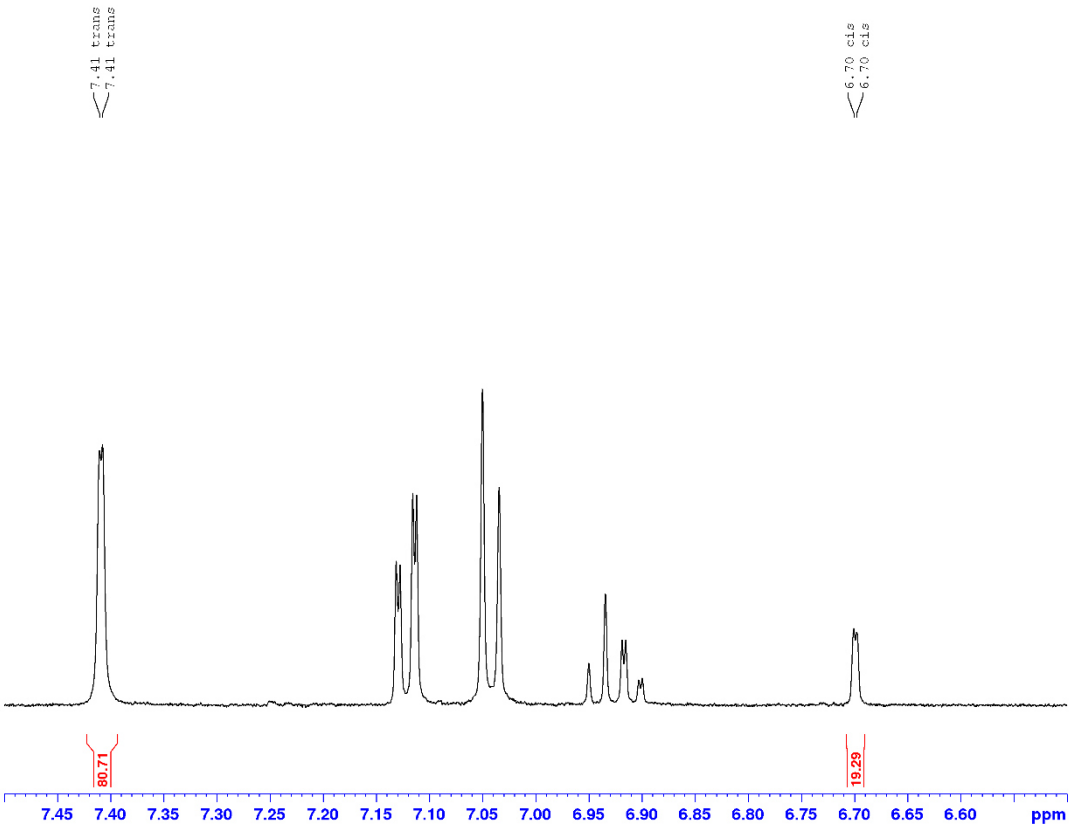

Figure S32: ^{1}H-NMR spectrum of compound **11b** at PSS (385 nm).

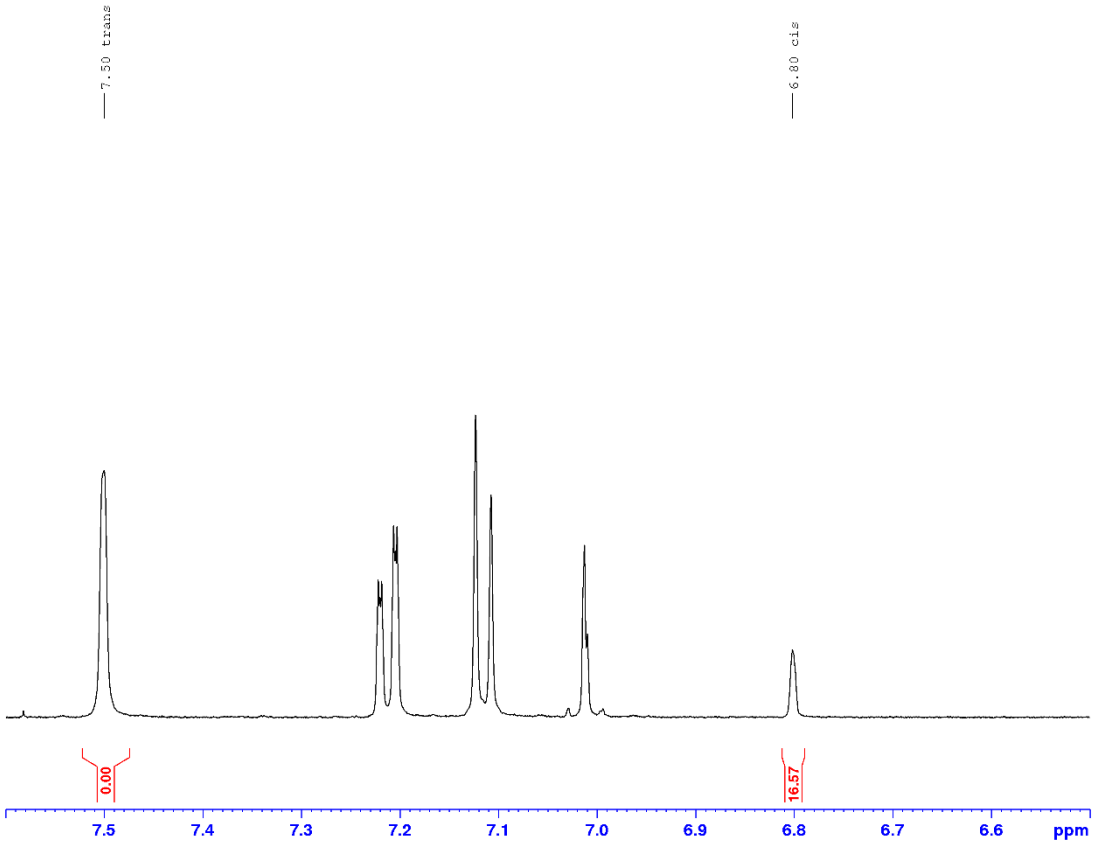

Figure S33: ^{1}H-NMR spectrum of compound **4a** at PSS (385 nm).

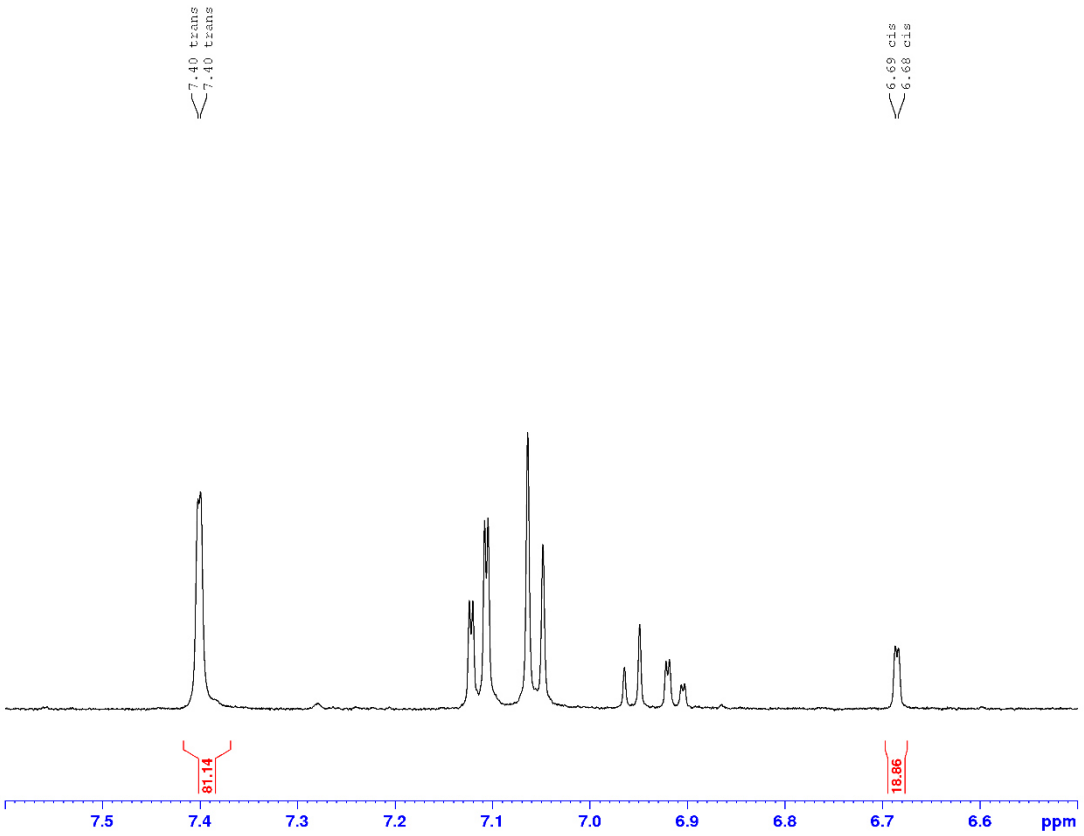

Figure S34: [1]H-NMR spectrum of compound **4b** at PSS (385 nm).

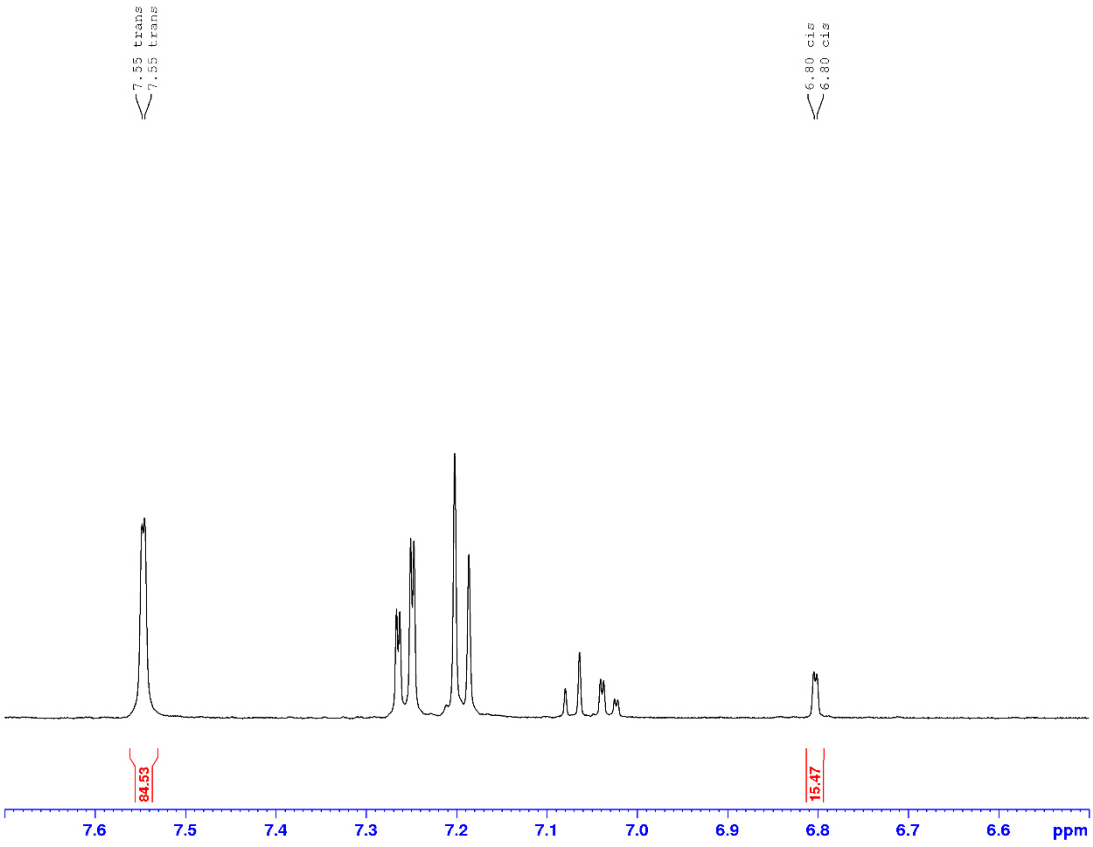

Figure S35: [1]H-NMR spectrum of compound **5a** at PSS (385 nm).

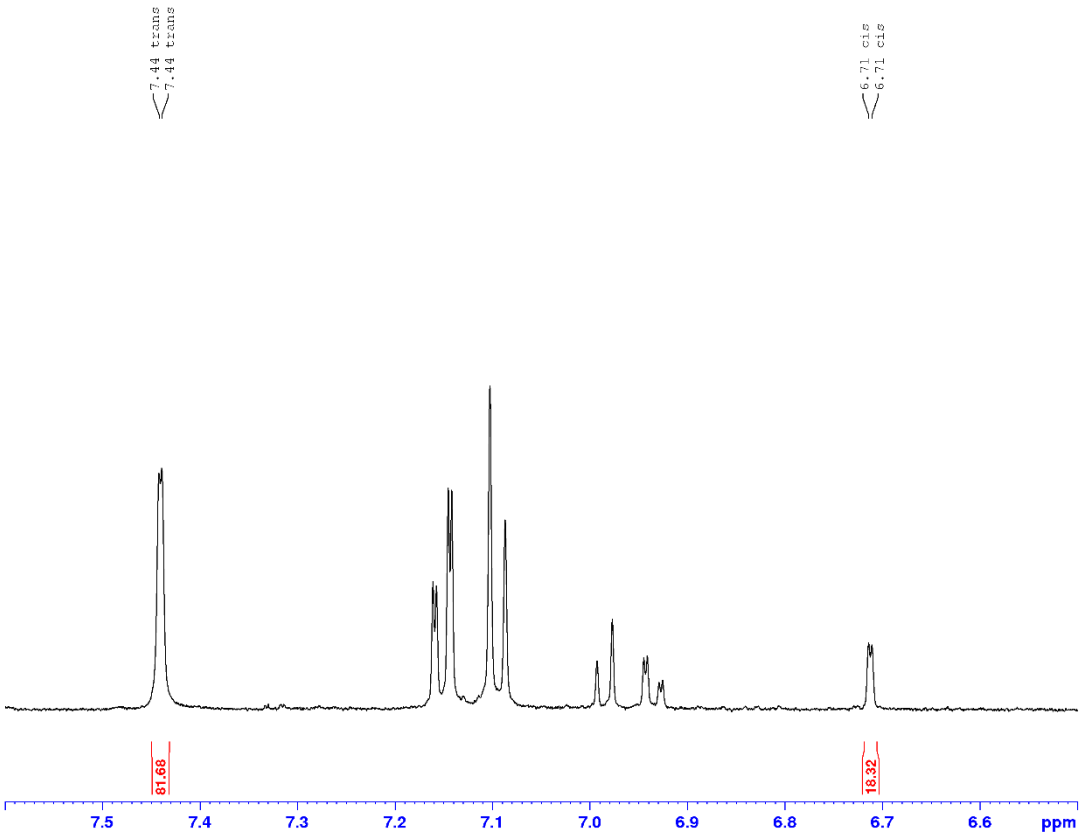

Figure S36: ^{1}H-NMR spectrum of compound **5b** at PSS (385 nm).

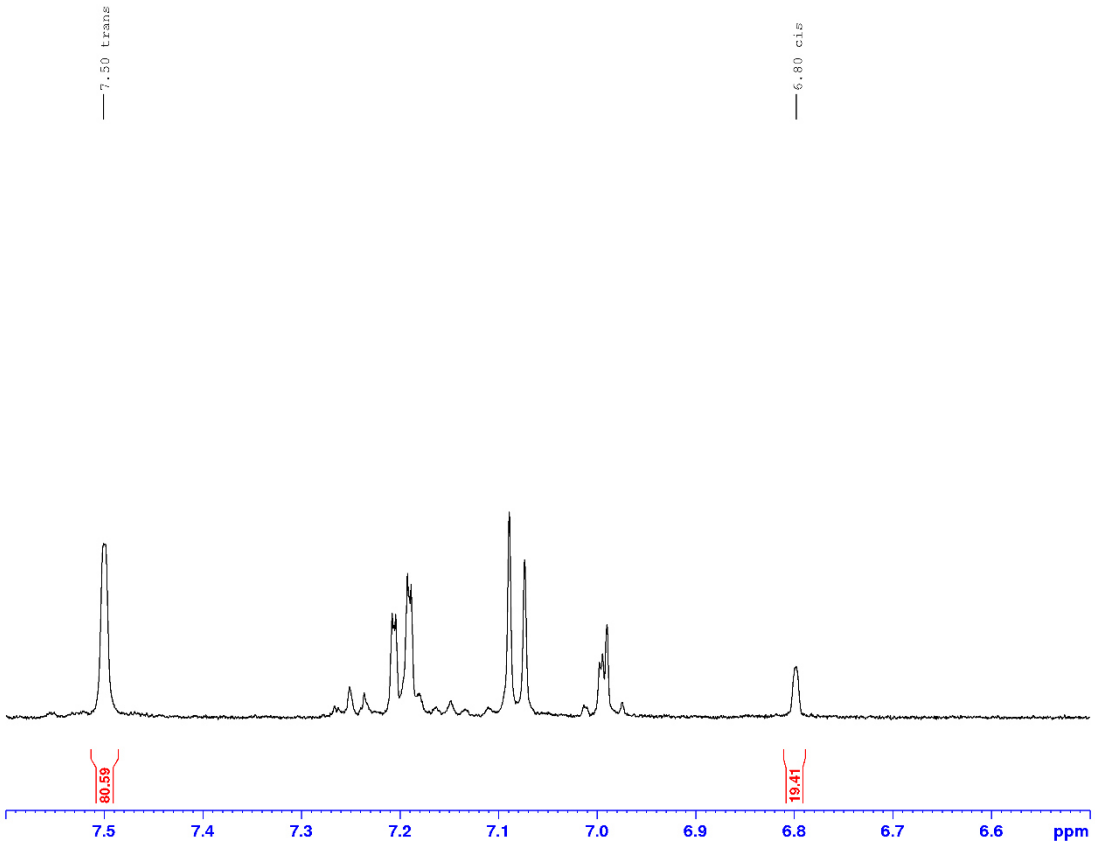

Figure S37: ^{1}H-NMR spectrum of compound **6a** at PSS (385 nm).

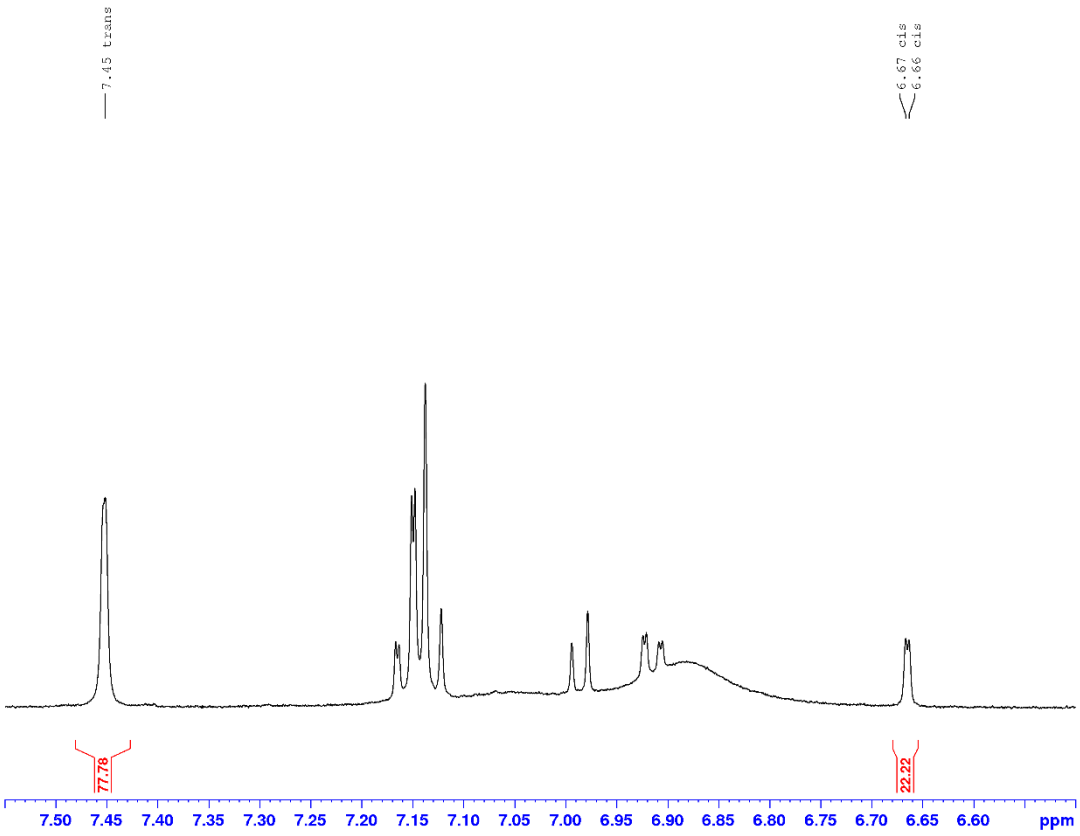

Figure S38: ^{1}H-NMR spectrum of compound **6b** at PSS (385 nm).

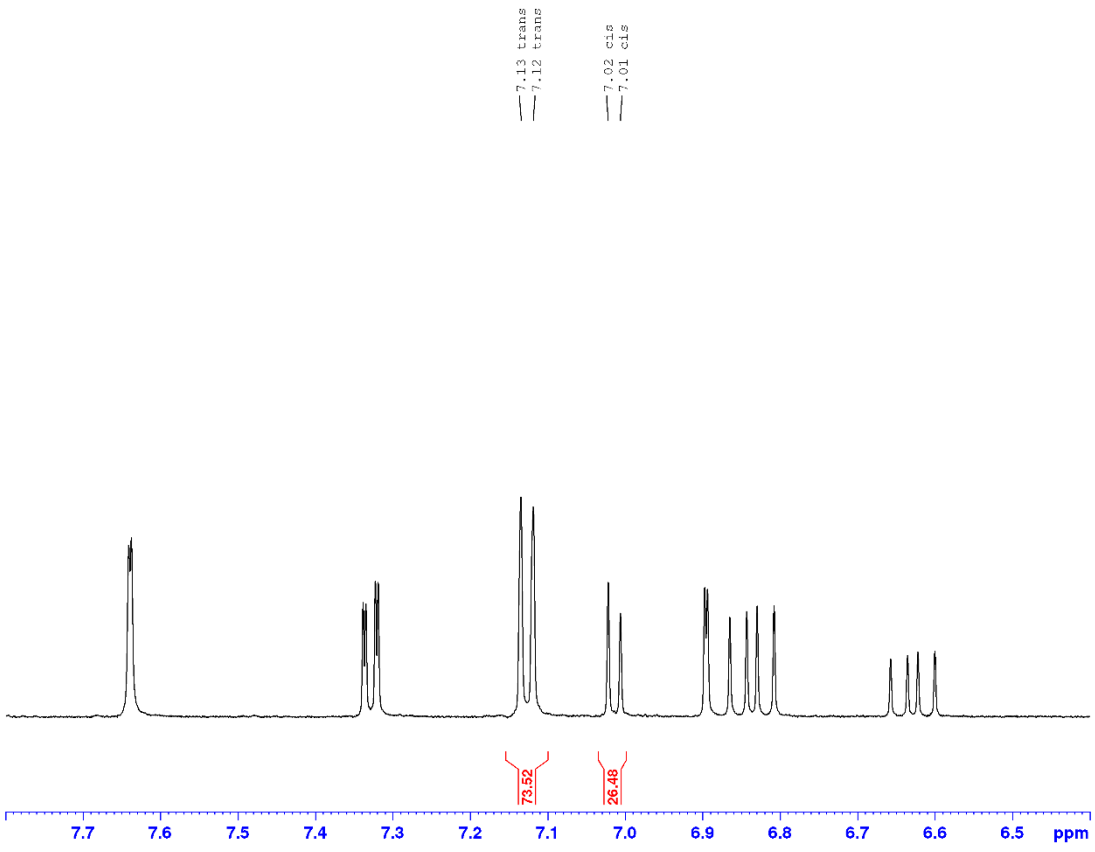

Figure S39: ^{1}H-NMR spectrum of compound **7** at PSS (385 nm).

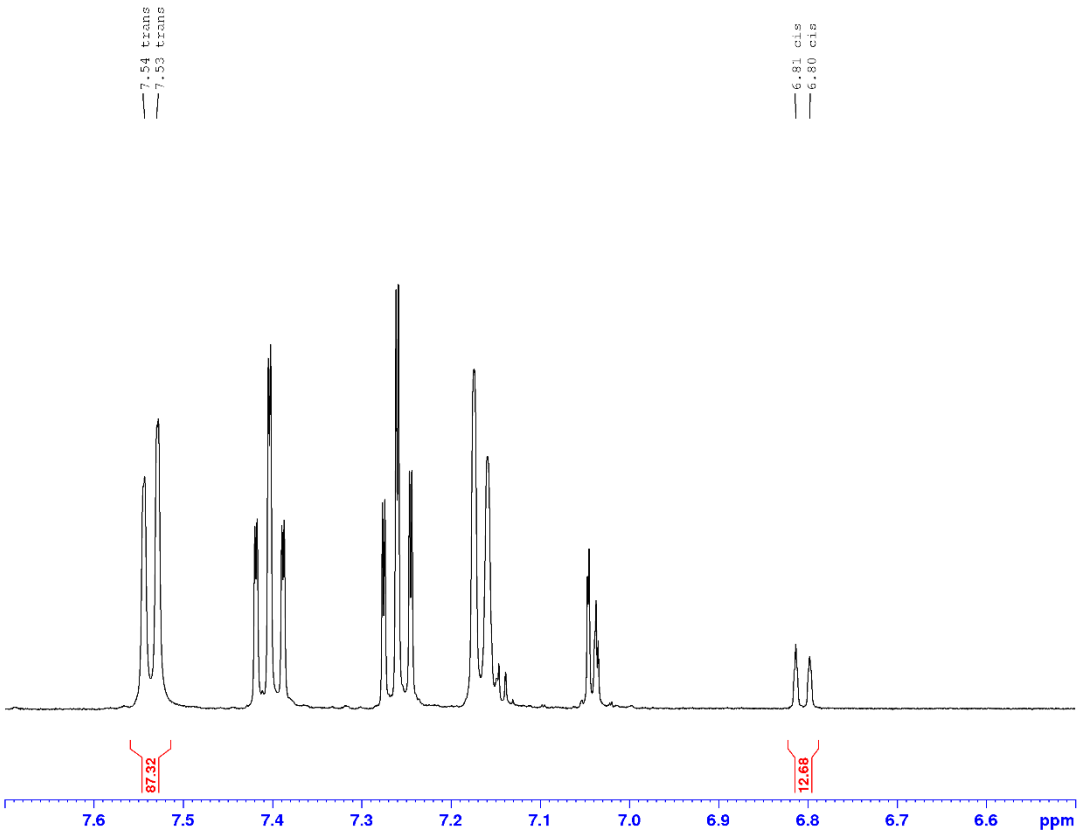

Figure S40: ^{1}H-NMR spectrum of compound **1** at PSS (385 nm).

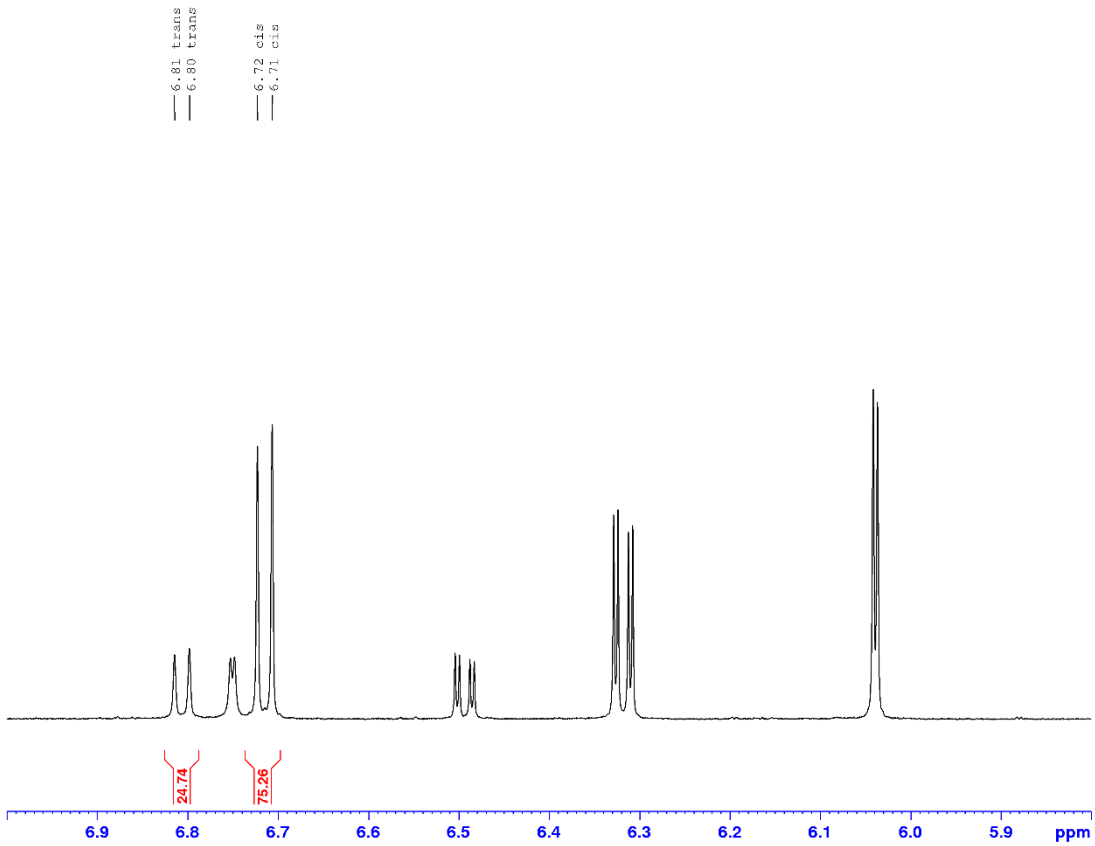

Figure S41: ^{1}H-NMR spectrum of compound **3** at PSS (385 nm).

Thermal half-lives determined by UV–vis spectroscopy

The functionalized diazocines **1**–**7**,**11a** and **11b** were dissolved in acetonitrile under the exclusion of light and UV–vis *cis* spectra were recorded at 298.15 K. Then the solutions were irradiated at 385 nm for 2 min. Spectra were recorded in appropriate intervals until complete relaxation. The absorption maxima were plotted as a function of time and the reaction time constants were determined after exponential fitting.

Table S1: Thermal half-lives (298.15 K), determined by UV–vis spectroscopy in acetonitrile.

molecule	concentration [mM]	$t_{1/2}$(UV) [h] at 298.15 K	standard error [h]
1	2.0	15.3	0.32
2	1.3	24.8	0.57
3	1.3	20	0.80
4a	1.5	11.4	0.01
4b	1.5	16.7	0.87
5a	1.0	11.2	0.22
5b	1.7	14.0	1.10
6a	1.2	14.7	0.29
6b	1.6	10.1	0.47
7	1.6	13.1	1.03
11a	1.5	10.2	0.01
11b	1.5	15.9	0.36

Supplementary Information

Visible-Light-Driven Photocontrol of the Trp-cage Protein Fold by a Diazocine Cross-Linker

Nils Preußke, Widukind Moormann, Katrin Bamberg, Matthias Lipfert, Rainer Herges, Frank D. Sönnichsen

Otto Diels-Institute for Organic Chemistry, Christian-Albrechts-University of Kiel, 24119 Kiel, Germany

Contents

1. Distance Computation

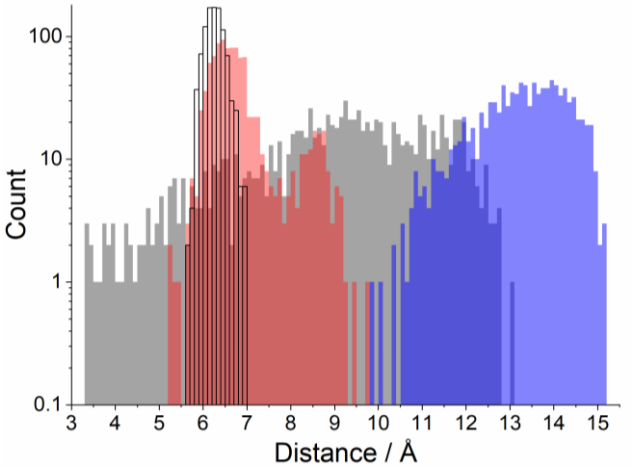

Fig. S 1: The same computed distances of the switchable Trp-cage 'cis-SC_a' (open), the uncross-linked Trp-cage 'TC(4,8)' (red), as well as the diazocines *cis*-**5** (gray) and *trans*-**5** (blue) as in **Fig. 3** (in the paper) are here displayed on a logarithmic scale.

2. Characterization of TC(4,8)

2.1. UHPLC-HRMS

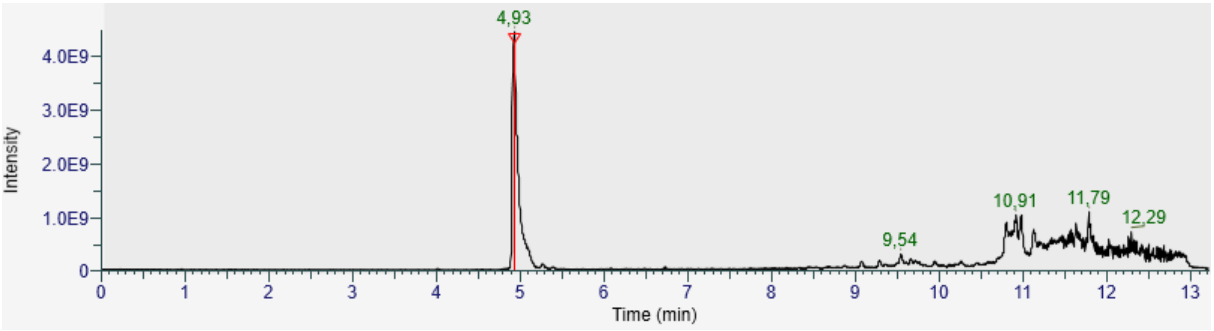

Fig. S 2: Chromatogram of TC(4,8). Peaks after 9 min are background noise.

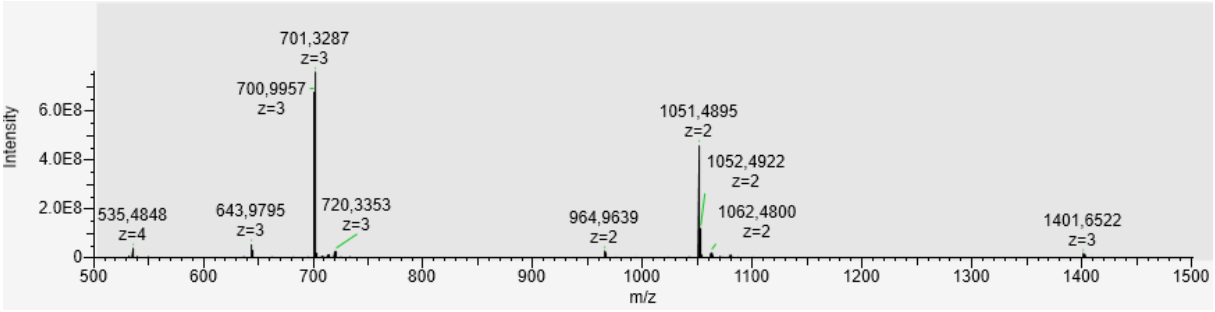

Fig. S 3: Mass spectrum of TC(4,8) at a retention time of 4.93 min. The peaks at 535, 701 and 1051 result from different charged states of TC(4,8). The small peaks immediately to the right of peak 701 and peak 1051 correspond to adducts of TC(4,8) with Na^+ and/or K^+. The peak at 1402 corresponds to the non-covalent homodimer of TC(4,8) $[2M + 3H]^{3+}$. The peaks at 644 and 965 belong to a side product from solid phase synthesis of TC(4,8) that possesses a similar retention time as TC(4,8). Based on the MS-detected chromatogram the sample is at least 80% pure.

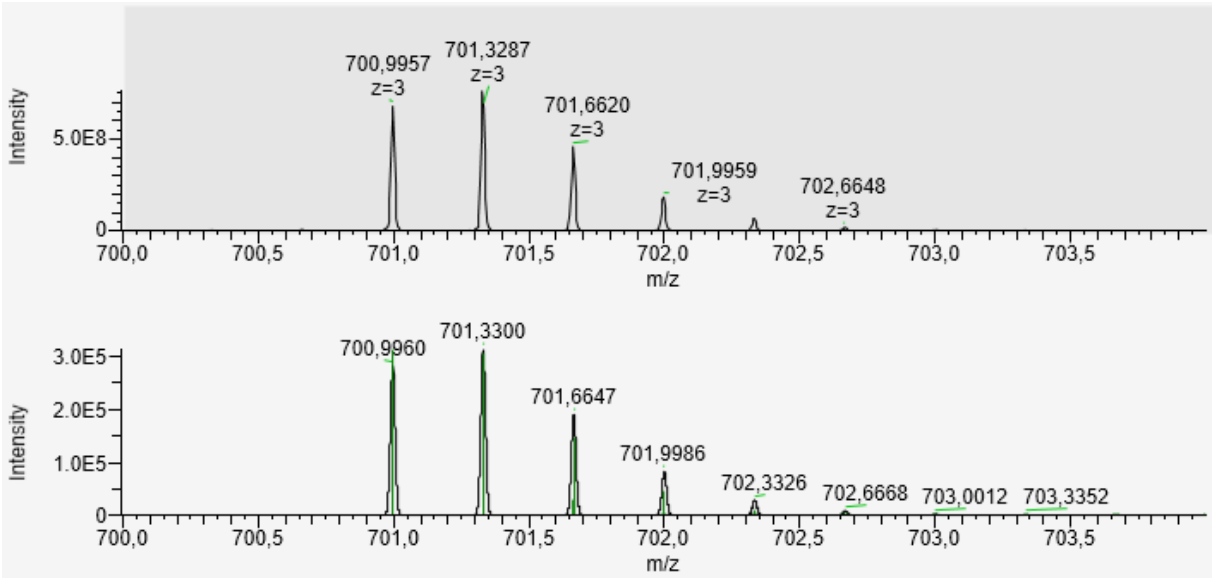

Fig. S 4: The expansion of the mass spectrum in **Fig. S 3** in the range between 700 and 704 demonstrates that the isotopic pattern of TC(4,8) (top) is identical with the isotopic pattern calculated based on its sum formula $[C_{91}H_{133}N_{27}O_{31} + 3H]^{3+}$ (bottom).

2.2. NMR data

Tab. S 1: Proton chemical shifts of the folded main form of TC(4,8).

No.	Res.	Proton: Shift / ppm
00	Ac	Me: 2.074
01	D	H^{N}: 8.245, H^{α}: 4.565, $H^{\beta 2/\beta 3}$: 2.828/2.726
02	A	H^{N}: 8.658, H^{α}: 4.185, H^{β}: 1.389
03	Y	H^{N}: 8.771, H^{α}: 4.248, H^{β}: 3.093, H^{δ}: 7.098, H^{ϵ}: 6.832
04	Γ	H^{N}: 8.622, H^{α}: 4.473, H^{β}: 3.470
05	Q	H^{N}: 8.465, H^{α}: 4.019, H^{β}: 2.114, H^{γ}: 2.311, $H^{\epsilon 21/\epsilon 22}$: 7.618/6.870
06	W	H^{N}: 8.228, H^{α}: 4.396, $H^{\beta 2/\beta 3}$: 3.394/3.204, $H^{\delta 1}$: 7.091, $H^{\epsilon 1}$: 9.873, $H^{\zeta 2}$: 7.308, $H^{\eta 2}$: 7.221, $H^{\epsilon 3}$: 7.135, $H^{\zeta 3}$: 7.226
07	L	H^{N}: 8.415, H^{α}: 3.696, $H^{\beta 2/\beta 3}$: 1.721/1.472, H^{γ}: 1.547, $H^{\delta 1/\delta 2}$: 0.937/0.854
08	Γ	H^{N}: 8.276, H^{α}: 4.467, $H^{\beta 2/\beta 3}$: 3.490/3.418
09	D	H^{N}: 8.055, H^{α}: 4.628, $H^{\beta 2/\beta 3}$: 2.840/2.699
10	G	H^{N}: 7.773, $H^{\alpha 2/\alpha 3}$: 4.100/3.657
11	G	H^{N}: 8.201, $H^{\alpha 2/\alpha 3}$: 3.420/1.983
12	P	H^{α}: 4.551, $H^{\beta 2/\beta 3}$: 2.440/2.040, H^{γ}: 2.102, $H^{\delta 2/\delta 3}$: 3.740/3.471
13	S	H^{N}: 7.963, H^{α}: 4.468, H^{β}: 3.906
14	S	H^{N}: 8.207, H^{α}: 4.260, $H^{\beta 2/\beta 3}$: 3.885/3.635
15	G	H^{N}: 8.071, $H^{\alpha 2/\alpha 3}$: 4.163/3.861
16	R	H^{N}: 8.096, H^{α}: 4.878, H^{β}: 1.819, $H^{\gamma 2/\gamma 3}$: 1.727/1.657, H^{δ}: 3.228, H^{ϵ}: 7.425
17	P	H^{α}: 4.708, $H^{\beta 2/\beta 3}$: 2.317/1.816, H^{γ}: 1.997, $H^{\delta 2/\delta 3}$: 3.837/3.634
18	P	H^{α}: 3.254, $H^{\beta 2/\beta 3}$: 1.547/1.046, H^{γ}: 1.816, $H^{\delta 2/\delta 3}$: 3.602/3.531
19	P	H^{α}: 4.376, $H^{\beta 2/\beta 3}$: 2.228/1.984, H^{γ}: 1.890, $H^{\delta 2/\delta 3}$: 3.369/3.180
20	S	H^{N}: 7.871, H^{α}: 4.191, H^{β}: 3.801

Assignments are according to IUPAC nomenclature.[1]

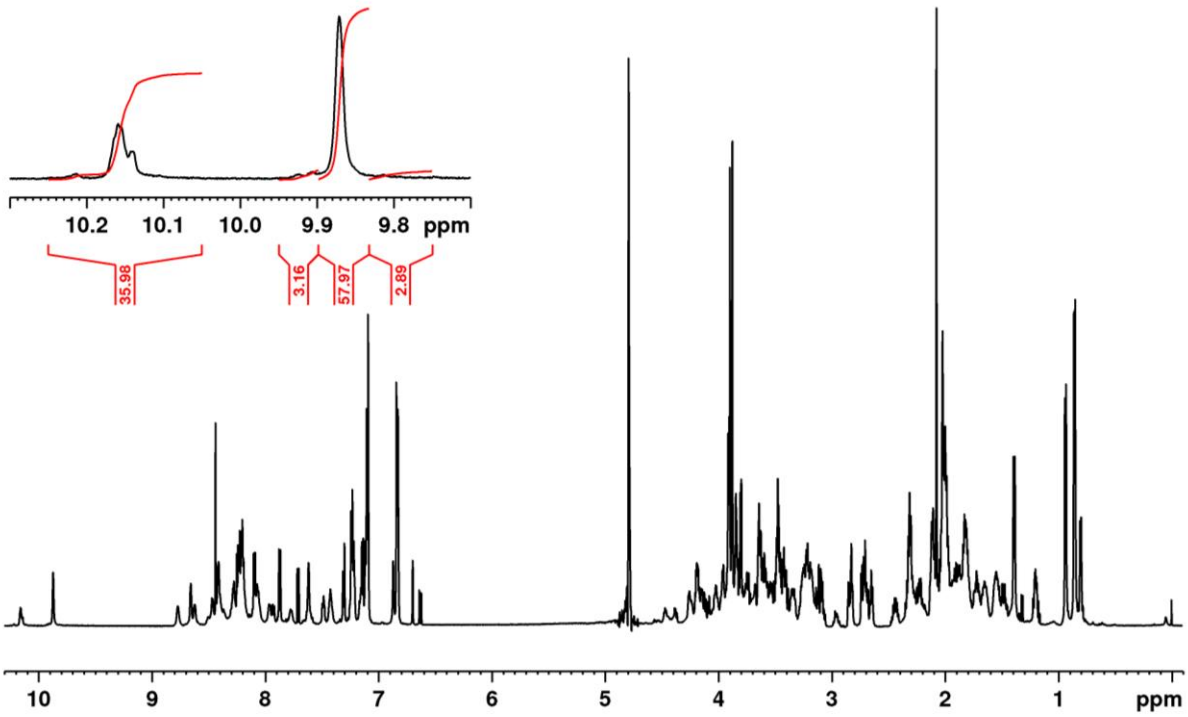

Fig. S 5: 1D ^{1}H-NMR spectrum of TC(4,8) in water with 10% D_2O at pH = 5.3, 298 K and a concentration of 1.6 mM. The expansion between 10.3 ppm and 9.7 ppm highlights the indole region. The highest peak (9.873 ppm) belongs to the Trp6 indole proton ($H^{\varepsilon 1}$) of the folded main form. Additional peaks in the indole region indicate unfolded by-forms of the Trp-cage with chemical shifts of the Trp6 indole proton ($H^{\varepsilon 1}$) around 10.15 ppm.

2.2.1. Trp-cage by-forms

Apart from the folded main-form described above, several by-forms of the Trp-cage are apparent in the indole NH-region in the ^{1}H-NMR spectrum (resonances between 9.7 ppm and 10.3 ppm). These by-forms belong to TC(4,8). They make up approximately 36% of the sample as determined by integration of the indole region (**Fig. S 5**) while ultra-high performance liquid chromatography coupled to high resolution mass spectrometry (UHPLC-HRMS) determined the amount of impurities of the sample to be <20% (**Fig. S 2** and **Fig. S 3**). These unfolded by-forms are detectable in NMR spectroscopy as separate resonances, because they are in slow equilibrium with the folded main population on the NMR chemical shift time scale.

In this paper, all NMR-based evaluations refer to the folded main population if not stated otherwise. In contrast, CD spectroscopy is averaged over every structure (including the folded and unfolded by-forms) weighted with respect to their population

2.3. Determination of midpoint of thermal unfolding of TC(4,8)

Fig 4a (in the paper) displays data of thermal unfolding of TC(4,8) (red triangles). The following function was fitted to the data

$$y = A_2 + \frac{A_1 - A_2}{1 + \exp(\frac{x - x_0}{dx})}$$

yielding the following values: A_1 = -13585.51999 ± 850.58255
A_2 = -3298.40652 ± 135.41215
x_0 = 31.62031 ± 2.69452 (in this case $x_0 = T_m$)
dx = 13.99868 ± 1.57008

3. Characterization of the folded *cis*-switch-cage

3.1. UHPLC-HRMS

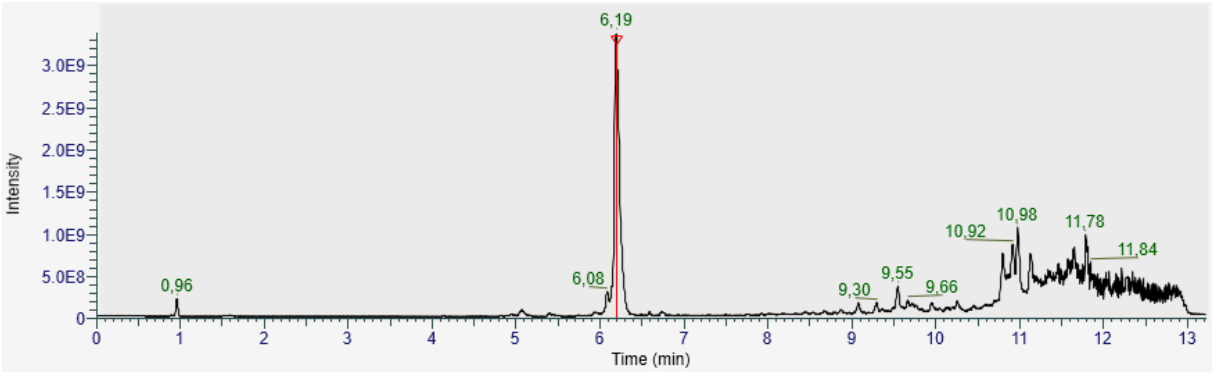

Fig. S 6: Chromatogram of the switch cage. An aliquot of the NMR sample (contains 10% D_2O) was subjected to UHPLC-HRMS analysis. Peaks after 9 min are background noise.

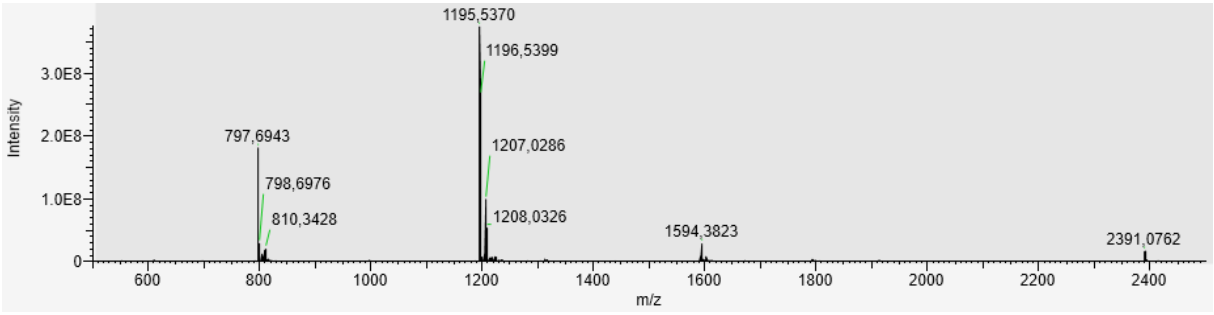

Fig. S 7: Mass spectrum of the switch cage at a retention time of 6.19 min. The peaks around 798, 1196 and 2391 result from different charged states of TC(4,8). The smaller peaks to the right of the product peaks correspond to adducts of the switch cage with Na^+ and/or K^+. The peak around 2391 can be assigned to singly charged switch cage $[M + H]^+$ overlaid the doubly charged non-covalent homodimer of the switch cage $[2M + 2H]^{2+}$. The peak around 1594 belongs to the triply charged non-covalent homodimer $[2M + 3H]^{3+}$. Based on the MS-detected chromatogram the sample is at least 85% pure.

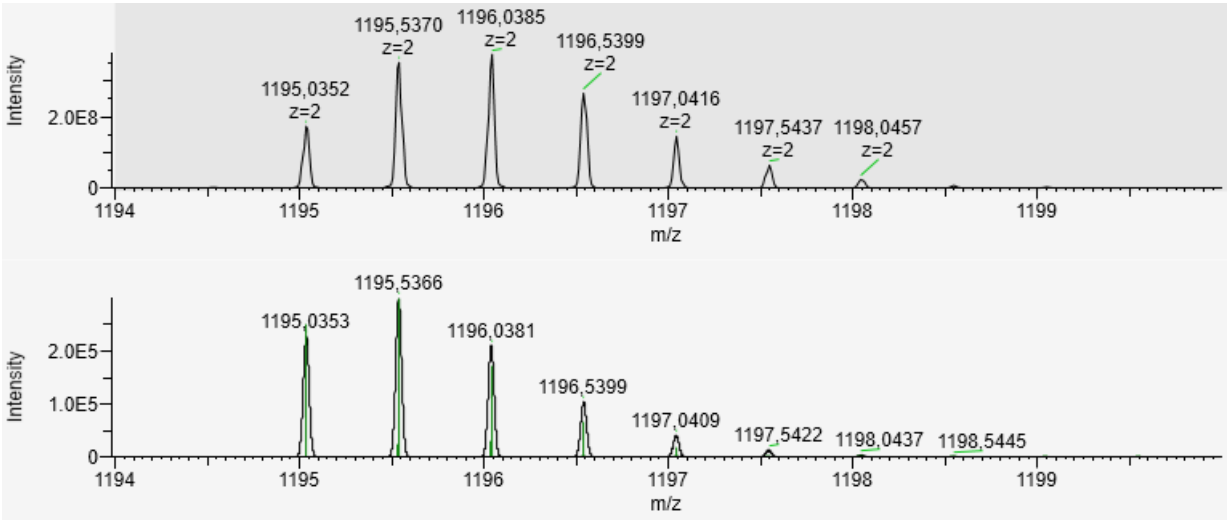

Fig. S 8: The expansion of the mass spectrum in **Fig. S 7** in the range between 1194 and 1200 demonstrates that the isotopic pattern of the switch cage (top) is almost identical with the isotopic pattern calculated based on its sum formula $[C_{109}H_{145}N_{29}O_{33} + 2H]^{2+}$ (bottom). The slight deviation is a result of exchanged protons for deuterons due to the D_2O content of the solvent (cf. **Fig. S 9**).

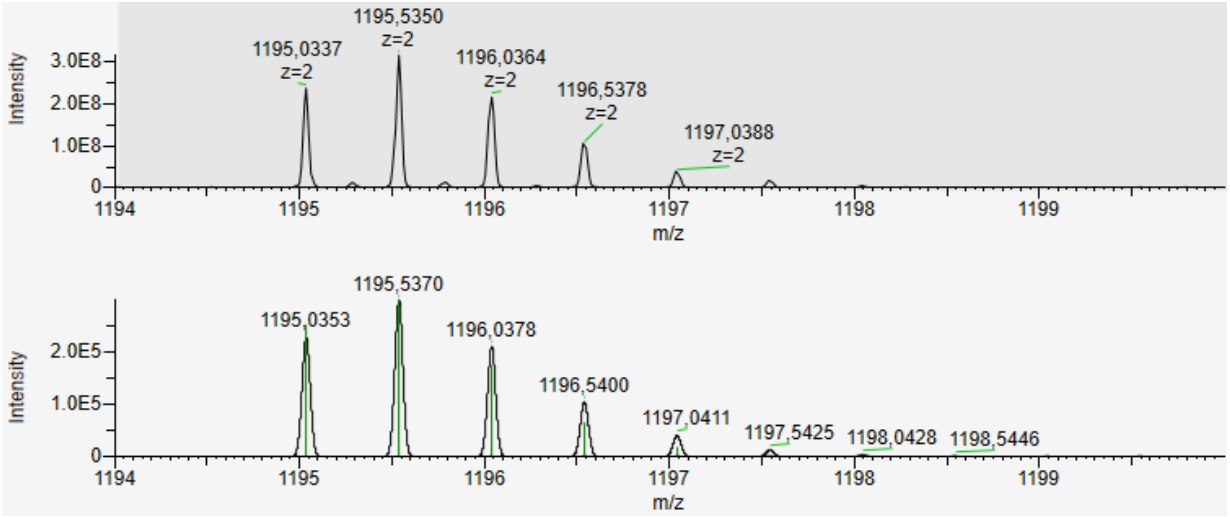

Fig. S 9: The sample from **Fig. S 6**, **Fig. S 7** and **Fig. S 8** was lyophilized and reconstituted with H_2O to exchange all deuterons in the protein with protons. The resulting isotopic pattern of the $[M + 2H]^{2+}$ species exactly matches the predicted pattern. The small peaks in between the isotopic pattern of $[M + 2H]^{2+}$ correspond to the non-covalent homodimer $[2M + 4H]^{4+}$.

3.2. NMR data

3.2.1. Chemical shifts

Tab. S 2: Proton chemical shifts of *cis*-SC$_a$.

No.	Res.	Proton: shift / ppm
00	Ac	Me: 2.060
01	D	H^N: 8.236, H^α: 4.622, $H^{\beta2/\beta3}$: 2.881/2.714
02	A	H^N: 8.688, H^α: 4.201, H^β: 1.483
03	Y	H^N: 8.709, H^α: 4.156, $H^{\beta2/\beta3}$: 3.203/3.128, H^δ: 7.118, H^ε: 6.888
04	Γ	H^N: 8.446, H^α: 3.543, H^β: 3.543, H^γ: 7.506, $H^{\varepsilon2/\varepsilon3}$: 3.654/3.418, H^2: 6.714, $H^{4,5}$: 7.030, H^{br}: 2.83 ± 0.07
05	Q	H^N: 8.353, H^α: 3.923, H^β: 2.173, H^γ: 2.360, $H^{\varepsilon21/\varepsilon22}$: 7.693/6.867
06	W	H^N: 8.004, H^α: 4.238, $H^{\beta2/\beta3}$: 3.501/3.195, $H^{\delta1}$: 7.009, $H^{\varepsilon1}$: 9.728, $H^{\zeta2}$: 7.229, $H^{\eta2}$: 7.153, $H^{\varepsilon3}$: 7.063, $H^{\zeta3}$: 7.148
07	L	H^N: 8.487, H^α: 3.414, $H^{\beta2/\beta3}$: 1.724/1.335, H^γ: 1.525, $H^{\delta1/\delta2}$: 0.853/0.655
08	Γ	H^N: 8.252, H^α: 4.412, $H^{\beta2/\beta3}$: 3.960/3.403, H^γ: 7.917, $H^{\varepsilon2/\varepsilon3}$: 3.488/3.400, H^2: 6.662, H^4: 6.442, H^5: 6.942, H^{br}: 2.83 ± 0.07
09	D	H^N: 7.871, H^α: 4.624, $H^{\beta2/\beta3}$: 2.892/2.683
10	G	H^N: 7.484, $H^{\alpha2/\alpha3}$: 4.148/3.497
11	G	H^N: 8.295, $H^{\alpha2/\alpha3}$: 3.123/0.969
12	P	H^α: 4.594, $H^{\beta2/\beta3}$: 2.516/2.069, H^γ: 2.144, $H^{\delta2/\delta3}$: 3.799/3.416
13	S	H^N: 7.698, H^α: 4.474, H^β: 3.920
14	S	H^N: 8.185, H^α: 4.166, $H^{\beta2/\beta3}$: 3.869/3.528
15	G	H^N: 7.926, $H^{\alpha2/\alpha3}$: 4.270/3.812
16	R	H^N: 8.138, H^α: 5.019, $H^{\beta2/\beta3}$: 1.888/1.818, H^γ: 1.658, H^δ: 3.269, H^ε: 7.563
17	P	H^α: 4.748, $H^{\beta2/\beta3}$: 2.339/1.798, H^γ: 2.000, $H^{\delta2/\delta3}$: 3.866/3.672
18	P	H^α: 2.580, $H^{\beta2/\beta3}$: 1.351/0.385, $H^{\gamma2/\gamma3}$: 1.736/1.651, H^δ: 3.519
19	P	H^α: 4.331, $H^{\beta2/\beta3}$: 2.199/1.981, H^γ: 1.857, $H^{\delta2/\delta3}$: 3.163/2.992
20	S	H^N: 7.819, H^α: 4.164, H^β: 3.775

The assignments are according to IUPAC nomenclature.[1] The nomenclature of the cross-linker assignments is shown in **Fig. S 10**.

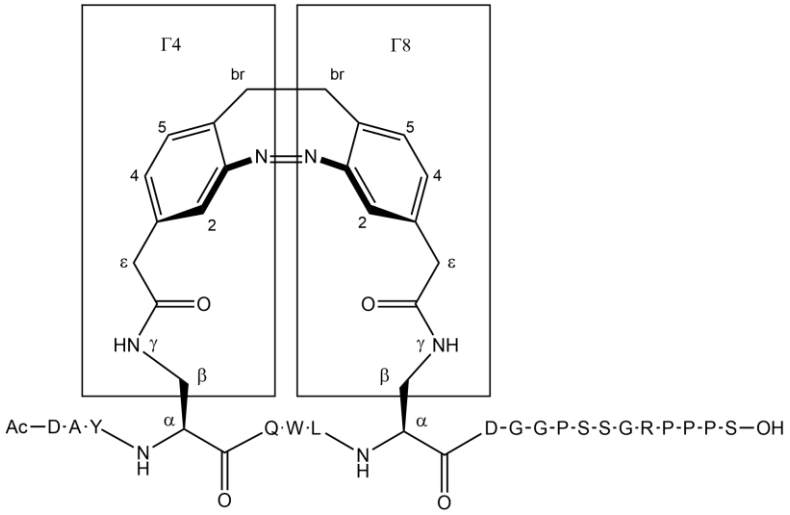

Fig. S 10: The nomenclature of the cross-linker assignments.

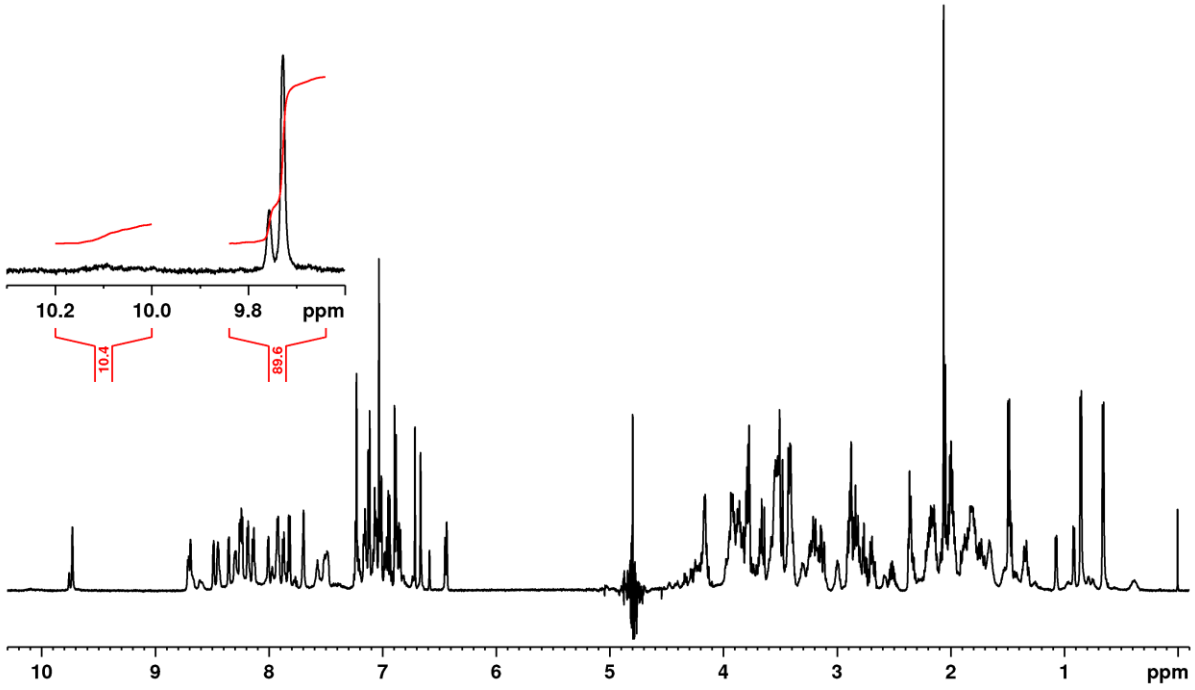

Fig. S 11: 1D ^{1}H-NMR spectrum of the dark-adapted switch cage in water with 10% D_2O at pH = 5.5, 298 K and a concentration of 0.5 mM. The expansion of the region between 10.3 ppm and 9.6 ppm shows that the amount of unfolded by-forms with chemical shifts of the Trp6 indole proton ($H^{\varepsilon 1}$) around 10.1 ppm adds up to approximately 10%, which is significantly reduced compared to TC(4,8) (cf. **Fig. S 5**). With approximately 10%, the amount of unfolded species lies within the range of impurity determined by UHPLC-MS. The broad signals may therefore also correspond to unfolded Trp-containing side-products from the synthesis and not necessarily belong to unfolded switch-cage species.

3.2.2. Chemical shift deviations

The chemical shift deviation (CSD, also referred to as $\Delta\delta$) is typically employed to assess the stability of the fold of a Trp-cage mutant.[2,3] The CSD is the difference between the observed chemical shift of a certain nucleus in a peptide and the corresponding nucleus in an unstructured random coil peptide:

$$\text{CSD} = \Delta\delta = \delta_{\text{obs.}} - \delta_{\text{random coil}}$$

Unfortunately, we were unable to find a comprehensive list of random coil shifts used by Andersen *et al.*[2,3]. Therefore, random coil shifts were taken from Wishart *et al.* and are listed in **Tab. S 3**.[4] The random coil value of the Trp indole proton was taken from Bundi and Wüthrich.[5] The random coil shifts by Wishart *et al.* are non-stereospecifically assigned. When two β-protons ($H^{\beta 2/\beta 3}$) from the same residue display different random coil shifts, their CSD was calculated by subtracting the larger random coil shift from the larger observed shift and the smaller random coil shift from the smaller observed shift.

Example from Asp1:	Observed shift:	$H^{\beta 2/\beta 3}$: 2.881/2.714 ppm
	Random coil shift:	$H^{\beta 2/\beta 3}$: 2.72/2.65 ppm
	CSD:	$H^{\beta 2/\beta 3}$: 0.16/0.06 ppm

No CSDs are given for the acetyl moiety of the N-terminus and for residues Dpr4 and Dpr8 as no random coil values are available for their nuclei.

Tab. S 3: Random coil shifts used for the calculation of CSDs.

No.	Res.	Proton: CSD / ppm
00	Ac	Me: n.d.
01	D	H^{N}: 8.34, H^{α}: 4.64, $H^{\beta2/\beta3}$: 2.72/2.65
02	A	H^{N}: 8.24, H^{α}: 4.32, H^{β}: 1.39
03	Y	H^{N}: 8.12, H^{α}: 4.55, $H^{\beta2/\beta3}$: 3.03/2.98, H^{δ}: 7.14, H^{ε}: 6.84
04	Γ	n.d.
05	Q	H^{N}: 8.32, H^{α}: 4.34, $H^{\beta2/\beta3}$: 2.12/1.99, H^{γ}: 2.360, $H^{\varepsilon21/\varepsilon22}$: 7.52/6.85
06	W	H^{N}: 8.25, H^{α}: 4.66, $H^{\beta2/\beta3}$: 3.29/3.27, $H^{\delta1}$: 7.27, $H^{\varepsilon1}$: 10.22, $H^{\zeta2}$: 7.50, $H^{\eta2}$: 7.25, $H^{\varepsilon3}$: 7.65, $H^{\zeta3}$: 7.18
07	L	H^{N}: 8.16, H^{α}: 4.34, H^{β}: 1.62, H^{γ}: 1.59, $H^{\delta1/\delta2}$: 0.92/0.87
08	Γ	n.d.
09	D	H^{N}: 8.34, H^{α}: 4.64, $H^{\beta2/\beta3}$: 2.72/2.65
10	G	H^{N}: 8.33, H^{α}: 3.96
11	G	H^{N}: 8.21, H^{α}: 4.13
12	P	H^{α}: 4.42, $H^{\beta2/\beta3}$: 2.29/1.94, H^{γ}: 2.02, H^{δ}: 3.63
13	S	H^{N}: 8.31, H^{α}: 4.47, $H^{\beta2/\beta3}$: 3.89/3.87
14	S	H^{N}: 8.31, H^{α}: 4.47, $H^{\beta2/\beta3}$: 3.89/3.87
15	G	H^{N}: 8.33, H^{α}: 3.96
16	R	H^{N}: 8.20, H^{α}: 4.65, H^{β}: 1.81, H^{γ}: 1.67, H^{δ}: 3.21, H^{ε}: 8.07
17	P	H^{α}: 4.73, $H^{\beta2/\beta3}$: 2.31/1.91, H^{γ}: 2.01, H^{δ}: 3.60
18	P	H^{α}: 4.73, $H^{\beta2/\beta3}$: 2.31/1.91, H^{γ}: 2.01, H^{δ}: 3.60
19	P	H^{α}: 4.42, $H^{\beta2/\beta3}$: 2.29/1.94, H^{γ}: 2.02, H^{δ}: 3.63
20	S	H^{N}: 8.31, H^{α}: 4.47, $H^{\beta2/\beta3}$: 3.89/3.87

Tab. S 4: Chemical shift deviations of *cis*-SC_a.

No.	Res.	Proton: CSD / ppm
00	Ac	n.d.
01	D	H^{N}: -0.10, H^{α}: -0.02, $H^{\beta2/\beta3}$: 0.16/0.06
02	A	H^{N}: 0.45, H^{α}: -0.12, H^{β}: 0.09
03	Y	H^{N}: 0.59, H^{α}: -0.39, $H^{\beta2/\beta3}$: 0.17/0.15, H^{δ}: -0.02, H^{ε}: -0.05
04	Γ	n.d.
05	Q	H^{N}: 0.03, H^{α}: -0.42, $H^{\beta2/\beta3}$: 0.05/0.18, H^{γ}: 0.00, $H^{\varepsilon21/\varepsilon22}$: 0.17/0.02
06	W	H^{N}: -0.25, H^{α}: -0.42, $H^{\beta2/\beta3}$: 0.21/-0.08, $H^{\delta1}$: -0.26, **$H^{\varepsilon1}$: -0.49**, $H^{\zeta2}$: -0.27, $H^{\eta2}$: -0.10, $H^{\varepsilon3}$: -0.59, $H^{\zeta3}$: -0.03
07	L	H^{N}: 0.33, **H^{α}: -0.93**, $H^{\beta2/\beta3}$: 0.10/-0.28, H^{γ}: -0.07, $H^{\delta1/\delta2}$: -0.07/-0.22
08	Γ	n.d.
09	D	H^{N}: -0.47, H^{α}: -0.02, $H^{\beta2/\beta3}$: 0.17/0.03
10	G	H^{N}: -0.85, $H^{\alpha2/\alpha3}$: 0.19/-0.46
11	G	H^{N}: 0.08, **$H^{\alpha2/\alpha3}$: -1.01/-3.16**
12	P	H^{α}: 0.17, $H^{\beta2/\beta3}$: 0.23/0.13, H^{γ}: 0.12, $H^{\delta2/\delta3}$: 0.17/-0.21
13	S	H^{N}: -0.61, H^{α}: 0.00, $H^{\beta2/\beta3}$: 0.03/0.05
14	S	H^{N}: -0.13, H^{α}: -0.30, $H^{\beta2/\beta3}$: -0.02/-0.34
15	G	H^{N}: -0.40, $H^{\alpha2/\alpha3}$: 0.31/-0.15
16	R	H^{N}: -0.06, H^{α}: 0.37, $H^{\beta2/\beta3}$: 0.08/0.01, H^{γ}: -0.01, H^{δ}: 0.06, H^{ε}: -0.51
17	P	H^{α}: 0.02, $H^{\beta2/\beta3}$: 0.03/-0.11, H^{γ}: -0.01, $H^{\delta2/\delta3}$: 0.27/0.07
18	P	**H^{α}: -2.15**, **$H^{\beta2/\beta3}$: -0.96/-1.52**, $H^{\gamma2/\gamma3}$: -0.27/-0.36, H^{δ}: -0.08
19	P	H^{α}: -0.09, $H^{\beta2/\beta3}$: -0.09/0.04, H^{γ}: -0.16, $H^{\delta2/\delta3}$: -0.47/-0.64
20	S	H^{N}: -0.49, H^{α}: -0.31, $H^{\beta2/\beta3}$: -0.12/-0.10

Large CSDs which are a result of and an indicator for the stable Trp-cage fold are highlighted in bold.

3.3. Determination of midpoint of thermal unfolding of the switch cage

Fig 4a (in the paper) displays data of thermal unfolding of the switch cage (black circles). The following function was fitted to the data

$$y = A_2 + \frac{A_1 - A_2}{1 + \exp(\frac{x - x_0}{dx})}$$

yielding the following values: A_1 = -13518.25883 ± 404.28719
A_2 = -3855.61105 ± 228.37507
x_0 = 48.50329 ± 1.42176 (in this case $x_0 = T_m$)
dx = 12.95674 ± 1.42566

4. Switching properties of the switch cage

4.1. UV/vis spectroscopy

UV/vis spectra were recorded at 25 °C on a Lambda 14 spectrometer (PerkinElmer, Waltham, MA, USA) equipped with a ecoline E100 thermostat mounted on an ecoline 003 water bath (Lauda, Lauda-Königshofen, Germany). Measurements were performed using low-volume (700 µL) Quartz cuvettes with an optical path length of 10 mm (Hellma, Müllheim, Germany) and water as a solvent at pH = 5.5 ± 0.1.

UV/vis spectroscopy was used to determine the which of the available light sources produces the largest *cis*→*trans*-conversion ratio (**Fig. S 12**). From the tested wavelengths, the highest conversion to *trans*-SC was achieved at 385 nm.

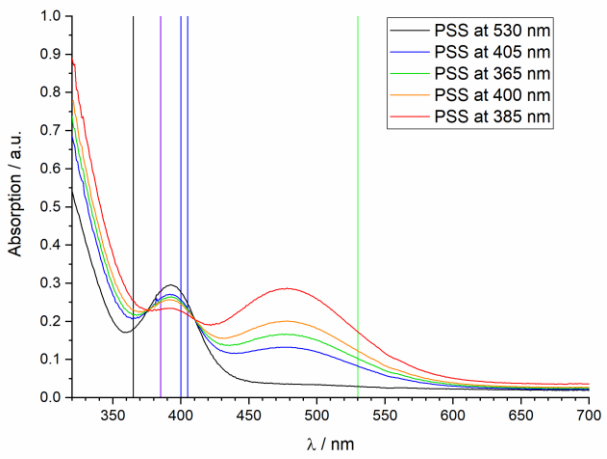

Fig. S 12: UV/vis spectra of the switch cage irradiated with light of different wavelengths (365 nm, 385 nm, 400 nm, 405 nm and 530 nm). The irradiation wavelengths are indicated by a vertical line. The baseline displays a small offset which is an artifact resulting from the narrow low-volume cuvettes.

4.2. Photostationary state at 385 nm and relaxation rates

4.2.1. Experimental setup

The photostationary state (PSS) and relaxation rate were determined by NMR spectroscopy. The sample with the switch cage was irradiated to the PSS at 385 nm and immediately afterwards a 1D-^{1}H-NMR spectrum was recorded (**Fig. S 13**). The NMR spectrometer had previously been calibrated to a temperature of 298 °C. The sample remained in the spectrometer in the dark for the entire time of the relaxation measurements. After the first spectrum (representing the PSS, recorded at t = 2 min after irradiation), a new spectrum was recorded every 30 min for the next 21 h. The last spectrum was recorded at t = 39 h.

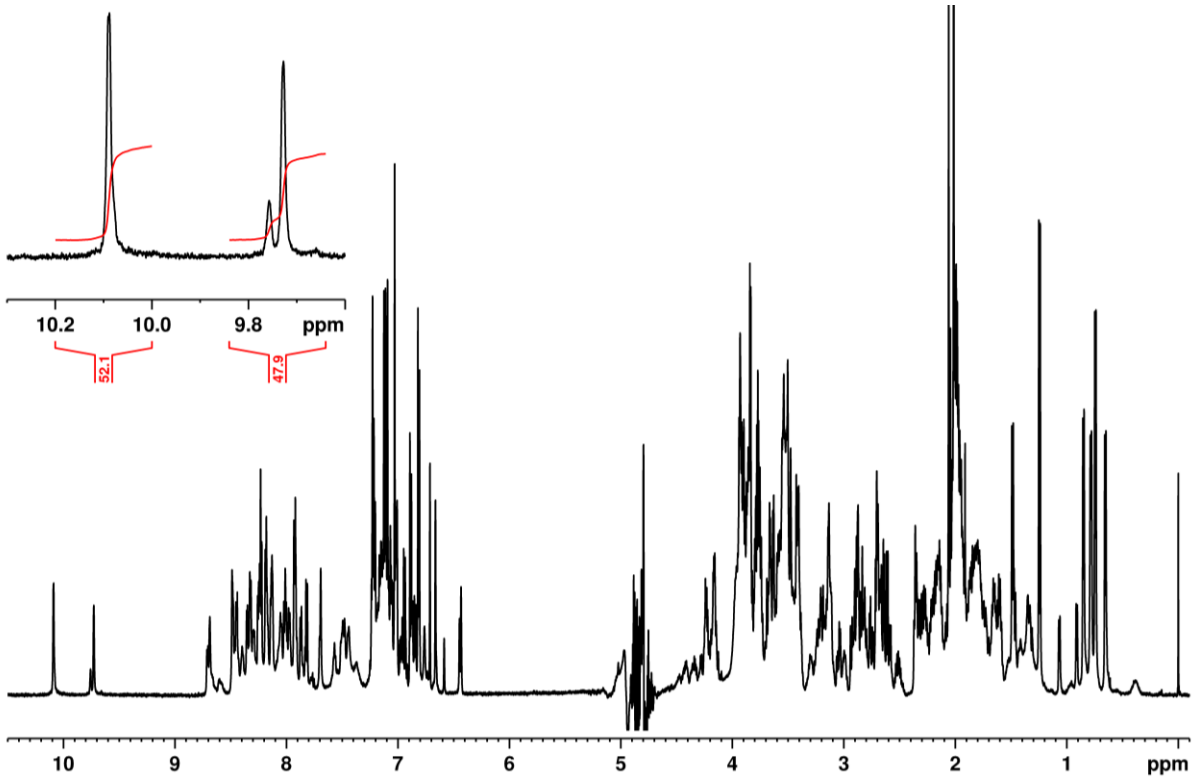

Fig. S 13: 1D-^{1}H-NMR spectrum of the switch cage after irradiation to the PSS at 385 nm in water with 10% D_2O at pH = 5.5, 298 K and a concentration of 0.5 mM. The same regions as in **Fig. S 11** are integrated in the expansion.

4.2.2. Selecting the nuclei for the determination of the PSS at 385 nm and the relaxation rate

Accurate determination of photostationary states and relaxation rates ideally requires baseline-separated signals of the *cis*- and the *trans* diazocine to allow for integration. Unfortunately, all signals of the *trans*-diazocine overlap with other aromatic signals of *trans*-SC, *cis*-SC_a or *cis*-SC_b. In consequence, six largely separated signals of *cis*-SC (signals b) – g)) and one signal (signal a)) of *trans*-SC were used to quantify the *cis*- and *trans*-populations and determine the relaxation rate (**Tab. S 5**, **Fig. S 14**).

The six chosen *cis*-SC-signals (b) – g)) represent either the switching state of the diazocine cross-linker or the fold state of the switch cage (**Tab. S 5**). This facilitates the discrimination between the state of the linker and the fold and it also allows for the determination of the PSS and relaxation rates for each

individual species, i.e. *cis*-SC_a and *cis*-SC_b. Signal a) was chosen to calculate the relaxation rate by monitoring a fold-indicating proton of *trans*-SC.

Tab. S 5: List of signals that were chosen to calculate the PSS and/or the relaxation rate of the switch cage.

Entry	Species	Proton	Integr. Region / ppm	Representing
a)	*trans*-SC	Trp6 indole NH	10.105 – 10.065	fold
b)	*cis*-SC_b	Trp6 indole NH	9.780 – 9.744	fold
c)	*cis*-SC_a	Trp6 indole NH	9.744 – 9.700	fold
d)	*cis*-SC_a	Dpr4 H^2	6.725 – 6.699	diazocine
e)	*cis*-SC_a	Dpr8 H^2	6.692 – 6.632	diazocine
f)	*cis*-SC_b	DprX H^2*	6.600 – 6.570	diazocine
g)	*cis*-SC_a: Dpr8 H^4; *cis*-SC_b: Dpr H^2**		6.473 – 6.413	diazocine

*) It was not possible to unequivocally assign the two protons, Dpr4 H^2 and Dpr8 H^2 of *cis*-SC_b, to their corresponding residue in the sequence. **) These two signals are overlapping and treated as one.

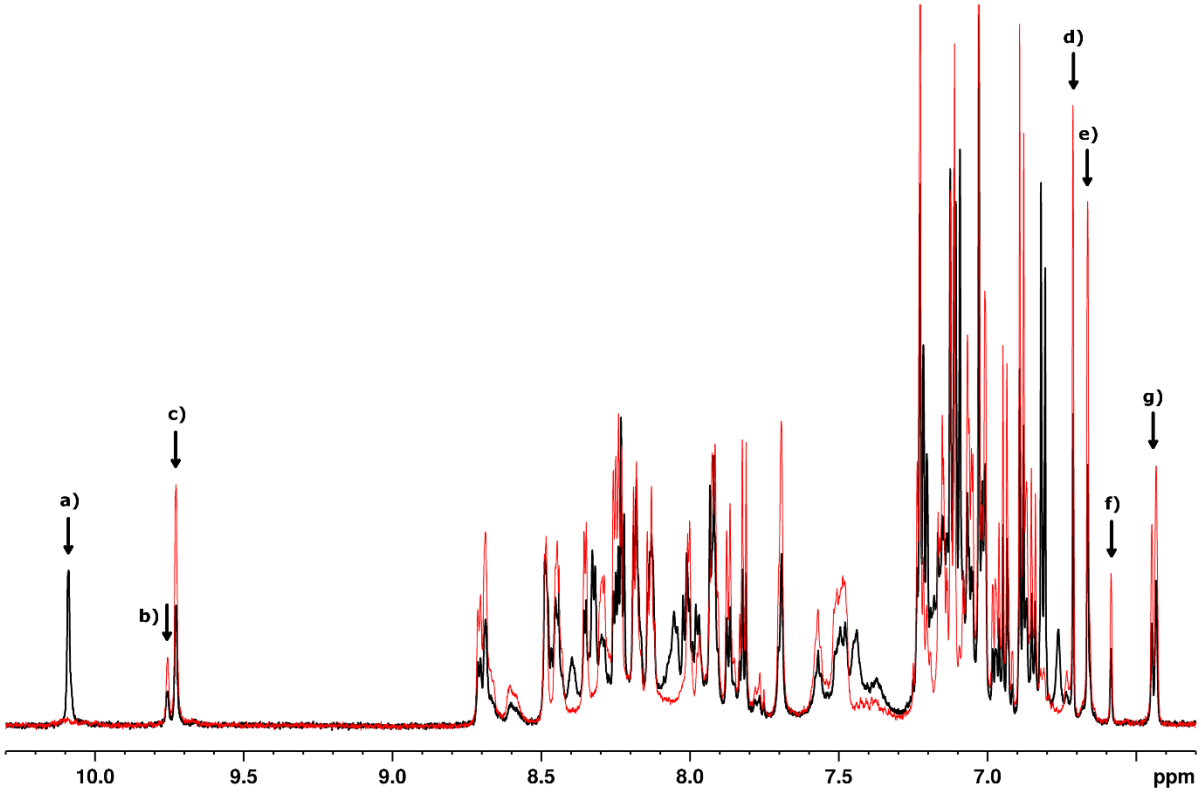

Fig. S 14: The indole, amide and aromatic region of the 1D-^{1}H-NMR spectra of the switch cage after irradiation to the PSS at 385 nm (red) and relaxation in the dark at 298 K for 39 h (black) are shown. The full spectra are depicted in **Fig. S 13** (PSS at 385 nm) and **Fig. S 11** (dark-adapted). The signals marked a) – g) were chosen for determination of the PSS and relaxation rates as they are more or less baseline-separated.

4.2.3. Determination of the PSS at 385 nm

The PSS at 385 nm was determined *via* the six signals of *cis*-SC (Signals b) – g) of **Tab. S 5** and **Fig. S 14**). The ratio of their intensity after irradiation to the PSS at 385 nm ($I_{385\ nm}$) and their intensity in the dark-adapted state ($I_{dark\text{-}adapted}$) is correlated to the *cis*→*trans*-conversion ratio in the PSS according to the following formula:

$$1 - \frac{I_{385\,nm}}{I_{dark-adapted}} = \textit{cis}\rightarrow\textit{trans}\text{-conversion ratio}$$

Note that this method can only be applied with signals of *cis*-SC, as signals of *trans*-SC are essentially zero in the dark-adapted state.

The first (recorded at t = 2 min after irradiation) and the last spectrum (t = 39 h) of the relaxation measurements were chosen to represent the PSS and the dark-adapted state, respectively. In order to determine the PSS, the intensity of signals b) – g) (**Tab. S 5**, **Fig. S 14**) was measured by integration. Their integrals were calibrated relative to the DSS integral which was arbitrarily set to 1. The obtained intensities were inserted in the formula to obtain the approximate fraction of *trans*-SC in the PSS listed in **Tab. S 6**.

4.2.4. Determination of the relaxation rate

In order to determine the relaxation rate, every 1D-^{1}H-NMR spectrum of the relaxation measurements was integrated within the ranges listed in **Tab. S 5** (signals a) – g)). These integrals were calibrated relative to the DSS signal, which was arbitrarily set to 1. The signal intensity was plotted over the time (**Fig. S 15**) and the following function of exponential decay was fitted to the data:

$$y = A_1 \cdot e^{\left(\frac{-x}{t_1}\right)} + y_0$$

In this formula, x is the time, y_0 is the offset to which the function approaches asymptotically, t_1 is the time constant of the decay and A_1 is the initial decaying quantity. The sum of y_0 and A_1 ($y_0 + A_1$) give the y-intercept (initial total quantity). The half-life $t_{1/2}$ was calculated by the following relationship:

$$t_{1/2} = t_1 \cdot \ln(2)$$

The results of the fitted data are listed in the table included in **Fig. S 15**, the final results are listed in **Tab. S 6**.

4.2.5. Results

Tab. S 6: Resulting PSS and relaxation rate from each signal a) – g).

Entry	Species	Representing	$PSS_{385\ nm}$ / % *trans*-state	$t_{1/2}$ / h
a)	*trans*-SC	fold	n.d.	6.7 ± 0.1
b)	*cis*-SC_b	fold	43	5.6 ± 0.3
c)	*cis*-SC_a	fold	49	6.1 ± 0.1
d)	*cis*-SC_a	diazocine	46	6.5 ± 0.1
e)	*cis*-SC_a	diazocine	45	6.3 ± 0.2
f)	*cis*-SC_b	diazocine	46	6.5 ± 0.3
g)	*cis*-SC_a / *cis*-SC_b	diazocine	47	6.0 ± 0.2
		Average:	**46 ± 2**	**6.2 ± 0.3**

There is no significant discrepancy in the PSS or half-life of either species, i.e. *cis*-SC_a, *cis*-SC_b or *trans*-SC, nor is there any significant deviation between the behavior of the fold and the diazocine. This implies a direct coupling of the fold and the photoswitchable cross-linker.

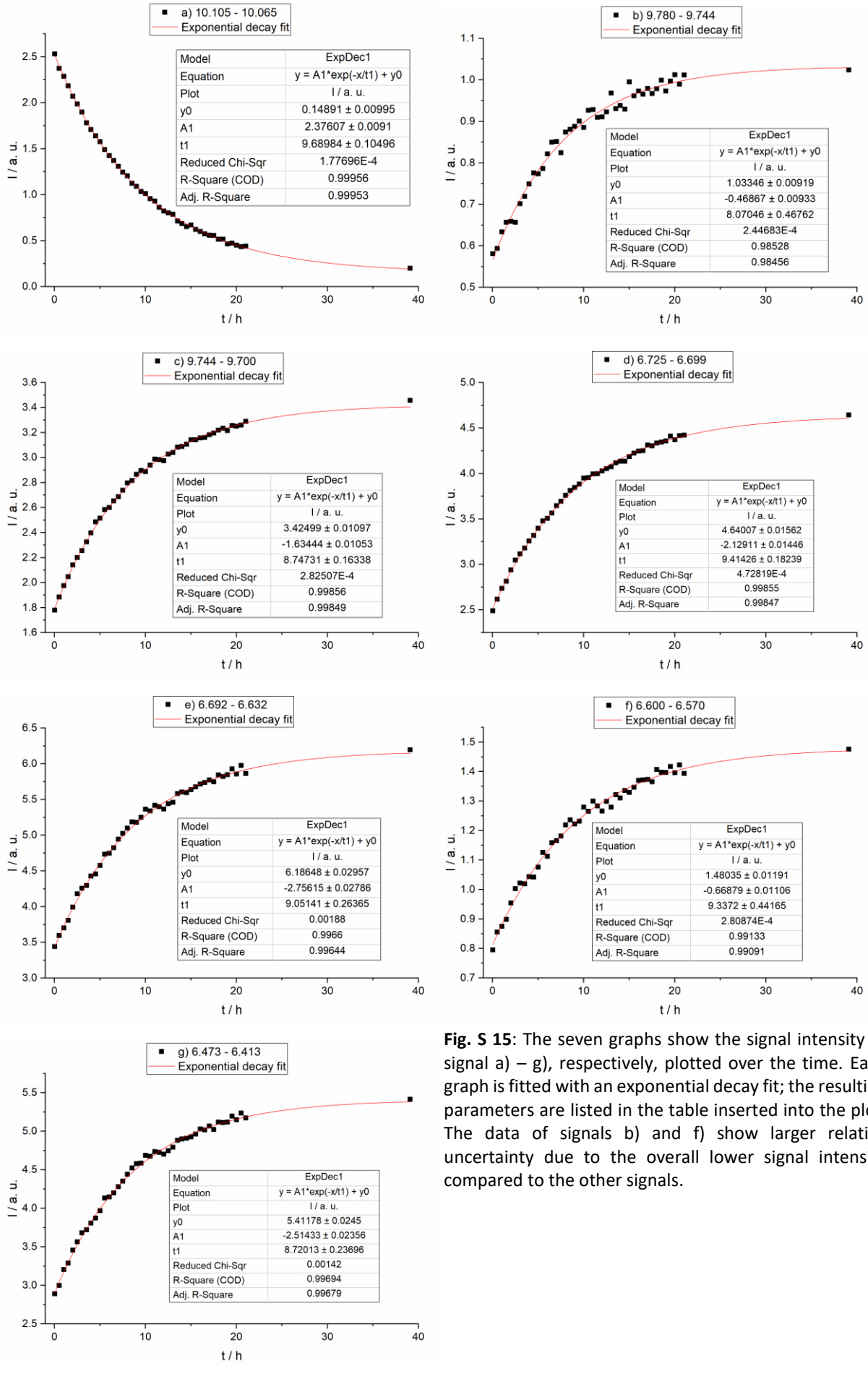

Fig. S 15: The seven graphs show the signal intensity of signal a) – g), respectively, plotted over the time. Each graph is fitted with an exponential decay fit; the resulting parameters are listed in the table inserted into the plot. The data of signals b) and f) show larger relative uncertainty due to the overall lower signal intensity compared to the other signals.

4.3. Photostationary state at 530 nm

The 1D-^{1}H-NMR spectrum of the switch-cage recorded immediately after irradiation to the PSS at 530 nm is virtually identical the spectra of the dark-adapted switch-cage (**Fig. S 16**). Therefore, irradiation with light of the wavelength 530 nm affords nearly complete conversion to the *cis*-switch cage.

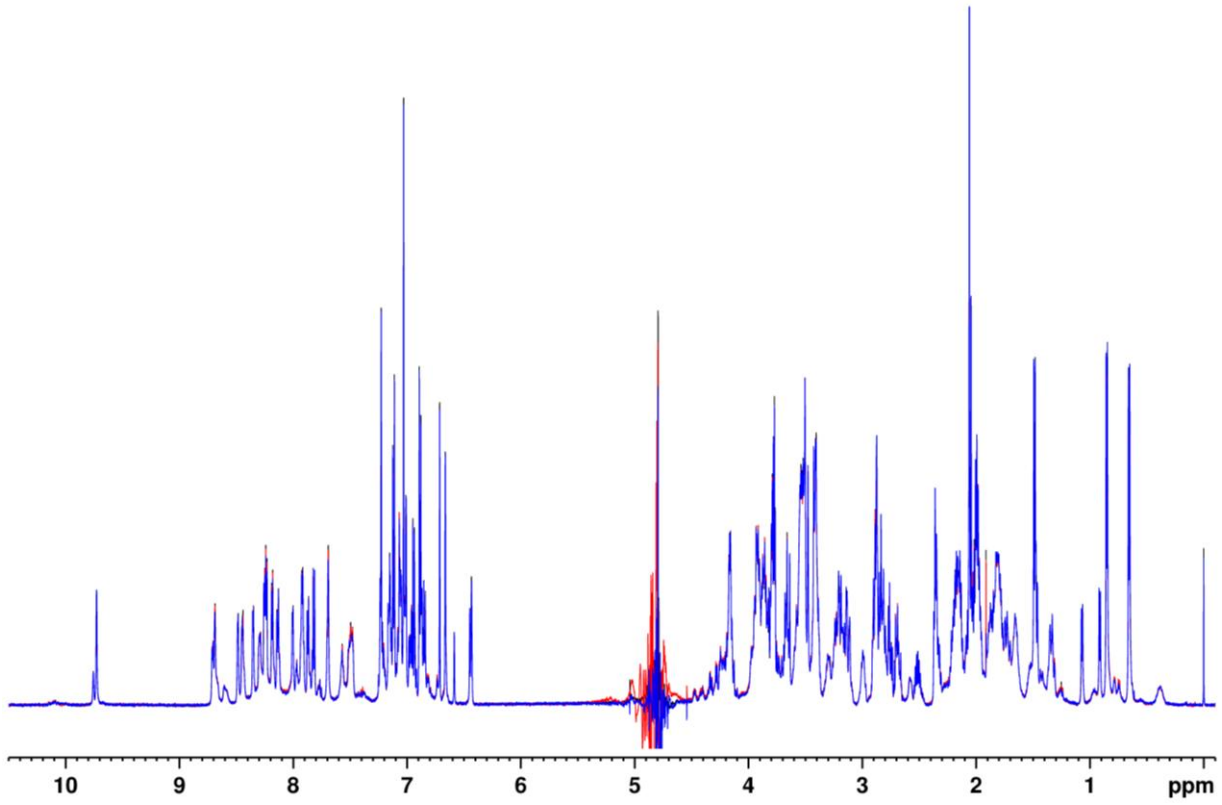

Fig. S 16: Overlay of the 1D-^{1}H-NMR spectra of dark-adapted *cis*-SC as obtained after purification (black), *cis*-SC immediately after irradiation to the PSS at 530 nm (red), and *cis*-SC after irradiation to the PSS at 385 nm and subsequent relaxation in the dark at 298 K (24.85 °C) for 39 h (blue). Apart from the water suppression artifact around 4.9 ppm, the three spectra are virtually identical.

4.4. Mechanism of interconversion between *cis*-SC_a and *cis*-SC_b

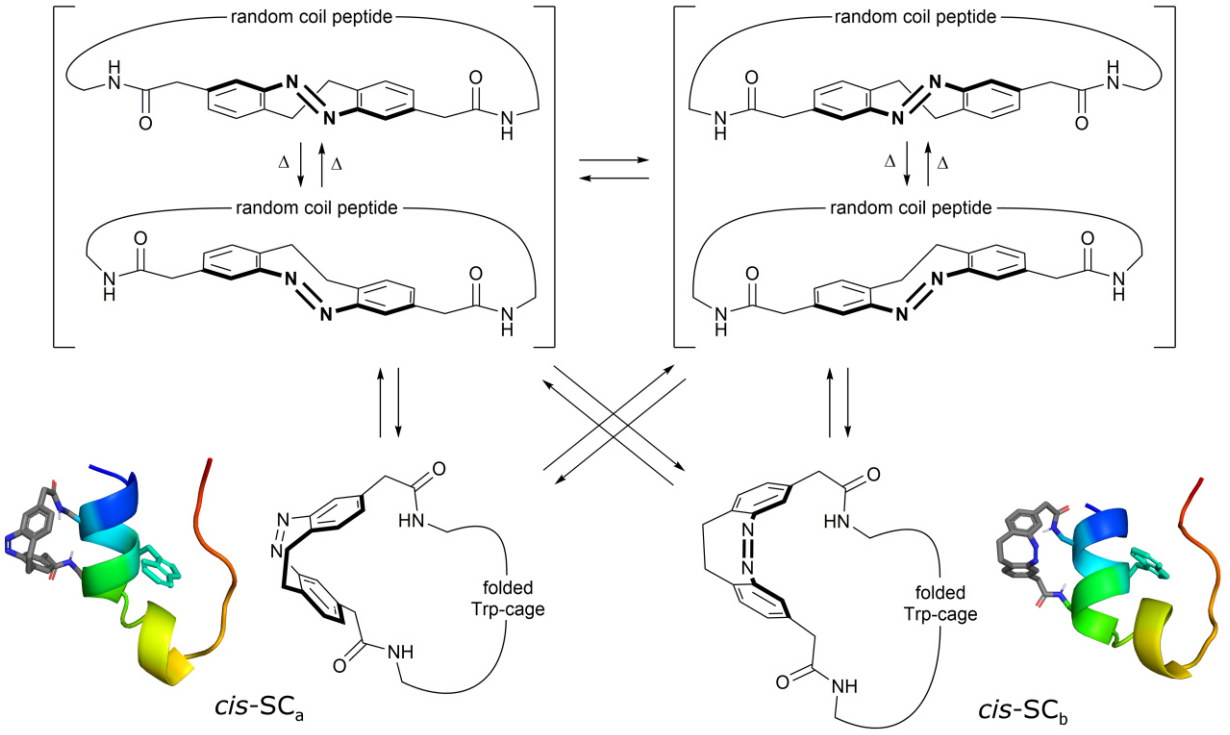

Scheme S 1: Mechanism of interconversion between *cis*-SC_a, *cis*-SC_b and the two diastereomers of *trans*-SC in the twist and chair conformation. Deltas (Δ) indicate thermal interconversion at ambient temperature. The other indicated equilibria are significantly slower and require higher temperatures or irradiation with light.

5. Cross-linker synthesis and characterization

5.1. Devices

5.1.1. Chromatography stationary phases

Flash column chromatography purfications were performed on a Biotage Isolera one with Biotage Ultra cartridges (HP-Sphere, particle diameter: 25 µm, cartridge sizes: 10 g, 25 g, 50 g and 100 g; Biotage, Uppsala, Sweden). R_f values were determined by thin layer chromatography on Polygram SilG/UV_{254} (0.2 mm particle size; Macherey-Nagel, Düren, Germany) and ALUGRAM Xtra SIL G/UV_{254} (0.2 mm particle size; Macherey-Nagel, Düren, Germany).

5.1.2. Melting point determination

Melting points were measured with a B-560 Melting Point Apparatus (Büchi, Essen, Germany) in melting point tubes.

5.1.3. NMR spectroscopy

NMR measurements of the cross-linker and its precursors were performed with a Bruker DRX 500 FT-NMR spectrometer (^{1}H-NMR: 500.1 MHz, ^{13}C-NMR: 125.8 MHz; Bruker, Billerica, MA, USA).

NMR spectra were measured in deuterated solvents (Deutero, Kastellaun, Germany). Spectra were referenced to TMS when acetone, acetonitrile or chloroform was the solvent. Otherwise the following solvent signals were used for referencing:

Tab. S 7: List of deuterated solvents.

Solvent	**Degree of deuteration**	**^{1}H signal**	**^{13}C signal**
Acetone-d_6	99.8%	2.05 (quintet)	29.84 (septet)
Acetonitrile-d_3	99.8%	1.94 (quintet)	118.26 (septet)
Chloroform-d_1	99.8%	7.26 (s)	77.16 (triplet)
DMSO-d_6	99.8%	2.50 (s)	39.52 (septet)
Methanol-d_4	99.8%	3.34 (s)	49.86 (septet)

5.1.4. IR spectroscopy

Infrared spectra were measured on a PerkinElmer 1600 Series FT-IR spectrometer with an A531-G Golden-Gate-Diamond-ATR-unit (PerkinElmer, Waltham, MA, USA). Signals were abbreviated with w for weak, m for medium and s for strong signal intensity.

5.1.5. Mass spectrometry

The high resolution-electron ionization (HR-EI) mass spectra were measured with an AccuTOF GCv 4G (Jeol Germany, Freising, Germany) with ionization energy of 70 eV and the high resolution-electrospray ionization (HR-ESI) mass spectra were measured with a Q Exactive Plus MS, Hybrid Quadrupol-Orbitrap (Thermo Fisher Scientific, Waltham, MA, USA).

5.2. Synthetic procedures and analysis results

General remark:

The 4-methyl-2,6,7-trioxabicyclo[2.2.2]octane-1-yl (OBO) protecting group that was employed during the cross-linker synthesis is highly labile against acids and a fraction may unintentionally be hydrolyzed to the open ester during the work-up of reaction ii) or iii) of **Scheme 2** in the paper.

5.2.1. Synthesis of (3-methyloxetan-3-yl)methyl 2-(4-methyl-3-nitrophenyl)acetate (8)

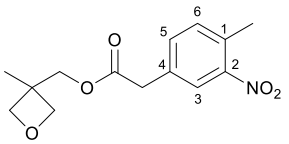

At 0 °C and under N_2 atmosphere 2-(4-methyl-3-nitrophenyl)acetic acid (**6**; 3.9 g, 20 mmol), 4-dimethylaminopyridine (DMAP; 244 mg, 2 mmol) and *N*,*N*'-dicyclohexylcarbodiimide (DCC; 4.13 g, 20 mmol) were dissolved in 30 ml dry dichloromethane (DCM). Immediately afterwards 3-methyl-3-oxetanemethanol (**7**; 1.98 ml, 20 mmol) was added. The reaction was stirred for 1 h at room temperature. The formed solid was filtered and washed with 100 ml DCM. The solvent was evaporated in vacuo and the crude product was purified by flash column chromatography (cyclohexane/ethyl acetate) to afford the product as a yellow oil (4.91 g, 17.6 mmol, 88%).

R_f: 0.29 (cyclohexane/ethyl acetate, 2:1).

^{1}H-NMR (500.1 MHz, Acetone-d_6, 300 K): δ = 7.96 (d, ^4J = 1.8 Hz, 1 H, *H*-3), 7.58 (dd, ^3J = 8.0 Hz, ^4J = 1.7 Hz, 1 H, *H*-5), 7.44 (d, ^3J = 7.8 Hz, 1 H, *H*-6), 4.41 (d, ^4J = 5.8 Hz, 2 H, C-CH_2-O-), 4.25 (d, ^4J = 5.8 Hz, 2 H, C-CH'_2-O-), 4.21 (s, 2 H, C-CH_2-OOC), 3.87 (s, 2 H, OOC-CH_2-C_4), 2.54 (s, 3H, C_1-CH_3), 1.29 (s, 3H, C-CH_3) ppm.

^{13}C-NMR (125.8 MHz, Acetone-d_6, 300 K): δ = 171.4 (*C*OO), 150.1 (*C*-2), 135.2 (*C*-5), 135.1 (C-4), 133.6 (*C*-6), 132.4 (C-1), 126.1 (*C*-3), 79.6 (*C*-CH_2-O-), 70.0 (C-*C*H_2-OOC), 40.2 (OOC-*C*H_2-C_4), 21.2 (C-*C*H_3), 19.7 (C_1-*C*H_3) ppm.

IR (ATR): $\tilde{\nu}$ = 2963 (w), 2872 (w), 1735 (s), 1526 (s), 1498 (w), 1454 (w), 1346 (s), 1298 (w), 1246 (m), 1223 (m), 1152 (s), 1031 (w), 977 (s), 833 (m), 815 (s), 751 (w), 732 (w), 678 (w) cm^{-1}.

MS (EI, 70 eV): m/z (%) = 279 (7), 262 (5), 196 (5), 177 (13), 150 (100).

HRMS (EI, 70 eV): $[C_{14}H_{17}N_1O_5]^+$, calc.: m/z = 279.11067, found: m/z = 279.11046.

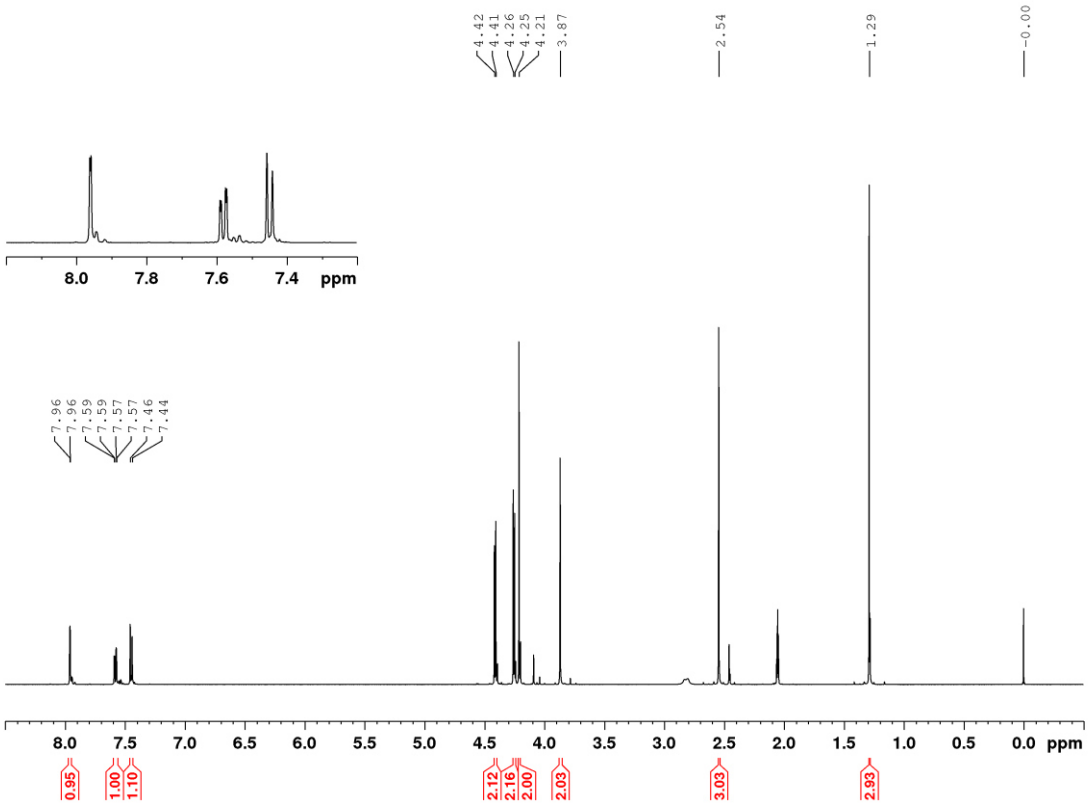

Fig. S 17: ^{1}H-NMR spectrum of compound **8** measured in deuterated acetone at 300 K.

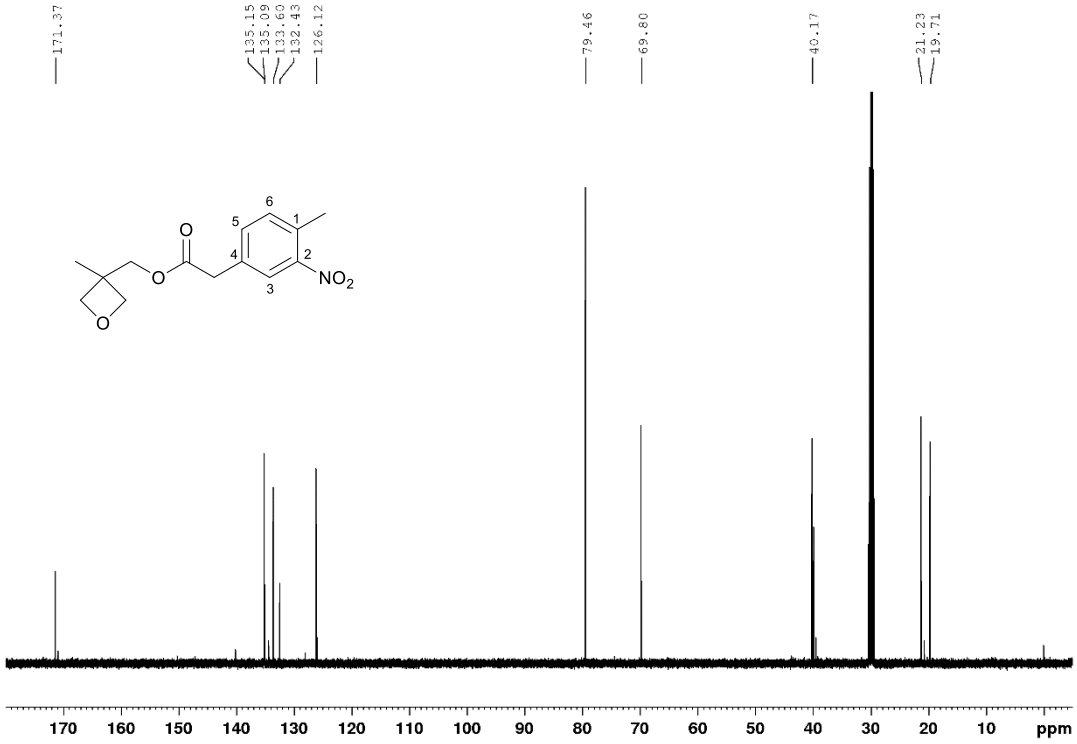

Fig. S 18: ^{13}C-NMR spectrum of compound **8** measured in deuterated acetone at 300 K.

5.2.2. Synthesis of 4-methyl-1-(4-methyl-3-nitrobenzyl)-2,6,7-trioxabicyclo[2.2.2]octane (9)

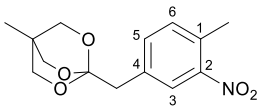

Under N_2 atmosphere (3-methyloxetan-3-yl)methyl 2-(4-methyl-3-nitrophenyl)acetate (**8**; 2.00 g, 7.16 mmol) was dissolved in 20 ml dry DCM, cooled to -10 °C and 48% $BF_3{\cdot}Et_2O$ solution (200µl, 716 µmol) was added dropwise. The reaction was stirred at room temperature for 2 h and stopped with trimethylamine (TEA; 1.00 ml, 7.16 mmol). The solvent was evaporated in vacuo and the residue was dissolved in ethyl acetate. The organic layer was washed with 5% ammonium chloride solution (150 ml), H_2O (2 x 100 ml), saturated sodium bicarbonate solution (2 x 100 ml), saturated sodium chloride solution (100 ml) and dried over magnesium sulfate. The solvent was evaporated in vacuo and the crude product was purified by flash column chromatography (cyclohexane/ethyl acetate, 1:2) to afford the product as colourless crystals (1.61 g, 5.79 mmol, 81%).

R_f: 0.48 (cyclohexane/ethyl acetate, 2:1).

T_m: 118 °C

^{1}H-NMR (500.1 MHz, Acetone-d_6, 300 K): δ = 7.85 (d, ^4J = 1.7 Hz, 1 H, *H*-3), 7.47 (dd, ^3J = 7.9 Hz, ^4J = 1.78 Hz, 1 H, *H*-5), 7.34 (d, ^3J = 7.9 Hz, 1 H, *H*-6), 3.86 (s, 6 H, C-CH_2-O-), 2.98 (s, 2 H, C-CH_2-C_4), 2.52 (s, 3H, C_1-CH_3), 0.79 (s, 3H, C-CH_3) ppm.

^{13}C-NMR (125.8 MHz, Acetone-d_6, 300 K): δ = 149.8 (*C*-2), 136.3 (*C*-5), 136.1 (C-4), 132.8 (*C*-6), 132.4 (C-1), 127.0 (*C*-3), 108.9 (O-*C*-CH_2), 73.1 (C-*C*H_2-O-), 42.5 (C-*C*H_2-C_4), 31.1 (*C*-CH_3), 19.7 (C_1-*C*H_3), 14.3 (C-*C*H_3).

IR (ATR): $\tilde{\nu}$ = 2966 (w), 2935 (w), 2886 (w), 1733 (m), 1526 (s), 1472 (w), 1464 (w), 1453 (w), 1440 (w), 1397 (w), 1384 (w), 1340 (w), 1309 (m), 1282 (m), 1264 (m), 1207 (m), 1190 (m), 1153 (m), 1043 (s), 1025 (s), 1011 (s), 984 (s), 928 (m), 923 (m), 895 (m), 886 (m), 851 (m), 837 (m), 818 (m), 768 (w), 755 (w), 718 (s), 688 (w), 675 (w) cm^{-1}.

MS (EI, 70 eV): m/z (%) = 279 (3), 249 (37), 179 (20), 150 (100).

HRMS (EI, 70 eV): $[C_{14}H_{17}N_1O_5]^+$, calc.: m/z = 279.11067, found: m/z = 279.11090.

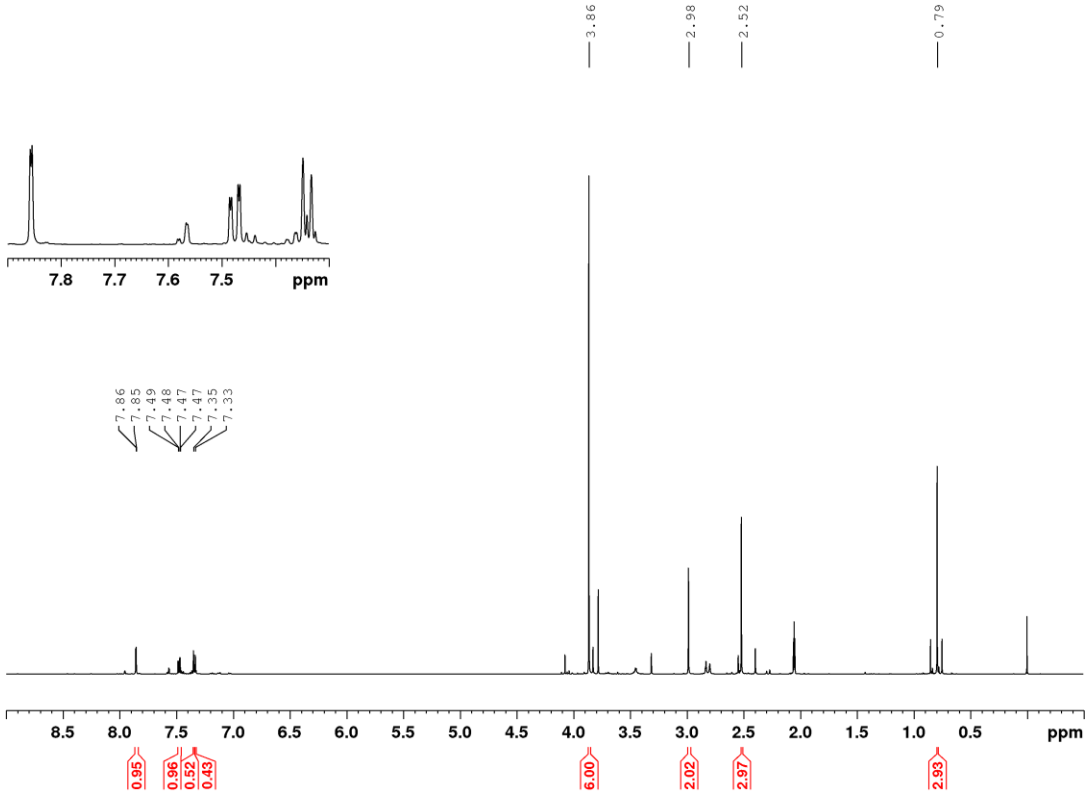

Fig. S 19: ^{1}H-NMR spectrum of compound **9** measured in deuterated acetone at 300 K.

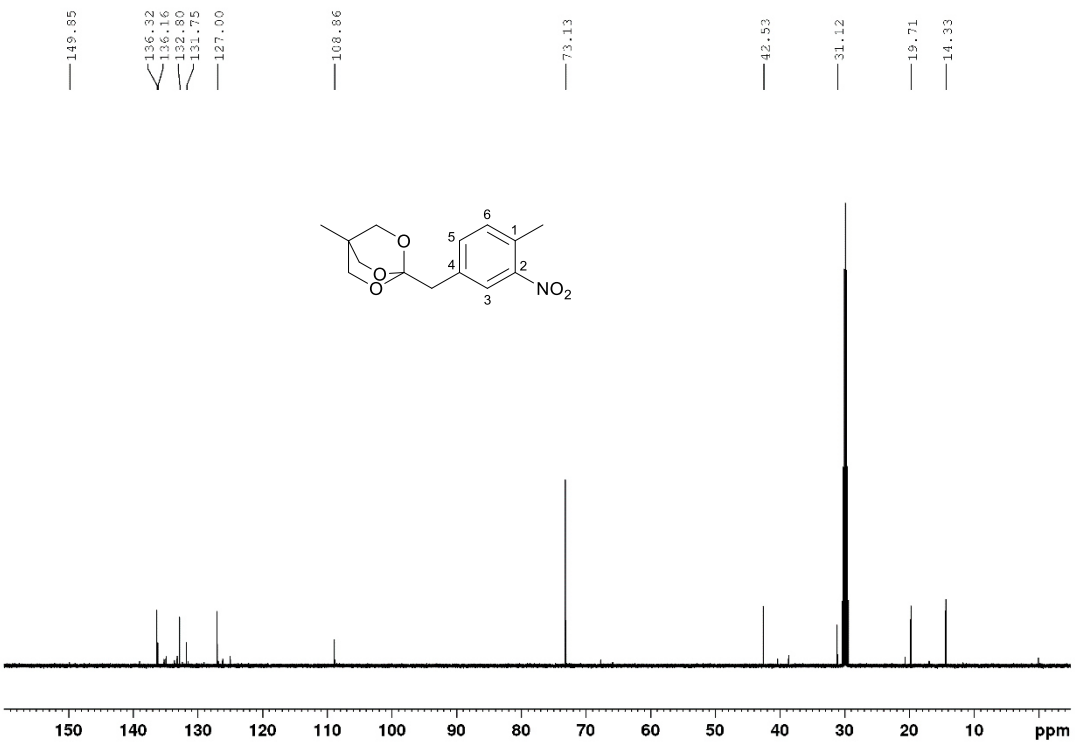

Fig. S 20: ^{13}C-NMR spectrum of compound **9** measured in deuterated acetone at 300 K.

5.2.3. Synthesis of 1,2-bis(4-((4-methyl-2,6,7-trioxabicyclo[2.2.2]octan-1-yl)methyl)-2-nitrophenyl)-ethane (10)

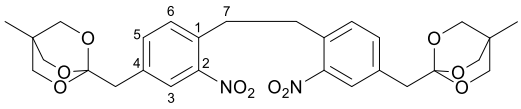

Under N_2 atmosphere 4-methyl-1-(4-methyl-3-nitrobenzyl)-2,6,7-trioxabicyclo[2.2.2]octane (**9**; 1.50 g, 5.37 mmol) was dissolved in 30 ml dry tetrahydrofuran (THF) and cooled to -5 °C, followed by addition of potassium butoxide (1.02 g, 9.13 mmol). The reaction was stirred for 40 s before addition of bromine (274 µl, 5.37 mmol). After further stirring for 10 min at room temperature the reaction mixture was added to a saturated sodium bicarbonate solution and extracted with ethyl acetate (3 x 100 ml). The combined organic layers were washed with 100 ml saturated sodium thiosulfate solution and dried over magnesium sulfate. The solvent was evaporated in vacuo and the crude product was purified by flash column chromatography (cyclohexane/ethyl acetate, 2:1) to afford the product as colourless crystals (680 mg, 2.44 mmol, 46%).

R_f: 0.28 (cyclohexane/ethyl acetate, 2:1).

T_m: 116 °C

^{1}H-NMR (500.1 MHz, Acetone-d_6, 300 K): δ = 7.86 (d, ^4J = 1.7 Hz, 2 H, *H*-3), 7.55 (dd, ^3J = 7.9 Hz, ^4J = 1.8 Hz, 2 H, *H*-5), 7.42 (d, ^3J = 7.9 Hz, 2 H, *H*-6), 3.87 (s, 12 H, C-CH_2-O-), 3.20 (s, 4 H, C-CH_2-C_4), 3.01 (s, 4H, *H*-7), 0.80 (s, 6H, C-CH_3) ppm.

^{13}C-NMR* (125.8 MHz, Acetone-d_6, 300 K): δ = 149.8 (*C*-2), 136.5 (*C*-5), 136.8 (*C*-4), 134.5 (*C*-1), 132.1 (*C*-6), 127.2 (*C*-3), 108.9 (O-*C*-CH_2), 73.1 (C-*C*H_2-O-), 42.6 (C-*C*H_2-C_4), 34.2 (*C*-7), 31.1 (*C*-CH_3), 14.3 (C-*C*H_3).

IR (ATR): $\tilde{\nu}$ = 3310 (w), 2883 (w), 1726 (s), 1526 (w), 1525 (s), 1458 (w), 1341 (s), 1227 (m), 1169 (s), 1038 (s), 1002 (s), 924 (s), 846 (s), 817 (m), 764 (w), 732 (w), 679 (m) cm^{-1}.

MS (EI, 70 eV): m/z (%) = 556(8), 539 (9), 294 (32), 278 (100).

HRMS (EI, 70 eV): $[C_{28}H_{32}N_2O_{10}]^+$, calc.: m/z = 556.20569, found: m/z = 556.20124.

*Frequencies were determined from the carbon dimension of the HMBC spectrum.

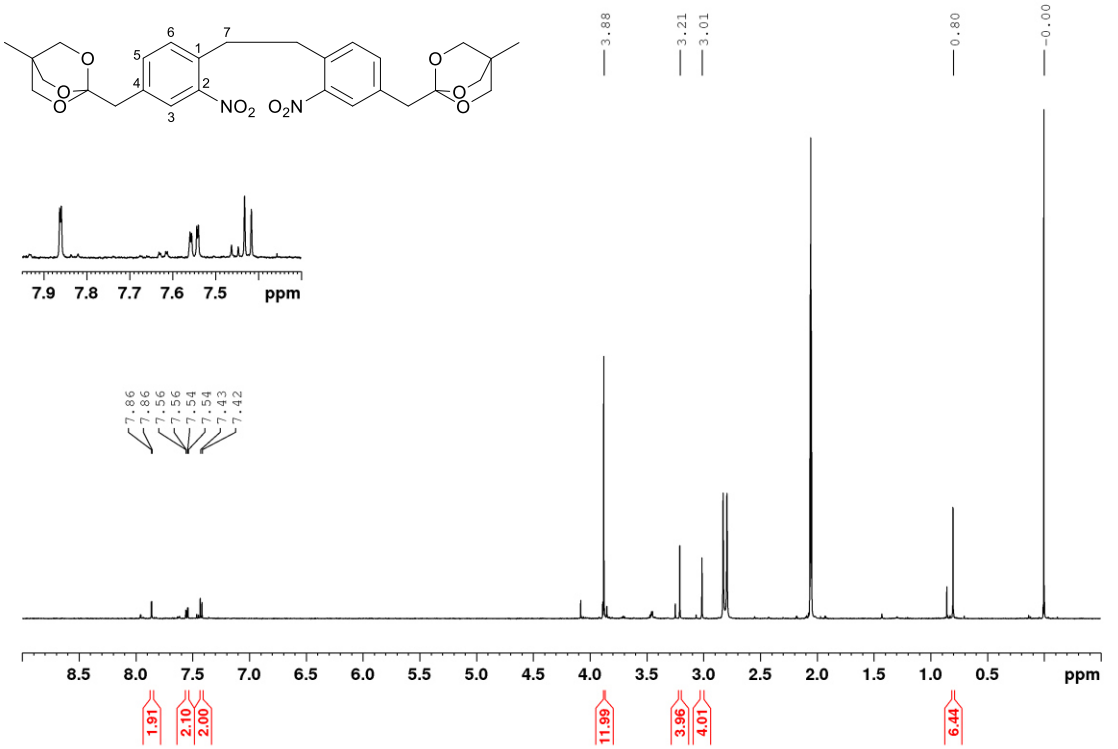

Fig. S 21: ^{1}H-NMR spectrum of compound **10** measured in deuterated acetone at 300 K.

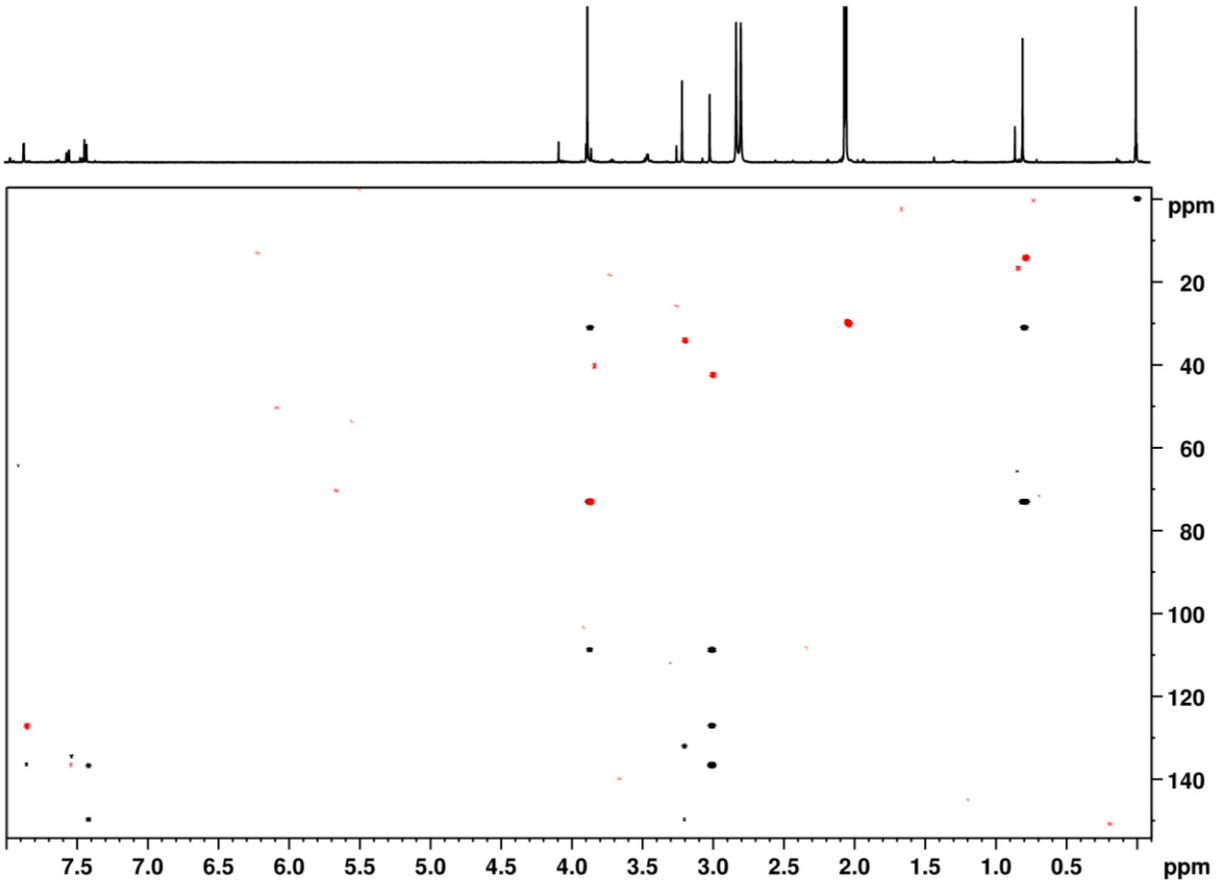

Fig. S 22: Overlay of the ^{1}H,^{13}C-HSQC (red) and the ^{1}H,^{13}C-HMBC (black) of compound **10** measured in deuterated acetone at 300 K.

5.2.4. Synthesis of (Z)-bis(3-hydroxy-2-(hydroxymethyl)-2-methylpropyl) 2,2'-(11,12-dihydro-dibenzo[c,g][1,2]diazocine-3,8-diyl)diacetate (11)

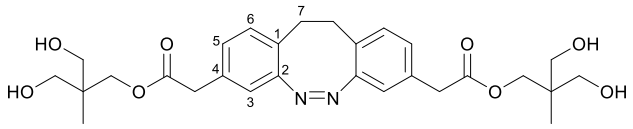

A mixture of 1,2-bis(4-((4-methyl-2,6,7-trioxabicyclo[2.2.2]octan-1-yl)methyl)-2-nitrophenyl)ethane (**10**; 431 mg, 775 µmol), $Ba(OH)_2 \cdot 8\ H_2O$ (732 mg, 2.33 mmol) and zinc powder (811 mg, 12.4 mmol) were dissolved in an ethanol-water mixture (60 ml, 2:1) and stirred for 5 h under reflux. After filtration trough Celite and evaporation of the solvent under reduced pressure, the crude product was dissolved in 90 ml 0.1 M methanolic NaOH solution, $CuCl_2$ (20 mg, 149 µmol) was added, and air was blown trough the solution for 4 h. The reaction was added to a saturated sodium bicarbonate solution, neutralized with 1 M HCl solution and extracted with DCM (3 x 75 ml). The combined organic layers were washed with a saturated sodium chloride solution and dried over magnesium sulfate. The solvent was evaporated in vacuo and the crude product was purified by flash column chromatography (cyclohexane/ethyl acetate, 2:1) to afford the product as a yellow solid (161 mg, 326 µmol, 42%).

R_f: 0.22 (cyclohexane/ethyl acetate, 2:1).

T_m: 132 °C

^{1}H-NMR (500.1 MHz, $CDCl_3$, 300 K): δ = 6.96 (s, 4 H, *H*-5, *H*-6), 6.79 (d, ^3J = 7.9 Hz, 2 H, *H*-3), 4.13 (s, 4 H, COO-CH_2-C), 3.57 (s, 4 H, COO-CH_2-C_4), 3.44 (d, ^3J = 11.4 Hz, 4 H, CH_2-OH), 3.36 (d, ^3J = 11.4 Hz, 4 H, CH'_2-OH), 2.85 (s, 4 H, *H*-7), 2.41 (s, 4H, CH_2-O*H*), 0.71 (s, 6H, C-CH_3) ppm.

^{13}C-NMR (125.8 MHz, $CDCl_3$, 300 K): δ = 172.0 (*C*OO), 155.3 (*C*-2), 132.5 (*C*-4), 130.0 (*C*-5), 128.1 (*C*-5), 127.0 (*C*-1), 125.6 (*C*-5), 119.8 (*C*-3), 67.5 (CH_3-*C*-$(CH_2)_3$) 67.4 (*C*H_2-OH) 66.9 (COO-*C*H_2-C), 40. (COO-*C*H_2-C_4), 31.4 (*C*-7), 16.7(C-*C*H_3) ppm.

IR (ATR): $\tilde{\nu}$ = 3312 (w), 2933 (w), 2880 (w), 1730 (s), 1458 (w), 1396 (w), 1334 (m), 1303 (m), 1253 (m), 1191 (m), 1151 (w), 1038 (s), 990 (s), 892 (w), 835 (w), 702 (w) cm^{-1}.

HRMS (HR-ESI): $[C_{28}H_{36}O_8N_2 + NH_4]^+$, calc.: m/z = 546.2806, found: m/z = 546.28099.

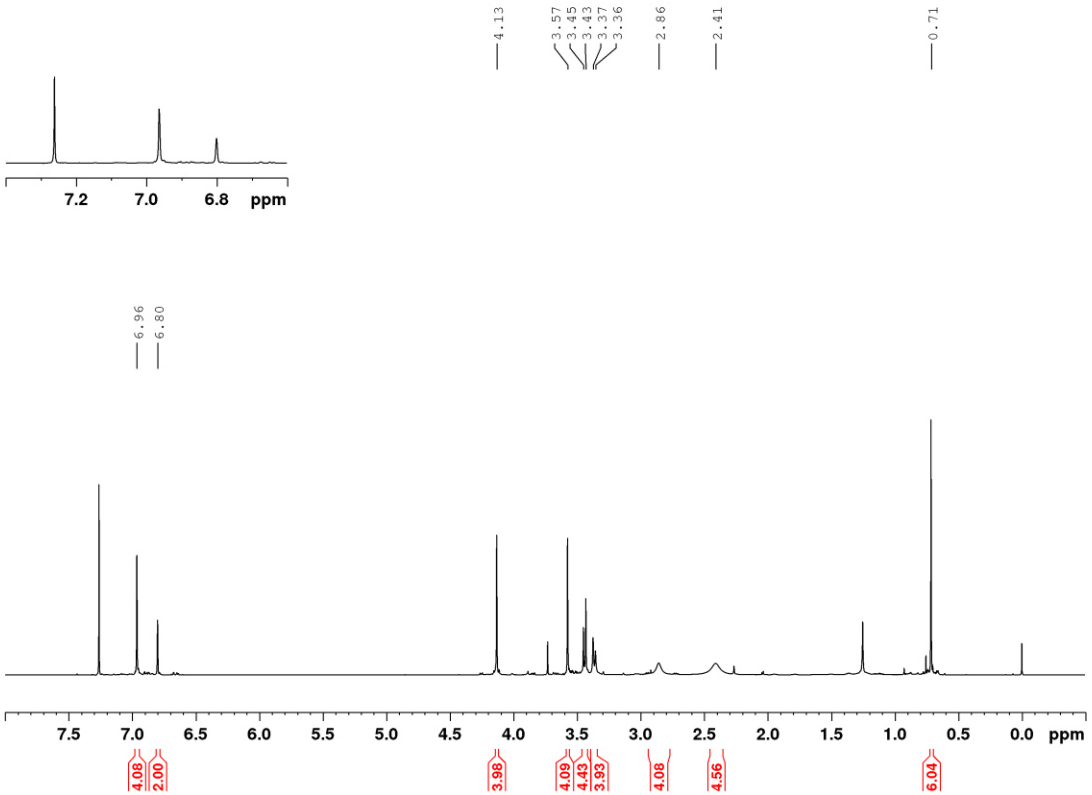

Fig. S 23: ^{1}H-NMR spectrum of compound **11** measured in deuterated chloroform at 300 K.

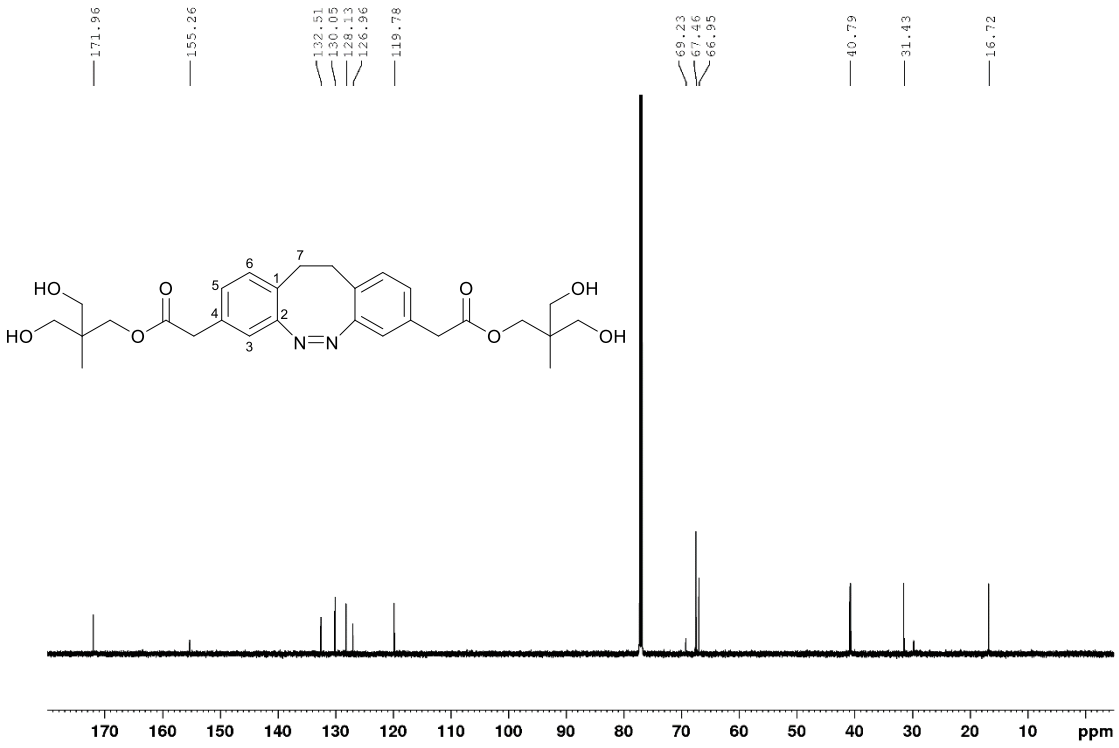

Fig. S 24: ^{13}C-NMR spectrum of compound **11** measured in chloroform at 300 K.

5.2.4.1. *Determination of the PSS of diazocine* 11

The PSS at 385 nm of diazocine **11** was determined in MeCN by integration of the *H*-3 signals of the *cis*- and the *trans*- isomer in the 1D-^{1}H-NMR spectrum of the PSS at 385 nm (**Fig. S 25**, red).

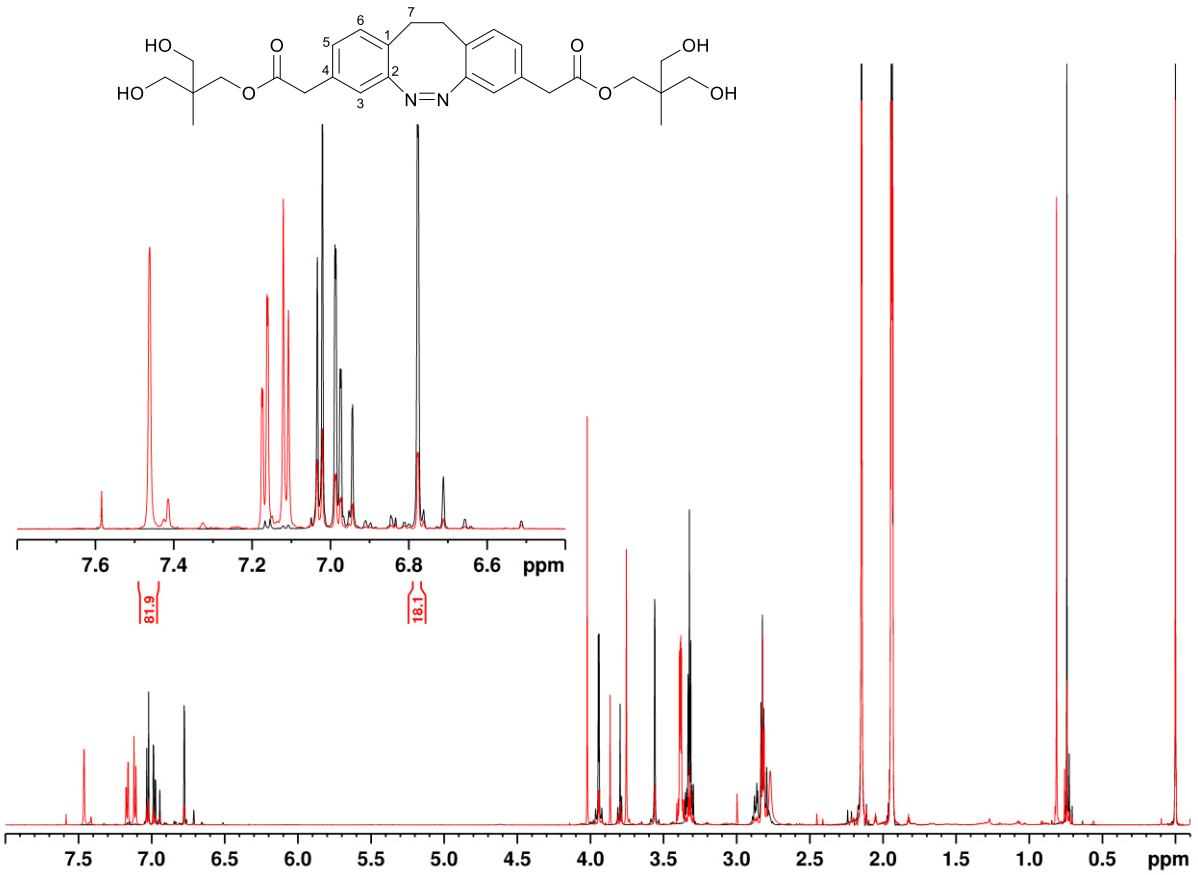

Fig. S 25: Overlay of the 1D-^{1}H-NMR spectra of diazocine **11** dissolved in MeCN-d_3. The spectrum displayed in black was recorded immediately after irradiation to the PSS at 530 nm, whereas the red spectrum represents the PSS at 385 nm. The expansion shows the aromatic region from which the PSS at 385 nm was determined by integration of the doublet at 7.46 ppm which represents the *trans*-species and at 6.78 ppm which represents the *cis*-isomer.

cis-diazocine 11 (black)

^{1}H-NMR (500.1 MHz, MeCN-d_3, 298 K): δ = 7.03 (d, ^3J = 7.9 Hz, 2 H, *H*-6), 6.98 (dd, ^3J = 7.9 Hz, ^4J = 1.6 Hz, 2 H, *H*-5), 6.79 (d, ^4J = 1.4 Hz, 2 H, *H*-3), 3.98-3.92 (m, 4 H, COO-CH_2-C), 3.56 (s, 4 H, COO-CH_2-C$_4$), 3.32 (m$_c$, 8 H, CH_2-OH, CH'_2-OH), 2.88-2.76 (m, 8 H, *H*-7, CH$_2$-O*H*), 0.74 (s, 6H, C-CH_3) ppm.

trans-diazocine 11 (red)

^{1}H-NMR (500.1 MHz, MeCN-d_3, 298 K): δ = 7.46 (s, 2 H, *H*-3), 7.17 (dd, ^3J = 7.8 Hz, ^4J = 1.6 Hz,2 H, *H*-5), 7.11 (d, ^3J = 7.8 Hz, 2 H, *H*-6), 4.02 (s, 4 H, COO-CH_2-C), 3.75 (s, 4 H, COO-CH_2-C$_4$), 3.38 (m$_c$, 8 H, CH_2-OH, CH'_2-OH), 2.86-2.72 (m, 8 H, *H*-7, CH$_2$-O*H*), 0.81 (s, 6H, C-CH_3) ppm.

5.2.5. Synthesis of (Z)-bis(2,5-dioxopyrrolidin-1-yl) 2,2'-(11,12-dihydrodibenzo[c,g][1,2]diazocine-3,8-diyl)diacetate (1)

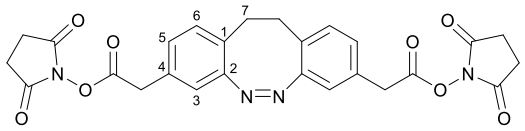

(Z)-bis(3-hydroxy-2-(hydroxymethyl)-2-methylpropyl) 2,2'-(11,12-dihydrodibenzo[c,g][1,2]diazocine-3,8-diyl)diacetate (**11**; 182 mg, 345 µmol) was dissolved in 5 ml MeOH/H_2O (4:1) and 5.5 ml 10% calcium carbonate solution was added. The reaction was stirred over night at room temperature. Afterwards the reaction was acidified to pH = 2 with 1 M hydrogen chloride solution and extracted with ethyl acetate (3 x 10 ml). The combined organic layers were washed with saturated sodium chloride solution, dried over magnesium sulfate and the solvent was evaporated in vacuo. Under N_2 atmosphere the crude product was dissolved in 5 ml DMF. 1-Ethyl-3-(3-dimethylaminopropyl)carbodiimide (EDC; 661 mg, 3.45 mmol) and *N*-hydroxysuccinimide (NHS; 199 mg, 1.73 mmol) were added at room temperature and the reaction stirred for 1 h. The reaction was added to 50 ml H_2O and extracted with (2 x 30 ml) DCM. The combined organic layers were washed with 10 % sodium bicarbonate solution, (2 x 50 ml) 0.1 M hydrogen chloride solution, 50 ml sodium chloride solution and dried over magnesium sulfate. The solvent was evaporated in vacuo and the crude product was purified by flash column chromatography (cyclohexane/ethyl acetate, 1:2) to afford the product as a yellow solid (45 mg, 87 µmol, 25%).

R_f : 0.43 (cyclohexane/ethyl acetate, 1:2)

T_m: 190 °C

^{1}H-NMR (500.1 MHz, DMSO-d_6, 300 K): δ = 7.12 (d, ^3J = 7.9 Hz, 2 H, *H*-6), 7.06 (dd, ^3J = 7.9 Hz, ^4J = 1.5 Hz 2 H, *H*-5), 6.89 (d, ^4J = 1.4 Hz, 2 H, *H*-3), 4.05 (s, 4 H, COO-CH_2-C_4), 2.82-2.81 (m, 12 H, *H*-7, CH_2-C*H*'$_2$) ppm.

^{13}C-NMR (125.8 MHz, DMSO-d_6, 300 K): δ = 170.0 (*C*O), 167.0 (*C*OO), 154.7 (*C*-2), 130.9 (*C*-1) 130.0 (*C*-6), 128.1 (*C*-5), 127 (*C*-4) 119.87 (*C*-3), 35.7 (COO-*C*H_2-C_4), 30.5 (*C*-7), 25.4 (*C*H$_2$-*C*'H$_2$) ppm.

IR (ATR): $\tilde{\nu}$ = 2925 (w), 1812 (w), 1781 (w), 1745 (s), 1727 (s), 1522 (w), 1497 (w), 1457 (w), 1426 (w), 1355 (m), 1205 (s), 1109 (m), 1062 (s), 991 (m), 963 (m), 892 (w), 877 (w), 846 (w), 807 (s), 758 (w), 738 (w), 646 (s) cm^{-1}.

HRMS (HR-ESI): $[C_{28}H_{36}O_8N_2 + NH_4]^+$, m/z = calc.: 536.1772, found 536.17759.

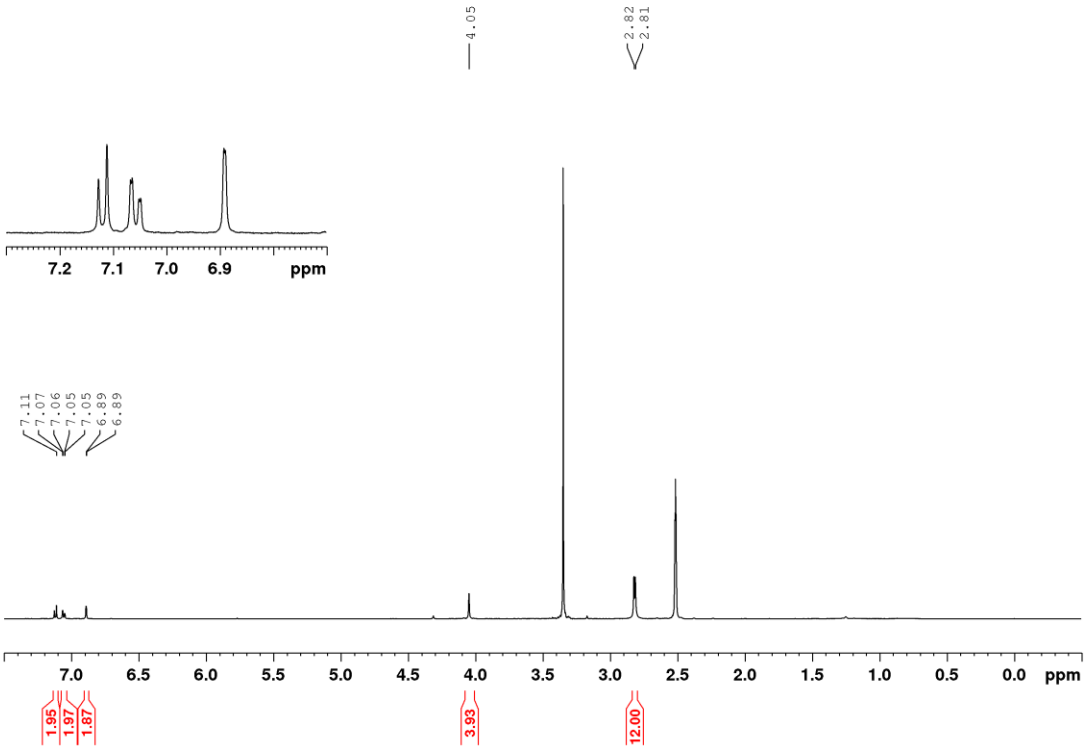

Fig. S 26: ^{1}H-NMR spectrum of compound **1** measured in deuterated DMSO at 300 K.

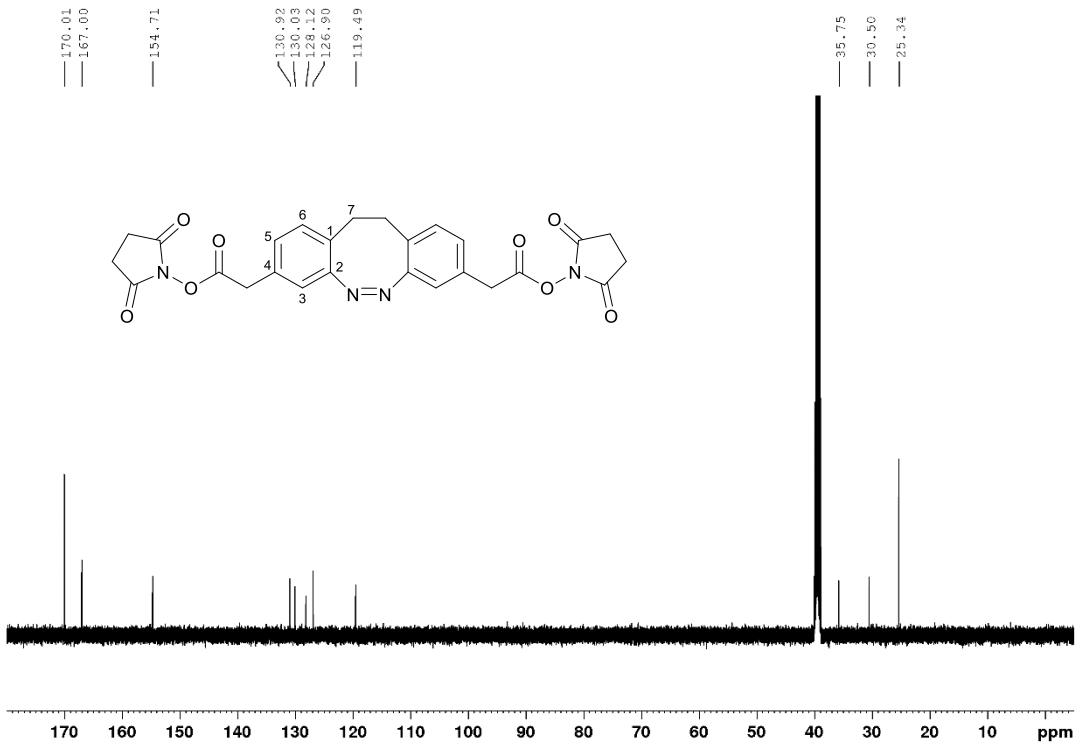

Fig. S 27: ^{13}C-NMR spectrum of compound **1** measured in deuterated DMSO at 300 K.

6. References

1. J. L. Markley, A. Bax, Y. Arata, C. W. Hilbers, R. Kaptein, B. D. Sykes, P. E. Wright and K. Wüthrich, *Pure and Applied Chemistry*, 1998, **70**(1), 117.
2. J. W. Neidigh, R. M. Fesinmeyer and N. H. Andersen, *Nat. Struct. Biol.*, 2002, **9**(6), 425.
3. B. Barua, J. C. Lin, V. D. Williams, P. Kummler, J. W. Neidigh and N. H. Andersen, *Protein Eng. Des. Sel.*, 2008, **21**(3), 171.
4. D. S. Wishart, C. G. Bigam, A. Holm, R. S. Hodges and B. D. Sykes, *J. Biomol. NMR*, 1995, **5**(1), 67.
5. A. Bundi and K. Wüthrich, *Biopolymers*, 1979, **18**(2), 285.

Supporting Information

Synthetic photoswitchable neurotransmitters based on bridged azobenzenes

Gisela Cabré[a,‡], Aida Garrido-Charles[b,‡], Àngels González-Lafont[a,c], Widukind Moormann[d], Daniel Langbehn[d], David Egea,[a] José M. Lluch[a,c], Rainer Herges[d], Ramon Alibés[a], Félix Busqué[a], Pau Gorostiza[b,e,f,*] and Jordi Hernando[a,*]

[a] *Departament de Química, Universitat Autònoma de Barcelona (UAB), Cerdanyola del Vallès 08193, Spain.*

[b] *Institut de Bioenginyeria de Catalunya (IBEC), Barcelona Institute of Science and Technology (BIST), Barcelona 08036, Spain.*

[c] *Institut de Biotecnologia i de Biomedicina (IBB), UAB, Cerdanyola del Vallès 08193, Spain.*

[d] *Otto Diels-Institute of Organic Chemistry, Christian Albrechts University Kiel, Kiel 24118, Germany.*

[e] *Institució Catalana de Recerca i Estudis Avançats (ICREA), Barcelona 08010, Spain.*

[f] *Centro de Investigación Biomédica en Red en Bioingeniería, Biomateriales y Nanomedicina (CIBER-BBN), Zaragoza 50018, Spain.*

[‡] *Equal contribution*

[*] *Corresponding authors: pau@icrea.cat (P. G.), jordi.hernando@uab.cat (J. H.)*

Contents

Experimental procedure for the synthesis of Glu_brAzo1 and Glu_brAzo2

***General procedure*:** The preparation of ligands **Glu_brAzo1** and **Glu_brAzo2** was achieved via a multistep synthetic sequence (see Scheme 1 in the article). In both cases, we took commercially available 4-bromo-2-nitrotoluene (**3**) as a starting material to form the bridged azobenzene core **6**, to which fully protected glutamate derivative **1** and, in the case of **Glu_brAzo2**, amine **2** were introduced. These fragments were obtained from commercially available products as described in refs. 1 (**1**) and 2 (**2**).

Materials and methods: Commercially available reagents were used as received. Solvents were dried by distillation over the appropriate drying agents. All reactions were monitored by analytical thin-layer chromatography (TLC) using silica gel 60 precoated aluminum plates (0.20 mm thickness). Flash column chromatography was performed using silica gel (230-400 mesh). ^{1}H NMR and ^{13}C NMR spectra were recorded at 250, 360 400 or 500 MHz and 90.5, 100.6 or 125.8 MHz, respectively. Proton chemical shifts are reported in ppm (δ) ($CDCl_3$, δ 7.26 or DMSO-d_6, δ 2.50). Carbon chemical shifts are reported in ppm (δ) ($CDCl_3$, δ 77.16 or DMSO-d_6, δ 39.5). NMR signals were assigned with the help of COSY, HSQC, HMBC and DEPT135. Infrared peaks are reported in cm^{-1}. Melting points were determined on hot stage and are uncorrected. HRMS were recorded using electron ionization (EI) or electrospray ionization (ESI). Optical rotations were measured at 20 ± 3 °C.

Synthesis of* Glu_brAzo1 *and* Glu_brAzo2*: The synthesis of **Glu_brAzo1** and **Glu_brAzo2** proceeded as follows.

1,2-bis(4-bromo-2-nitrophenyl)ethane, 4

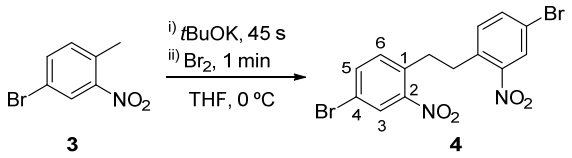

To an ice-cooled solution of 4-bromo-2-nitrotoluene, **3**, (4.00 g, 18.5 mmol) in anhydrous THF (130 mL), *t*BuOK (3.10 g, 27.7 mmol) was added and the solution was stirred for 45 s. Then, Br_2 (1.4 mL, 27.3 mmol) was added and the mixture was stirred for 1 min. The reaction mixture was let warm up to rt and then was poured into ice. The resulting suspension was filtrated and the solid was washed with acetone to furnish **4** (2.84 g, 6.60 mmol, 71%) as an orange solid: mp 219 ºC (from acetone); ^{1}H NMR (500 MHz, $CDCl_3$) δ 8.16 (d, $J_{3,5}$ = 2.1 Hz, 2H, H-3), 7.87 (dd, $J_{5,6}$ = 8.3 Hz, $J_{5,3}$ = 2.1 Hz, 2H, H-5), 7.41 (d, $J_{6,5}$ = 8.3 Hz, 2H, H-6), 3.10 (s, 4H, 2xCH_2); ^{13}C NMR (125.8 MHz,

$CDCl_3$) δ 149.3 (C-2), 134.0 (C-5), 133.9 (C-6), 133.7 (C-1), 126.8 (C-3), 119.6 (C-4), 31.9 (CH_2); IR (ATR) 3088, 1557, 1519, 1473, 1390, 1335 cm^{-1}; MS (EI, 70 eV) *m/z* (%) 213.97 (100) [M^{2+}], 155.97 (66) [M-$C_8H_7BrN_2O_4$]; Anal calcd. for [$C_{14}H_{10}Br_2N_2O_4$]: C, 39.10; H, 2.35; N, 6.51; found: C, 39.17; H, 2.33; N, 6.29. COSY and $^1H/^{13}C$ correlation were recorded.

6,6'-(ethane-1,2-diyl)bis(3-bromoaniline), 5

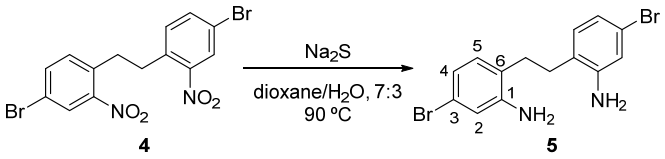

4 **5**

Compound **4** (100 mg, 0.23 mmol) was dissolved in a 7:3 degassed mixture of 1,4-dioxane and water (2.6 ml) under N_2 atmosphere. The reaction mixture was heated to 90 ºC and sodium sulfide (168 mg, 2.15 mmol) was added portion-wise over 2 h. The mixture was stirred overnight. Then, the reaction was quenched with a saturated aqueous solution of $NaHCO_3$ (4 mL) and the crude product was extracted with CH_2Cl_2 (3 x 5 ml). The combined organic layers were washed with H_2O, dried over anhydrous $MgSO_4$ and the solvent was evaporated under vacuum to furnish a crude solid identified as **5** (77 mg, 0.21 mmol, 90% yield): mp 158.8 ºC (from CH_2Cl_2); ^1H NMR (500 MHz, $CDCl_3$) δ 6.84 (m, 4H, H-4, H-5), 6.81 (m, 2H, H-2), 3.63 (br s, 4H, 2x-NH_2), 2.71 (s, 4H, 2xCH_2); ^{13}C NMR (125.8 MHz, $CDCl_3$) δ 145.8 (C-1), 131.1 (C-5), 124.7 (C-6), 121.9 (C-4), 120.7 (C-3), 118.5 (C-2), 30.4 (CH_2); IR (ATR): 3430, 3354, 1619, 1491, 1409, 1179 cm^{-1}; HRMS (HR-EI) calcd. for [$C_{14}H_{14}{}^{79}Br_2N_2$]: 367.9524; found: 367.9525. COSY and $^1H/^{13}C$ correlation were recorded.

(*Z*)-3,8-dibromo-11,12-dihydrodibenzo[*c,g*][1,2]diazocine, 6

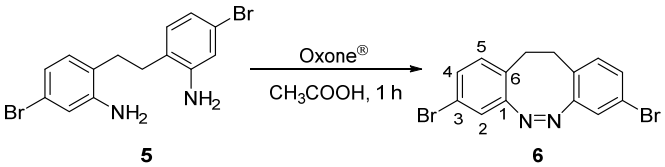

5 **6**

To a solution of **5** (204 mg, 0.55 mmol) in 150 mL glacial acetic acid was added Oxone® (126 mg, 0.83 mmol) in portions. The mixture was stirred at room temperature for 1 h. The solvent was evaporated under reduced pressure. The residue was dissolved in CH_2Cl_2 (25 mL) and washed with saturated $NaHCO_3$ solution (30 mL) and saturated NaCl solution (30 mL). The organic layer was dried over anhydrous $MgSO_4$ and the solvent was evaporated in vacuo. The crude product was purified by column

chromatography (from cyclohexane/ethyl acetate 10% to ethyl acetate 100%) to give **6** as a yellow solid (80 mg, 0.22 mmol, 40% yield).: mp 179 ºC (from EtOAc); ^{1}H NMR (500 MHz, $CDCl_3$) δ 7.16 (dd, $J_{4,5}$ = 8.2 Hz, $J_{4,2}$ = 2.0 Hz, 2H, H-4), 7.00 (d, $J_{2,4}$ = 2.0 Hz, 2H, H-2), 6.86 (d, $J_{5,4}$ = 8.2 Hz, 2H, H-5), 2.82 (m, 4H, 2xCH_2); ^{13}C NMR (125.8 MHz, $CDCl_3$) δ 155.9 (C-1), 131.2 (C-5), 130.4 (C-4), 126.8 (C-6), 121.3 (C-2), 120.3 (C-3), 31.0 (CH_2); IR (ATR) 3042, 2162, 2046, 1743, 1585, 1559, 1465, 1382 cm^{-1}; MS (EI, 70 eV) *m/z* (%) = 365.92 (6) [M$^+$], 257.99 (14) [M-BrN_2], 205.08 (3) [M-Br_2], 178.03 (100) [M-Br_2N_2]; HRMS (EI) calcd. for [$C_{14}H_{10}{}^{79}Br_2N_2$]$^+$: 363.9211; found: 363.9201; Anal calcd. for [$C_{14}H_{10}Br_2N_2$]: C, 45.94; H, 2.75; N, 7.65; found: C, 45.83; H, 2.80; N, 7.50. COSY and ^{1}H/^{13}C correlation were recorded.

(*Z*)-8-bromo-11,12-dihydrodibenzo[*c*,*g*][1,2]diazocine-3-carbonitrile, 7

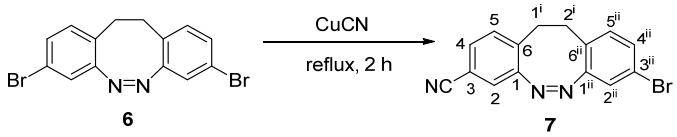

To a solution of **6** (600 mg, 1.64 mmol) in dry DMF (4 mL), CuCN (147 mg, 1.64 mmol) was added. The reaction mixture was stirred for 2 h under reflux conditions. Then, it was let cool down to rt and a 10% aqueous solution of ethylendiamine (45 mL) was added. The product was extracted with CH_2Cl_2 (3 x 50 mL). The combined organic extracts were washed with H_2O (2 x 50 mL), dried over anhydrous $MgSO_4$ and concentrated under vacuum. The resulting residue was purified by column chromatography (cyclohexane/EtOAc, 3:1) to furnish unreacted **6** (210 mg, 0.57 mmol, 35%) and compound **7** (260 mg, 0.83 mmol, 51% yield, 78% yield considering recovered **6**) as a yellow solid. Compound **7**: Mp 179.3 ºC (from EtOAc); ^{1}H NMR (500 MHz, $CDCl_3$) δ 7.34 (dd, $J_{4,5}$ = 7.9 Hz, $J_{4,2}$ = 1.6 Hz, 1H, H-4), 7.18 (dd, $J_{4^{ii},5^{ii}}$ = 8.2 Hz, $J_{4^{ii},2^{ii}}$ = 2.0 Hz, 1H, H-4^{ii}), 7.14 (d, $J_{2,4}$ = 1.6 Hz, 1H, H-2), 7.12 (d, $J_{5,4}$ = 7.9 Hz, 1H, H-5), 7.02 (d, $J_{2^{ii},4^{ii}}$ = 2.0 Hz, 1H, H-2^{ii}), 6.87 (d, $J_{5^{ii},4^{ii}}$ = 8.2 Hz, 1H, H-5^{ii}), 2.90 (m, 4H, H-1^{i}, H-2^{i}); ^{13}C NMR (125.8 MHz, $CDCl_3$) δ 155.8 (C-1^{ii}), 155.1 (C-1), 133.6 (C-6), 131.3 (C-5^{ii}), 130.9 (C-4), 130.7 (C-5), 130.7 (C-4^{ii}), 126.2 (C-6^{ii}), 122.5 (C-2), 121.7 (C-2^{ii}), 120.6 (C-3^{ii}), 117.9 (CN), 111.2 (C-3), 31.7 (C-1^{i}), 30.8 (C-2^{i}); IR (ATR) 3045, 2922, 2231, 1587, 1471 cm^{-1}; HRMS (HR-EI) calcd. for [$C_{15}H_{10}{}^{79}BrN_3$]: 311.0058; found: 311.0056; calcd. for [$C_{15}H_{10}{}^{81}BrN_3$]: 313.00361; found: 313.00361. COSY and ^{1}H/^{13}C correlation were recorded.

di-*tert*-butyl (2*S*,4*R*)-2-((*tert*-butoxycarbonyl)amino)-4-((*E*)-3-((*Z*)-8-cyano-11,12-dihydrodibenzo[*c*,*g*][1,2]diazocin-3-yl)allyl)pentanedioate, 8

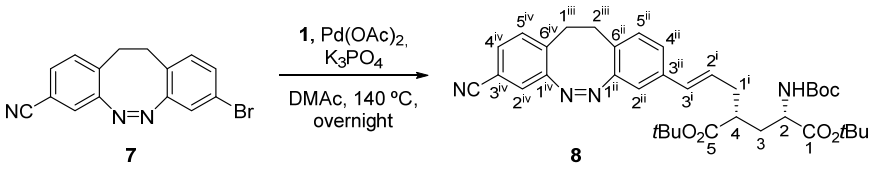

7 **8**

A mixture of diazocine **7** (30 mg, 96 μmol), glutamate derivative **1** (46 mg, 0.12 mmol), $Pd(OAc)_2$ (3 mg, 10 μmol) and K_3PO_4 (30 mg, 0.14 mmol) in DMAc (0.5 mL) under argon atmosphere was heated at 140 ºC overnight. Then, the solvent was evaporated and the resulting residue was purified by column chromatography (hexane/EtOAc, 3:1) to give **8** (37 mg, 59 μmol, 61% yield) as a yellow solid: mp 66.5 ºC (from EtOAc); $[\alpha]_D^{20}$ 14.4 (*c* 1.0, $CHCl_3$); ^{1}H NMR (500 MHz, $CDCl_3$) δ 7.30 (dd, $J_{4^{iv},5^{iv}}$ = 7.9 Hz, $J_{4^{iv},2^{iv}}$ = 1.7 Hz, 1H, H-4^{iv}), 7.11 (d, $J_{5^{iv},4^{iv}}$ = 7.9 Hz, 1H, H-5^{iv}), 7.09 (d, $J_{2^{iv},4^{iv}}$ = 1.7 Hz, 1H, H-2^{iv}), 7.00 (d, $J_{4^{ii},5^{ii}}$ = 8.0 Hz, 1H, H-4^{ii}), 6.89 (d, $J_{5^{ii},4^{ii}}$ = 8.0 Hz, 1H, H-5^{ii}), 6.87 (s, 1H, H-2^{ii}), 6.29 (d, $J_{3^{i},2^{i}}$ = 15.8 Hz, 1H, H-3^{i}), 6.07 (m, 1H, H-2^{i}), 4.99 (d, $J_{NHBoc,2}$ = 8.5 Hz, 1H, NHBoc), 4.23 (m, 1H, H-2), 2.90 (m, 4H, H-1^{iii}, H-2^{iii}), 2.44 (m, 2H, H-1^{i}, H-4), 2.35 (m, 1H, H-1^{i}), 2.15 (m, 1H, H-3), 1.68 (m, 1H, H-3), 1.44 (s, 9H, $C(CH_3)_3$), 1.43 (s, 9H, $C(CH_3)_3$), 1.40 (s, 9H, $C(CH_3)_3$); ^{13}C NMR (125.8 MHz, $CDCl_3$) δ 173.9 (C-5), 171.7 (C-1), 155.6 (C-1^{ii}), 155.1 (C-1^{iv}), 136.7 (C-3^{ii}), 134.3 (C-6^{iv}), 130.8 (C-3^{i}, C-5^{iv}), 130.7 (C-4^{iv}), 130.2 (C-5^{ii}), 128.2 (C-2^{i}), 126.0 (C-6^{ii}), 125.4 (C-4^{ii}), 122.5 (C-2^{iv}), 118.1 (CN), 116.3 (C-2^{ii}), 111.0 (C-3^{iv}), 82.1 ($C(CH_3)_3$), 81.1 ($C(CH_3)_3$), 79.8 ($C(CH_3)_3$), 52.7 (C-2), 42.7 (C-4), 36.2 (C-1^{i}), 34.4 (C-3), 32.0 (C-1^{i}), 31.2 (C-2^{i}), 28.4 ($C(CH_3)_3$), 28.1 (2x$C(CH_3)_3$); IR (ATR): 2978, 2932, 2232, 1714, 1367, 1148 cm^{-1}; HRMS (HR-ESI) calcd. for [$C_{36}H_{46}N_4O_6$+Na]: 653.3310; found: 653.3296. COSY and ^{1}H/^{13}C correlation were recorded.

(1*S*,3*R*,*E*)-1,3-dicarboxy-6-((*Z*)-8-cyano-11,12-dihydrodibenzo[*c*,*g*][1,2] diazocin-3-yl)hex-5-en-1-aminium chloride, Glu_brAzo1

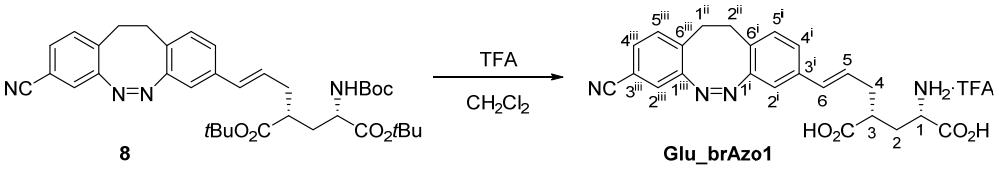

8 **Glu_brAzo1**

To a solution of **8** (45 mg, 0.07 mmol) in CH_2Cl_2 (11 mL), trifluoroacetic acid (4 mL, 52.2 mmol) was added. After stirring 2 h at rt, the solution was concentrated under vacuum. The resulting solid was washed with Et_2O, hexane and EtOAc to furnish **Glu_brAzo1** (30 mg, 0.06 mol, 81% yield) as a brown solid: mp 134-139 ºC (from EtOAc); $[\alpha]_D^{20}$ 20.8 (*c* 0.18, DMSO-d_6); ^{1}H NMR (360 MHz, DMSO-d_6) δ 7.55 (d, $J_{4^{iii},5^{iv}}$ = 7.8 Hz, 1H, H-4^{iii}), 7.44 (s, 1H, H-2^{iii}), 7.34 (d, $J_{5^{iii},4^{iii}}$ = 7.8 Hz, 1H, H-5^{iii}), 7.12 (d, $J_{4^{i},5^{i}}$ =

7.9 Hz, 1H, H-4^{i}), 7.04 (d, $J_{5i,4i}$ = 7.9 Hz, 1H, H-5^{i}), 6.88 (s, 1H, H-2^{i}), 6.37 (d, $J_{6,5}$ = 15.6 Hz, 1H, H-6), 6.15 (m, 1H, H-5), 3.80 (m, 1H, H-1), 2.87 (m, 4H, H-1^{ii}, H-2^{ii}), 2.71 (m, 1H, H-3), 2.50 (m, 2H, H-4), 2.13 (m, 1H, H-2), 1.77 (m, 1H, H-2); ^{13}C NMR (90.5 MHz, DMSO-d_6) δ 175.0/170.9 (2xCOOH), 155.1 (C-1^{iii}), 155.0 (C-1^{i}), 135.9 (C-3^{i}), 134.6 (C-6^{iii}), 131.2 (C-5^{iii}), 131.0 (C-4^{iii}), 130.8 (C-6), 130.4 (C-5^{i}), 127.7 (C-5), 126.3 (C-6^{i}), 125.0 (C-4^{i}), 122.2 (C-2^{iii}), 118.1 (CN), 115.8 (C-2^{i}), 109.6 (C-3^{iii}), 50.9 (C-1), 40.4 (C-3), 35.0 (C-4), 31.3 (C-2), 30.9 (C-1^{ii}), 30.3 (C-2^{ii}); IR (ATR) 2934, 2231, 1675, 1606, 1243, 1200, 1134 cm^{-1}; HRMS (HR-ESI) calcd. for $[C_{23}H_{23}N_4O_4]^+$: 419.1714; found: 419.1718. COSY and ^{1}H/^{13}C correlation were recorded.

(*Z*)-8-bromo-11,12-dihydrodibenzo[*c*,*g*][1,2]diazocine-3-carboxylic acid, 7a

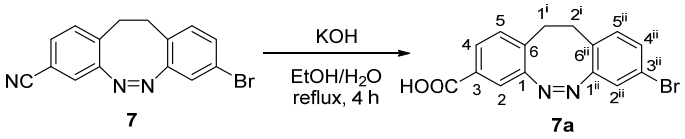

To a solution of nitrile **7** (260 mg, 0.84 mmol) in EtOH (36 mL), a solution of KOH (5.20 g, 92.7 mmol) in H_2O (11 mL) was added dropwise. The mixture was heated at reflux temperature for 4 h. Then, the EtOH was removed under vacuum and the resulting aqueous solution was acidified to pH 4. The product was extracted with EtOAc (3 x 50 mL) and the combined organic extracts were dried over anhydrous Na_2SO_4 and concentrated under vacuum to give **7a** (265 mg, 0.80 mmol, 95% yield) as a black solid: mp > 230 ºC (from EtOAc); ^{1}H NMR (400 MHz, acetone-d_6) δ 7.72 (dd, $J_{4,5}$ = 7.9 Hz, $J_{4,2}$ = 1.7 Hz, 1H, H-4), 7.48 (d, $J_{2,4}$ = 1.7 Hz, 1H, H-2), 7.24 (d, $J_{5,4}$ = 7.9 Hz, 1H, H-5), 7.22 (dd, $J_{4ii,5ii}$ = 8.2 Hz, $J_{4ii,2ii}$ = 2.0 Hz, 1H, H-4^{ii}), 7.11 (d, $J_{2ii,4ii}$ = 2.0 Hz, 1H, H-2^{ii}), 7.06 (d, $J_{5ii,4ii}$ = 8.2 Hz, 1H, H-5^{ii}), 2.94 (m, 4H, H-1^{i}, H-2^{i}); ^{13}C NMR (100.6 MHz, acetone-d_6) δ 166.5 (-COOH), 157.5 (C-1^{ii}), 156.2 (C-1), 134.4 (C-6), 132.7 (C-5^{ii}), 131.3 (C-4^{ii}), 130.9 (C-5), 130.3 (C-3), 129.2 (C-4), 128.4 (C-6^{ii}), 122.1 (C-2^{ii}), 120.5 (C-2), 120.5 (C-3^{ii}), 31.9 (C-1^{i}), 31.3 (C-2^{i}); IR (ATR) 2922, 2852, 2538, 1683, 1430, 1296, 1226 cm^{-1}; HRMS (HR-ESI) calcd. for $[C_{15}H_{10}BrN_2O_2+H]^+$: 331.0077; found: 331.0082. COSY and ^{1}H/^{13}C correlation were recorded.

***tert*-butyl (*Z*)-4-(8-bromo-11,12-dihydrodibenzo[*c*,*g*][1,2]diazocine-3-carboxamido) benzoate, 9**

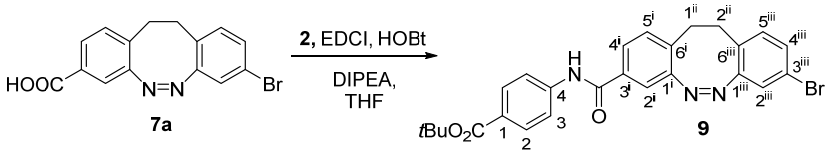

To a solution of acid **7a** (50 mg, 0.15 mmol) in dry THF (7 mL), a solution of amine **2** (35 mg, 0.18 mmol), EDCI·HCl (40 mg, 0.21 mmol), HOBt (32 mg, 0.24 mmol) and DIPEA (0.11 mL, 0.63 mmol) in dry THF (3.6 mL) were added. The reaction mixture was stirred at rt overnight. Then, H_2O (20 mL) was added and the resulting mixture was extracted with CH_2Cl_2 (3 x 20 mL). The combined organic extracts were dried over anhydrous Na_2SO_4, filtered and concentrated under vacuum. The resulting residue was purified by column chromatography (hexane/EtOAc, 3:1) to furnish **9** (60 mg, 0.12 mmol, 78% yield) as a pale yellow solid: mp 226-230 ºC (from EtOAc); ^{1}H NMR (400 MHz, $CDCl_3$) δ 7.98 (d, $J_{2,3}$ = 8.7 Hz, 2H, H-2), 7.90 (br s, 1H, CONH), 7.67 (d, $J_{3,2}$ = 8.7 Hz, 2H, H-3), 7.57 (dd, $J_{4^i,5^i}$ = 8.0 Hz, $J_{4^i,2^i}$ = 1.9 Hz, 1H, H-4^i), 7.37 (d, $J_{2^i,4^i}$ = 1.9 Hz, 1H, H-2^i), 7.16 (dd, $J_{4^{iii},5^{iii}}$ = 8.2 Hz, $J_{4^{ii},2^{ii}}$ = 2.0 Hz, 1H, H-4^{iii}), 7.13 (d, $J_{5^i,4^i}$ = 8.0 Hz, 1H, H-5^i), 7.01 (d, $J_{2^{iii},4^{iii}}$ = 2.0 Hz, 1H, H-2^{iii}), 6.88 (d, $J_{5^{ii},4^{ii}}$ = 8.2 Hz, 1H, H-5^{iii}), 2.90 (m, 4H, H-1^{ii}, H-2^{ii}), 1.59 (s, 9H, C(CH$_3$)$_3$); ^{13}C NMR (100.6 MHz, $CDCl_3$) δ 165.3 (C, ester), 164.5 (C, amide), 156.1 (C-1^{iii}), 155.4 (C-1^i), 141.5 (C-4), 133.6 (C-3^i), 132.5 (C-6^i), 131.4 (C-5^{iii}), 130.8 (C-2, C-4^{iii}), 130.6 (C-5^i), 128.2 (C-1), 126.8 (C-6^{iii}), 126.2 (C-4^i), 122.0 (C-2^{iii}), 120.6 (C-3^{iii}), 119.3 (C-3), 118.0 (C-2^i), 81.1 (*C*(CH$_3$)$_3$), 31.7 (C-1^{ii}), 31.1 (C-2^{ii}), 28.4 (C(*C*H$_3$)$_3$); IR (ATR) 3415, 2965, 1705, 1673, 1521, 1290, 1161, 1103 cm^{-1}; HRMS (HR-ESI) calcd. for $[C_{26}H_{24}BrN_3O_3+H]^+$: 506.1074; found: 506.1085. COSY and ^{1}H/^{13}C correlation were recorded.

di-tert-butyl (2*S*,4*R*)-2-((*tert*-butoxycarbonyl)amino)-4-((*E*)-3-((*Z*)-8-((4-(*tert*-butoxy carbonyl)phenyl)carbamoyl)-11,12-dihydrodibenzo[c,g][1,2]diazocin-3-yl)allyl)pentanedioate, 9a

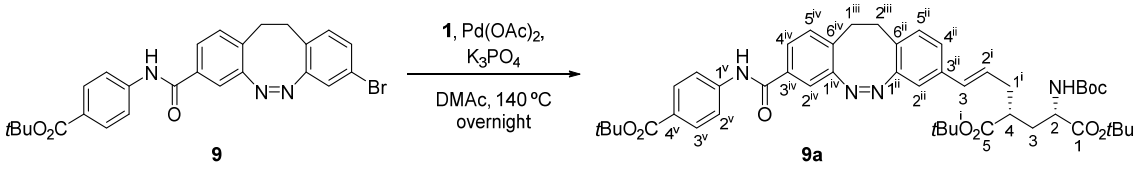

A mixture of diazocine **9** (60 mg, 0.12 mmol), glutamate derivative **1** (57 mg, 0.14 mmol), $Pd(OAc)_2$ (3 mg, 13 μmol) and K_3PO_4 (35 mg, 0.16 mmol) in DMAc (1.0 mL) under argon atmosphere was heated at 140 ºC overnight. Then, the solvent was evaporated and the resulting residue was purified by column chromatography (hexane/EtOAc, 5:1) to give **9a** (50 mg, 60 μmol, 51% yield) as a yellow foam: ^{1}H NMR (360 MHz, $CDCl_3$) δ 8.10 (s, 1 H, -NHCO), 7.95 (d, $J_{3^v,2^v}$ = 8.2 Hz, 2H, H-3^v), 7.66 (d, $J_{2^v,3^v}$ = 8.2 Hz, 2H, H-2^v), 7.55 (d, $J_{4^{iv},5^{iv}}$ = 8.0 Hz, 1H, H-4^{iv}), 7.36 (s, 1H, H-2^{iv}), 7.11 (d, $J_{5^{iv},4^{iv}}$ = 8.0 Hz, 1H, H-5^{iv}), 6.98 (d, $J_{4^{ii},5^{ii}}$ = 8.0 Hz, 1H, H-4^{ii}), 6.90 (d, $J_{5^{ii},4^{ii}}$ = 8.0 Hz, 1H, H-5^{ii}), 6.79 (s, 1H, H-2^{ii}), 6.26 (d, $J_{3^i,2^i}$ = 15.7 Hz, 1H, H-3^i), 6.02 (m, 1H, H-2^i), 4.99 (d,

$J_{NHBoc,2}$ = 8.5 Hz, 1H, NHBoc), 4.21 (m, 1H, H-2), 2.97 (m, 2H, H-1^{iii}, H-2^{iii}), 2.79 (m, 2H, H-1^{iii}, H-2^{iii}), 2.43 (m, 2H, H-1^{i}, H-4), 2.31 (m, 1H, H-1^{i}), 2.13 (m, 1H, H-3), 1.68 (m, 1H, H-3), 1.58 (s, 9H, C(CH_3)$_3$), 1.40 (s, 18H, C(CH_3)$_3$), 1.37 (s, 9H, C(CH_3)$_3$); ^{13}C NMR (90.6 MHz, $CDCl_3$) δ 173.9 (C-5), 171.7 (C-1), 165.4 (C, ester), 164.7 (C, amide), 155.4 (C, carbamate, C-1^{ii}, C-1^{iv}), 141.7 (C-1^{v}), 133.5 (C-3^{ii}), 133.3 (C-3^{iv}), 132.9 (C-6^{iv}), 131.1 (C-3^{i}), 130.7 (C-3^{v}), 130.5 (C-5^{iv}), 130.1 (C-5^{ii}), 127.9 (C-2^{i}, C-4^{v}), 126.4 (C-6^{ii}), 126.0 (C-4^{iv}), 125.3 (C-4^{ii}), 119.2 (C-2^{v}), 118.0 (C-2^{iv}), 116.5 (C-2^{ii}), 82.1 (*C*(CH_3)), (81.0 (*C*(CH_3)$_3$), 79.8 (*C*(CH_3)$_3$), 52.7 (C-2), 42.7 (C-4), 36.2 (C-1^{i}), 34.4 (C-3), 31.8 (C-1^{i}), 31.4 (C-2^{i}), 28.4 (C(*C*H_3)$_3$), 28.3 (C(*C*H_3)$_3$), 28.1 (2xC(*C*H_3)$_3$); IR (ATR) 3343, 2983, 2931, 1710, 1528, 1148 cm^{-1}; HRMS (HR-ESI) calcd. for [$C_{47}H_{60}N_4O_9$+H]: 825.4433; found: 825.4418. COSY and ^{1}H/^{13}C correlation were recorded.

(1*S*,3*R*,*E*)-1,3-dicarboxy-6-((*Z*)-8-((4-carboxyphenyl)carbamoyl)-11,12-dihydro dibenzo[c,g][1,2]diazocin-3-yl)hex-5-en-1-aminium trifluoroacetate, Glu_brAzo2

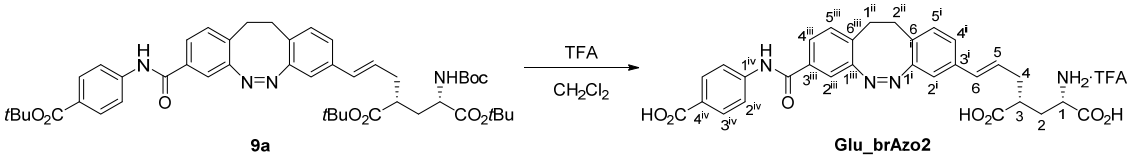

9a **Glu_brAzo2**

To a solution of **9a** (50 mg, 61 µmol) in CH_2Cl_2 (9 mL), trifluoroacetic acid (4.5 mL, 59 mmol) was added. The mixture was stirred for 2 h and the solvent was evaporated under vacuum. The resulting solid was washed with Et_2O, hexane and EtOAc to give **Glu_brAzo2** (33 mg, 0.049 mmol, 82% yield) as a pale orange solid: mp > 230 ºC (from EtOAc); $[\alpha]_D^{20}$ -6.0 (*c* 0.25, DMSO-d_6); ^{1}H NMR (400 MHz, DMSO-d_6) δ 10.50 (s, 1 H, -NHCO), 7.92 (d, $J_{3^{iv},2^{iv}}$ = 8.7 Hz, 2H, H-3^{iv}), 7.85 (d, $J_{2^{iv},3^{iv}}$ = 8.7 Hz, 2H, H-2^{iv}), 7.68 (d, $J_{4^{iii},5^{iii}}$ = 7.9 Hz, 1H, H-4^{iii}), 7.46 (s, 1H, H-2^{iii}), 7.29 (d, $J_{5^{iii},4^{iii}}$ = 7.9 Hz, 1H, H-5^{iii}), 7.11 (d, $J_{4^{i},5^{i}}$ = 8.0 Hz, 1H, H-4^{i}), 7.06 (d, $J_{5^{i},4^{i}}$ = 8.0 Hz, 1H, H-5^{i}), 6.90 (s, 1H, H-2^{i}), 6.34 (d, $J_{6,5}$ = 15.5 Hz, 1H, H-6), 6.15 (m, 1H, H-5), 3.29 (m, 1H, H-1), 2.86 (m, 4H, H-1^{ii}, H-2^{ii}), 2.68 (m, 1H, H-3), 2.50 (m, 2H, H-4), 2.04 (m, 1H, H-2), 1.65 (m, 1H, H-2); ^{13}C NMR (90.6 MHz, DMSO-d_6) δ 172.8/171.8 (2xCOOH), 166.9(COOH), 164.7 (C, amide), 155.1 (C-1^{iii}), 154.6 (C-1^{i}), 143.0 (C-1^{iv}), 135.9 (C-3^{i}), 133.0 (C-3^{iii}), 132.3 (C-6^{iii}), 130.2 (C-5^{i}, C-5^{iii}, C-3^{iv}), 128.2 (C-6), 126.6 (C-5, C-6^{i}), 125.6 (C-4^{iii}, C-4^{iv}), 124.7 (C-4^{i}), 119.5 C-2^{iv}), 118.0 (C-2^{iii}), 116.0 (C-2^{i}), 50.7 (C-1), 40.1 (C-3), 35.5 (C-4), 31.1 (C-2), 30.9 (C-1^{ii}), 30.5 (C-2^{ii}); IR (ATR) 2923, 1676, 1599, 1521, 1247, 1176 cm^{-1}; HRMS (HR-ESI) calcd. for [$C_{30}H_{29}N_4O_7$]: 557.2031; found: 557.2040. COSY and ^{1}H/^{13}C correlation were recorded.

Computational, photochemical and biological supplementary methods

Molecular docking calculations: Docking calculations were performed with GOLD5.6.3[3] program on the rigid crystallographic structure of GluK2 Ligand Binding Domain retrieved from the Protein Data Bank (PDB code: 4H8I).[4] H++ web-server[5] was used to add missing hydrogen atoms to the protein pdb file and to determine the protonation states of ionizable residues at pH = 7.0. All co-crystallized ligands, and water molecules were removed. The structures of *trans*-**Glu_brAzo1** and *cis*-**Glu_brAzo1** were built with standard bond lengths and angles using Gaussview[6] and UCSF Chimera[7] codes. Those structures were further minimized using Quantum Mechanics at the B3LYP/6-31G(d) level with the Gaussian09 package.[8] The *trans*-**Glu_brAzo2** and *cis*-**Glu_brAzo2** initial structures were built from the coordinates of *trans*-**Glu_brAzo1** and *cis*-**Glu_brAzo1** QM minima, respectively, by replacing the cyano substituent by the bulky -CONH-*p*-C6H4COOH group, and the corresponding QM minima were also located. The four minimized compounds and the protein were further prepared for docking by assigning GOLD atom types to all the atoms by means of Hermes (GOLD 3D Visualizer).

To ensure a complete exploration of the conformational space of the four ligands in the binding site of the protein, the maximum efficiency of the genetic algorithm was selected in the docking setup. All the parameters of the genetic algorithm were set to the default values of the program and partial flexibility was assigned to the ligands. The binding site of the receptor was defined as all atoms within 15 Å of a conveniently specified central point (given by its X, Y, Z coordinates). 100 binding solutions for each ligand were generated. The Chemscore fitness function[9] was selected to estimate the binding affinities of the four ligands. The obtained poses were ranked based on those affinity docking scores (kJ/mol) and the best solution for each ligand was selected.

Photochemical characterization of Glu_brAzo1 and Glu_brAzo2: All spectroscopic and photochemical experiments were carried out in HPLC- or spectroscopy-quality solvents. Steady-state UV-vis absorption measurements were recorded on a HP 8453 spectrophotometer with temperature control. The UV-vis absorption spectra of *trans*-**Glu_brAzo1** and *trans*-**Glu_brAzo2** in PBS:DMSO 1:1 was estimated from the absorption spectra of as-synthesized *cis*-**Glu_brAzo1** and *cis*-**Glu_brAzo2** and of a well-known mixture of their *cis* and *trans* isomers, the composition of which was measured by ^{1}H NMR in DMSO-d_6. Isomerization quantum yields were determined relative to 1,2-bis(5-chloro-2-methyl-3-thienyl)perfluorocyclopentene in hexane ($\Phi_{ring\ opening}$ = 0.13[10]). Different excitation sources were used in the photochemical

experiments depending on the spectral requirements: a cw DPSS laser (λ_{exc} = 405 nm, SciTec) for *cis-trans* photoisomerization, and the second harmonic of a ns-pulsed Nd:YAG laser (λ_{exc} = 532 nm, Brilliant, Quantel) for *trans-cis* photoisomerization.

Cell line and transfection: HEK293 tsA201 cell line (SV40-transformed, Human Embryonic Kidney 293 cells) was maintained at 37 ºC in a 5% CO_2 humid incubator with Dulbecco's Modified Eagle Medium/Nutrient Mixture F-12 media (DMEM) (1:1, Invitrogen) supplemented with 10% Fetal Bovine Serum (FBS) and 1% Penicillin/Streptomycin. Cells transiently expressed the receptor subunit GluK2 or GluK1(Q)-2b(GGAA). The expression plasmid for GluK2 was kindly provided by Ehud Y. Isacoff (University of California). GluK2 was subcloned into EcoRI site of the pCDNA3.1 expression vector. To obtain the GluK2-eGFP pCDNA3 construct, a fragment spanning the C-terminal domain of GluK2 and eGFP was amplified by PCR using AfeI/XbaI flanked primers and subcloned into GluK2-pCDNA3 plasmid by replacing the former AfeI/XbaI cassette. GluK1(Q)-2b(GGAA) was kindly provided by G. Swanson (Northwestern University, Feinberg School of Medicine), with the endoplasmic reticulum retention motif of the carboxy-terminal mutated to increase surface expression.[11] DNA–X-tremGENE 9 Transfection Reagent (Roche) mix was used following manufacturer's instructions with a Reagent:DNA ratio of 3:1. GluK1(Q)-2b-GGAA plasmid was co-transfected with peGFP with a Transfection Reagent:GluK1:eGPF ratio of 3:1:0.1.

The mix was incubated for 20 min at room temperature, meanwhile cells were detached and freshly plated into a 12-mulltiwell plate at a density of 3 × 105 cells before the DNA-Transfection Reagent mix was added dropwise into each well. Experiments were performed after 48–72 h, and the day before the experiment cells were plated at low density on 16-mm coverslips (Fisher Scientific) treated with collagen(Sigma-Aldrich) to allow cell adhesion.

Electrophysiology: Whole-cell voltage-clamp recordings were done using an EPC-10 amplifier and data at 10 kHz was acquired with amplifier's software Patch Master (HEKA). Bath solution was composed of (in mM): 140 NaCl, 1 $MgCl_2$, 2.5 KCl, 10 HEPES, 2.5 $CaCl_2$ and 10–20 glucose to fix osmolarity to 310 mOsm·kg^{-1}, while pH 7.42 was adjusted with NaOH. Borosilicate glass pipettes were pulled with a typical resistance of 4–6 MΩ for HEK293 cells. Pipette solution contained (in mM): 120 cesium methanosulfonate, 10 TEA-Cl, 5 $MgCl_2$, 3 Na_2ATP, 1 Na_2GTP, 20 HEPES, 0.5 EGTA; osmolarity was 290 mOsm·kg^{-1} and pH 7.2 was adjusted with CsOH.

Before starting the recording, cells were incubated 10 min with 0.3 mg mL^{-1} Concanavalin A (Sigma) —to block GluK1 and GluK2 desensitization— on an ES based on $NMDG^+$ (to avoid depolarization due to open GluRs, in mM): 110 $NMDG^+$, 2.5 KCl, 1 $MgCl_2$, 10 HEPES, 10–20 glucose to fix osmolarity to 300 $mOsm \cdot kg^{-1}$, while pH 7.4 was adjusted with HCl. Before placing the coverslip to the recording chamber, cells were washed again with bath solution.

Light stimulation was done by illumination of the entire focused field using a Polychrome V monochromator (TILL Photonics) connected through the back port of an IX71 inverted microscope (Olympus) with a XLUMPLFLN 20XW x20/1 water immersion objective (Olympus). For automatically controlling wavelength, the monochromator was connected to the EPC-10 amplifier via Photochromic Manual Control (TILL Photonics) and controlled with the photometry module of Patch Master. Light power density measured with a Newport 1916-C light meter after the objective was 22.0 $\mu W\ mm^{-2}$ for 380 nm, 45.9 $\mu W\ mm^{-2}$ for 460 nm and 47.4 $\mu W\ mm^{-2}$ for 500 nm.

One-photon action spectrum characterization was done during voltage-clamp recordings applying a train of 1 s light-pulses at different wavelengths (for the whole action spectrum, we ranged wavelengths from 300 to 600 nm, with 10 nm steps) with 5 s delay between pulses in which light was switched to 530 nm to *trans-cis* back-isomerize for activation spectrum, and to 390nm for deactivation spectrum.

Rat hippocampal neural primary culture. All procedures were conducted in accordance with the European guidelines for animal care and use in research, and were approved by the Animal Experimentation Ethics Committee at the University of Barcelona (Spain). Low-density primary hippocampal cultures were prepared from newborn P0-P3 pups from Sprague Dawley rat and maintained in cell culture for 1-2 weeks in coverslips coated with poly-L-lysine (Sigma-Aldrich), as previously described.[12-14].

Cells were cultured with complete medium (Neurobasal A, B-27 5%, GlutaMax (0.5x), glucose 15mM, penicillin (5 U ml−1) and streptomycin (5 µg ml−1)). Within 48-72 h an anti-mitotic treatment with AraC 5 µM is done to avoid fibroblast and astrocyte proliferation. Half of the medium in each well was changed every 3-4 days.

***Electrophysiology recording conditions for rat hippocampal neurons*:** Voltage and current-clamp recordings under whole-cell configuration were done using an EPC-10 amplifier and data at 10 kHz was acquired with amplifier's software Patch Master

(HEKA). Bath solution was composed of (in mM): 140 NaCl, 2 MgCl, 2.5 KCl, 10 HEPES, 0.2 $CaCl_2$ and 10–20 mM glucose to fix osmolarity to 310 mOsm·kg–1, pH 7.42 adjusted with NaOH. Borosilicate glass pipettes were pulled with a typical resistance of 6–8 MΩ for neurons. Pipette solution contained (in mM): 130 KCl, 5 $MgCl_2$, 3 Na_2ATP, 1 Na_2GTP, 20 HEPES, 0.5 EGTA. Osmolarity is adjusted at 289 mOsm·kg–1 and pH 7.2 adjusted with KOH. During recordings, neurons were maintained at room temperature (r.t., 25-27 °C) in a continuous perfusion of bath solution.

Data analysis and statistics: Amplitude of photocurrents were analyzed using IgorPro (Wavemetrics). Displayed whole-cell current traces have been filtered using the infinite impulse response digital filter from IgorPro (low-pass filter with cutoff of 50 Hz). The drift in current observed during light spectra recordings was corrected where appropriate with the IgorPro (WaveMetrics) software using a custom-made macro for drift correction.

Figure S1. Molecular docking simulations

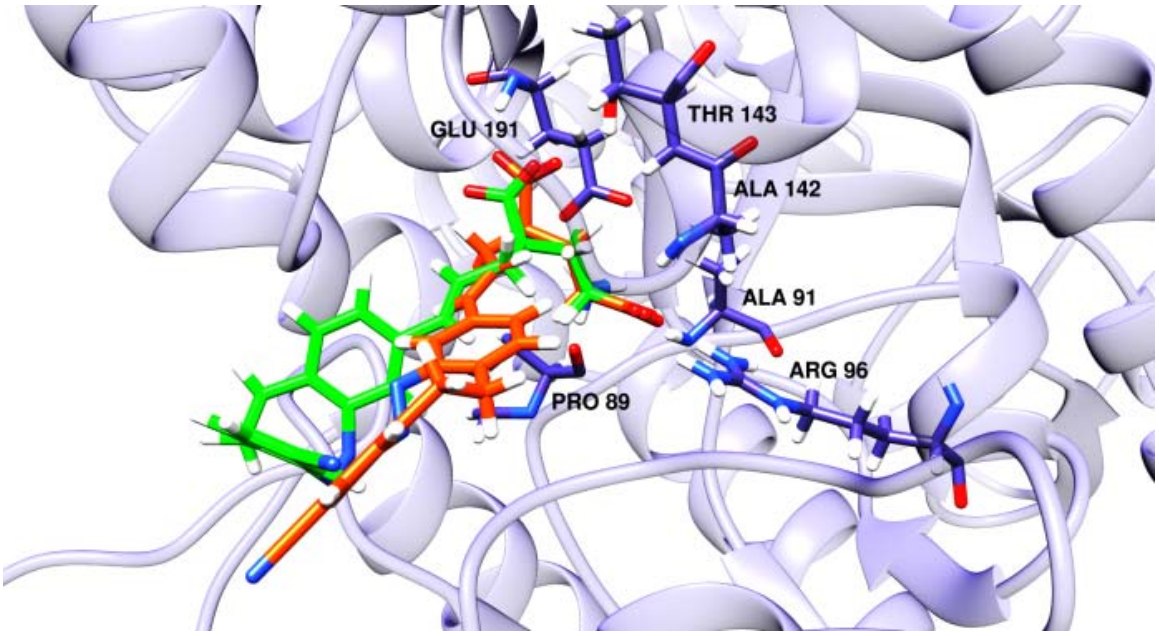

Figure S1. Best docking solutions for *trans*-**Glu_brAzo1** (orange) and *cis*-**Glu_brAzo1** (green) in GluK2. The protein residues interacting with the glutamate groups are also indicated. Oxygen, nitrogen and hydrogen atoms are depicted in red, blue and white, respectively.

Figures S2-S7 and Table S1. Photoisomerization of Glu_brAzo1 and Glu_brAzo2

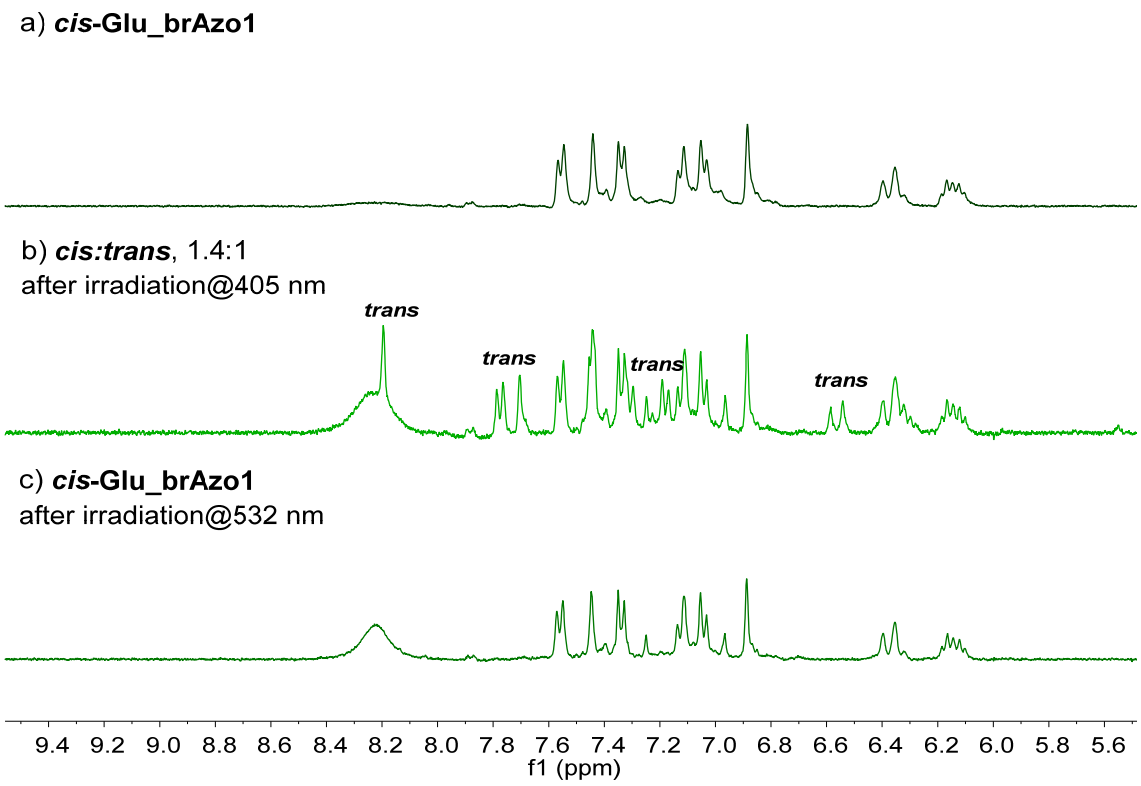

Figure S2. Low-field region of the ^{1}H NMR spectra (360 MHz, DMSO-d_6) of **Glu_brAzo1**: (a) freshly prepared (*cis* isomer); (b) after irradiation at λ_{exc} = 405 nm (power = 280 mW) for 3 h (*cis*:*trans* 1.4:1 mixture); (c) after irradiation of (b) at λ_{exc} = 532 nm (power = 100 mW) for 3 h (*cis* isomer).

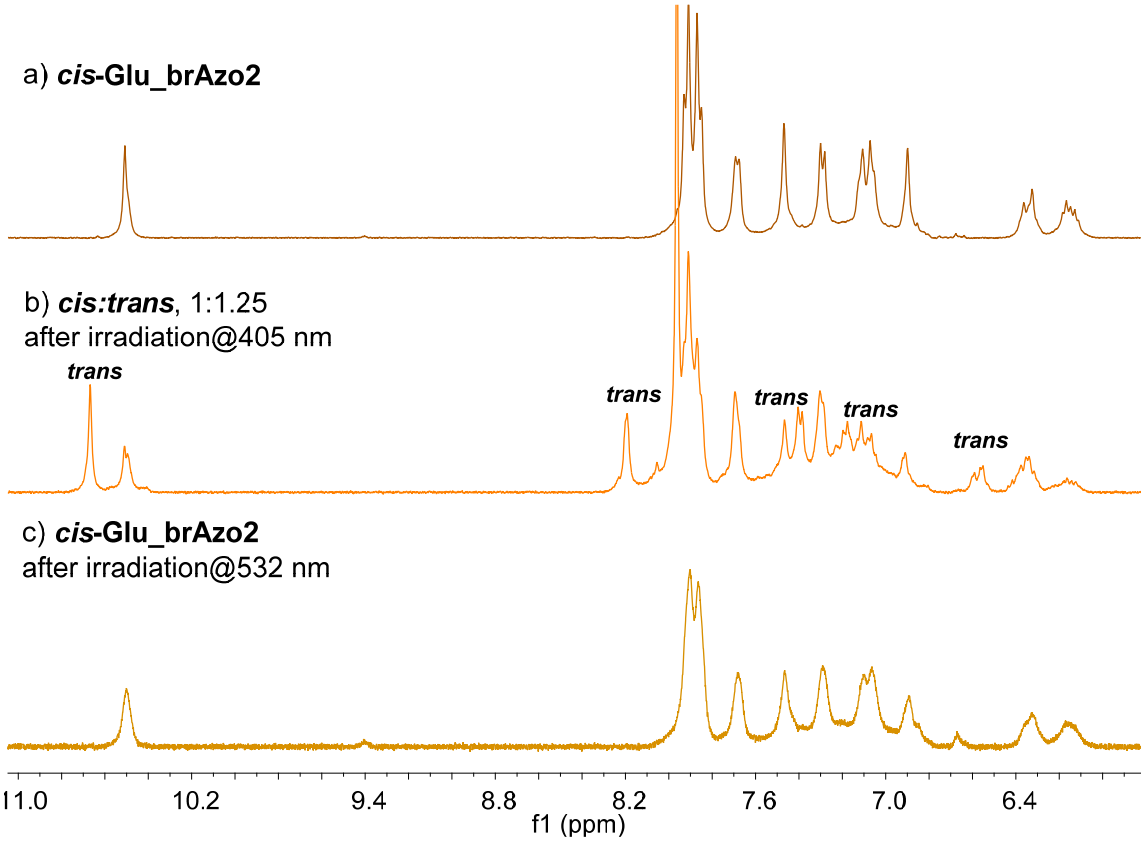

Figure S3. Low-field region of the ^{1}H NMR spectra (400 MHz, DMSO-d_6) of **Glu_brAzo2**: (a) freshly prepared (*cis* isomer); (b) after irradiation at λ_{exc} = 405 nm (power = 280 mW) for 3 h (*cis*:*trans* 1:1.25 mixture); (c) after irradiation of (b) at λ_{exc} = 532 nm (power = 100 mW) for 3 h (*cis* isomer).

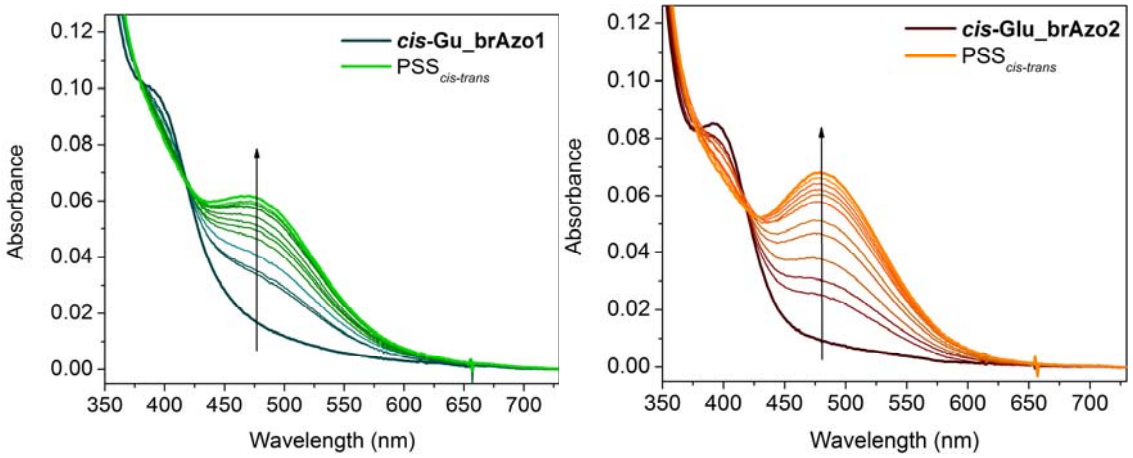

Figure S4. Absorption spectra of **Glu_brAzo1** and **Glu_brAzo2** in PBS:DMSO 1:1 upon irradiation of their *cis* isomer at λ_{exc} = 405 nm (power = 88 mW).

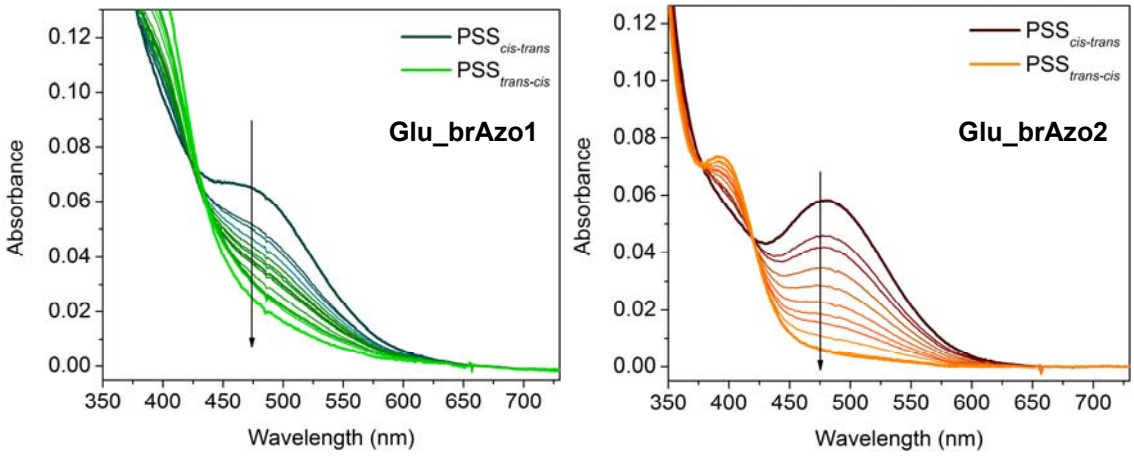

Figure S5. Absorption spectra of **Glu_brAzo1** and **Glu_brAzo2** in PBS:DMSO 1:1 upon irradiation at λ_{exc} = 532 nm (power = 10 mW) of the *cis-trans* photostationary mixture previously prepared at λ_{exc} = 405 nm.

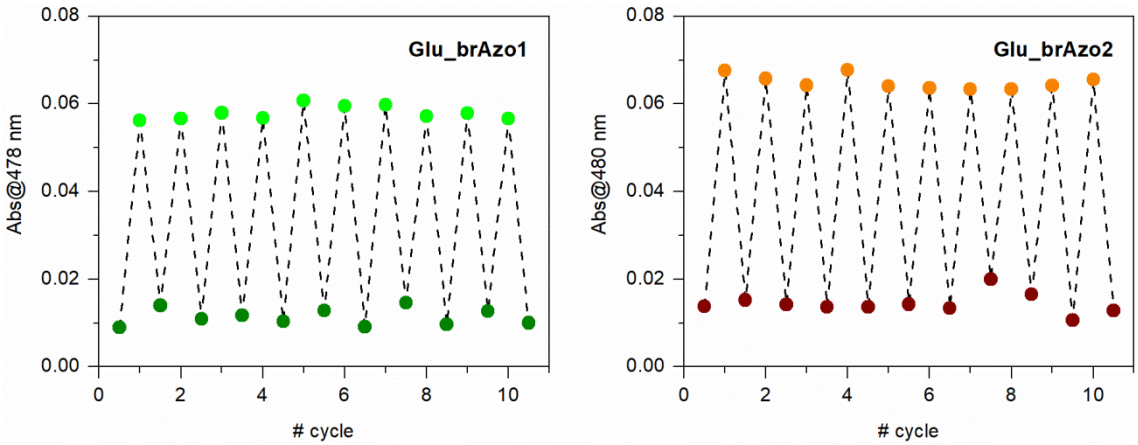

Figure S6. Variation of the absorption at 395 and 478 nm of **Glu_brAzo1** and **Glu_brAzo2** in PBS:DMSO 1:1 upon consecutive cycles of *cis-trans* (λ_{exc} = 405 nm, 280 mW) and *trans-cis* photoisomerization (λ_{exc} = 532 nm, power = 230 mW).

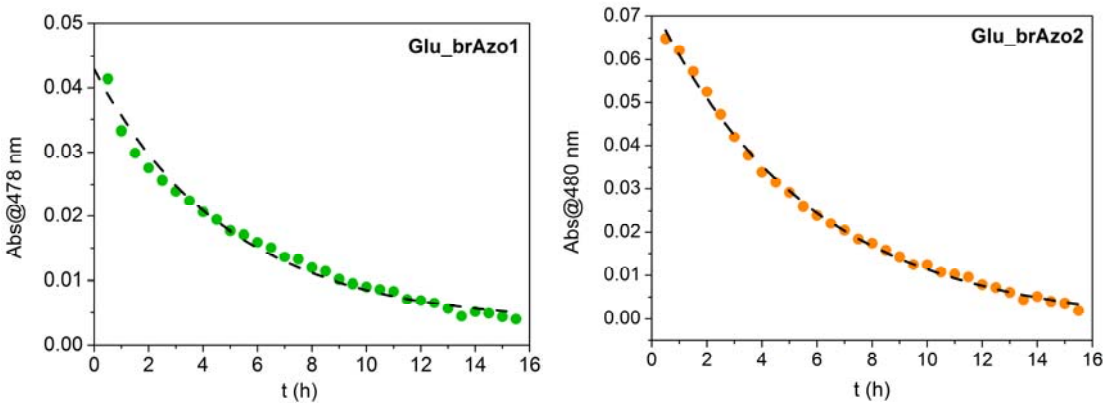

Figure S7. Variation of the absorption at $\lambda_{abs,max}^{trans}$ of the *cis-trans* photostationary state mixture of **Glu_brAzo1** and **Glu_brAzo2** in the dark at 25ºC in PBS:DMSO 1:1. At these conditions, thermal *trans-cis* back-isomerization takes place, thus restoring the initial concentration of the *cis* state of the ligands. Points correspond to the experimental data, while lines were obtained from monoexponential fits.

Table S1. Photochemical properties of **Glu_brAzo1** and **Glu_brAzo2** in PBS:DMSO 1:1.

	$\lambda^{cis}_{abs,max}$ [a] (nm)	$\lambda^{trans}_{abs,max}$ [a] (nm)	$\Phi_{cis\text{-}trans}$	$\Phi_{trans\text{-}cis}$	%*trans* **PSS**$_{cis\text{-}trans}$	%*cis* **PSS**$_{trans\text{-}cis}$	τ_{trans} (h) [b]
Glu_brAzo1	392	478	0.11	0.89	47	100	6.8
Glu_brAzo2	395	480	0.13	0.86	60	100	5.6

[a] Data for the n-π* band. [b] $t_{1/2}$ = 4.7 and 3.9 h, respectively.

Figures S8-S11. Photomodulation of GluK1 and GluK2 in HEK293 cells using Glu_brAzo1 and Glu_brAzo2

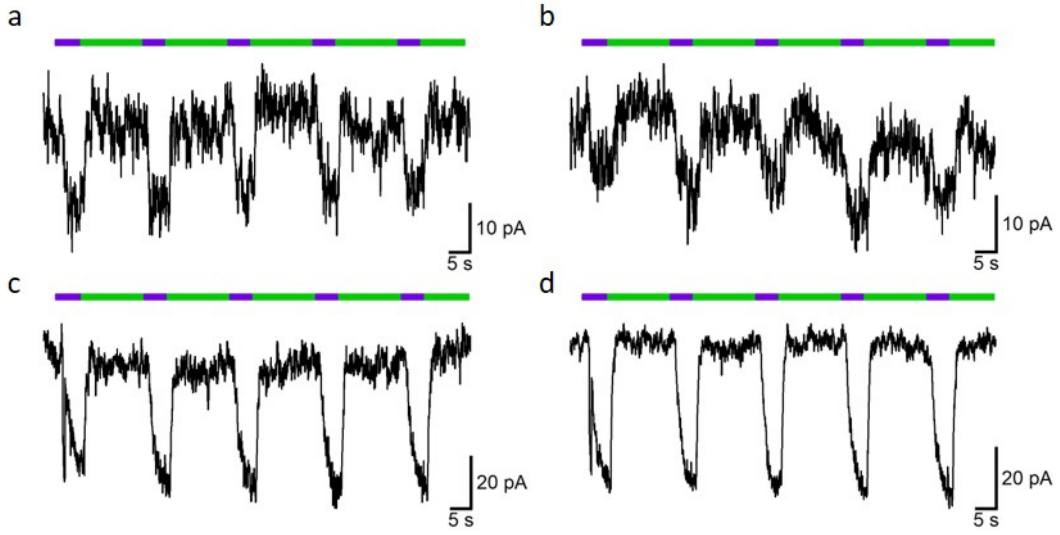

Figure S8. Light-dependent inward currents measured for HEK293 cells expressing GluK1 and GluK2. (a-b) HEK293 cells transfected with GluK1 and perfused with (a) *cis*-**Glu_brAzo1** (100 μM), and (b) *cis*-**Glu_brAzo2** (100 μM). (c-d) HEK293 cells transfected with GluK2 and perfused with (c) *cis*-**Glu_brAzo1** (100 μM), and (d) *cis*-**Glu_brAzo2** (100 μM). Light pulses at λ_{exc} = 390 nm (purple bars) were employed to induce *cis-trans* photoisomerization, which in all the cases resulted in larger electrophysiological currents (i.e. receptor activation and channel opening). Irradiation at λ_{exc} = 530 nm (green bars) was used to trigger *trans-cis* back-isomerization and recover the initial signal (i.e. receptor deactivation and channel closing).

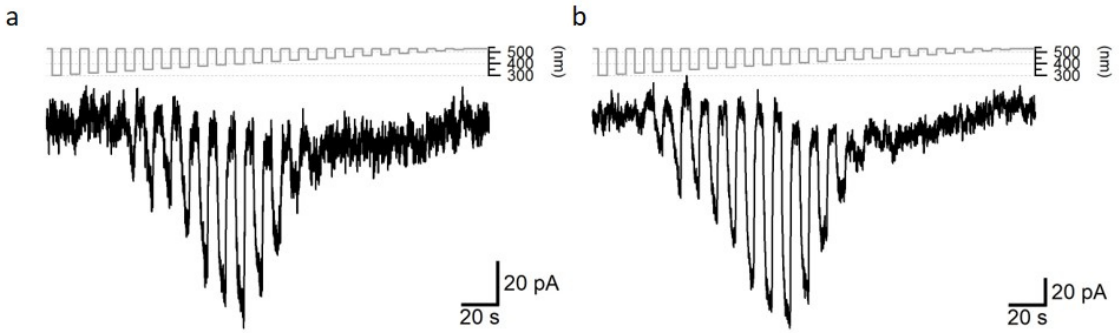

Figure S9. Activation spectra of (a) **Glu_brAzo1** (100 μM) and (b) **Glu_brAzo2** (100 μM) in HEK293 cells transfected with GluK2. Wavelength excitation to promote *cis-trans* photoisomerization and receptor activation ranges from 300 nm to 530 nm. In all the cases, *trans-cis* back-isomerization was achieved with pulses at λ_{exc} = 530 nm.

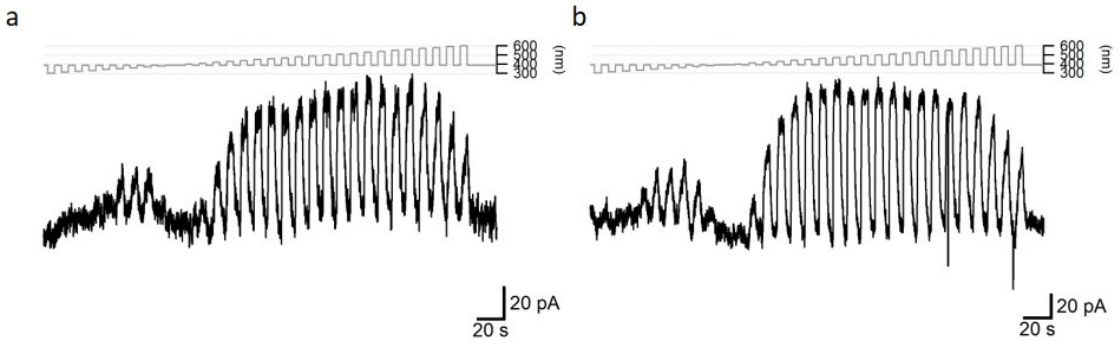

Figure S10. Deactivation spectra of (a) **Glu_brAzo1** (100 μM) and (b) **Glu_brAzo2** (100 μM) in HEK293 cells transfected with GluK2. Wavelength excitation to promote *trans-cis* photoisomerization and receptor deactivation ranges from 300 nm to 600 nm. In all the cases, *cis-trans* isomerization was previously conducted with pulses at λ_{exc} = 390 nm.

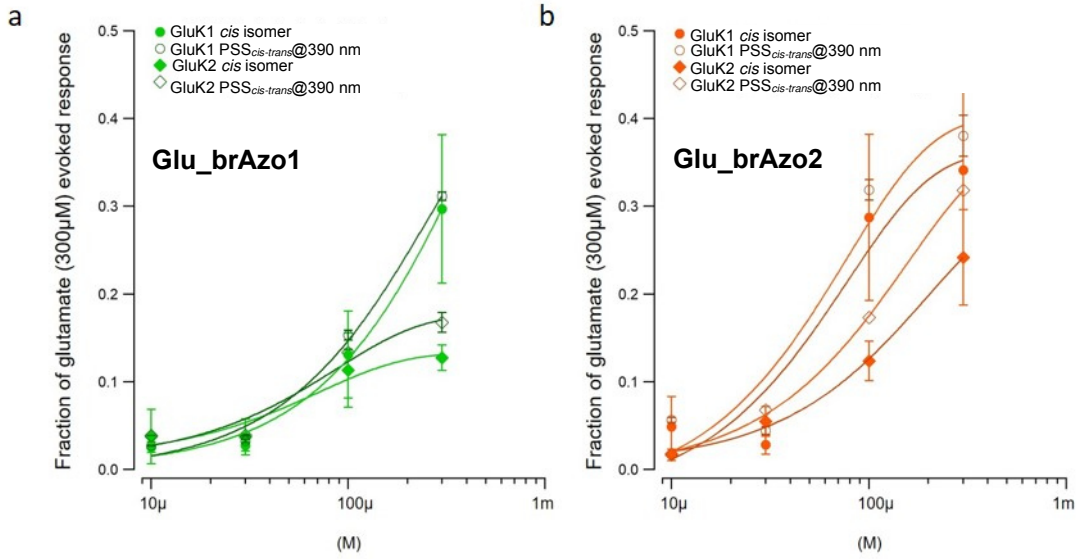

Figure S11. Dose-response curves of (a) **Glu_brAzo1** and (b) **Glu_brAzo2** in HEK293 cells transfected with GluK1 and GluK2. Measurements were conducted from 10 to 300 μM for their *cis* isomer and the *trans-cis* mixture obtained at λ_{exc} = 390 ($PSS_{cis\text{-}trans}$@390 nm).

Figures S12. Photoactivation of rat hippocampal neurons using Glu_brAzo1 and Glu_brAzo2

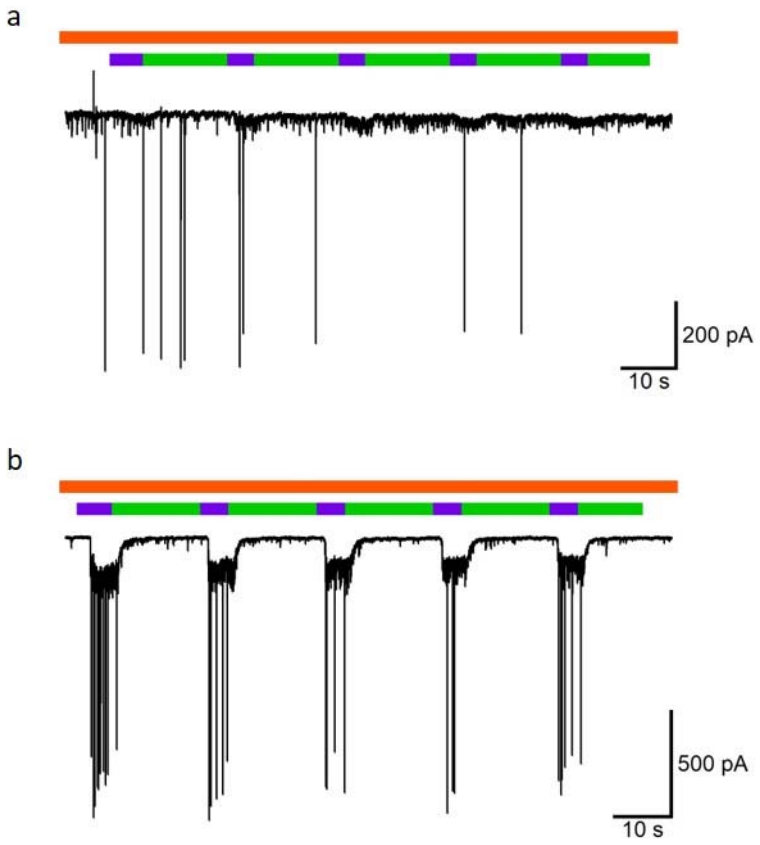

Figure S12. Whole-cell voltage clamp recording of rat hippocampal neurons in culture. Perfusion of 30 μM of (a) **Glu_brAzo1** and (b) **Glu_brAzo2**. Light activation is induced by pulses at λ_{exc} = 390 and 530 nm (purple and green bars, respectively).

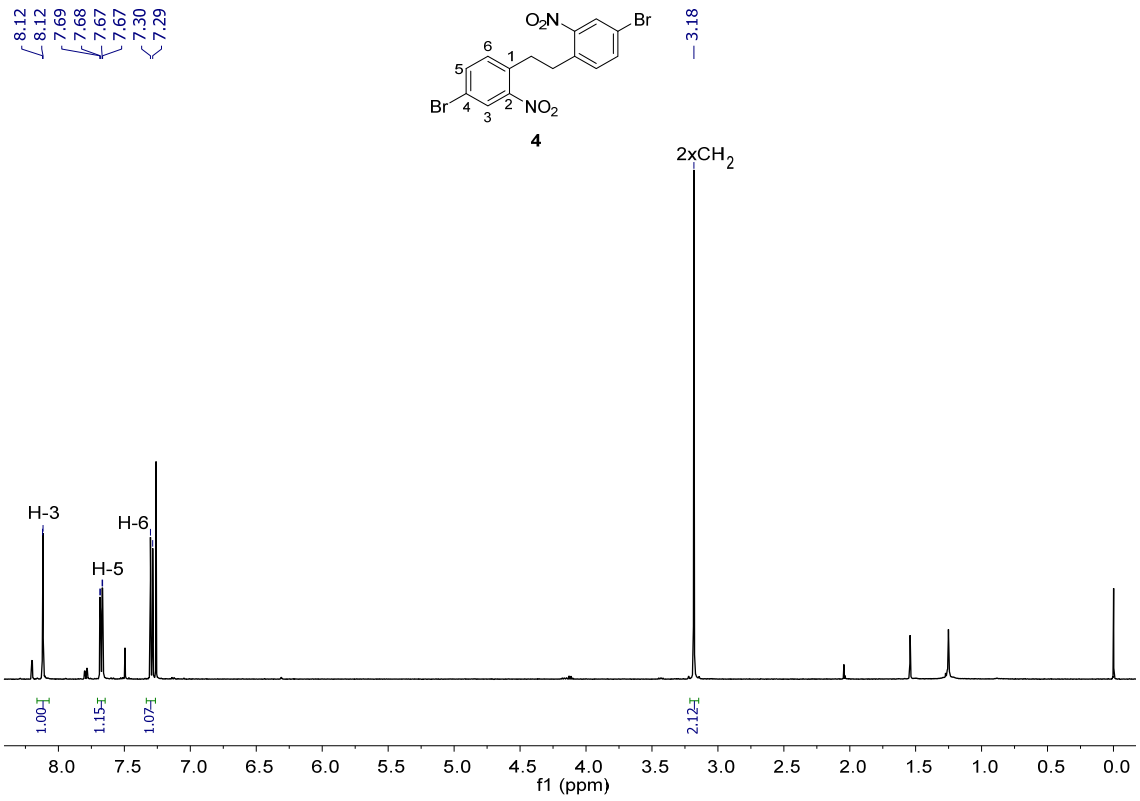

^{1}H NMR (500 MHz, $CDCl_3$)

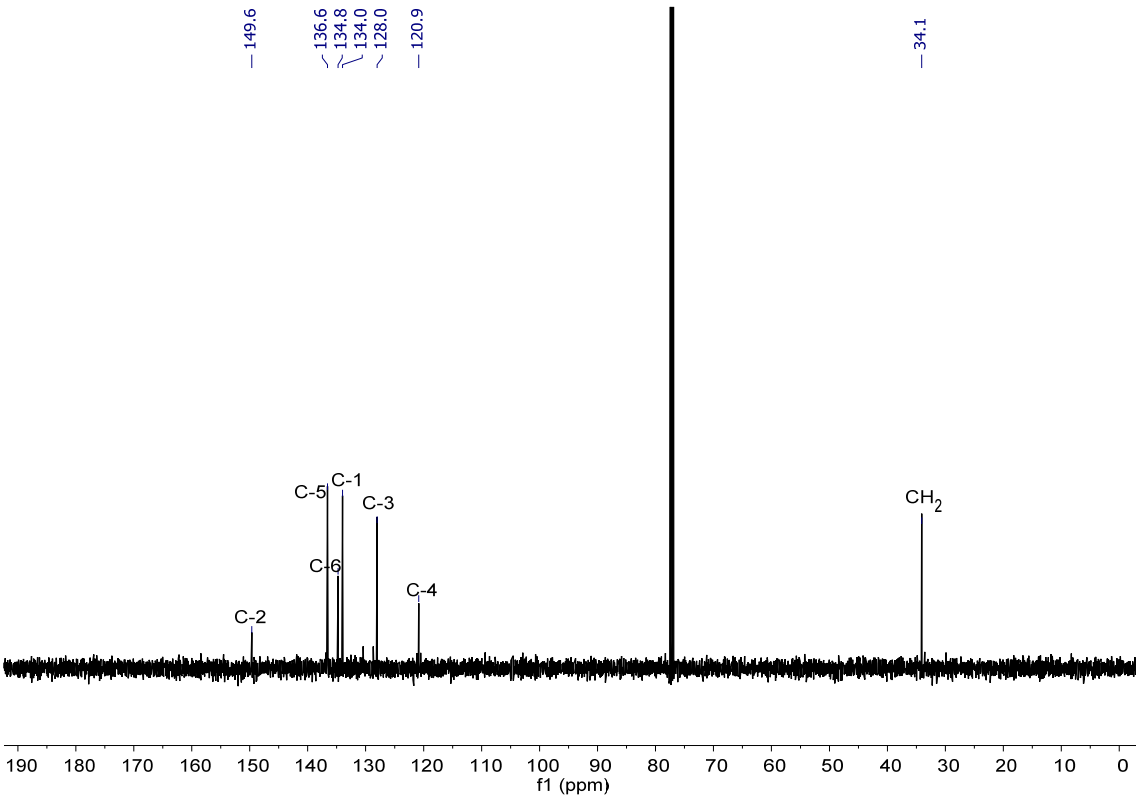

^{13}C NMR (125.8 MHz, $CDCl_3$)

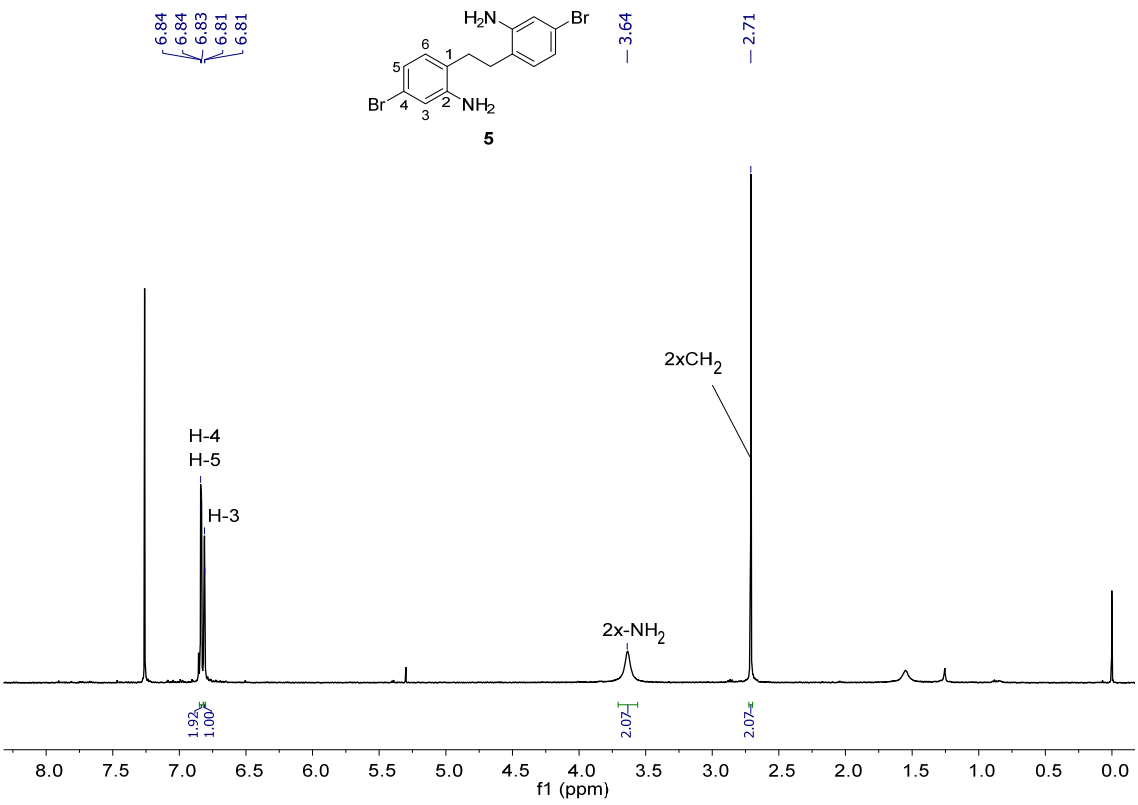

^{1}H NMR (500 MHz, $CDCl_3$)

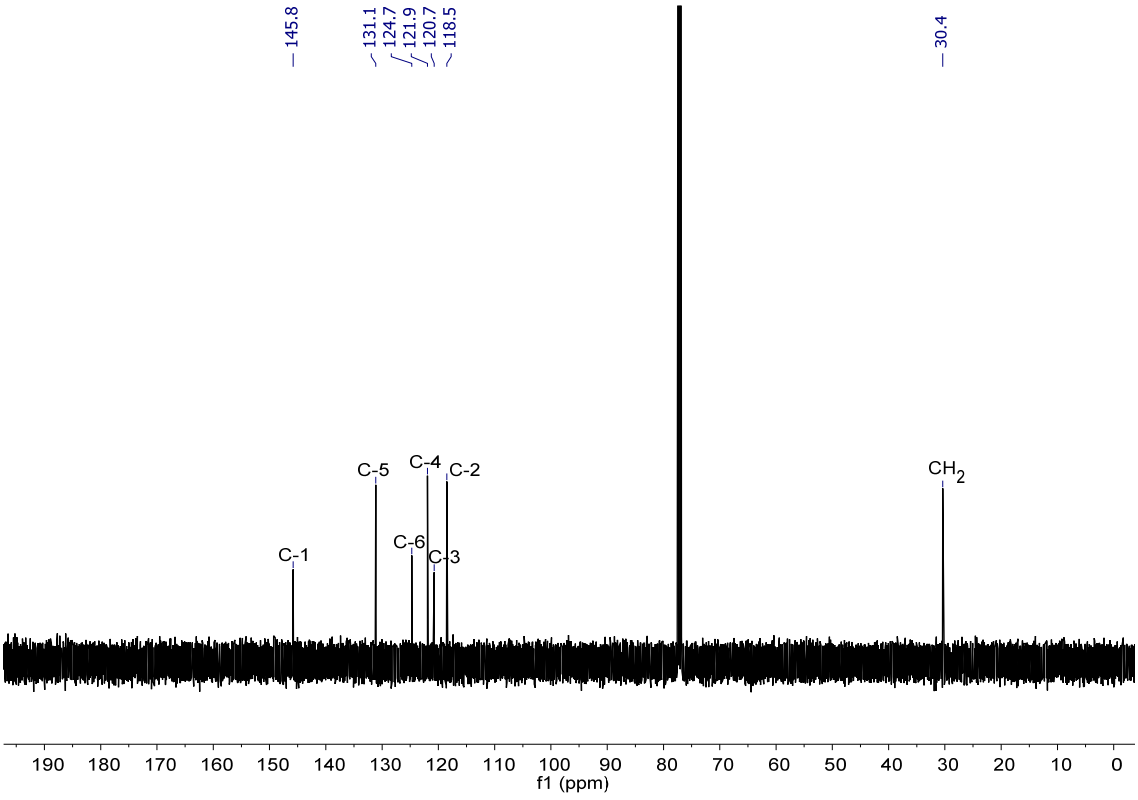

^{13}C NMR (125.8 MHz, $CDCl_3$)

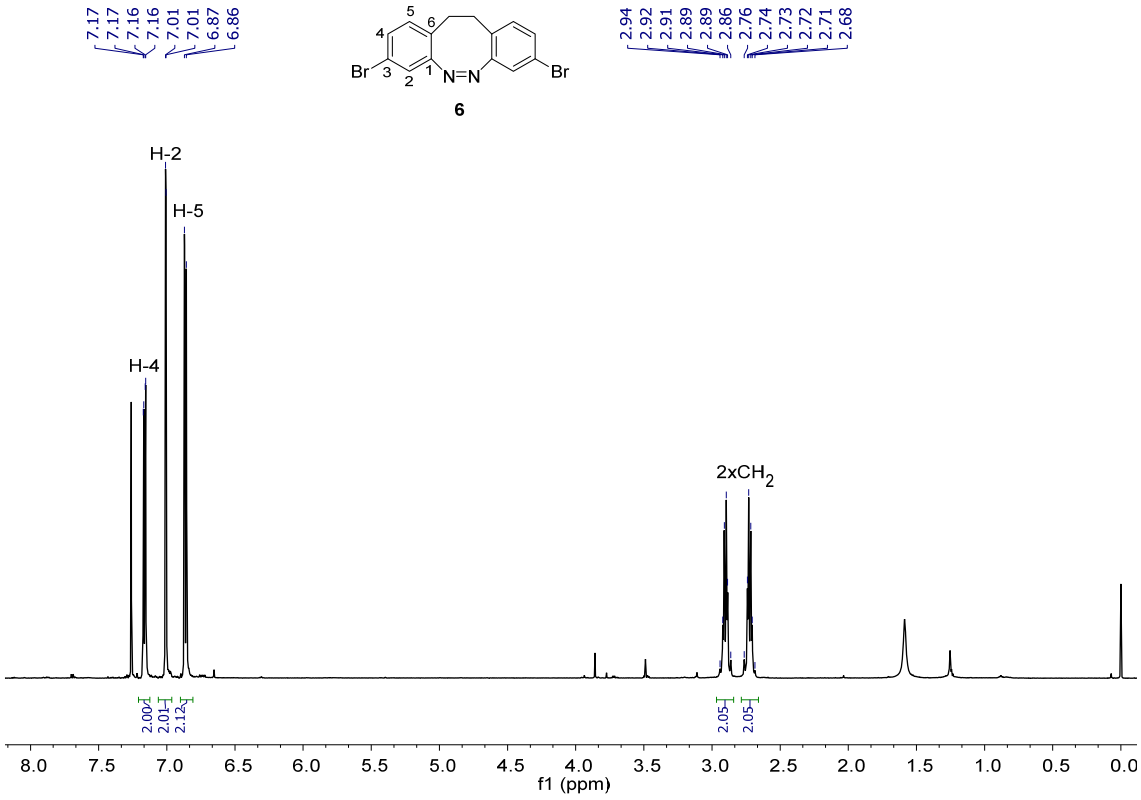

^{1}H NMR (500 MHz, $CDCl_3$)

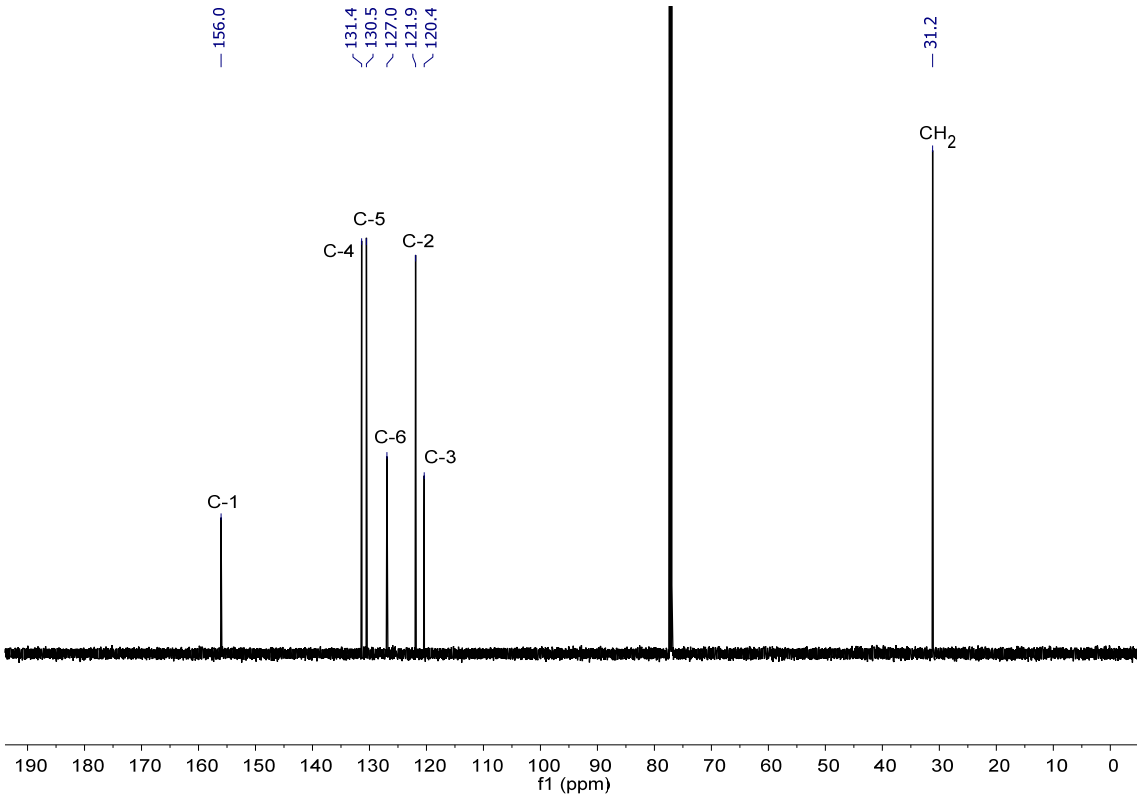

^{13}C NMR (125.8 MHz, $CDCl_3$)

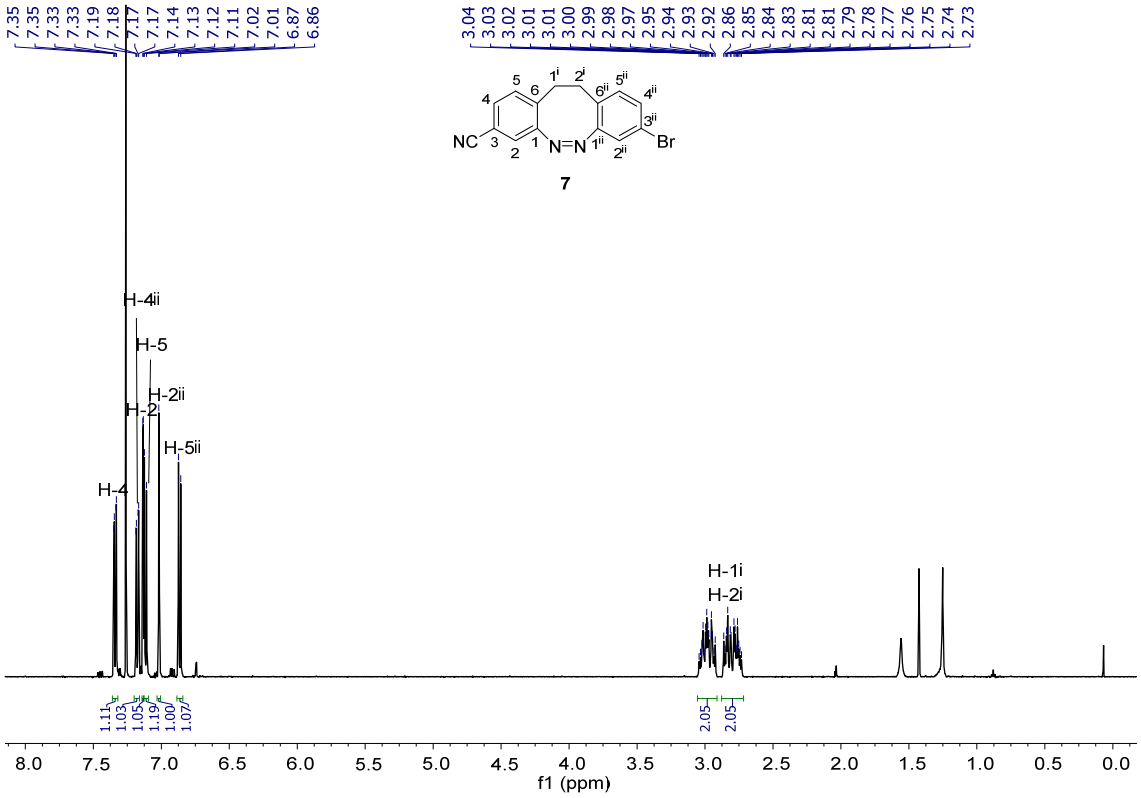

^{1}H NMR (500 MHz, $CDCl_3$)

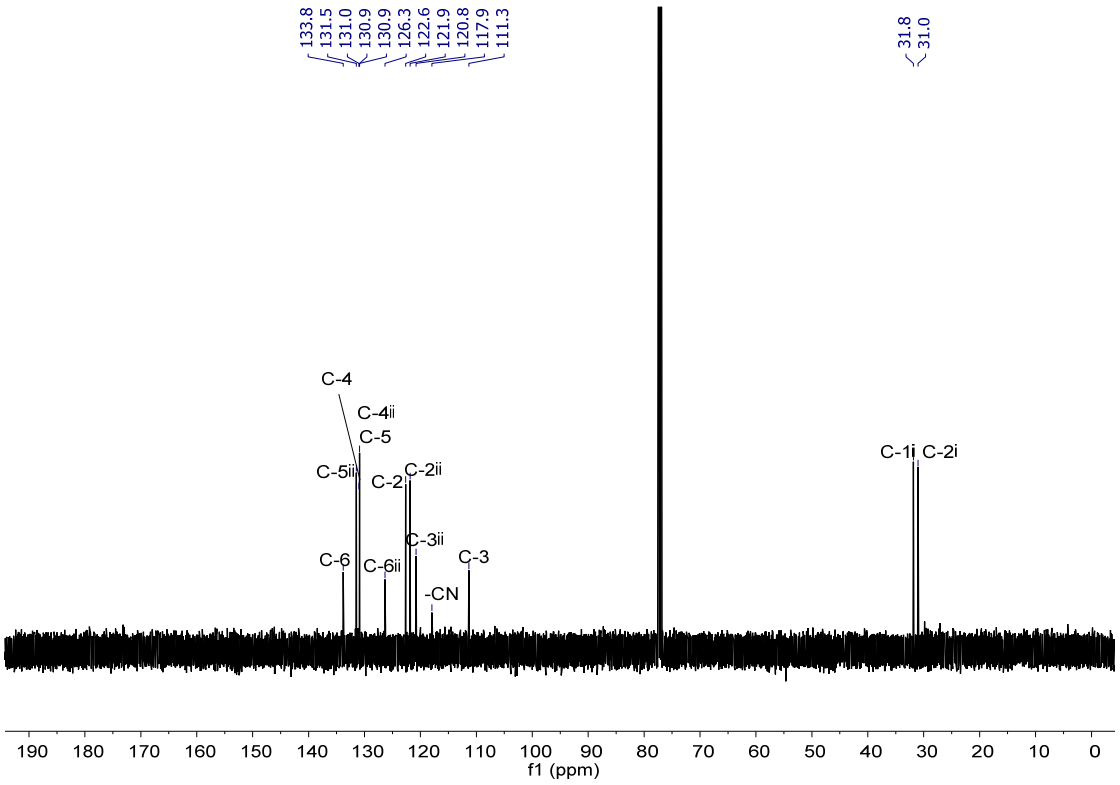

^{13}C NMR (125.8 MHz, $CDCl_3$)

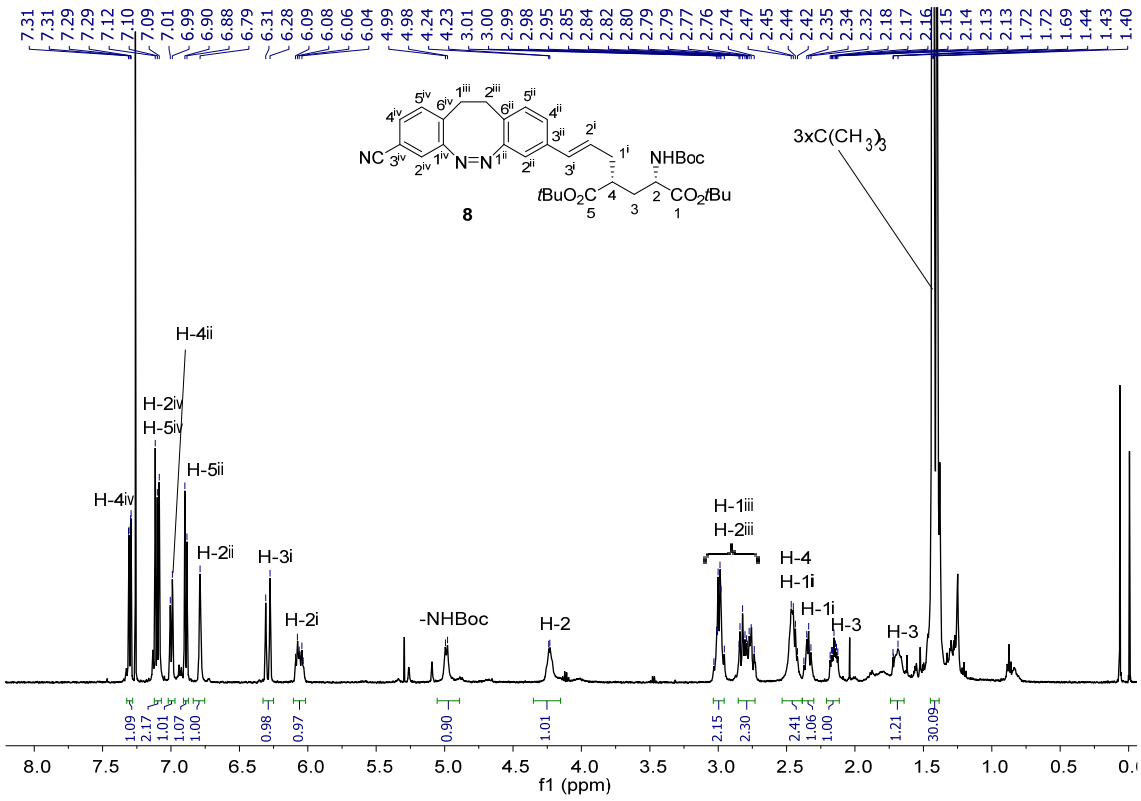

^{1}H NMR (500 MHz, $CDCl_3$)

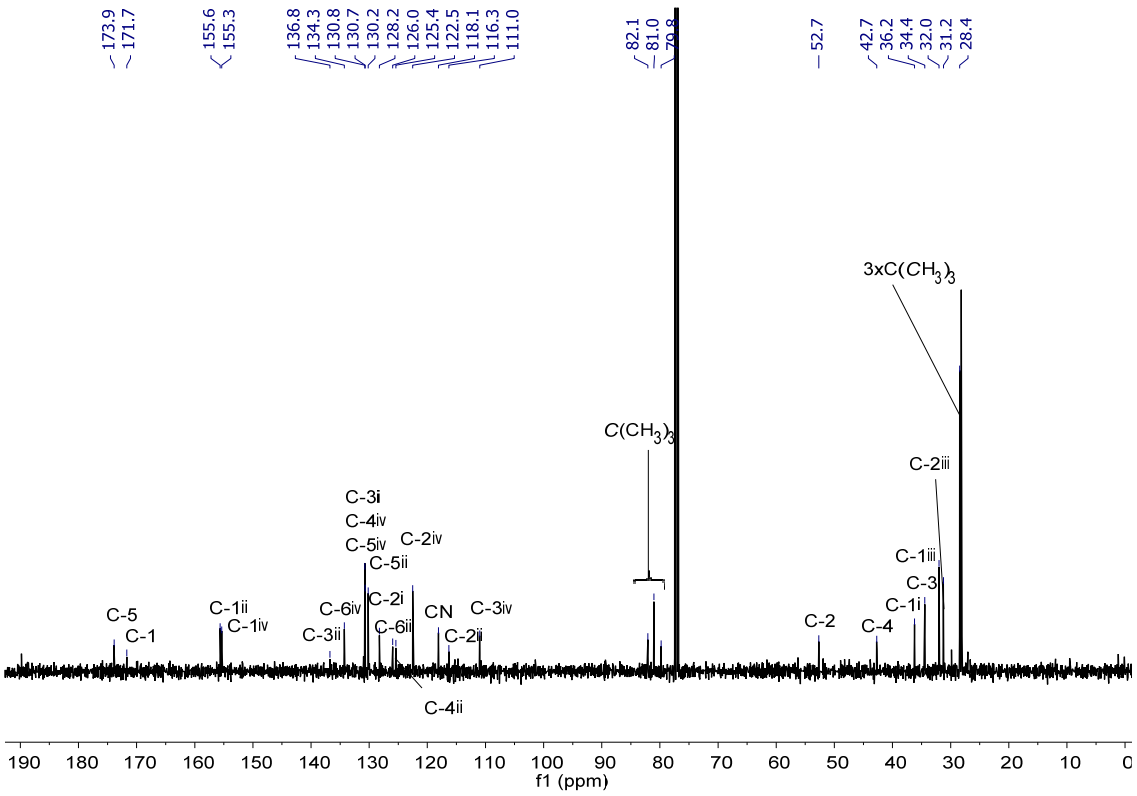

^{13}C NMR (125.8 MHz, $CDCl_3$)

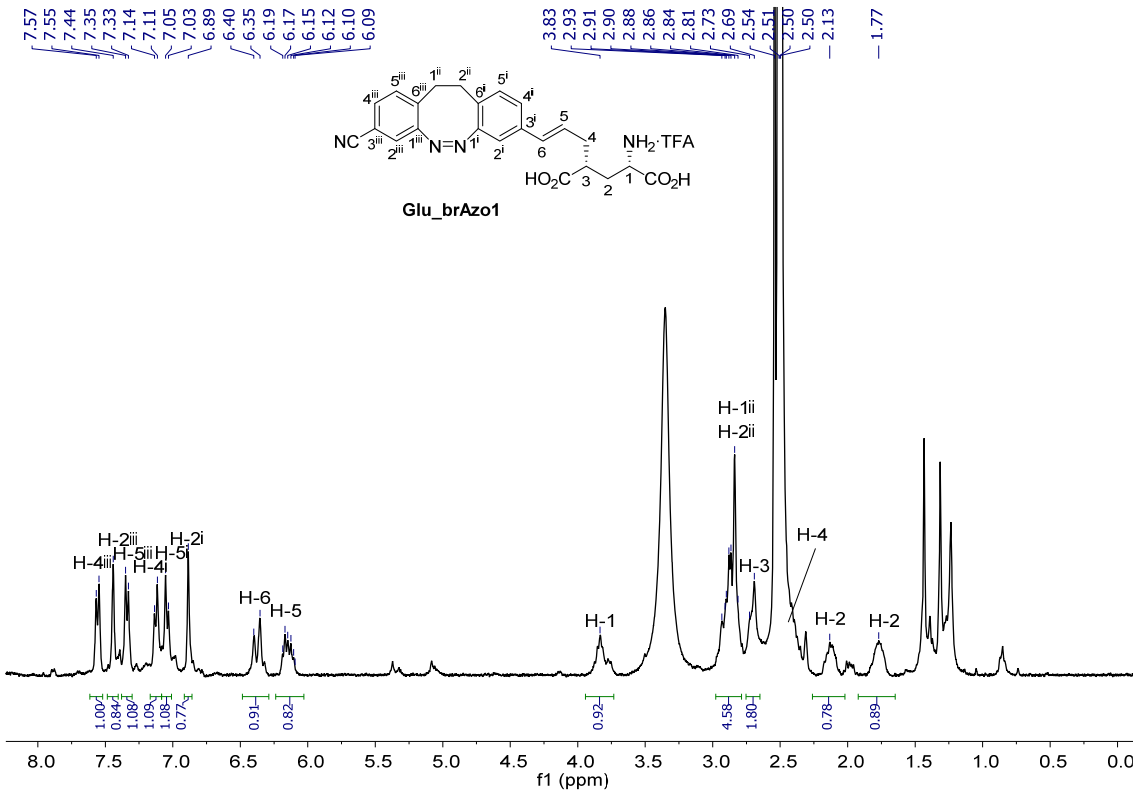

^{1}H NMR (360 MHz, DMSO-d_6)

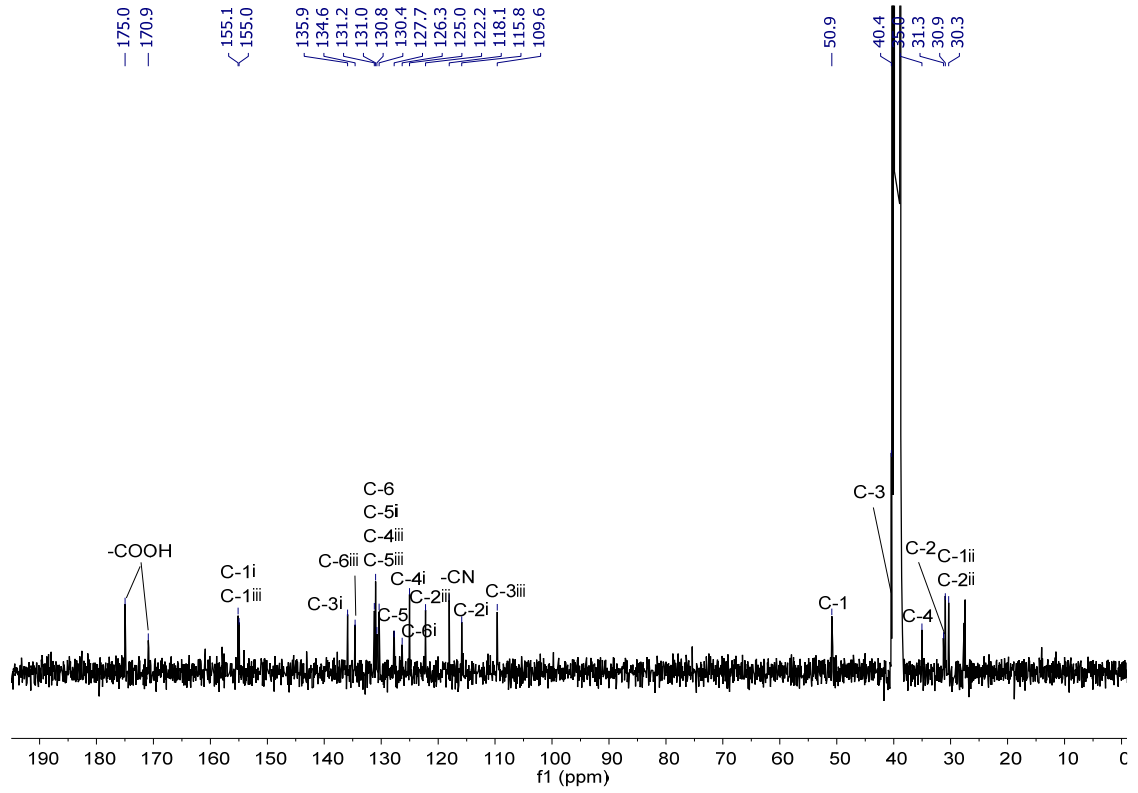

^{13}C NMR (90.5 MHz, DMSO-d_6)

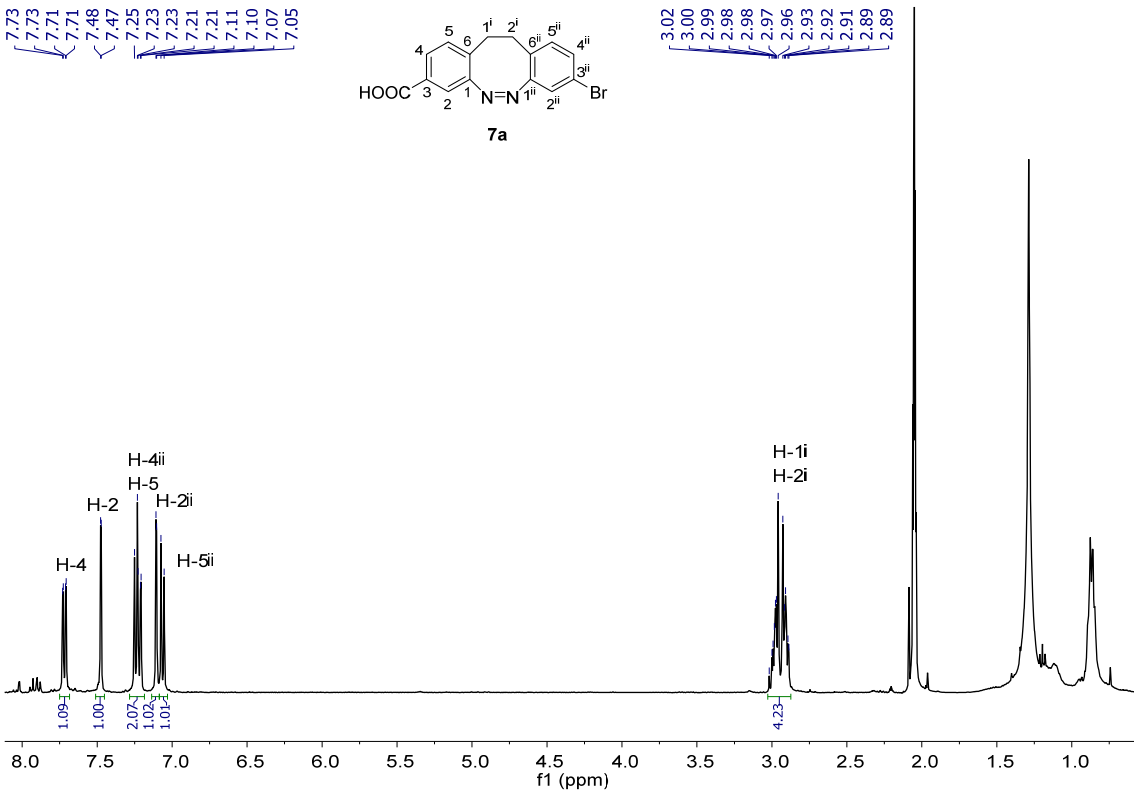

^{1}H NMR (400 MHz, acetone-d_6)

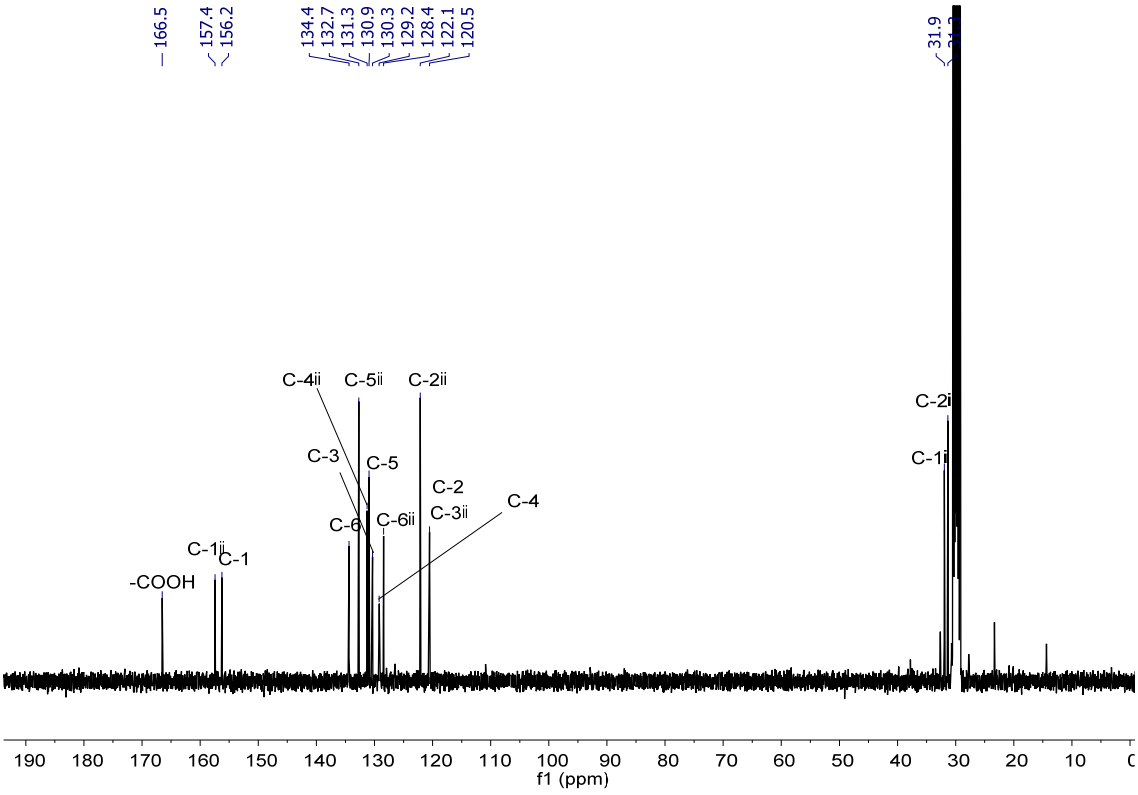

^{13}C NMR (100.6 MHz, acetone-d_6)

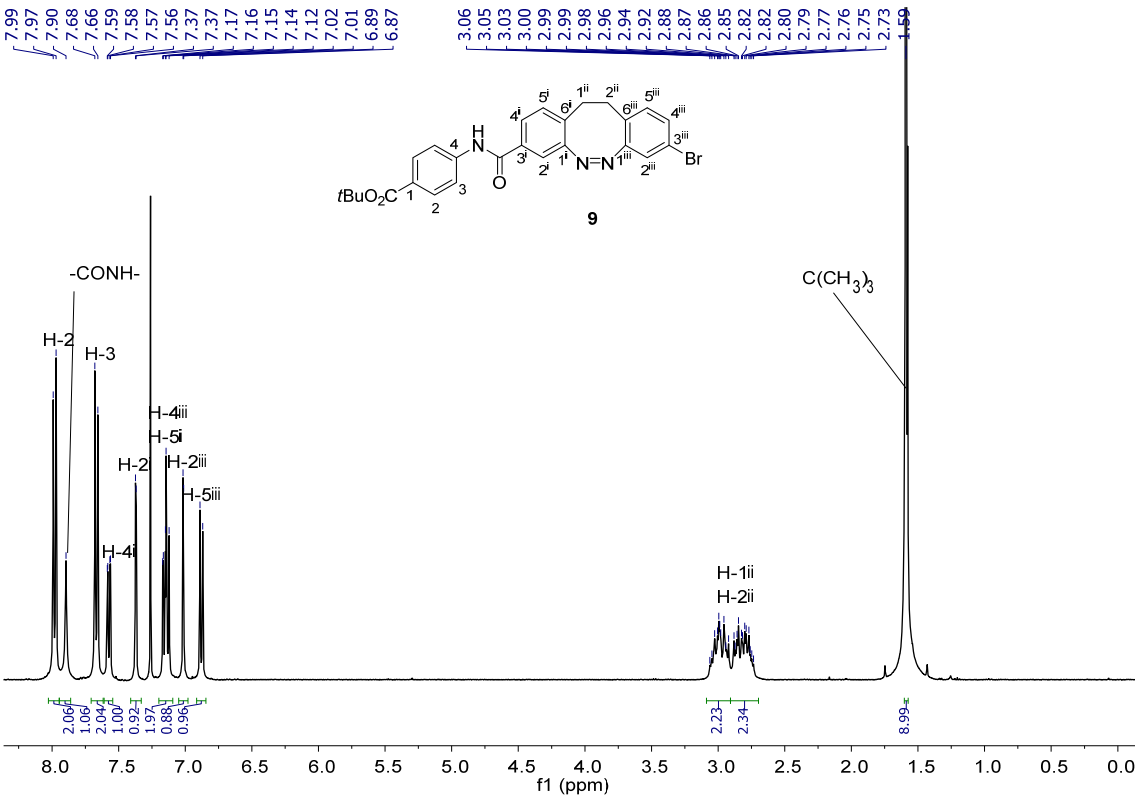

^{1}H NMR (400 MHz, $CDCl_3$)

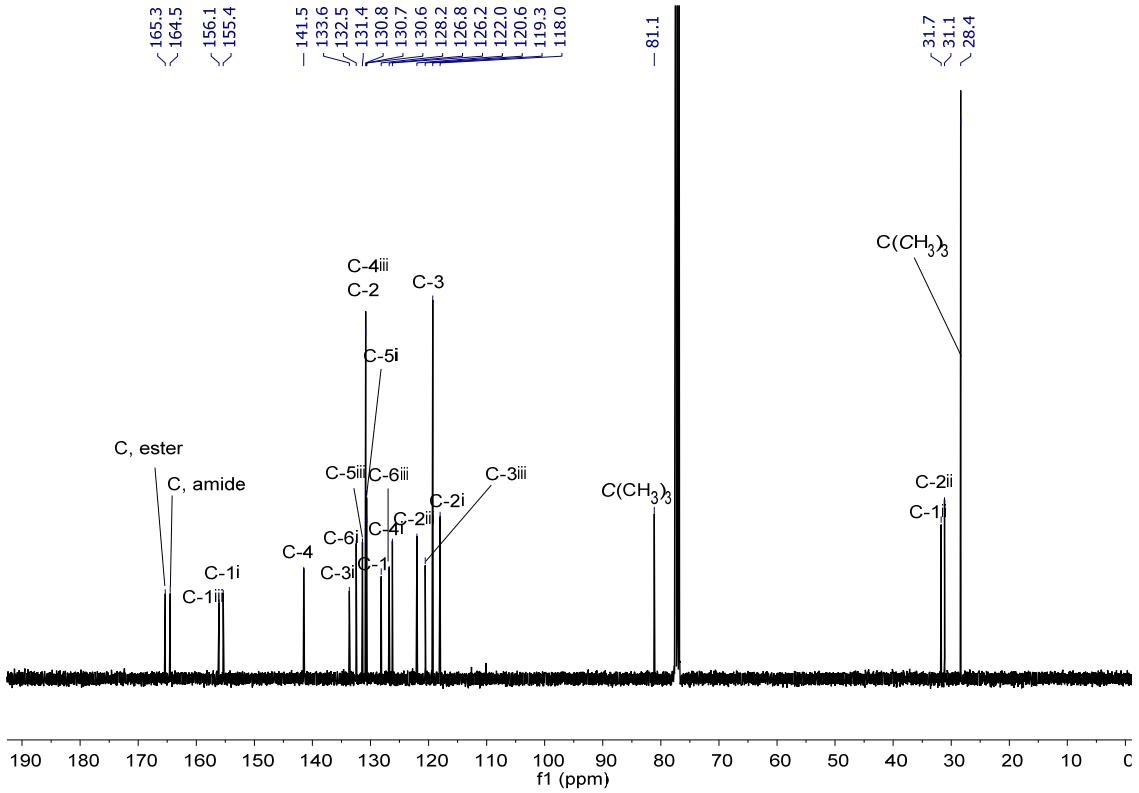

^{13}C NMR (100.6 MHz, $CDCl_3$)

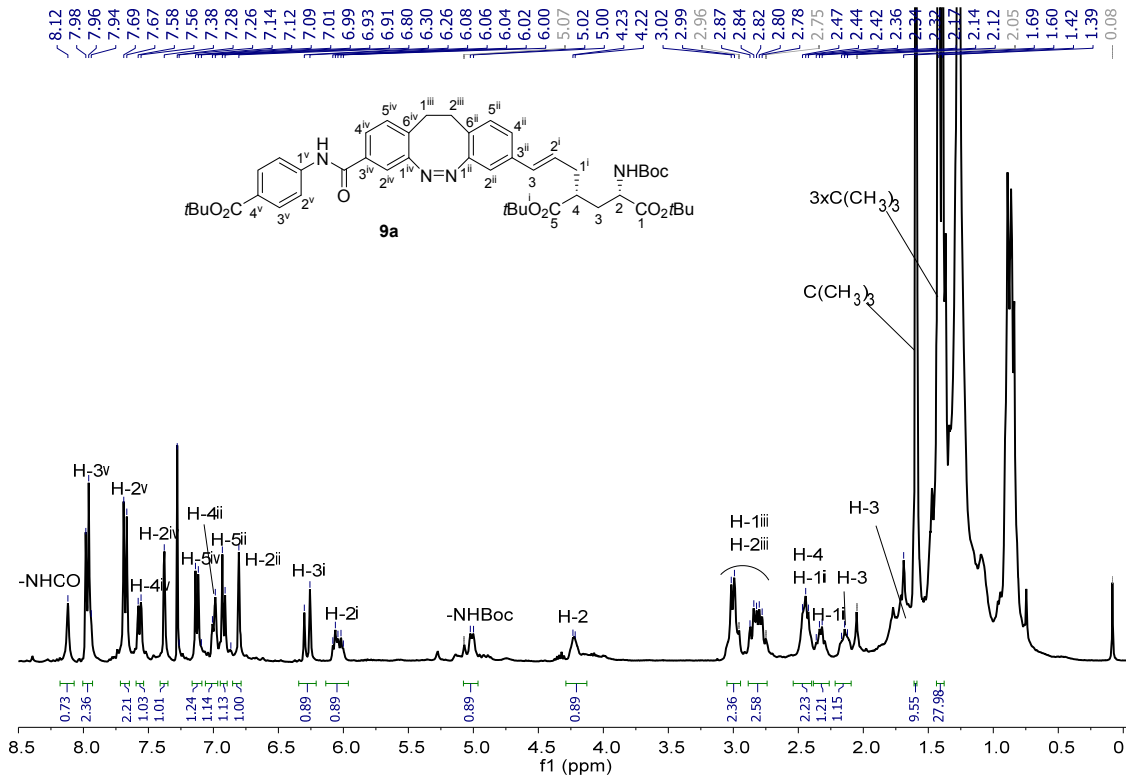

^{1}H NMR (360 MHz, $CDCl_3$)

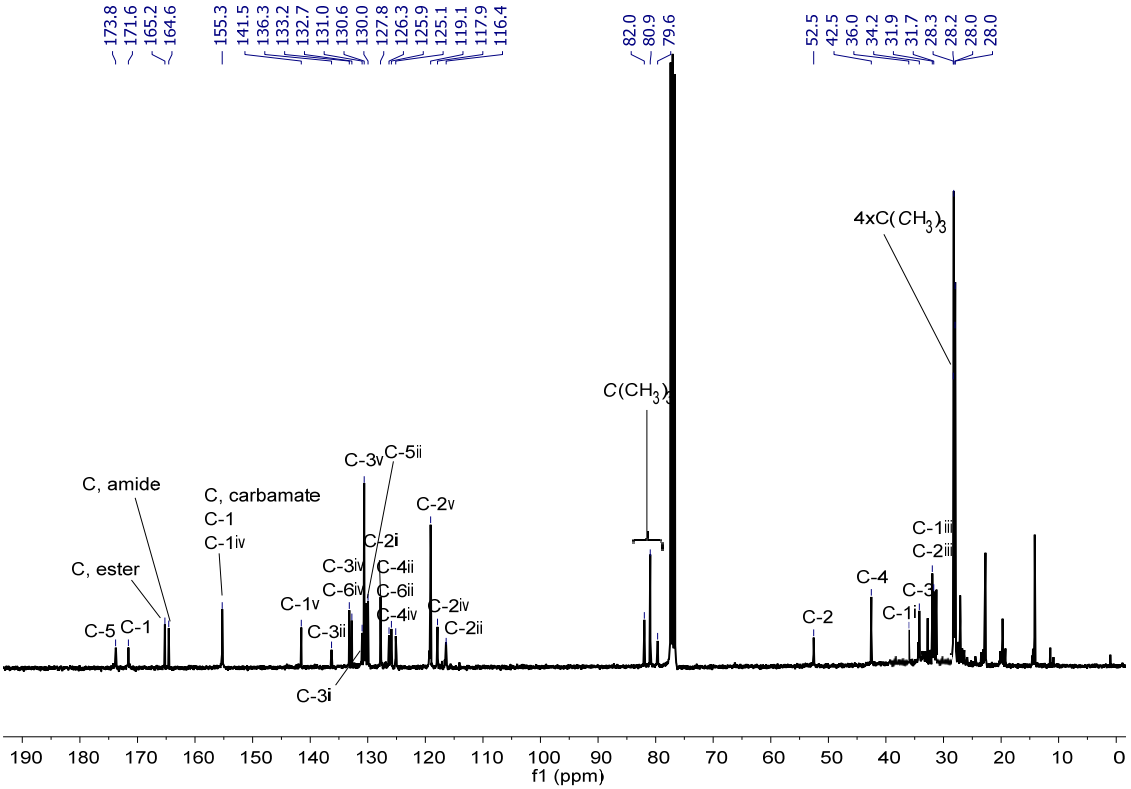

^{13}C NMR (90.6 MHz, $CDCl_3$)

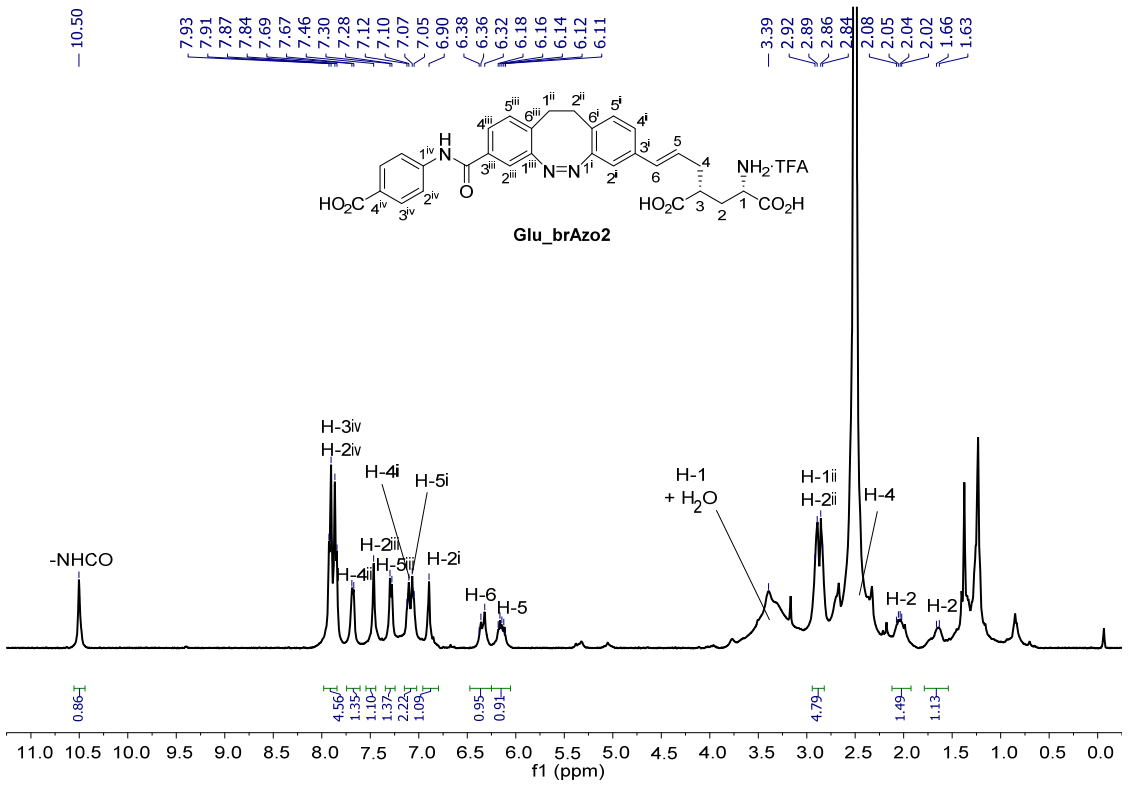

^{1}H NMR (400 MHz, DMSO-d_6)

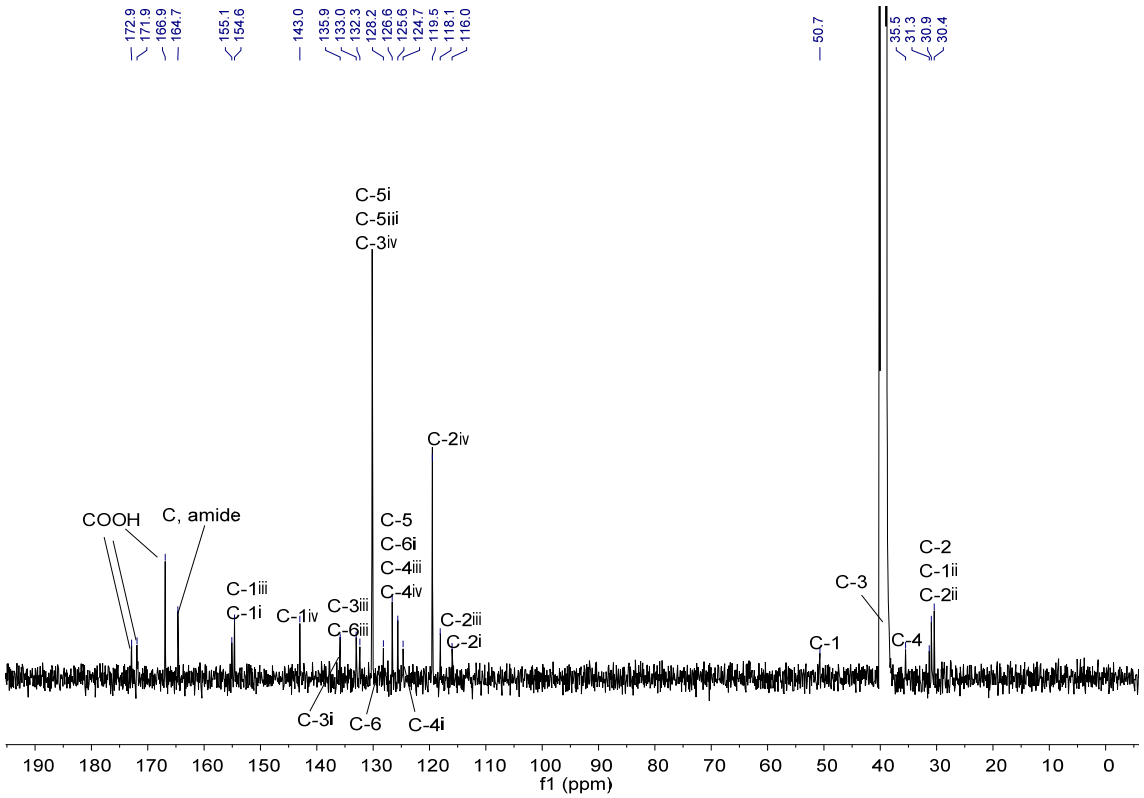

^{13}C NMR (90.6 MHz, DMSO-d_6)

References

[1] Gascón-Moya, M.; Pejoan, A.; Izquierdo-Serra, M.; Pittolo, S.; Cabré, G.; Hernando, J: Alibés, R.; Gorostiza, P.; Busqué, F. *J. Org. Chem.* **2015**, *80*, 9915-9925.

[2] Venkatachalam, T. K.; Huang, H.; Yu, G.; Uckun, F. M. *Synth. Commun.* **2004**, *34*, 1489-1497.

[3] Verdonk, M. L.; Cole, J. C.; Hartshorn, M. J.; Murray, C. W.; Taylor, R. D. *Proteins Struct. Funct. Biogenet.* **2003**, *52*, 609–623.

[4] Reiter, A.; Skerra, A.; Trauner, D.; Schiefner, A. *Biochemistry* **2013**, *52*, 8972-8974.

[5] Anandakrishnan, R.; Aguilar, B.; Onufriev, A. V. *Nucleic Acids Res.* **2012**, *40*, 537-541.

[6] GaussView, Version 6, Dennington, R.; Keith, T. A.; Millam, J. M. Semichem Inc., Shawnee Mission, KS, **2016**.

[7] Pettersen E. F.; Goddard, T. D.; Huang, C. C.; Couch, G. S.; Greenblatt, D. M.; Meng, E. C.; Ferrin, T. E. *J. Comput. Chem.* **2004**, *25*, 1605-1612.

[8] Gaussian 09, Revision C.01, Frisch, M. J.; Trucks, G. W.; Sch-legel, H. B.; Scuseria, G. E.; Robb, M. A.; et al. Gaussian, Inc., Wallingford CT, **2009**.

[9] Eldridge, M. D.; Murray, C. W.; Auton, T. R.; Paolini, G. V.; Mee, R. P. *J. Comput.-Aided Mol. Des.* **1997**, *11*, 425–445.

[10] Higashiguchi, K., Matsuda, K., Asano, Y.; Murakami, A.; Nakamura, S.; Irie, M. *Eur. J. Org. Chem*. **2005**, 91-97.

[11] Ren, Z.; Riley, N. J.; Needleman, L. A.; Sanders, J. M.; Swanson, G. T.; Marshall, J. *J. Biol. Chem*. **2003,** 278, 52700–52709.

[12] Halliwell, R. F.; Peters, J. A.; Lambert, J. J. *Br. J. Pharmacol.* **1989**, *96*, 480-494.

[13] Beaudoin, G. M.; Lee, S. H.; Singh, D.; Yuan, Y.; Ng, Y. G.; Reichardt, L. F.; Arikkath, J. *Nat. Protoc.* **2012**, *7*, 1741-1754.

[14] Kaech, S.; Banker; G. *Nat. Protoc.* **2006**, *1*, 2406-2415.